Hannu Kärkkäinen

ANALYSIS OF THEORY AND METHODOLOGY USED IN DETERMINATION OF ELECTRIC MOTOR DRIVE SYSTEM LOSSES AND EFFICIENCY

ACTA UNIVERSITATIS LAPPEENRANTAENSIS 958

Hannu Kärkkäinen

ANALYSIS OF THEORY AND METHODOLOGY USED IN DETERMINATION OF ELECTRIC MOTOR DRIVE SYSTEM LOSSES AND EFFICIENCY

Dissertation for the degree of Doctor of Science (Technology) to be presented with due permission for public examination and criticism in the Auditorium 1316 at Lappeenranta-Lahti University of Technology LUT, Lappeenranta, Finland on the 23rd of April, 2021, at 3 p.m.

Acta Universitatis
Lappeenrantaensis 958

Supervisors Professor Juha Pyrhönen
LUT School of Energy Systems
Lappeenranta–Lahti University of Technology LUT
Finland

Docent Lassi Aarniovuori
LUT School of Energy Systems
Lappeenranta–Lahti University of Technology LUT
Finland

Reviewers Professor Martin Doppelbauer
Institute of Electrical Engineering
Karlsruhe Institute of Technology
Germany

Associate Professor Emmanuel Agamloh
Department of Electrical and Computer Engineering
Baylor University
United States of America

Opponents Professor Martin Doppelbauer
Institute of Electrical Engineering
Karlsruhe Institute of Technology
Germany

Associate Professor Emmanuel Agamloh
Department of Electrical and Computer Engineering
Baylor University
United States of America

ISBN 978-952-335-647-4
ISBN 978-952-335-648-1 (PDF)
ISSN-L 1456-4491
ISSN 1456-4491

Lappeenranta–Lahti University of Technology LUT
LUT University Press 2021

Abstract

Hannu Kärkkäinen
Analysis of theory and methodology used in determination of electric motor drive system losses and efficiency

Lappeenranta 2021
84 pages
Acta Universitatis Lappeenrantaensis 958
Diss. Lappeenranta-Lahti University of Technology LUT
ISBN 978-952-335-647-4, ISBN 978-952-335-648-1 (PDF)
ISSN-L 1456-4491, ISSN 1456-4491

This research is divided into two main parts: loss determination of motors, converters, and motor drive systems and determination of measurement uncertainty. With its accurate measurements and data analysis, the work provides significant findings. For example, it is now clear that converter-caused additional losses in a motor depend on the load and excitation frequency.

The measurement uncertainty related to converter-fed machines and pulse-width-modulated power is a controversial topic. It has been shown that in the practical measurement uncertainty analysis of converters and electric machines, the PWM supply can be analyzed using fundamental wave values, and they can be treated in the uncertainty analysis similar to the analysis of a typical sinusoidal supply.

To the author's knowledge, there has not been a procedure to thoroughly analyze the measurement uncertainty of electric motors and drives. A method to determine the overall measurement uncertainty for direct-on-line and converter-fed motor drive systems is developed starting from measurement instrument datasheets and resulting in the total expanded measurement uncertainty. The main uncertainty contributors are demonstrated, and it is shown that it is important to identify all uncertainty sources, as a single high uncertainty contributor can have a significantly deteriorating effect on the overall measurement uncertainty.

So far, there has not been general guidance available on how the data should be collected from the measurement instruments in the case of electric motor and converter efficiency determination. The number of samples and measurement time needed to achieve an acceptable level of measurement uncertainty are demonstrated in this work.

Although the international standards are generally well prepared and widely studied, the methods for loss and efficiency determination have room for improvement. The results published in the papers of this study show that there are grounds for criticism of some of the present standard methods.

The open and balance type calorimeter used in this study has been considered one of the most accurate types of calorimetric systems. However, the method consists of two separate tests, and the impact of changes in air properties between the tests has not been clear. In this work, it is shown that humidity and barometric pressure measurements are, after all, not essential for an open and balance type calorimeter. A comprehensive procedure to establish a measurement system has been set up to make compliance measurements possible in general.

Keywords: Electric motor, frequency converter, variable frequency drive, complete drive module, power drive system, efficiency, measurement uncertainty

Acknowledgments

The research documented in this doctoral dissertation was carried out at the Laboratory of Electrical Drives Technology at Lappeenranta-Lahti University of Technology LUT, Finland, between 2015 and 2020. Part of the laboratory measurements conducted for this work relied on collaboration projects with ABB Oy.

First, I would like to thank my supervisors Professor Juha Pyrhönen and Docent Lassi Aarniovuori for the opportunity to continue within the topic after my Master's Thesis, and their invaluable guidance, ideas and support throughout the research and dissertation process. I am grateful for Dr. Markku Niemelä for discussions, comments, and help with several parts of the research.

Special thanks go to Mr. Kyösti Tikkanen for the laboratory arrangements and help with measurements and for Dr. Hanna Niemelä for reviewing and improving the language of this work.

I express my gratitude for pre-examiners Professor Martin Doppelbauer and Associate Professor Emmanuel Agamloh for their effort and comments for improving this work in its final stages.

I would also like to thank my colleagues and friends for their help and support during this process.

Hannu Kärkkäinen
March 2021
Lappeenranta, Finland

Contents

List of publications

This doctoral dissertation is based on the following papers. The rights have been granted by the publishers to include the papers in the dissertation.

I. Kärkkäinen, H., Aarniovuori, L., Niemelä, M., and Pyrhönen, J., "Converter-fed induction motor losses in different operating points," in *2016 18th European Conference on Power Electronics and Applications (EPE'16 ECCE Europe)*, Karlsruhe, 2016, pp. 1−8.

II. Kärkkäinen, H., Aarniovuori, L., Niemelä, M., and Pyrhönen, J., "Converter-Fed Induction Motor Efficiency: Practical Applicability of IEC Methods," *IEEE Industrial Electronics Magazine*, vol. 11, no. 2, pp. 45–57, June 2017.

III. Kärkkäinen, H., Aarniovuori, L., Niemelä, M., Pyrhönen, J., and Kolehmainen, J., "Technology comparison of induction motor and synchronous reluctance motor," in *IECON 2017 - 43rd Annual Conference of the IEEE Industrial Electronics Society*, Beijing, 2017, pp. 2207–2212.

IV. Kärkkäinen, H., Aarniovuori, L., Niemelä, M., Pyrhönen, J., Kolehmainen, J., Känsäkangas, T., and Ikäheimo, J., "Direct-On-Line Synchronous Reluctance Motor Efficiency Verification with Calorimetric Measurements," in *2018 XIII International Conference on Electrical Machines (ICEM)*, Alexandroupoli, 2018, pp. 171–177.

V. Kärkkäinen, H., Aarniovuori, L., Niemelä, M., and Pyrhönen, J., "Induction Motor Efficiency Verification Using a Balance-Type Calorimeter Equipped with a Mass Flow Meter," in *2018 20th European Conference on Power Electronics and Applications (EPE'18 ECCE Europe)*, Riga, 2018, pp. P.1–P.10.

VI. Kärkkäinen, H., Aarniovuori, L., Niemelä, M., and Pyrhönen, J., "Advanced Uncertainty Calculation Method for Frequency Converter Loss Determination," in *2018 20th European Conference on Power Electronics and Applications (EPE'18 ECCE Europe)*, Riga, 2018, pp. P.1–P.10.

VII. Kärkkäinen, H., Aarniovuori, L., Niemelä, M., and Pyrhönen, J., "Advanced Uncertainty Calculation Method for Converter-Fed Motor Loss Determining," in *2019 IEEE International Electric Machines and Drives Conference (IEMDC)*, San Diego, CA, 2019.

VIII. Kärkkäinen, H., Aarniovuori, L., Niemelä, M., and Pyrhönen, J., "The Instrumentation Influence on the Motor Loss Determination Uncertainty," in *IECON 2017 – 45th Annual Conference of the IEEE Industrial Electronics Society*, Lisbon, 2019.

IX. Aarniovuori, L., Kärkkäinen, H, Anuchin, A., Pyrhönen, J., Lindh, P., and Cao, W., "Voltage Source Converter Energy Efficiency Classification in Accordance with IEC 61800-9-2," in *IEEE Transactions on Industrial Electronics*, vol. 67, no. 10, pp. 8242–8251, Oct. 2020.

Author's contribution

Hannu Kärkkäinen is the principal author and the main investigator in **Publications I–VIII.** In these publications, all the data analyses were performed by Hannu Kärkkäinen. In **Publications I**, **II**, **IV**, and **V**, the experimental measurements were conducted by Hannu Kärkkäinen. In **Publications III**, **VI**, and **VII**, data from previous measurements conducted by Dr. Markku Niemelä were used. In **Publication VIII**, the theoretical analysis was carried out by Hannu Kärkkäinen by using the technical specifications of motors and measurement devices instead of actual measurements. Hannu Kärkkäinen performed the postprocessing of the experimental data and conducted the uncertainty analysis presented in **Publication IX.**

Nomenclature

Latin alphabet

f	frequency	Hz
I	current	A
k	coverage factor	–
m	mass	kg
n	rotational speed	min^{-1}
P	power	W
R	resistance	Ω
T	torque	Nm
p	pressure	Pa
u	uncertainty	–
u_A	uncertainty of type A	–
u_B	uncertainty of type B	–
t	time	s

Greek alphabet

η	efficiency	–
θ	temperature	K, °C
σ	standard uncertainty	–
φ	relative humidity	%
Ω	mechanical angular velocity	rad/s
ω	electrical angular velocity	rad/s

Subscripts

C	constant
c	coolant
Fe	iron
fw	friction and windage
in	input
indirect	indirect method, determined using an indirect method
LL	stray load loss, additional load loss
LH	linearity and hysteresis
loss	loss
nom	nominal
out	output
para	parasitic
PWM	pulse width modulated
R&D	research and development
REP	repeatability

r	rotor
s	stator
SEN	sensitivity tolerance
sine	sinusoidal
max	maximum
min	minimum
tot	total
θZ	temperature influence on zero value
θS	temperature influence on span

Abbreviations

AC	alternating current
Cal	calorimetric method
CDM	complete drive module (frequency converter)
DC	direct current
DOL	direct-on-line
DTC	direct torque control
DUT	device under test
FEM	finite element method
GaN	gallium nitride
IGBT	insulated gate bipolar transistor
IEA	International Energy Association
IE0	efficiency class for frequency converters when the losses are more than 25% higher than the reference losses
IE1	standard efficiency class for motors or for frequency converters when the losses are at the same level as with the reference CDM losses
IE2	high efficiency class for motors or for frequency converters whose losses are 25% below the reference losses
IE3	premium efficiency class for motors
IE4	super premium efficiency class for motors
IE5	the following efficiency class for motors
IES0	PDS efficiency class if the losses are at least 20% higher than the reference losses
IES1	PDS efficiency class if the losses are at the same level as the reference losses
IES2	PDS efficiency class if the losses are at least 20% lower than the reference losses
IEC	International Electrotechnical Commission
IM	induction motor
In-Out	input-output method
JCGM	Joint Committee for Guides in Metrology
LUT	Lappeenranta-Lahti University of Technology LUT
PDS	power drive system (frequency converter driven motor system)
PMSM	permanent magnet synchronous motor

PWM	pulse width modulation
RPM	realistic perturbation method
SiC	silicon carbide
SM	synchronous motor
SynRM	synchronous reluctance motor
TS	technical specification
VSC	voltage source converter

1 Introduction

Global awareness of human-induced environmental problems has increased over the past few decades. Alternative solutions have been presented to curb the climate change; in any case, the fact is that electric machines play a major role in this task. It has been estimated that electric motor systems account for more than half of the global electricity consumption (IEA, 2016). The significance of electric motors is even greater considering industry, where electric motors consume over 70% of electric energy (IEA, 2016). Legislation and regulations are used to drive the users and manufacturers towards more energy-efficient products. For instance, the European Commission has put in action gradually tightening efficiency regulations for electric motors (European Commission, 2009), and this development is expected to continue in the future (European Commission, 2019).

The efficiencies of motor systems can be increased by selecting a motor of the optimal technology considering the usage scenario and by optimizing the motor design (materials and structure). In addition, the energy consumption can be reduced by using frequency converters to control motor drive systems. In some cases, a direct-on-line (DOL) motor is the optimal choice. However, because of the constant grid-frequency supply, DOL motors are, in practice, running at a fixed speed. In many situations, the ability to control the motor speed can lead to energy savings. In a motor drive system, a frequency converter is used to supply a motor, and the speed can be controlled optimally according to the load. In the case of converter-fed motor systems, further efficiency improvements can be obtained by improving the efficiency of the frequency converters—for instance by using better semiconductors—and by optimizing the operation of the motor and the frequency converter at the drive system level.

The progress of increasing the efficiencies and tightening regulations is reflected also in the development of standards covering motor efficiency classification and testing. New DOL motor efficiency classes have been introduced in the latest edition of the classification standard from the International Electrotechnical Commission (IEC, 2014a). Determination of the motor losses and efficiency becomes more challenging when the efficiency increases. Consequently, the standard for DOL motor loss and efficiency determination has been updated with tighter requirements for instrument accuracy and refined test methods (IEC, 2014b). Considering converter-fed motor systems, a completely new IEC standard has been released (IEC, 2017). The standard provides international efficiency classifications and efficiency determination methods for frequency converters and complete motor drive systems. Converter-fed motors are not covered by (IEC, 2017). Instead, another completely new standard (IEC, 2020) was recently released defining methods for loss and efficiency determination of converter-fed motors.

1.1 Power drive systems

The electric grid frequencies are, in general, either 50 Hz or 60 Hz, and as the operation principle of AC motors is based on a rotating magnetic field produced by the alternating supply current, the operating speed of an AC motor is determined by the frequency of the supply current and the number of pole pairs in the machine. A frequency converter—as the name suggests—can be used to adjust the frequency of its output voltage and consequently, to control the motor speed. There are several different frequency converter technologies, but by far the most common converter type in industry is the two-level three-phase voltage source converter. In a voltage source converter, the input grid voltage is first rectified to intermediate circuit DC voltage. Secondly, a switching inverter bridge is used to achieve the desired output voltage by controlling the power electronic switches accordingly using pulse width modulation (PWM). At present, the switches are typically insulated gate bipolar transistors (IGBT) based on traditional silicon technology, but the deployment of wide bandgap devices is rapidly expanding. The new wide bandgap power switches are a future technology, even though they are already available in the market with a high price. The market is not yet ready for the uptake of new devices as the full potential of the new devices has not yet been demonstrated.

The construction in which a motor is supplied with a variable-frequency voltage provided with a frequency converter is referred to with a number of different terms. The most typical ones are “electric drive system,” “variable speed drive system,” and “adjustable speed drive system.” In addition, the IEC standard for converters and drive systems (IEC, 2017) uses the term “power drive system.” The terms should be used carefully, as it is not uncommon to see a frequency converter referred to with similar terms: “electric drive,” “variable speed drive,” or “adjustable speed drive” even though a converter is only capable of supplying a motor that then is capable of driving a mechanical load. In fact, the European Commission regulation on electric motor efficiency (European Commission, 2009) uses misleadingly the term “variable speed drive” of the electronics that provide variable supply frequency for an electric motor. In the standard (IEC, 2017), however, a more illustrative term “complete drive module” is used. In this dissertation, the standardized terms power drive system (PDS) and complete drive module (CDM) are used for clarity.

The number of speed-controlled motor installations has been increasing rapidly in recent years, and this progress is expected to continue. In 2014, the share of power drive systems of new industrial motor installations was 30%, and it was estimated to rise to 50% by 2020 (Sander, 2016).

In principle, any rotating field DOL motor can be used in a PDS, but the loadability of the motor is reduced compared with a DOL supply for several reasons. Because of the pulse width modulation, the output voltage of frequency converters is distorted, which causes additional losses in motors. Furthermore, in typical industrial motors, the motor cooling fan is attached to the motor shaft, and hence, cooling is weaker when operating at lower speeds. This is partly compensated by lower iron losses at low fundamental

frequencies and by possible energy efficiency optimization procedures in partial load conditions, which reduce iron losses. In addition, limitations of the available voltage amplitude typically reduce the loadability near the rated operating frequency of the motor. However, there are also motors designed and rated specifically for variable speed use, and some motor technologies are optimally suitable for a frequency converter supply, as will be discussed later.

1.2 Electric motor technologies

There are various rotating field motor types based on different technologies in use and in the market. Considering industrial applications of electric motors and variable speed motor drive systems, the most important motor technologies are the squirrel-cage induction motor (IM), the permanent magnet synchronous motor (PMSM), and the synchronous reluctance motor (SynRM). In some—especially in very large—applications, also synchronous motors (SM) are used. The IM, PMSM, and SynRM technologies naturally share some features, but have also major differences in operating principles, although motors combining these technologies also exist. All three technologies are AC machines, and typically in industry, have three phases. In addition, the basic operating principle is based on supplying the total electric power through the stator windings, which produce a rotating magnetic field. Therefore, a similar stator structure can be used in IMs, PMSMs, and SynRMs. It should, however, be noted that PMSMs can also use stator constructions not suitable for IMs or SynRMs.

The major differences between the technologies are found on the rotor side. The common air-gap flux is produced in different ways: In the case of an IM, the air-gap flux density induces currents in the rotor short-circuited cage, which, in turn, starts carrying currents and affects the common air-gap flux, while in a PMSM, the rotor permanent magnets contribute to the common flux in a permanent way. In the case of a SynRM, the common flux is built by the stator windings alone, but the rotor saliency modulates the flux in a way that torque production becomes possible. The common air-gap flux modulation in SynRM is based on the tendency of the magnetic flux to take the minimum reluctance path, and the rotor of a SynRM is constructed to maximize this effect. The permanent magnets in PMSM and SynRM rotor saliency are physical structures in the rotor, hence the rotor speed in both these technologies is, on average, the same as the speed of the common air-gap field. For induction to take place, the IM rotor cage has to move in relation to the air-gap field. Therefore, in the IM, the speed of the rotor, depending on the operating mode, is slightly lower or higher than the speed of the common air-gap field.

The IM has been the workhorse of the industry for decades, but it has a disadvantage in efficiency when compared with the PMSM and the SynRM. As an advantage of the IM, it can be considered to have a wide operational speed area when fed by a converter. Still, most industrial motors are IMs, but this may change as the efficiency regulations are tightened and IMs may not be able to keep up with the progress (de Almeida, et al., 2014). PMSMs and SynRMs, instead, are well suited to be used with frequency converters.

Capabilities to start and operate with a direct-on-line supply can, however, be incorporated in PMSM and SynRM structures, but not without compromising the efficiency to some degree.

1.3 Efficiency and losses of electric motors

Lately, the efficiency of electric motors has been increasing in general. This is due to the use of improved materials and manufacturing technologies and more accurate product development, which, however, is to some extent driven by regulations. Standards define the common rules in efficiency determination and classification of motors. Regulations, in turn, are issued by authorities to limit the minimum allowed efficiency levels; the European Commission has set minimum efficiency limits for motors in the European market. The limits are given as international efficiency (IE) classes that are defined in the standard IEC 60034-30-1 (IEC, 2014a) for DOL motors. In Figure 1.1, the IE class limits are given for four-pole, three-phase motors for the power range covered by the standard. The efficiency limits consider the higher efficiency of larger motors, and in practice, the curves in Figure 1.1 show which efficiency values the electric motor has to reach as a function of motor power rating. Motors rated for converter supply will soon have their own IE efficiency limits, which were introduced in the technical specification IEC TS 60034-30-2 (IEC, 2016). Converter-fed motor IE efficiency limits will be slightly lower

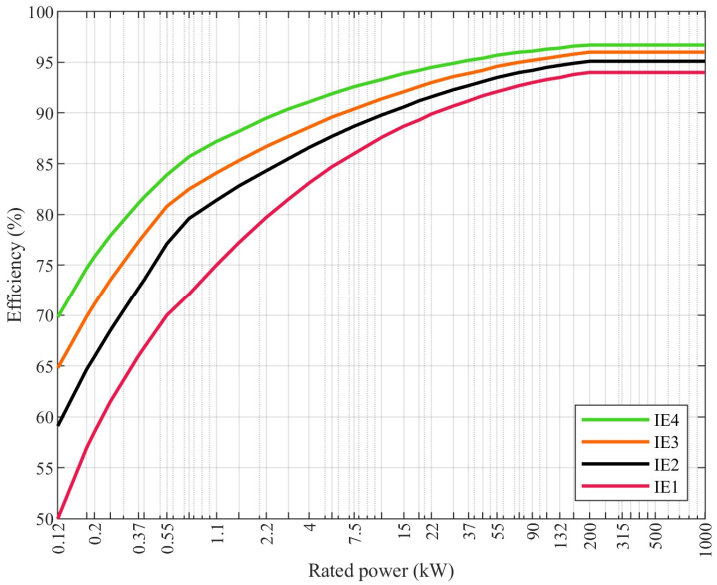

Figure 1.1. IE efficiency class limits for four-pole, three-phase Direct-On-Line AC motors according to IEC 60034-30-1 (IEC, 2014a). IE5 class is not yet standardized, but the IE5 limits for DOL motors are already included in the technical specification IEC TS 60034-30-2 (IEC, 2016).

than the corresponding DOL motor limits, allowing 15%–25% higher total motor losses for each IE class to account for converter-modulation-caused additional motor losses.

Currently, the Commission requires induction motors from 0.75 kW to 375 kW to meet the DOL motor IE3 efficiency level in the direct-on-line use. However, if a DOL-rated IM is used in a power drive system, only a lower IE2 class efficiency is required from the motor. This allowance of a less efficient motor relates to the savings in overall energy consumption that the speed control enables in several applications compared with a fixed-speed DOL motor. There are, though, further plans for tighter regulations already, and the timetable for them is shown in Table 1.1. The table also includes the previous stages of the progress of the Commission regulations for reference. Each new stage in Table 1.1 introduces evolving progress over the previous regulations, extending the power range

Table 1.1: Current timetable of the European Commission regulations for the energy efficiency electric motors (European Commission, 2009), (European Commission, 2019).

Applies from	Requirements
16 June 2011	Motors[1] with rated output power of 0.75 kW–375 kW shall meet the limits of **IE2** efficiency class.
1 January 2015	Motors[1] with rated output power of **7.5 kW**–375 kW shall meet the limits of **IE3** efficiency class, **or IE2 efficiency class, if used in a variable speed drive system**[2].
1 January 2017	Motors[1] with rated output power of **0.75 kW**–375 kW shall meet the limits of IE3 efficiency class, or IE2 efficiency class, if used in a variable speed drive system[2].
1 July 2021	Motors[1] with rated output power of **0.75 kW–1000 kW** shall meet the limits of IE3 efficiency class.[1] Motors[1] with rated output power of **0.12–0.75 kW** shall meet the limits of IE2 efficiency class. [1] **Note: Motors[1] used in a variable speed drive system[2] are from this date on covered by the same IE class requirements.**
1 July 2023	**Ex eb increased safety motors**[1] with 2, 4, 6, or 8 poles and rated output power of 0.12 kW–1000 kW shall meet the limits of IE2 efficiency class. **Single-phase motors**[1] with rated output power of $\geq$ 0.12 kW shall meet the limits of IE2 efficiency class. Motors[1] with rated output power of **75 kW–200 kW** shall meet the limits of **IE4** efficiency class.[4]

[1] "Motor" in the table refers, unless otherwise stated, to a single-speed three-phase induction motor with 2, 4, or 6 poles rated for 50 Hz or 50/60 Hz and up to 1000 V, which is rated for continuous duty operation S1.

[2] The commission regulation refers to a PDS with the term variable speed drive system.

[3] Excluding Ex eb increased safety motors.

[4] Excluding brake motors, Ex eb increased safety motors and other explosion-protected motors.

and motor types covered and requiring higher minimum IE classes. In addition, the IE class requirements for DOL-rated induction motors used in power drive systems will no longer be specified separately after July 2021. Instead, motors rated for DOL supply must meet the same efficiency class requirements even if used with a frequency converter. It should be noted that motors rated for converter supply are not included in the timetable as the standards are not finalized yet. The Commission regulations have also numerous exclusions and exceptions for specific motor types or applications, but many of those are under evaluation to be removed in the future. For instance, the previously excluded *Ex eb increased safety motors* and *single-phase motors* will be included in the regulations from July 2023. Considering the availability of high-efficiency induction motors, IE3- and IE4-rated motors are widely available in the market already, and also some IE5 motors exist.

1.3.1 Direct-on-line motor loss components

The losses of an electric motor are typically divided into four or five main components as listed in Table 1.2. The loss component classification used here is based on typical measurement-based loss segregation, where the loss component boundaries are not physically exact. The differences between a measurement-based loss components and loss components of actual electromagnetic origin are discussed in the context of additional load losses later in this section. Joule losses, also known as copper losses, are the ohmic losses taking place in the stator and rotor windings. Stator Joule losses are present in all common rotating field motor technologies, but rotor Joule losses only take place if there are windings in the rotor, such as the induction motor rotor cage. Iron losses

Table 1.2. Electric motor loss components and their approximate dependence on operating conditions

Loss component	Dependence	Load dependence	Speed/frequency dependence
Stator Joule Losses	• Square of stator current and stator winding resistance (I^2R) • Stator winding temperature	Torque squared	No significant dependence
Rotor Joule losses [1]	• Slip and winding temperature	Torque squared	No significant dependence
Iron losses	• Supply frequency • Peak flux density	Slightly decreases with load [2]	Increases with supply frequency
Friction and windage losses	• Rotational speed	Somewhat load dependent [3]	Increases with rotational speed
Additional load losses	• Relative to torque squared • Supply voltage quality	Torque squared	Increases with supply frequency

[1] Only considered for motors with rotor windings, i.e., not present in PMSM or SynRM.

[2] Stator winding resistive voltage drop decreases the fundamental flux density.

[3] Friction in bearings is temperature dependent. Additionally, DOL induction motor slip increases with load and decreases speed, causing a slight load dependence also in friction and windage losses.

are caused by the alternating magnetic field in the steel and iron parts of the motor. Friction and windage losses are mechanical losses caused by the friction of the bearings and the air resistance of the rotating parts. Stray load losses, or additional load losses, lump together the rest of the electric motor losses. The relative share of each of the loss components is presented in Figure 1.2 as a function of the rated power of the motor. The Joule losses are more dominant in smaller motors, while additional load losses are the largest component in larger motors. The share of mechanical losses and iron losses is similar throughout the power scale shown in the figure.

The Joule losses of the stator and rotor account for a significant part of the total motor losses especially under high load. These losses are proportional to the resistance of the winding and the square of the current running in it. Stator winding losses are caused by the magnetizing current and the torque-dependent component of the stator current. The measurement-based stator Joule losses are, in practice, defined by the winding DC resistance in the operating temperature and the RMS current as

$$P_s = I_s^2 R_s, \tag{1.1}$$

where I_s is the stator line current, and R_s is the stator line-to-line resistance. However, the resistive losses in windings are, in reality, higher as the AC resistance is higher because of the skin effect, the proximity effect, and circulating currents, but the losses caused by these phenomena are counted as additional load losses. Considering the most common industrial motor technologies, the rotor Joule losses are only present in IMs and SMs,

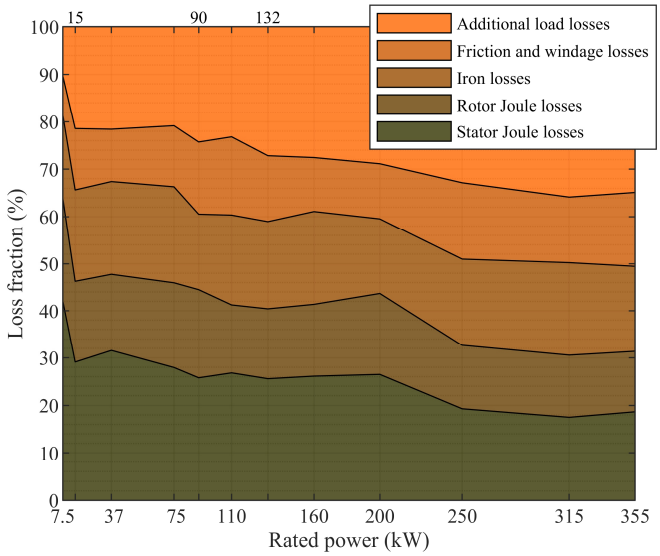

Figure 1.2. Relative share of motor loss components of four-pole DOL IE3 induction motors from the same model series as a function of rated power with sinusoidal voltage (Aarniovuori, et al., 2018).

which is also one of their major disadvantages compared with PMSMs and SynRMs. In the SM, excitation current causes Joule losses in the field winding in the rotor. In the IM rotor, the Joule losses are caused by the slip-speed-induced current, which is proportional to the load. Winding losses are also affected by the temperature characteristics of the conductor resistance. When the winding temperature rises, the conductor resistance increases depending on the material-specific temperature coefficient, which increases the Joule losses as Eq. (1.1) indicates.

Iron or core losses occur in the magnetic core materials of the stator and the rotor. Iron losses in the stator are more significant than in the rotor. In the SynRM and the PMSM, the rotor is spinning synchronized with the fundamental flux, and therefore, there is no changing fundamental flux density in the steady state, and thereby practically no iron losses in the rotor. In the IM, the fundamental frequency in the rotor is proportional to slip, which in 50 Hz and 60 Hz machines is typically only a few percent in rated operation. In large IMs, the rated slip can be close to one percent. As the fundamental frequency in the IM rotor is very low, the IM rotor fundamental iron losses are practically insignificant.

Iron losses are caused by two separate phenomena: eddy currents and hysteresis. Eddy currents are induced by a changing magnetic flux in any conductive material. The rotating flux wave produced by all the windings together induces eddy currents in the stator core. The stator core is constructed from thin steel laminations to minimize eddy currents. Naturally, any flux density changes in the rotor cause some eddy currents also in the rotor, but they are typically negligible in DOL motors and are included in the additional load losses. Hysteresis losses are caused by the magnetic properties of the core material. When a ferromagnetic material, such as steel, is brought to a magnetic field, magnetic dipoles of the material are aligned with the field. After the magnetic field is removed, part of the alignment is retained. When opposite magnetic field is then applied, the magnetic dipoles turn correspondingly. During this process, energy is needed to align the dipoles and remove the retained alignment. Hysteresis losses can be minimized by selection of the core material. Hysteresis losses are, in principle, proportional to frequency, but the effect of frequency may be higher than only to the power of one. Eddy-current losses are proportional to the square of the peak flux density.

What makes the iron loss analysis complicated in an electric machine is the existence of different higher flux density harmonics caused by permeance variations and supply harmonics. In addition, part of the losses is caused by alternating flux densities and part by rotating flux densities, which both have iron loss mechanisms of their own. Finally, calculating the iron loss is very difficult, and empirical models are used even in the case of finite element analysis.

Friction and windage losses include all mechanical losses of the motor. Friction occurs in the bearings and seals of the motor. Windage losses are caused by the motor cooling fan, if one is attached to the shaft, which is the typical industrial motor configuration, and by the air resistance of the rotor. Friction and windage losses are, in principle, independent of the load. They are, however, proportional to the speed of the motor, which in the case

of the induction motor decreases slightly with load because of the slip. Friction losses can be minimized by the selection of bearings, and windage losses by optimizing the cooling: the smaller the required air flow, the smaller the fan and the windage losses. The bearing friction loss depends on the amount of grease and its temperature.

Additional load losses, or stray load losses, consist of all the losses not accounted for by mechanical losses and fundamental winding and iron losses. As the name implies, this loss component, or a collection of load-dependent portions of different loss components, is considered to be present only when operating under load. As already mentioned, additional load losses include the losses taking place in the stator windings because of the skin effect, the proximity effect, and circulating currents. Extra iron losses caused by the increased current under load also end up in additional load losses. There are also some losses induced in the frame of the machine, and also these losses are load dependent because for instance the stator leakage flux increases as a result of the increased torque. In addition, the machine mechanical losses may be slightly affected by the load. A major source of additional load losses is space harmonics caused by the nonideal behavior of the air-gap flux. The air-gap flux density waveform is a distorted sinus wave, as stator windings are not ideally distributed along the stator bore. The windings are placed in slots, and the distribution of the slots causes a stepped waveform. The stepped waveform contains harmonics, and the flux harmonics induce harmonic currents in the rotor. These space harmonics cause additional iron and Joule losses in the rotor and the stator. Space harmonics also cause torque ripple, vibrations, and noise, which increase the total losses. Space harmonics can be reduced by choices made in the motor design. A higher stator winding slot number per pole and phase results in a more sinusoidal air-gap flux-density wave. The IM rotor cage is often skewed to reduce the effects of some space harmonics. In addition, it is preferable to avoid certain stator and rotor slot number combinations (Boldea & Nasar, 2002). Additional load losses are load dependent and usually assumed proportional to the torque squared (IEC, 2014b).

Traditionally, another cause for additional load losses has been the time harmonic components of the supply voltage. The time harmonics are significant when a motor is supplied with a frequency converter, but the grid voltage is not purely sinusoidal either, especially when there are power electronic devices present in the same network nearby. Similar to space harmonics, time harmonics cause additional iron and Joule losses and vibrations. Time harmonics are dampened by the stator leakage inductance, but they may still cause substantial losses also in the rotor. Recently, however, the trend has been that only the losses caused by the harmonics formed when the motor is supplied with a purely fundamental frequency voltage are included in the additional load losses, and the losses caused by the supply voltage harmonics are called additional high frequency losses. (IEC, 2020).

1.3.2 Additional high frequency losses in converter-fed motors

Frequency converters enable optimization of the motor speed according to the application to reduce the overall energy consumption. However, the frequency converter pulse width

modulation (PWM) causes voltage and current harmonics and, inevitably, additional high frequency harmonic losses in the motor. The harmonic losses increase the temperature in the motor and the windings, which leads to an increase in the resistive winding losses. Furthermore, if a DOL-rated motor is driven with a converter instead of grid, the fundamental flux-producing voltage is typically limited near the rated operating speed and, in practice, the motor is running in field weakening, which can cause a substantial increase in the motor current and, consequently, in the Joule losses, if the load is not limited. At partial speeds and loads, in contrast, the flux linkage can be optimized according to the operating point in order to maximize efficiency.

The additional high frequency harmonic losses caused by PWM are a function of PWM switching frequency and modulation method. Using a higher switching frequency, the resulting motor current is less distorted and has a waveform closer to sinusoidal, which reduces the harmonic losses to some degree. In addition, a higher switching frequency helps to provide a somewhat higher fundamental voltage and alleviate the effect of the limited motor voltage close to the rated operating speed. Similarly, the modulation method applied influences the current waveform and the maximum fundamental voltage achieved.

1.4 Efficiency and losses of power drive systems

While international motor efficiency standards have been in use for decades, standards for frequency converters (CDM, complete drive module) and converter driven motor systems (PDS, power drive system) have been released only recently. The international efficiency classes for CDMs and PDSs are defined in the standard IEC 61800-9-2 (IEC, 2017), which also sets the methods for the determination of efficiencies. The standard covers converters and drive systems from 0.12 kW to 1000 kW. While the motor IE class limits are given for each IE class individually, the classes for CDMs and PDSs are defined using reference losses for IE1 and IES1 classes: a CDM is rated for IE0 if the losses are more than 25% higher than the reference losses and for IE2 if the losses are 25% below the reference losses. Similarly, a PDS is rated as IES0 if the losses are at least 20% higher and as IES2 if they are more than 20% lower. The class limits for CDMs and PDSs are given as efficiencies in Figure 1.3a and Figure 1.3b, respectively.

As the standards for CDMs and PDSs are now publicly available, the European Commission has already planned regulations for CDM efficiency: “From 1 July 2021, the power losses of variable speed drives rated for operating with motors with a rated output power equal to or above 0,12 kW and equal to or below 1 000 kW shall not exceed the maximum power losses corresponding to the IE2 efficiency level” (European Commission, 2019).

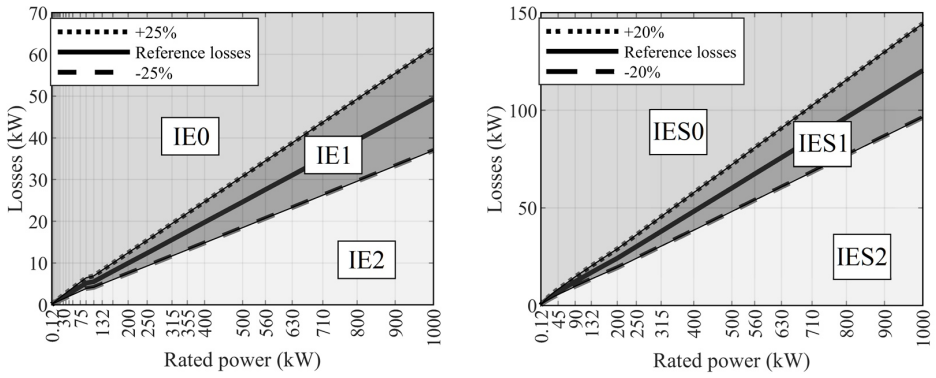

(a) (b)

Figure 1.3. Reference losses and efficiency class limits for complete drive modules (a) and power drive systems (b) presented as efficiency curves as a function of rated power.

1.4.1 Frequency converter losses

The most common type of CDM used in power drive systems is a voltage source converter (VSC). The VSC losses are divided into the following main components: input choke losses, input bridge losses, DC link losses, output bridge losses, control losses, and cooling losses.

The semiconductor losses consist of switching and conduction losses. With silicon switches, the majority of the VSC losses are generated in the inverter bridge. The semiconductor conduction losses are proportional to current and depend on the power factor and the modulation principles. The switching losses increase as a function of switching frequency. The DC link losses are, to a large extent, caused by voltage-balancing resistors connected in parallel with the DC link capacitors but also by the resistance of the busbar. The choke losses are proportional to current. The cooling losses increase along with an increase in converter losses. The control losses are caused by the control hardware, and they do not depend on the converter load (Aarniovuori, et al., 2015).

It is well known that the new wide bandgap switching devices consume less energy. However, only replacing the silicon switches with SiC or GaN ones does not significantly enhance the efficiency of a whole converter or motor drive system. The new wide-bandgap power switches with lower switching losses make it possible to use a very high switching frequency and reduce the inverter bridge losses and motor harmonic losses. But when a relatively high switching frequency is used, the harmonic losses do not decrease anymore (Boglietti, et al., 2005); further, there is some evidence that when an ultra-high switching frequency is used, the losses actually increase rapidly because of minor-loop hysteresis losses. The extra losses caused by a very high switching frequency can also

partly be explained with capacitive currents, which also cause losses in the motor construction.

1.4.2 Drive system losses

The efficiency of a PDS consists of the efficiencies of the motor and the CDM. The efficiency of the power electronics used in a modern frequency converter is typically significantly higher than the efficiency of a motor that it is designed to drive. An example of the share of the motor and converter losses in a power drive system is illustrated in Figure 1.4, where the motor losses are 75% and the converter losses 25% of the total drive system losses.

The overall PDS efficiency, however, is somewhat more complicated than only the product of the given motor and converter efficiencies. As discussed in the previous section, a frequency converter causes additional losses in the motor, but the converter losses also depend on the motor that is being supplied. For instance, the inductance and power factor of the motor have an effect on the converter losses. In addition, the switching frequency and the fundamental voltage affect both the motor and converter losses. The overall PDS efficiency is thus a combination of the operating states of both the motor and the converter.

The higher the switching frequency, the more sinusoidal current can be produced using a specific PWM. In motor applications, the higher number of switching instants consumes more energy in the frequency converter, but at the same time, the current harmonics and the resulting harmonic losses in the motor are decreased. Similarly, the lower number of switching instants consumes less energy in the frequency converter but increases

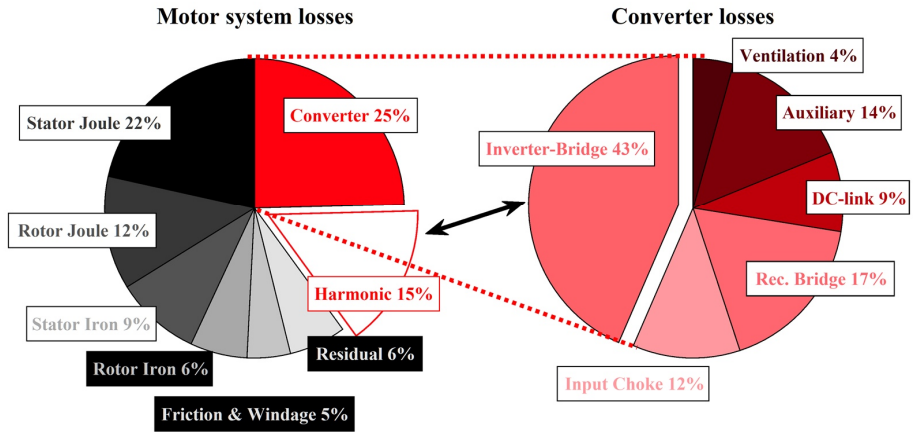

Figure 1.4. Proportions of losses in a frequency-converter-driven premium efficiency induction motor drive with a typical 3–6 kHz switching frequency, producing a few tens of kilowatts of mechanical output power. Composed based on the information found in (Aarniovuori, 2010).

harmonic losses in the motor. The motor losses have a follow-up effect, and the loss increase in the motor increases the current drawn by the motor. This, in turn, increases the conduction losses in the converter, canceling out the reduction in the converter switching losses. Similarly, the power factor of the motor has an influence on the converter losses; delivering the same active power with the lower power factor requires a higher current value, and with the unity power factor, the current is in its minimum value. Nevertheless, the switching frequency of a voltage source converter is a key design parameter when minimizing the losses of a converter-fed motor system.

The behavior of the loss distribution in a PDS is naturally a function of operating point, providing an optimizable situation where both the motor and converter losses, and the drive system as a whole, have to be considered. The control strategy used by the frequency converter has an effect on losses, and it can be used in optimizing the losses in the converter (CDM), motor, or on the power drive system (PDS) level. In such a complex dependence system, a single efficiency value in a single operating point is not enough to represent the overall efficiency of a PDS.

Optimizing the motor losses in a power drive system may also have an effect on the reliability of the motor. The lower the losses in the motor, the lower the motor temperature, and the lower the risk of failure caused by the heating of the motor.

1.5 Methods for determining power drive system losses and efficiency

There are two different main principles of how the efficiency of any device can be determined: direct and indirect, that is, from the input and output power of the device, or from the losses and either the input or output power of the device. Thus, the efficiency η can be presented as

$$\eta = \frac{P_{\text{out}}}{P_{\text{in}}} = \frac{P_{\text{in}} - P_{\text{loss}}}{P_{\text{in}}} = \frac{P_{\text{out}}}{P_{\text{out}} + P_{\text{loss}}} \tag{1.2}$$

where P_{out} is the output power, P_{in} is the input power, and P_{loss} represents the motor losses. Here, it has to be noted that motors are rated based on their output power P_{out}. The first part in (1.2) corresponds to efficiency determination directly from input and output power measurements. The second and third parts of (1.2) are used when the motor losses are determined by alternative methods other than input–output measurements, in which case only either input or output power measurement is needed to calculate the efficiency.

The most common methods used in loss and efficiency determination of frequency converters, electric motors, and power drive systems are listed in Table 1.3. The table summarizes the applicability of each method for high efficiency devices, the uncertainty relative to other methods in the table, and the relative complexity of each method. In addition, the last column indicates whether the method (or some variant of it) is included in efficiency determination standards. The IEC standard methods for loss and efficiency determination of polyphase DOL motors are defined in IEC 60034-2-1 (IEC, 2014b), for

Table 1.3. Most common methods used in determining losses and efficiency of electric motors, frequency converters, and power drive systems.

Method	Applicable to	Ease of use/ complexity	Uncertainty[3]	Standard method for
Input–output	All devices (if input and output power can be measured)	Easy and simple	High	DOL motors[1], frequency converters[2], drive systems[2]
Loss segregation	DOL induction motors (Possibly also DOL PMSM and DOL SynRM)	Complex	Low	DOL induction motors[1]
Calorimetric method	All devices	Extremely complex	Very low	Frequency converters[2]
Analytic calculation	Motors and frequency converters	Complex	High	Motors[1], Frequency converters[2]
Finite element method	Motors	Complex	Very high	-

[1] IEC 60034-2-1 (IEC, 2014b), IEEE 112 (IEEE, 2017)

[2] IEC 61800-9-2 (IEC, 2017)

[3] In the case of high-efficiency devices. The lower the efficiency of the DUT, the lower the uncertainty of the input-output method.

loss and efficiency determination of converter-fed AC motors in IEC 60034-2-3 (IEC, 2020), and for loss and efficiency determination of frequency converters and power drive systems in IEC 61800-9-2 (IEC, 2017).

The first method listed in Table 1.3 is the input–output method, which is by far the simplest of the methods for determining losses and efficiency: For a frequency converter, the electric power needs to be measured from both the input and output of the converter. For motors, the input is naturally electric power, and the output is the mechanical shaft power. Considering a complete power drive system, the losses and efficiency can be calculated from the converter input power and the motor output power. Using the input–output methods, the efficiency is simply the proportion of the output power to the input power (the first form of (1.2)), and the total losses are the difference of the power values

$$P_{\mathrm{loss}} = P_{\mathrm{in}} - P_{\mathrm{out}}. \tag{1.3}$$

The input–output method is a standard method for motors, converters, and power drive systems (IEC, 2014b), (IEC, 2017). The only major disadvantage of the input–output method is rather high uncertainty when testing high efficiency devices. For low efficiency devices, such as small induction motors, the input-output method is the obvious choice as its uncertainty can be similar or even lower compared to the loss segregation or calorimetric methods when the motor losses are relatively high. The uncertainty of the

input–output method in motor, converter and drive system measurements is investigated in detail in Chapter 3.

The loss segregation methods, or the summation of losses methods, are based on determining the motor loss components indirectly using several separate tests and summing the loss components to achieve the total losses of the motor under test. When calculating the final efficiency results, the second form of (1.2) is used, in other words, the efficiency is calculated only based on the electric input power measurement and the indirectly determined total loss value. For polyphase induction motors, loss segregation has been a standard method for decades, but the testing methodology and test requirements have been refined in the recent standard editions. As the losses are determined separately and not directly based on large input and output power measurements, the loss segregation methods are considered low uncertainty methods. Consequently, the IEC adaptation of loss segregation is the recommended method for direct-on-line polyphase induction motors in the standard IEC 60034-2-1 (IEC, 2014b). The loss segregation methods are, however, not perfect. As they rely on determining the motor loss components indirectly using three separate tests, several assumptions and simplifications are made that always result in procedural errors. In addition, the operating conditions are never identical during the separate tests which increases possible error. The main advantage of the loss segregation methods over the input-output method has been that the results are less dependent on the torque measurement as the torque value is only needed when determining the additional load losses, while the output power measurement in the input-output method relies completely on the torque value.

The loss segregation methods have also been considered for other motor technologies than induction motors. Loss segregation of the (DOL) PMSM has been investigated and found plausible (Deusinger, et al., 2014), and assumedly, the same applies also to DOL SynRMs. An extension of the loss segregation method for converter-fed IMs was introduced in the IEC technical specification 60034-2-3 (IEC, 2013), which is the main topic in Publication II. The method for converter-fed motors, however, was revised and simplified in the final standard (IEC, 2020), and it is not the preferred method for converter-fed motors.

Calorimetric methods are based on determining the losses of the device under test by measuring its heat dissipation from the coolant. In electric motors and frequency converters, the primary coolant is usually air or water, and both can be used in calorimetric measurements. Calorimetric measurements can be performed for any device, but in practice, the device to be tested must run in exactly the same load conditions for a sufficiently long period for any temperature transients to settle, which is not always possible. Electric motors and converters can usually be tested calorimetrically within their rated continuous operation specifications. There are several different calorimetric measurement principles and calorimetric measurement systems; a comprehensive review of different calorimetric systems used in electric motor and frequency converter loss measurements is presented in (Aarniovuori, et al., 2017). Out of the five groups of methods in Table 1.3, calorimetric measurements are by far the most complex to organize

and analyze the data, but calorimetric methods can achieve very low uncertainty levels. Calorimetric methods have been included in standards for electric motors before (IEC, 1974), but currently, only water-cooled large motors have a calorimetric method option defined in (IEC, 2010). Calorimetric measurement is especially complex to arrange for motors because of insulation problems related to the test bench and the shaft. For converters, the calorimetric measurement is easier to implement, and the method is included in the new standard (IEC, 2017).

In addition to the purely measurement-based methods, analytical calculations can be used to evaluate losses in electric motors and frequency converters. Equivalent-circuit-based loss calculations for motors require certain motor parameters, which can be either design parameters (if available) or determined by separate tests. Equivalent circuit methods are incorporated in the testing standards (IEC, 2014b), (IEEE, 2017), which also include the tests required to obtain the parameters needed in the calculations. The equivalent circuit methods, however, cannot be considered very accurate, and the IEC recommends using them only if a load test is not possible. Calculation methods for frequency converters involve parameters usually only available for manufacturers, which limits their usability. However, calculation is one of the methods for converters in the new standard (IEC, 2017).

Finite element methods (FEM) for electric motors are used as design tools that allow both transient and steady-state analysis of the performance of a motor design before building an actual prototype. The FEM can also be used to obtain the losses. However, because of the limitations in modeling, the results can be considered only rough estimates at best, especially in the case of iron losses, which are not included in the modeling but instead, are calculated by postprocessing the modeling data according to empirical iron loss models.

Besides the methods listed in Table 1.3 there are some methods that are needed in special cases, such as in very large motors where torque measurement is not feasible. There are variants of the loss segregation method where for example load tests are made at a reduced load, or stray load losses are determined by alternative methods or from predefined values. In addition, back-to-back methods are worth mentioning: the basic idea is to measure two identical machines using one as a motor and the other as a load. In such a setup, only electrical quantities have to be measured to determine the total losses of the two identical machines. However, in this case, the losses are not fully similar in both machines as the flux density levels in the generator and the motor differ slightly.

1.6 Measurement uncertainty

Measurement uncertainty represents a doubt of the validity of a measurement result. In applied sciences such as electrical engineering, measurement uncertainty is often omitted, and the results are presented without any information of the quality of the measurement result. In classical physical sciences, however, the results are usually considered useless without knowledge of the uncertainty. Uncertainty is typically given as a range of values

that most likely include the correct value. The narrower the range, the stronger the weight of the result. Uncertainty should not be mixed with error, which is a part of the result that can be corrected, but uncertainty is present also in the correct value. The uncertainty should not be mixed with resolution or number of digits either. Resolution is only one uncertainty contributor, and the number of digits is often higher than would be required considering accuracy. As a practical example, a cheap thermometer offered in a supermarket can be mentioned. It may have a high resolution, creating an image of high quality and accuracy. The meter may for instance show a room temperature of 21.14 °C, while the real temperature is 19.5 °C. However, there are principles on how to evaluate the uncertainty in any measurement. With the knowledge of the measurement uncertainty and the factors influencing it, the amount of the uncertainty can be controlled.

Measurement uncertainty is divided into two fundamentally different parts, which are called type A and type B uncertainties. Type A uncertainty is related to the variations in the quantity that is being measured, and type B uncertainty covers the accuracies—or inaccuracies—of the measurement instruments. The principles of both type A and type B uncertainties are covered in detail in Publication VI. In Publication VII, example calculations for determining both type A and type B uncertainties of the electric power and mechanical power measurements of a converter-fed induction motor are presented.

The final measurement uncertainty value is a combination of the type A and type B uncertainty values. The Joint Committee for Guides in Metrology (JCGM, 2008) suggests that the realistic perturbation method (RPM) should be used to combine individual uncertainty contributors that are not correlated. The type A uncertainty u_A and the type B uncertainty u_B do not correlate, as the measurement device accuracies have nothing to do with the fluctuations of the measured values. According to the RPM principle, the combined uncertainty is thus

$$u = \sqrt{u_A^2 + u_B^2}. \tag{1.4}$$

Furthermore, measurement uncertainty is usually given as expanded uncertainty, which is described by a coverage factor k. Figure 1.5 represents the normal distribution and different coverage factors. Standard uncertainty corresponds to a coverage factor $k = 1$. Typically, uncertainty values are given as expanded uncertainties using a coverage factor $k = 2$ or $k = 3$, which correspond to 95.4% or 99.7% level of confidence, respectively.

In the loss and efficiency testing standards, uncertainty analysis is not required. Instead, the uncertainty is controlled by setting requirements for the accuracy of the measurement devices and the measurement procedure itself. It is, however, still important to thoroughly understand the uncertainty issues. Although accuracy specifications of measurement instruments may be complex and confusing, the principles of determining measurement uncertainty are quite straightforward.

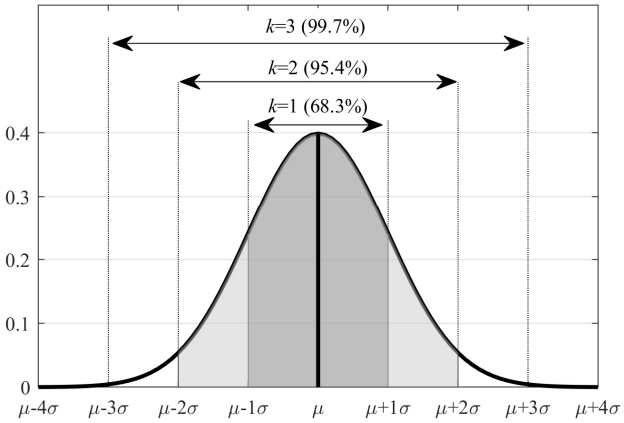

Figure 1.5. Standard uncertainty σ (coverage factor k = 1), and the expanded uncertainties and their probability distributions up to k = 4. At k = 4, the level of confidence is already higher than 99.99%.

In principle, the electric machines and power converters have high efficiencies, and the accuracy of the input–output method is thus limited. The loss uncertainty approaches infinity when the device efficiency is approaching unity. However, it is the only practical method to perform the efficiency evaluation quickly. The measurement equipment has to be selected carefully in the case of the input–output method. The calorimetric method, instead, offers a high-accuracy means of determining efficiency. The calorimetric method is, however, extremely slow and laborious and thus cannot be used on a larger scale, but mainly for verifying for instance the results of the input–output method. The loss segregation method for induction machines has a higher accuracy than the input–output method, but it is also significantly more complicated, and generally suitable only for IMs—although it has been successfully applied also to PMSMs (Deusinger, et al., 2014). For the above reasons, the uncertainty of the input–output method in motor, converter, and power drive system measurements is covered in detail in Chapter 3.

1.7 Outline of the doctoral dissertation

In this doctoral dissertation, the methods used in loss and efficiency determination of electric motors, frequency converters, and power drive systems are analyzed. Different methods are used both together and separately in the measurements of different motor systems, and the results are compared and analyzed. In addition, the measurement uncertainty of electric power measurement, mechanical power measurement, and input–output losses is covered in detail: the uncertainty analysis procedure is explicated and applied to various measurements in order to analyze the uncertainty of the input–output method. The requirements for the measurement instrument accuracies and details in setting up and performing the input–output loss measurements are discussed based on the results.

The focus is on the methods for determining losses and efficiency of electric motors, converters, and power drive systems, and on the converter-caused additional motor losses. The main topics are:

- Methods for determining losses and efficiency of converter-fed electric motors, including the converter-caused additional harmonic losses in the motors.
- Methods for determining the losses and efficiency of frequency converters and power drive systems, considering the loss and efficiency behavior at the motor, converter, and drive system level.
- Measurement uncertainty of the electric power, mechanical power, and input–output losses. Establishing an uncertainty analysis methodology for the input–output loss and efficiency measurements in electric motors, frequency converters, and power drive systems.

The topics are discussed in a total of nine scientific publications. Publications I–V and IX focus on the loss and efficiency determination in motor drive systems, while publications VI, VII, and VIII investigate the loss measurement uncertainty.

In Publication I, the losses and efficiency of a converter-fed 15 kW induction motor are investigated over a wide operating range. The measurements are performed with both a frequency converter and a generator supply over a wide operating range between 25% and 100% rated load and between 25% and 100% rated operating frequency of the motor. The behavior of motor loss components with both the generator and converter supply is compared in order to analyze the impacts of the converter supply.

Publication II offers an analysis of the loss segregation methodology that the IEC introduced for converter-fed motors in its technical specification IEC/TS 60034-2-3 (IEC, 2013). The method requires a specifically predefined converter output voltage PWM waveform. A more typical commercial frequency converter is used for comparison. The results of the loss segregation method are also compared with input–output results.

In Publication III, a comparison between a 15 kW induction motor and a 15 kW synchronous reluctance motor is conducted. Both motors are supplied with the same frequency converter in order to compare the losses and efficiency of the motors, the converter, and the drive systems. The measurements are performed over a wide operating range between 10% and 100% motor load and between 10% and 140% rated operating frequency of the motor.

Publication IV presents the efficiency verification measurements of two direct-on-line synchronous reluctance machine (DOL SynRM) prototypes. Measurements are performed using a calorimetric method and the input–output method simultaneously in four operating points. The results of the two methods are compared in detail. The loss and efficiency results of the DOL SynRM prototypes are compared with the performance of corresponding high-efficiency induction motors.

Publication V provides another set of efficiency verification measurements, where a prototype induction motor is tested in three different operating points using the input–output, loss segregation, and calorimetric methods. The results of the three methods are compared in detail. Additionally, in this study, a mass flow meter is incorporated in the calorimetric system to evaluate the calorimetric method used.

In Publication VI, the measurement uncertainty in the input–output loss measurements of frequency converters is analyzed. Measurement data over a wide operating range (25%–100% rated load and 25%–100% rated operating frequency) from three different motor drive systems are used in the analysis. Both type A and type B uncertainty analyses for the electric power measurement and for the calculated losses are addressed in detail. Uncertainty results are presented over the whole operating range.

Publication VII uses the same measurement data as Publication VI, but here the input–output power and loss analyses are performed for each of the three motors. The mechanical power measurement uncertainty and loss uncertainty analyses are presented in detail, and the results are provided for the whole operating range.

Publication VIII applies the analysis methods from Publications VI and VII to evaluate the uncertainty of the measurement instruments available at LUT University. Twelve motors from the same model series representing the power range that could be measured at LUT are considered. The analysis is made using the nameplate data of the motors. The uncertainty caused by the inevitable mismatch of the measurement instrument ratings and the tested devices is analyzed and discussed.

Publication IX evaluates the experimental methods of determination of the frequency converter power losses according to the new standard IEC 61800-9-2. The input–output method and the calorimetric method are used, and the results and the uncertainty of the methods are analyzed. The validity of the efficiency classes and the effect of the measurement uncertainty in the efficiency classification are discussed.

1.8 Scientific contributions of the doctoral dissertation

The research conducted in this doctoral dissertation can be divided into two parts: the loss determination of the devices and the determination of the measurement uncertainty. However, these topics are tightly intertwined. The main scientific contributions are highlighted in the following. As the novelty of the scientific contributions is not necessarily clear in all cases, the background or context of each contribution is explained in brief.

There has been a lively discussion in the scientific community whether the frequency-converter-induced additional losses in the machine depend on load torque or not, and results against and in favor have been presented. An important scientific contribution to this topic is that

- *In extensive laboratory tests with frequency converter and generator supply comparison, it has been verified up to the rated operating point, that the converter-caused additional losses in the motor depend on the load torque and the excitation frequency.* (Publication I).

The measurement uncertainty related to converter-fed machines and pulse-width-modulated power is a controversial topic. It has been shown that

- *In the practical measurement uncertainty analysis of converters and electric machines, the PWM supply can be analyzed using fundamental wave values, and they can be treated in the uncertainty analysis similar to the analysis of a typical sinusoidal supply* (Publication VII).

To the author's knowledge, there has not been a procedure to thoroughly analyze the complete measurement uncertainty of electric motors, frequency converters and power drive systems considering the uncertainty contributors from different origins.

- *A method to determine the overall measurement uncertainty for DOL and PWM motor drives is developed starting from measurement instrument datasheets and resulting in the total expanded measurement uncertainty* (Publications VI and VII).
- *The main uncertainty contributors are demonstrated, and it is shown that it is important to identify all uncertainty sources, as a single high uncertainty contributor can have a significantly deteriorating effect on the overall measurement uncertainty* (Publication VII).

To the author's knowledge, there has not been general guidance available on how the data should be collected from the measurement instruments in the case of electric motor and converter efficiency determination.

- *The number of samples and measurement time needed to achieve an acceptable level of measurement uncertainty are demonstrated* (Publication VI).

Although the international standards are generally well prepared and widely studied, the methods for loss and efficiency determination have room for improvement.

- *The results published in the papers of this study show that there are grounds for criticism of some of the present standard methods*.

The open and balance type calorimeter used in this study has been considered one of the most accurate types of calorimetric systems. However, the method consists of two separate tests, and the impact of changes in air properties between the tests has not been clear.

- *It is shown that humidity and barometric pressure measurements are, after all, not essential for an open and balance type calorimeter* (Publication V).
- *A comprehensive procedure to establish a measurement system has been set up to make compliance measurements possible in general* (Publications at large).

2 Determination of losses and efficiency of high-efficiency devices

A motor-driven system can consist of either a stand-alone direct-on-line (DOL) motor and a load or a frequency converter and a motor (a power drive system), and a load. In this chapter, the methods for determining losses and efficiency of motors, converters, and power drive systems are examined, applied to experimental measurements, analyzed, and criticized. Three methods were used in the measurements: The input–output method was included in all the motor and converter measurements. Loss segregation of induction motors was also used in several measurements. The calorimetric method was applied to only two sets of measurements.

To properly evaluate the methods, the conditions during the measurements of each of the methods have to be kept as similar as possible. This includes avoiding any unnecessary alterations in the test setup. In practice, apart from the calorimetric arrangements, exactly the same test setup can be used with all three methods. There are, however, some differences in the setups between Publications. For instance, motors of different sizes and rated powers were measured in different test beds and in DOL motor tests, some test series were performed using a grid supply, and some with a more stable and configurable generator supply.

In the calorimetric tests, both the input and output power were measured, and the data can also be used in the input–output method to obtain fully comparable results with the two methods. Considering the loss segregation method, the first of the three tests— the rated load test—is, in practice, an input–output test, and the same data can be used for the input–output analysis. However, some nonidealities considering the comparability of the results of the three methods can be found, and they are discussed later in this chapter.

This chapter is arranged as follows: section 2.1 covers DOL motors, section 2.2 converter-fed motors, section 2.3 frequency converters, and section 2.4 power drive systems. All the different methods used in this dissertation were applied to direct-on-line motors, and therefore, the principles of the methods and the measurement procedures are explained in section 2.1. For converter-fed motors, frequency converters, and power drive systems, only the differences with the DOL motor methods are addressed.

2.1 Direct-on-line motors

Direct-on-line motor measurements are included in Publications I, II, IV, and V. In Publication I, the input–output method was used for a 15 kW induction motor driven both with a sinusoidal supply and a frequency converter supply over a wide operating range consisting of 16 test points. In Publication II, both the input–output and loss segregation methods were used for the 15 kW IM with different input voltages. In Publication IV, the input–output method and the calorimetric method were used to perform efficiency verification measurements of two DOL SynRM prototypes. In Publication V, the input–

output, loss segregation, and calorimetric method were used for efficiency verification measurements of a 5.5 kW DOL induction motor. In the measurements of Publication II, grid voltage was used to feed the motor in the DOL tests, while in Publications I, IV, and V, the DOL tests were carried out using a synchronous generator supply to ensure the quality and stability of the supply voltage.

2.1.1 Input–output method

The input–output measurements of DOL electric motors require electric input power measurements, mechanical output power measurements, and a mechanical load for the motor. The measurement setup for DOL motors using the input–output method is illustrated in Figure 2.1. The electric input quantities are measured with a power analyzer, the output power measurement consists of torque and speed measurements, and the motor winding temperature is measured during these measurements in order to ensure that the temperature has stabilized before taking the input–output recordings. In addition, some form of soft starting is needed to avoid overload damages to the measurement instruments. Here, the DOL measurements are performed either by using an adjustable transformer when the DOL motor can be started by slowly increasing the 50 Hz voltage amplitude, or by using a fully adjustable synchronous generator supply where both the frequency and the voltage can be slowly ramped up.

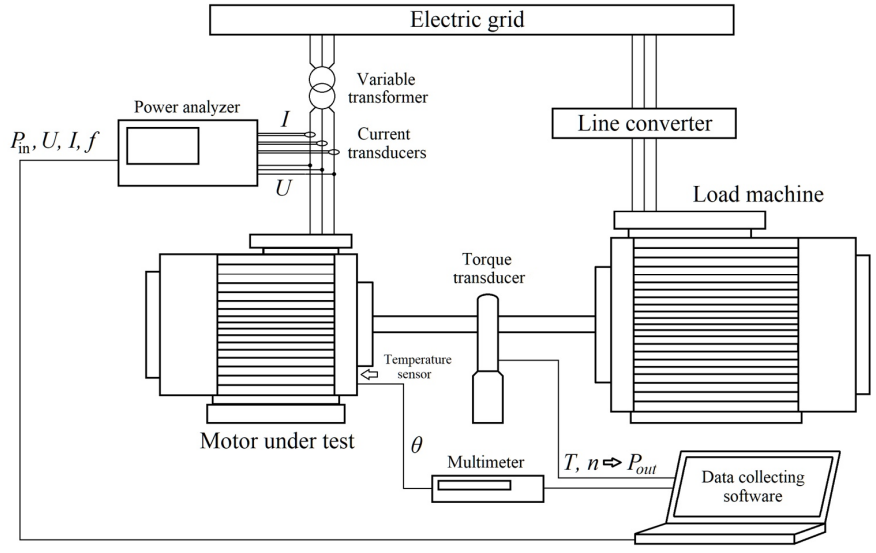

Figure 2.1. Test setup used in the DOL motor input–output measurements. The setup consists of a larger machine acting as a load, electric and mechanical power measurements, and temperature measurement. Instead of the grid supply and the variable transformer shown here, also a generator supply can be used when stable voltage quality is critical.

In the input–output method, the losses and efficiency are calculated from the input power P_{in} and the output power P_{out}. The losses are thus

$$P_{\text{loss}}=P_{\text{in}}-P_{\text{out}}. \tag{2.1}$$

The efficiency is obtained according to the first form of (1.2), that is,

$$\eta=\frac{P_{\text{out}}}{P_{\text{in}}}. \tag{2.2}$$

The basic outline of the input–output method used in Publications is in accordance with (IEC, 2014b), and further details specific to each set of measurements are given in each Publication.

In Publications I, III, VI, and VII, the input–output measurements were made in several operating points, and the data were interpolated and presented over the whole measurement range. This was accomplished in MATLAB by interpolating the data into a much denser matrix over the measurement range. The interpolation procedure is covered in Publications I and III.

2.1.2 Loss segregation

The loss segregation procedure has several variants, but the one used in this dissertation is the current IEC loss segregation method (IEC 60034-2-1 method 2-1-1B). The IEC loss segregation procedure for DOL motors is illustrated in Figure 2.2. As with other loss segregation methods, the different loss components of the motor under test are determined individually using three separate tests: a rated load test, a no-load test, and a load curve test. In the rated load test, the motor is run DOL at its rated load as long as it is needed to reach a stable operating temperature while keeping the ambient temperature constant. After having documented the rated operating point measurement data, the motor is

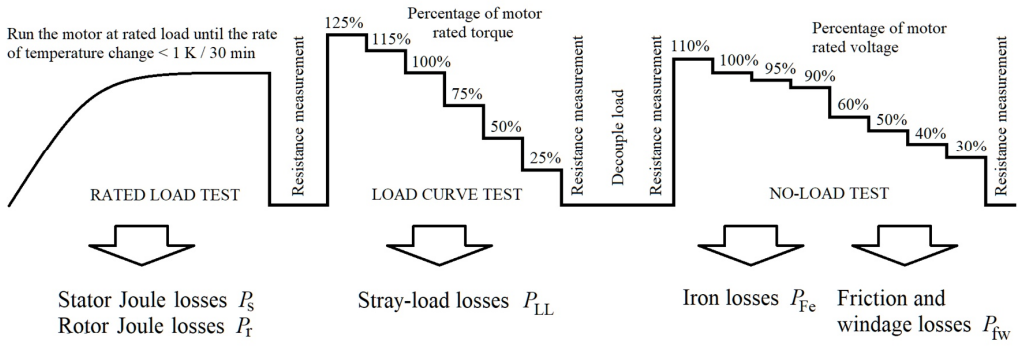

Figure 2.2. Test procedure of the IEC loss segregation method 2-1-1B.

quickly stopped, and resistance measurement is applied to its stator terminals to determine the stator resistance at the operating temperature. The hot motor is then started again for a load curve test and loaded by 125% rated torque. Thereafter, the load torque is, with a swift pace, gradually reduced using the torque values given in the figure. This means that the motor temperature will decrease slightly during the test. Therefore, the test must be performed fast, typically in approximately three minutes using 30 s load points. After the 25% torque test, the motor stator resistance is measured again, and the motor is decoupled from the mechanical load. Thereafter, the no-load test run is started with 110% voltage, then coming down in voltage stepwise according to the values given in Figure 2.2. The test run is ended with a final stator resistance measurement.

The test setup for the loss segregation measurements is shown in Figure 2.3. There are only a few differences from the input–output setup in Figure 2.1: A coolant temperature measurement is needed because the Joule losses are adjusted to the reference coolant temperature of 25°C. A mechanical coupling and support bearings are needed for quick decoupling of the load machine as the IEC loss segregation method requires that the no-load test is performed immediately after the load tests when the motor under test is still hot.

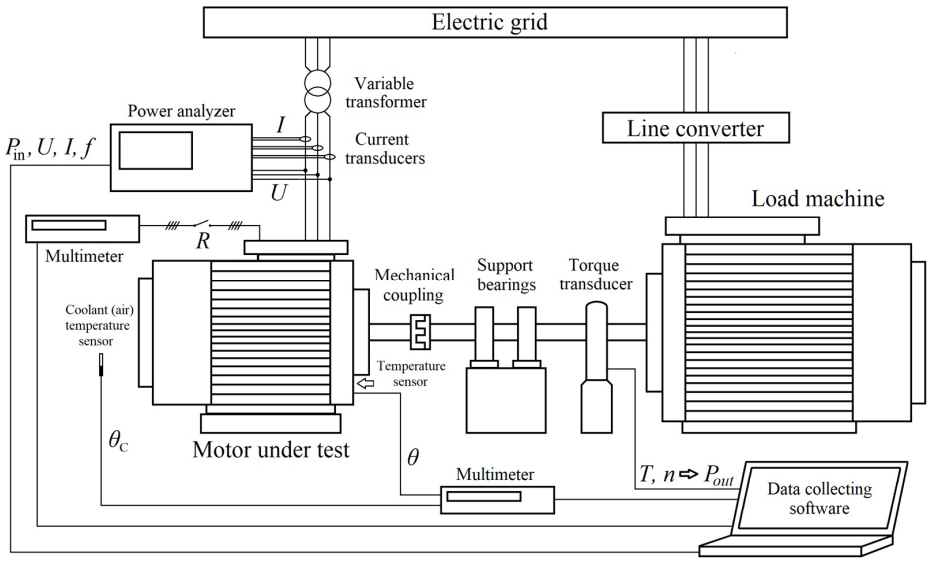

Figure 2.3. Test setup used in the DOL motor loss segregation measurements. Compared with the input–output setup in Figure 2.1, a stator winding resistance measurement and a coolant (here air) temperature measurement are needed in the loss segregation tests. In addition, a mechanical jaw coupling and support bearings are needed for fast detaching of the motor shaft between the tests. The difference from the setup in Fig. 2.1 is that in this case, the motor can be mechanically decoupled to perform the no-load test immediately after the load test. Instead of the grid supply and the variable transformer shown here, also a generator supply can be used when stable voltage quality is critical.

The stator Joule losses P_s are calculated based on the rated load test line current and line-to-line resistance. The IM rotor Joule losses P_r are calculated based on the per-unit slip during the rated load test. The no-load test with different voltage amplitude levels is used to determine the iron losses P_{Fe} and the mechanical losses P_{fw}. The load curve test is used to obtain the additional losses P_{LL}. The total losses of the motor are calculated as the sum of the individual loss components

$$P_{loss}=P_s+P_r+P_{Fe}+P_{fw}+P_{LL}\,, \tag{2.3}$$

and the second form of (1.2) is applied to calculate the efficiency

$$\eta=\frac{P_{in}-P_{loss}}{P_{in}}\,. \tag{2.4}$$

Despite the fact that only the electric power is needed to calculate the efficiency, the rated load test and the load curve test also require mechanical power measurement. Mechanical power measurement is typically regarded as more uncertain than electric power measurement. Altogether, the accuracy of the mechanical power measurement when using the indirect loss segregation method is less important because it is mainly needed for load setting. The torque value is only required in the analysis of the load curve test, where, in fact, only changes in the measured values are used rather than absolute values, and several sources of uncertainty are thus avoided.

2.1.3 **Calorimetric method**

The calorimetric system developed at LUT was used in Publications IV and V. The calorimeter is of an open and balance type, where the test procedure is based on two separate tests: a main test and a balance test. In the main test, the motor under test is running until the thermal stability of the whole system is reached. In the balance test, all other conditions are kept as similar as possible, but the motor as a heat source is replaced with a DC resistor that is used to replicate the motor heat output. The motor loss amount can be accurately determined from the resistor power measurement. The balance test practically equals calibrating the calorimetric system for the motor heat output in each measurement using a known heat power (DC resistor loss), which is one of the reasons for the very high accuracy of this specific calorimeter type.

The basic structure of the calorimetric system is shown in Figure 2.4. In principle, the setup is similar to the one used for loss segregation tests (Figure 2.3) with the calorimetric equipment added. The calorimetric method requires a chamber, an air exchange blower, an adjustable resistor, barometric pressure and humidity sensors, and several temperature sensors. In addition, for efficiency determination and load adjustment, either input or output power measurement is required—although in the measurements at LUT both the electric and mechanical power are measured. The calorimetric method is explained in detail in Publication IV.

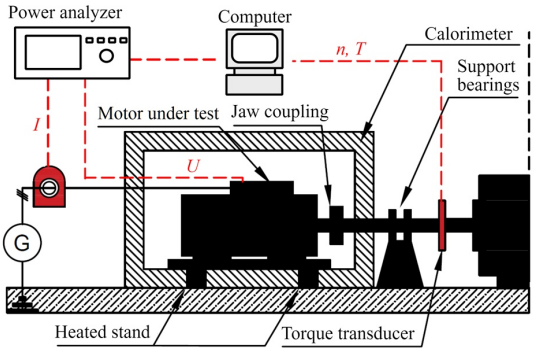

Figure 2.4. Test setup in the DOL motor calorimetric measurements.

The open and balance type calorimetric method is reliable and, in principle, easy to arrange, but the analysis procedure taking into account changes in the air properties is complicated to perform and verify. Largely, the reliability of the method arises from the excessive number of measured variables: the numerous temperature sensors immediately indicate any faults in the system, and measurements performed during drastic changes in weather conditions that could compromise the accuracy can be identified from air pressure and humidity measurements. The changes in barometric pressure and humidity are taken into account in the analysis, and moderate changes in weather conditions are well manageable. However, drastic changes in air conditions (weather) during measurements either require prolonging the measurement to ensure thermal equilibrium, or if the difference between the main test and the balance test is significant, it is preferable to repeat the test point when the conditions are more stable. The effect of corrections in the calorimetric analysis based on air properties is analyzed in Publication V.

There are several benefits when the calorimetric method is applied; it is independent of the power factor, the measurement bandwidth, and other factors affecting the electric or mechanical power measurement accuracy. The loss result itself is completely independent of electric or mechanical power measurements. The main disadvantages are the complexity of the final analysis and an extremely long measurement time. The analysis procedure can, however, be almost fully automated, but the measurement time for a single operating point with the open and balance type calorimeter is roughly 10 to 20 h depending on the device being tested. In the motor measurement, some nonidealities in the system also have to be accepted: The motor shaft requires a hole in the calorimetric chamber, which, however, is sealed with a labyrinth seal (Gamal Eldin, 2007) to minimize the air leakage through the shaft opening. In addition, some heat also leaks by conduction in the shaft, although this is also largely prevented by the insulated jaw coupling. In addition, to keep the air circulation during the main test and the balance test similar, the motor is rotated by the load machine during the balance test. This causes mechanical losses in the motor, and thus, these losses have to be taken into account by determining them by other means. In this study, the mechanical losses were determined by performing

a retardation test afterwards with the motor heated to the same temperature as in the balance test. The retardation test procedure is described in Publication VI.

2.1.4 Direct-on-line motor loss and efficiency results and analysis

Direct-on-line motor measurements were performed and analyzed in Publications I, II, IV, and V. Publications I and II apply the principles of the loss segregation and input–output methods, but the focus of these papers is on comparisons of the motor loss and efficiency results between a sinusoidal supply and a frequency converter supply. Therefore, the main results of these publications are discussed in the context of converter-fed motors in section 2.2. Publications IV and V present the efficiency verification measurements for two DOL SynRM prototypes and an IM prototype, respectively. In Publications IV and V, a variety of test methods were used: The DOL SynRM prototypes were tested in four operating points using the calorimetric method and the input–output method concurrently. The IM prototype was tested in three operating points using concurrent calorimetric and input–output tests, and additionally, the IEC loss segregation method was applied.

In Publication I, the measurements were made using a 16-point matrix measurement and analysis procedure, which is briefly covered in section 2.2.1 and in more detail in Publication I. The matrix measurement results with a generator supply illustrate well the behavior of the IM losses and efficiency over a wide operating range, Figure 2.5. The efficiency of the tested 15 kW IM at its rated operating frequency is optimal at around 70%. At lower operating frequencies or partial speeds, the efficiency is highest at a slightly lower load percentage. The losses naturally increase as a function of both load and operating frequency, as some of the loss components are more load dependent and some are more frequency (or speed) dependent. For more detailed information, the 15 kW IM loss components are presented as similar contour plots in Publication I.

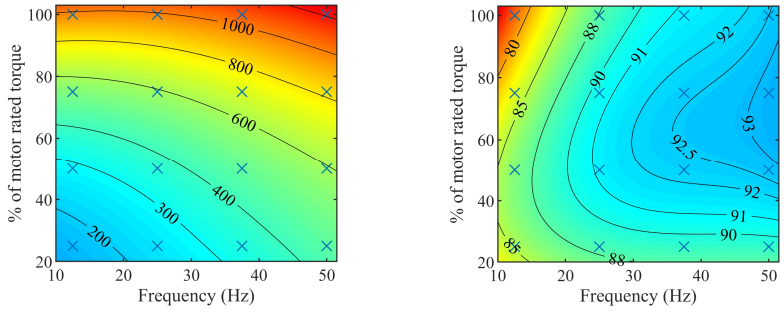

(a) (b)

Figure 2.5. Total losses (a) in watts (W) and efficiency (b) as a percentage (%) of a 15 kW IE3 induction motor with a nearly sinusoidal generator supply over the operating range between 20% and 103% of the rated torque and frequency. The 16 measurement points are indicated in the plots.

The calorimetric loss results and the input–output loss results from the DOL SynRM measurements of Publication IV are compared in Figure 2.6. Considering that the methods are completely independent, the results are extremely close showing that the input–output method can give very good results when the test bench is carefully built and the torque measurement calibrated. Here, the torque measurement was calibrated by detaching the shaft from the machine under test and rotating the detached shaft using the load machine at each of the speeds tested in order to determine the combined value for the torque measurement offset error and the torque needed to overcome the friction of the support bearings.

In Figure 2.7, the efficiency results of the two DOL SynRM prototypes are compared with their closest IM counterparts. The four-pole DOL SynRM is compared with two different IMs. At 45 kW, the four-pole DOL SynRM is comparable with an IM with a larger frame size, while an IM with a similar frame size is rated for 37 kW. Consequently, both 45 kW and 37 kW were among the operating points included in the DOL SynRM tests. The comparison in Figure 2.7 clearly shows that these prototypes have one percent efficiency advantage over a similar-sized IM. At 45 kW, the four-pole DOL SynRM is slightly more efficient than its physically larger 45 kW IM counterpart. Furthermore, it is shown in Publication IV by comparing the four-pole IM and DOL SynRM at 37 kW that their efficiency difference can be explained almost completely by the absence of the rotor losses in the SynRM when also the power factor difference is taken into account. The higher power factor of the IM somewhat compensates for the rotor losses as the IM stator current, and consequently the stator Joule losses, are lower. Hence, the difference in total losses between a comparable IM and a SynRM is somewhat lower than the IM rotor loss.

The two-pole induction motor analyzed in Publication V was tested in the load points of 5.5 kW and 7.5 kW at 50 Hz (3000 min^{-1}), and 6.3 kW at 60 Hz (3600 min^{-1}). The

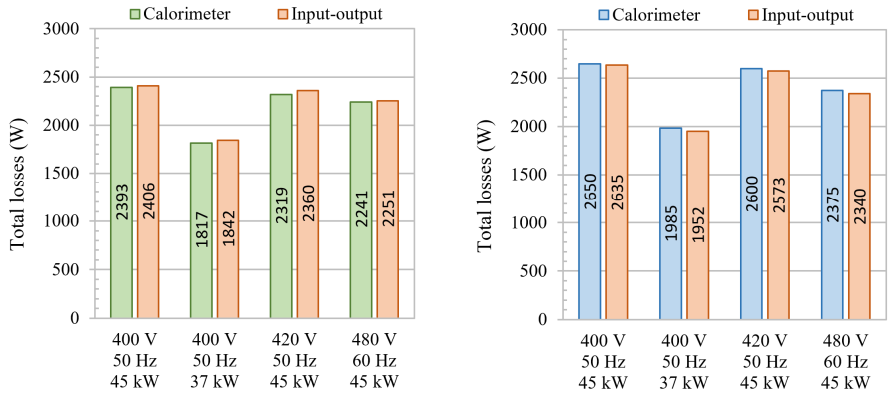

Figure 2.6. Losses of 2-pole (a) and 4-pole (b) DOL SynRM prototypes determined with the calorimetric method and the input–output method. The loss values are corrected to the reference coolant temperature of 25°C (ambient air temperature).

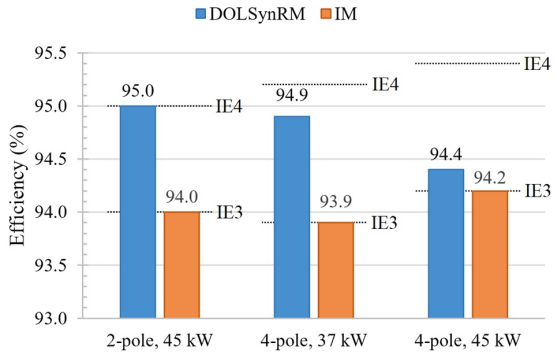

Figure 2.7. Comparison of the efficiencies of the DOL SynRMs and their IM counterparts. The 4-pole DOL SynRM is compared with an IM having the same power rating but a larger frame size, and also with a 37 kW IM, which, in turn, has the same frame size.

efficiency results obtained with the three different methods are presented in Figure 2.8. The values in Figure 2.8 are slightly different from the values presented in the corresponding figure of Publication V, as here the calorimetric loss results are corrected to the reference coolant temperature of 25°C to correspond the IEC loss segregation results, which are also corrected to 25°C. The air temperature inside the calorimetric chamber was close to 40°C, and the temperature correction improved the calorimetric result by 0.3–0.4 %-units. The IEC loss segregation results and the calorimetric results were similar in all three test points, while the input–output results were consistently lower. A clear reason for this discrepancy was found after the paper was published: there was a mechanical fault on the test bench that caused significant vibrations at 3000 min^{-1} and 3600 min^{-1}. Vibration causes inaccuracy in the torque measurement, which affects

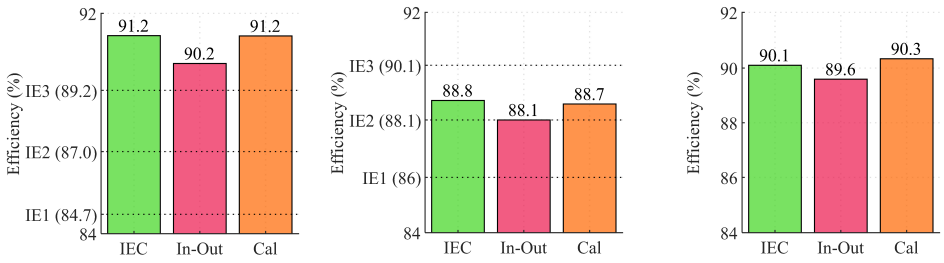

(a) 5.5 kW/50 Hz (b) 7.5 kW/50 Hz (c) 6.3 kW/60 Hz

Figure 2.8. Efficiencies of the induction prototype measured using the IEC loss segregation method (IEC), the input–output method (In-Out), and the calorimetric method (Cal) in the operating points of 5.5 kW/50 Hz (a), 7.5 kW/50 Hz (b), and 6.3 kW/60 Hz (c). The limits for the IE1, IE2, and IE3 efficiency classes are included for the operating points of 5.5 kW and 7.5 kW. The third operating point of 6.3 kW/60 Hz is not an official IEC power class, and thus, no limits exist. The input–output results are erroneous in this very case because of a fault in the measurement system.

especially the input-output results and, to a significantly lesser extent, the loss segregation results. The fault was not found earlier as the test bench is normally used only up to 1800 min^{-1}, and some vibrations were to be expected at higher speeds. However, the fault was found partly because of the discrepancy of these results, which underlines the benefit of using different methods when possible. Furthermore, the good match of the loss segregation and calorimetric results can be interpreted as an example of the relatively high error resilience of the loss segregation method.

In the calorimetric tests of Publication V, mass flow measurement was used to analyze the open and balance type calorimetric method. The open and balance type method is based on replicating the DUT heat dissipation in the main test with a reliably measurable DC resistor during the balance test. In the main test, the input and output air temperatures and the speed of the outlet blower are fixed, and therefore, changes in the barometric pressure p and the relative humidity φ between the main test and the balance test affect the results. In the calorimetric tests at LUT, p and φ were measured during the tests and were taken into account in the final analysis. Using the direct mass flow measurement, the validity of the indirect mass flow corrections based on p and φ was analyzed. The results showed that the corrections based on p and φ and the real mass flow were inconsistent but negligible, and the results would have been just as usable without the corrections. These results indicate that the p and φ measurements are not crucial for the analysis of the open and balance type calorimetric method, but there has to be a means to verify that there are no drastic changes in the air properties (weather) between the main test and the balance test. Further analysis is needed, but for instance local weather data could be used, and in case of significant changes in weather, the test point should be repeated in more stable conditions.

The analysis of the mass flow measurement revealed that the insulating properties of the calorimetric chamber had changed after the initial determination of the chamber wall heat transfer coefficient. This is probably due to numerous changes in the setup and possibly also the wear of gaskets over time. However, despite the inaccurate coefficient, the effect on the results was very small, which indicates the error tolerance of this calorimeter method. Of course, also here, relatively stable weather conditions significantly contribute to the situation, and if the air characteristics had changed more between the main test and the balance test, the result would also have been less accurate. However, the transmission coefficient is easily measurable even without a mass flow measurement, and thus, similar situations can be avoided by including the transmission coefficient test in the measurement set whenever the setup changes.

2.2 Converter-fed motors

Loss and efficiency measurements involving motors supplied with a frequency converter were performed and analyzed in Publications I, II, III, and VII. In Publication I, the input–output method was used for comparing the losses and efficiency of a 15 kW IM when supplied with a frequency converter and with a synchronous generator in matching

operating points over a wide operating range. In Publication II, a modification of the loss segregation method proposed for converter-fed motors was analyzed and the results were compared with the input–output results. Publication III presents a comparison between a similarly sized and rated 15 kW SynRM and IM with a frequency converter supply over a wide operating range. Publication VII focuses on the uncertainty of the input–output method in converter-fed motor measurements, and the results are therefore discussed in Chapter 3.

The methods used for loss and efficiency determination of converter-fed motors are the input–output method and the calorimetric method, and for induction motors, a variation of the loss segregation method can be applied. The traditional loss segregation method is not directly applicable to converter-fed motors, but different variations for converter-fed IMs have been introduced (IEC, 2013), (IEC, 2020).

2.2.1 Input–output method and calorimetric method

In the case of converter-fed motors, the input–output method and the calorimetric method can be applied similarly as in the case of DOL motors (see section 2.1). When testing converter-fed motors, the bandwidth of the electric power measurement devices must be higher than with a sinusoidal supply, as accurate results also require measuring the high-frequency harmonic power induced by the frequency converter. For motor measurements, recording the input electric power of the motor would suffice. However, in the converter-fed motor measurements at LUT, the input power of the frequency converter is always measured at the same time as the input power of the motor. Therefore, another power analyzer—or alternatively a power analyzer with six or more channels—is needed before the frequency converter, as shown in Figure 2.9. A variable transformer is not compulsory, but experience has shown that the grid voltage is not necessarily stable enough to obtain properly comparable results without the ability to adjust the voltage.

In Publications I and III, the measurements were made using the input–output method in several operating points, and the test data were interpolated over the whole test range using MATLAB. The interpolation procedure is similar in both publications: The data from the test points are interpolated to a fixed and a lot more dense matrix of reference points, which allows making calculations and comparisons between tests and machines, and presenting the data in smooth maps. The test procedures of Publications I and III, however, are different in several ways. The 16 data points used in Publication I covered the operating range between 25% and 100% motor load and operating frequency, while in Publication III, there were 48 operating points with the SynRM and 49 operating points with the IM, and the load spanned from 10% to 100% and the operating frequency from 10% to 140%. In addition, the tests points were run differently. In Publication I, all the test points were applied until a sufficient thermal equilibrium was reached, while in Publication III, the load changes were applied at short intervals, and only after each frequency change there was a 30 min settling time. Before starting the matrix measurements, the motors were run into thermal equilibrium in all the test series of Publications I and III. The test procedures are described in more detail in the publications.

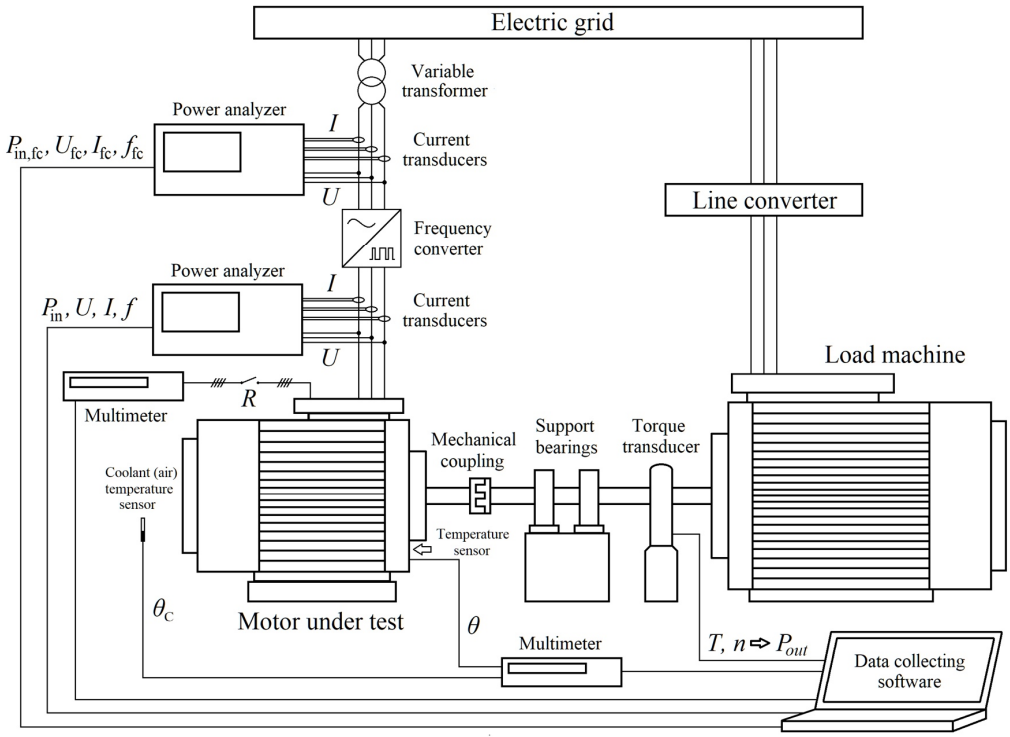

Figure 2.9. Test setup used in the measurements of converter-fed motors, frequency converters, and complete power drive systems. Compared with the loss segregation setup in Figure 2.3, another power analyzer is needed to measure the converter input in the frequency converter and drive system measurements.

The purposes of the matrix measurements in Publications I and III were different. In Publication I, the 16-point matrix measurement was performed first with a frequency converter supply and after that with a generator supply. The operating frequency (fundamental frequency), the fundamental voltage, and the load torque were carefully adjusted in the generator measurements to match the frequency converter test values. The main purpose here was to determine the converter-caused loss increase as a difference between the frequency converter results and the generator measurement results. In Publication III, in turn, the measurements were performed using the same frequency converter that can be used with both an IM and a SynRM in order to analyze the differences in the IM and SynRM performance. In the IM and SynRM comparison measurements, the test points had some differences because the operation of the two motor technologies is different. Matching the operating points (the fundamental operating frequency and the load torque) was therefore performed as part of the interpolation procedure to achieve comparable results.

2.2.2 Loss segregation methods for converter-fed motors

Possibilities for extending the loss segregation methodology to converter-fed motors have been considered by the IEC in the development of the standard 60034-2-3, which is the first international standard to define loss and efficiency determination methods for converter-fed motors.

The first release of 60034-2-3 (IEC, 2013) was a technical specification (IEC/TS) instead of a final standard. The main method of the technical specification is a variation of the loss segregation method suited for converter-fed motors. The method consists of five separate tests, Figure 2.10. As the figure illustrates, the method includes the complete loss segregation procedure with a sinusoidal supply (according to the IEC method 2-1-1B, see section 2.1.2). With the frequency converter supply, a second load curve test is made in the exact same manner as with the sinusoidal supply, and a no-load test is performed at the rated voltage and frequency of the motor. The principal idea in the IEC/TS main method is that the converter-caused additional harmonic losses in the motor consist of a constant component that is measurable as the difference between the no-load results with a frequency converter supply and a sinusoidal supply, and a load-dependent component that can be determined based on the additional load loss difference, when additional load losses are determined separately with the sinusoidal supply and with the frequency converter supply. The method sets strict requirements for the tests including the converter PWM waveform, which is not producible with all commercial frequency converters and thus limits the usability of the method. The IEC/TS loss segregation method is thoroughly analyzed in Publication II.

The IEC/TS variation of loss segregation did not end up in the final standard when it was released in 2020 (IEC, 2020). Instead, the main method in the standard is the input–output method. A loss segregation method is included in the final standard, but it is somewhat

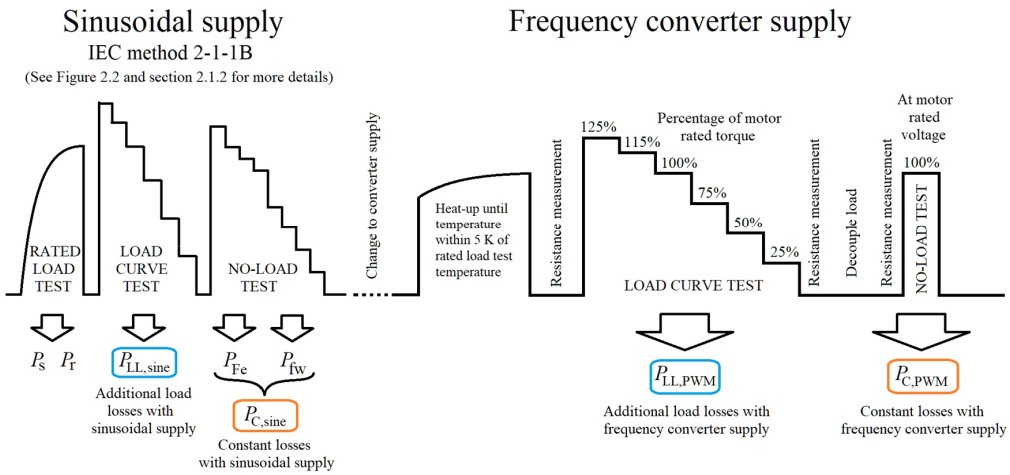

Figure 2.10. Test procedure of the IEC/TS 60034-2-3:2013 loss segregation method.

simplified from the IEC/TS method, and the standard also acknowledges that the method is suitable rather for final application testing purposes than for efficiency classification.

2.2.3 Converter-fed motor loss and efficiency results and analysis

The loss segregation method for converter-fed IMs defined in the IEC/TS (IEC, 2013) was applied for a 15 kW IM in Publication II. The results from the main loss segregation method 2-3-A are compared with the input–output results in Figure 2.11. The input–output results in Figure 2.11 were obtained with the "test converter" required for the IEC/TS method and with a commercial frequency converter employing direct torque control (DTC), which produces a very different PWM voltage waveform compared with the test converter. The term "test converter" refers to the very specific PWM waveform required by the IEC/TS method. All three results of the total losses with the frequency converter supply are practically the same. This is, however, partially an artificial result, because the method requires the rated fundamental voltage for the motor, which for the DOL-rated motor under study is 400 V, 50 Hz. Normally, when a DOL-rated motor is supplied with a frequency converter at the rated frequency of the motor, the fundamental voltage is less than the rated motor voltage, and the motor losses are higher. In addition, the input voltages of the test converter and the DTC converter were different. The IEC/TS method requires that the input voltage has to be just enough to produce the rated fundamental voltage of the motor, and the same rule was applied to the input–output measurements. Here, the test converter required 460 V, while 433 V was sufficient for

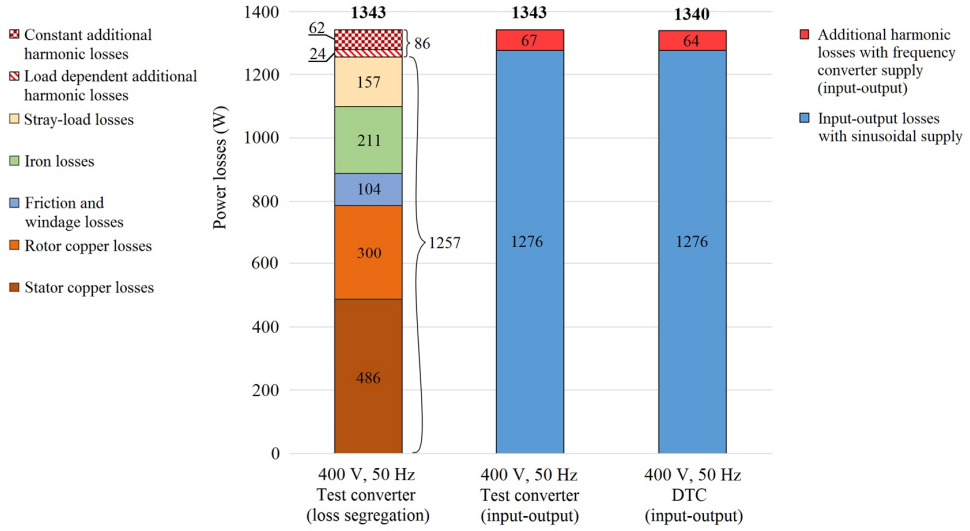

Figure 2.11. Results from the IEC/TS 60034-2-3:2013 loss segregation method compared with the input–output results with the same converter (IEC-defined test converter) and another commercial frequency converter. Switching frequency of the test converter was 4 kHz and the average switching frequency of the DTC converter was 1.5 kHz.

the DTC converter to achieve the rated fundamental voltage (400 V, 50 Hz) for the motor. In addition, Figure 2.11 includes the input–output losses with a sinusoidal supply, and the additional converter-caused loss increase calculated as the difference from the PWM supply results. The sinusoidal supply results and thereby the converter-caused losses are also similar in all the three cases.

The results of Publication II showed that the IEC/TS loss segregation method itself is usable for determining converter-fed motor losses when all the very specific requirements of the method 2-3-A are met. However, the requirements of the method also limit its usability: The strictly defined "test converter" waveform and the requirement for the rated fundamental operating voltage of a converter motor at its rated operating point mean that the results do not represent the motor losses in any practical operation of a converter-fed induction motor. In addition, the method and its analysis are complicated as the method adds two more tests to the already quite complicated DOL motor loss segregation.

In Publication I, the 15 kW IM losses with a frequency converter supply were compared with its losses with a generator supply. The total losses with the frequency converter supply are presented in Figure 2.12a, while Figure 2.12b shows the loss difference—or the converter-caused loss increase. In plot c, the converter-caused loss increase is given as a percentage of the losses with the generator supply. The results show that the converter-caused loss increase is dependent on both the load and operating frequency. The load dependence of additional harmonic losses has been a topic of much discussion in recent years and this result sheds some light on this matter. Here, however, the loss difference is not purely the additional harmonic loss, as the total loss value contains the increased stator and rotor Joule losses caused by the higher temperature of the motor with the frequency converter supply. The total increase caused by the temperature rise, however, was only a few watts at most, which is presented in Publication I by comparing the Joule losses between the converter supply and the generator supply. The choice of using the actual total losses rather than temperature-matched losses was made in

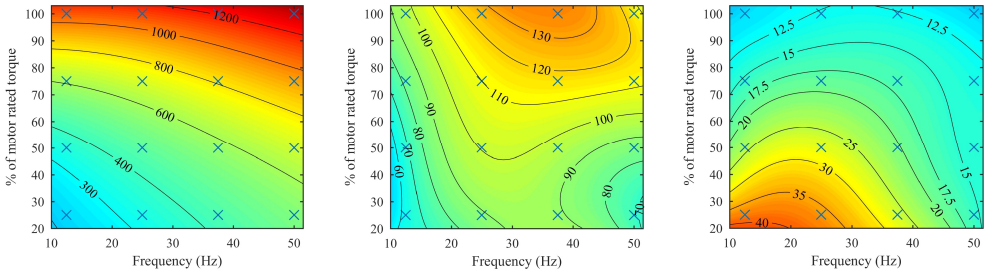

(a) Total losses with converter supply (W)

(b) Converter-caused loss increase (W)

(c) Converter-caused loss increase (%)

Figure 2.12. 15 kW IM losses with the frequency converter supply in watts (a), the converter-caused loss increase compared with the generator supply in watts (b), and as a percentage (c). 15 kW IM losses with the generator supply are presented in Figure 2.5a. The converter switching frequency was 4 kHz.

Publication I to give a practical overview of the losses caused by the frequency converter. In fact, quite a few choices had to be made to enable comparison: All efficiency optimizations were disabled from the frequency converter, and the converter input voltage was increased high enough to avoid field weakening and overmodulation up to 50 Hz. In addition, the modulation method used was classic space vector modulation without any modifications, and the actual resultant switching frequency was confirmed by postprocessing the recorded waveform data to stay at 4 kHz in all 16 test points. All these choices were made to achieve results where only the interaction of the motor and the converter affects the motor losses without any optimizations or limitations over the operating range in the tests. Naturally, a similar comparison made with all the optimizations activated and applying a manufacturer-specific modulation method with the converter input voltage limited to the grid voltage would be an interesting topic, but such an arrangement was outside the scope of Publication I and this dissertation. To properly analyze motor losses in a real-usage situation, a variety of frequency converters from different manufacturers would have to be used to get an overview of such results, as the efficiency optimizations, modulation techniques, and field weakening and overmodulation behavior tend to be manufacturer-specific.

Figure 2.13 illustrates the 15 kW IM efficiency with the frequency converter supply (a) and the efficiency difference compared with the sinusoidal supply (b). The efficiency decreases the least at the rated operating point and the most in the low load and speed range. This behavior is natural, because the converter-caused loss increase is far less load and operating frequency dependent than the other motor loss components, and therefore, the proportion of the converter-caused loss share is higher when the total losses are lower (this can be seen also in Figure 2.12).

In Figure 2.14, the efficiency comparisons between the induction motor and the synchronous reluctance motor from Publication III are presented. Overall, the SynRM efficiency is higher over the whole measurement range. In the rated operating point, the

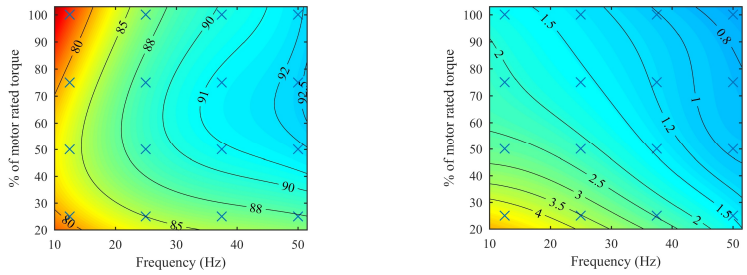

(a) Efficiency with converter supply (%) (b) Efficiency reduction (%-units)

Figure 2.13. 15 kW IM efficiency with the frequency converter supply (a) and the converter-caused decrease in the motor efficiency compared with the generator supply (b). The 15 kW IM efficiency with the generator supply is presented in Figure 2.5b. The converter switching frequency was 4 kHz.

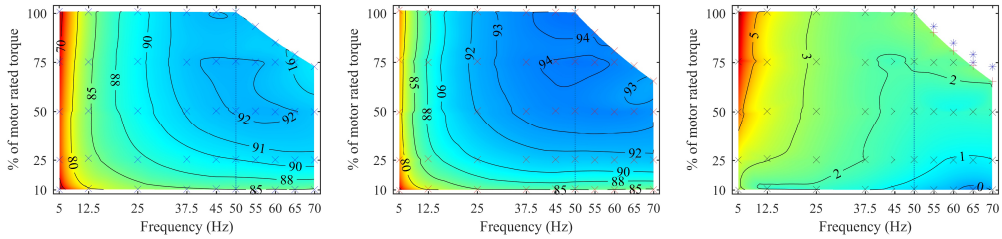

(a) Induction motor efficiency (%)

(b) SynRM efficiency (%)

(c) Motor efficiency difference (%-units)

Figure 2.14. Efficiencies of a 15 kW IM (a) and a 15 kW SynRM (b) supplied with the same frequency converter, and the difference in the motor efficiencies (c). The converter switching frequency was automatically adjusted by the converter control system and the exact value is not available.

SynRM has more than 2% higher efficiency, but there are also clear differences in the distribution of the efficiency of the two tested motors over the operating range. The highest efficiency values for the SynRM are around the rated frequency (45 Hz–55 Hz) and at quite high load values of 60% to 100% of the rated load. For the IM, the highest efficiency values are over a similar frequency range between 45 Hz and 60 Hz, but in a lower load range between 40% and 80% of the rated load. The efficiency difference is highest at very low operating frequencies with high load values, where the SynRM efficiency is more than 5%-units higher. In the high operating speeds with a very low load, the efficiency difference is reduced to zero. Both the different optimal efficiency ranges and the distribution of the efficiency difference are largely due to the rotor Joule losses of the IM. The rotor Joule losses are load dependent but not operating frequency dependent, and therefore, the proportion of the rotor Joule losses of the total losses behaves similarly to the efficiency difference in Figure 2.14c.

2.3 Frequency converters

The losses and efficiency of frequency converters are among the topics of Publications III, VI, and IX. In Publication III, the same frequency converter was used with an IM and a SynRM, and the difference in the converter losses when using different motors was analyzed. Publication VI focused on the measurement uncertainty in frequency converter loss measurements, but also the input–output losses for three frequency converters with different current ratings were presented. In Publication IX, the recently released standard IEC 61800-9-2 (IEC, 2017) was analyzed.

In the frequency converter measurements, the methods used are the input–output method and the calorimetric method. These are the only two practical methods for frequency converter loss and efficiency determination with tests, and they are consequently defined as standard test methods in the standard IEC 61800-9-2. The input–output measurements in the case of frequency converters only require accurate electric power measurements from both the input and output sides. The load in the frequency converter measurements

does not necessarily need to be a motor, and only some electrical requirements are given for the loading in the standard (IEC, 2017). In practice, however, the load of the converter in the tests performed at LUT is always a motor, as the motor measurements are usually made at the same time. Therefore, the full measurement setup in the frequency converter measurements is the same as in the converter-fed motor measurements, Figure 2.9.

The calorimetric tests are, in fact, easier to arrange for converters than for motors, which is an obvious reason why the calorimetric method is included as a standard method in the standard IEC 61800-9-2. Motors have to be loaded mechanically from outside the calorimetric chamber via a rotating shaft, which requires a hole in the chamber wall. Although the shaft opening is carefully sealed, the input and output power of the frequency converter are simply transferred by cables and do not need any insulation-compromising openings in the chamber.

The standard IEC 61800-9-2 (IEC, 2017) defines eight reference points with the purpose of giving a good overview of the loss and efficiency results in different applications, Figure 2.15. Points 1, 4, and 7 can be used to illustrate losses with quadratic loads, such as centrifugal blowers or pumps, and points 1, 2, and 3 show the loss behavior in constant load applications, such as conveyer belts or hoisting machines.

In Publication IX, the input–output and calorimetric measurements were made for a 160 kW (200 kVA) frequency converter. The input–output measurements were conducted in a total of ten test points, which include the eight standardized test points from Figure 2.15. The calorimetric measurements were made simultaneously in five test points, which included four of the standard test points (points 1, 2, 5, and 7). The results

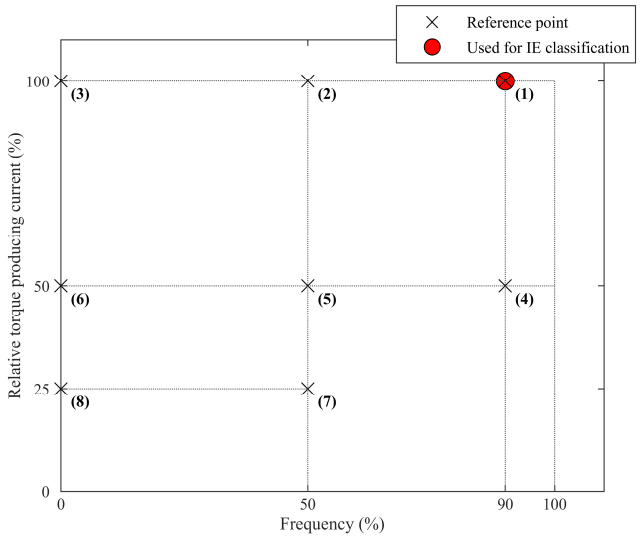

Figure 2.15. Frequency converter (Complete Drive Module) measurement points according to IEC 61800-9-2. Efficiency classification (IE-class) is based on measurement point (1).

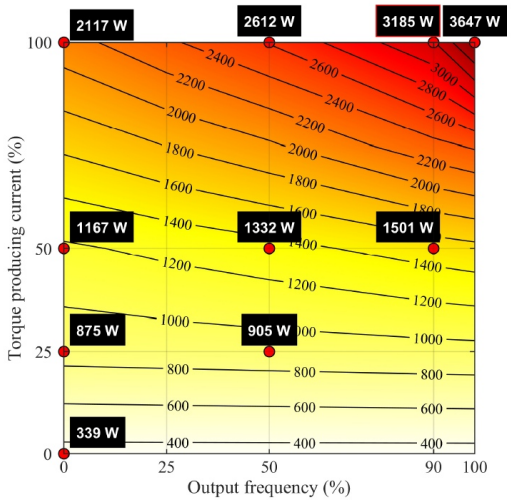

Figure 2.16. Input–output loss results for the 160 kW frequency converter in ten test points. The switching frequency was 2 kHz as specified in IEC 61800-9-2 (IEC, 2017) for converters with rated power higher than 90 kW.

from the input–output method are presented in Figure 2.16. As described already in section 1.4.1, the converter losses increase as a function of both current and operating frequency. The steep increase above 45 Hz output frequency is a result of overmodulation and the increased harmonic content of the produced voltage. In the low torque range, information about the output frequency dependence of the losses is probably lost in the interpolation process because there are no test points except for the 0%/0% point. The ventilation of the converter was kept constant, and the ventilation losses were 270 W. Hence, the converter losses in the 0%/0% point are dominated by the ventilation losses, and the control electronics power consumption is therefore only 69 W. The converter efficiency in both the rated point and the classification point was 97.9%.

The calorimetric loss results for the 160 kW frequency converter are compared with the input–output results in Table 2.1. The calorimetric loss results are higher in all five points. However, the uncertainty of the input–output method was determined in Publication IX, and the difference of the loss results fits within the uncertainty margin of the input–output method.

Figure 2.17 shows the input–output results and the calorimetric results, and the measurement uncertainty in the classification point (point 1). IEC 61800-9-2 requires the loss measurement uncertainty to be added on top of the loss results, and the total value shall be used in the efficiency classification. The figure shows that although the initially lower input–output losses become higher when defining the IE classification, the resulting classification is not affected, and according to both methods, the converter meets the

Table 2.1. 160 kW frequency converter loss results obtained with the calorimetric method. The simultaneously obtained input–output results are included for comparison.

	Measurement point				
Quantity	**0**	**1**	**2**	**5**	**7**
Output frequency (% of rated value)	100%	90%	50%	50%	50%
Torque-producing current (% of rated value)	100%	100%	100%	50%	25%
Calorimetric losses (W)	3964	3405	2907	1527	997
Input–output losses (W)	3647	3185	2612	1332	905
Difference in the loss results	8%	6%	10%	13%	9%

requirements of the currently highest IE2 class. The results are less than half of the IE2 limit, which would indicate that there is a need to revise the class or to introduce higher IE efficiency classes in the future editions of the standard.

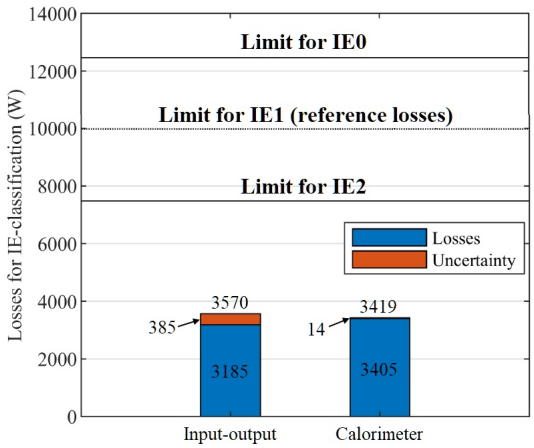

Figure 2.17. Losses of the 160 kW frequency converter obtained with the input–output method and the calorimetric method. The loss uncertainties are added on top of the determined losses. The reference losses (IE1 class limit) for the 200 kVA (160 kW) converter and the limits for the IE0 and IE2 efficiency classes are included in the figure.

2.4 Power drive systems

The methods suitable for the loss and efficiency determination of power drive systems are, naturally, the same as for motors and converters. The drive system losses and efficiency can be determined separately for the motor and the converter using suitable methods and then combined to represent the whole drive system. Alternatively, the losses

and efficiency can be determined directly for the drive system. When using the input–output method, this means simply that the input power is the electric input power of the frequency converter and the output power is the mechanical output power of the motor. Therefore, the losses and efficiency are calculated by (2.1) and (2.2), respectively. When using the calorimetric method, on the other hand, the motor and the converter can be measured either in separate chambers or both inside the same chamber (Aarniovuori, et al., 2016b).

As previously mentioned, the complete power drive system input-output data are recorded, in practice, in all the frequency converter measurements and converter-fed motor measurements at LUT. However, the losses and efficiency were analyzed in the drive system level only in Publication III, where the efficiency difference between the IM and SynRM drive systems was presented and the IES efficiency classes were determined for both drive systems. A loss and efficiency analysis for five different drive system measurements performed at LUT was presented in (Aarniovuori, et al., 2019), where the measurements were made using the same 75 kW IM supplied with five frequency converters from different manufacturers. The measurements were performed in a total of 30 operating points with each of the converters, and the results were interpolated over the test range. The loss results with one of the frequency converters are presented in Figure 2.18 and the corresponding efficiency results in Figure 2.19. The behavior of the converter, motor, and drive system losses is quite similar. The motor losses are more dependent on the operating frequency than the converter losses. The motor losses are around 50% higher than the converter losses in the low frequency and torque range and more than 100% higher in the high frequency and torque range. As the motor losses are higher than the converter losses, the loss distribution of the drive system is more similar to the motor loss distribution.

As the loss distributions of the converter, the motor, and the complete power drive system were similar, the same applies naturally to the efficiencies. Although the losses are highest in the high torque and frequency range, the highest efficiency values can also be found in

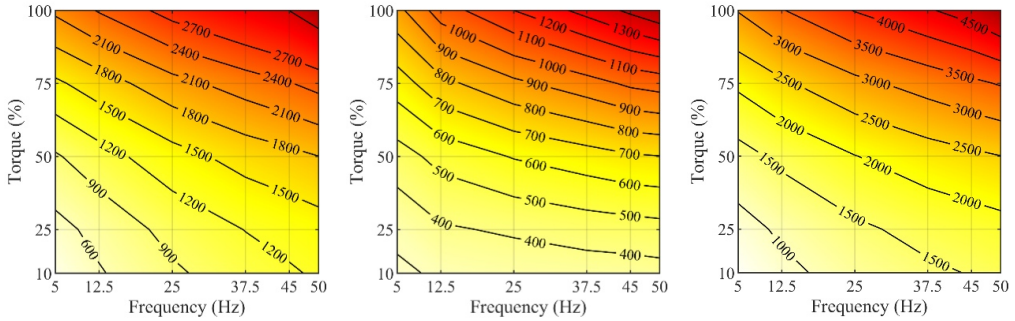

(a) Motor losses (W) (b) Converter losses (W) (c) Drive system losses (W)

Figure 2.18. Losses of the frequency converter (a), the motor (b), and the power drive system (c) in a 75 kW induction motor drive system. The converter switching frequency was 2.66 kHz.

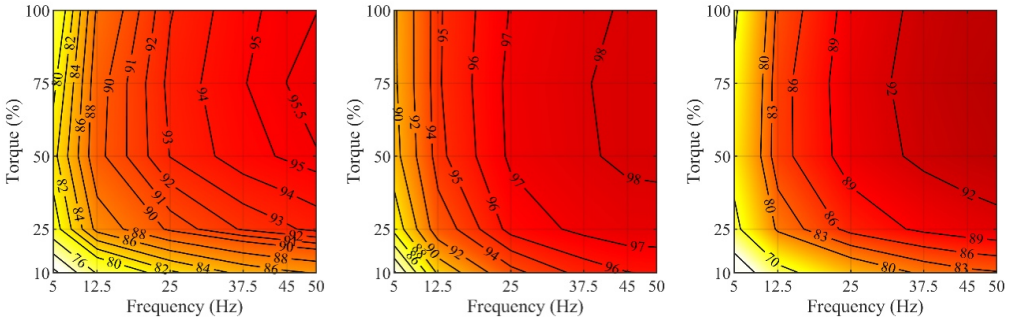

(a) Motor efficiency (%) (b) Converter efficiency (%) (c) Drive system efficiency (%)

Figure 2.19. Efficiencies of the frequency converter (a), the motor (b), and the power drive system (c) in a 75 kW induction motor drive system. The converter switching frequency was 2.66 kHz.

the same range as the proportion of the constant losses in both the motor and the converter becomes less significant when the load and the frequency increase.

The choice of the frequency converter can have a significant effect on the motor losses, or vice versa. In Publication III, the same converter was used with the IM and the SynRM. Although the SynRM losses and thereby the motor power consumption were lower, the frequency converter losses were higher when it was supplying the SynRM. This is due to the lower power factor of the SynRM compared with the IM, which causes a higher motor current in the SynRM. In the 75 kW IM measurements with five different frequency converters in (Aarniovuori, et al., 2019), there were clear differences between the motor losses with each of the converters, and some differences were quite high. Clear differences were also found in the frequency converter losses and the drive system losses. These are illustrative examples of the complex relationships of the losses in power drive systems, but also of the manufacturer-specific choices in the frequency converter technology, including for instance the electric components used in the converter, the motor control principles, the PWM methods, and the efficiency optimizations.

The efficiency of the motor decreases when supplied with a frequency converter. In Table 2.2, the 75 kW IM drive system efficiencies from Figure 2.19 in a total of eight operating points at 45 Hz and 50 Hz are compared with the motor efficiency DOL use (50 Hz). In the DOL use, the motor is, in practice, either running at the rated speed or brought to a standstill. Therefore, if lower speeds are sufficient in a significant part of the usage scenario, a frequency converter supply can easily be more energy efficient compared with the DOL use.

The DOL supply efficiencies (grid-connected) in Table 2.2 are the input–output efficiencies with the rated load when the motor has reached thermal stability, and the partial load efficiencies are from the load curve test measured directly after the heat run test measured in the ambient temperature of 25°C. Similarly, the converter and the converter-fed motor efficiencies were in thermal stability at the end of the rated load test,

Table 2.2. Efficiency behavior of a 75 kW motor in different operating modes in the DOL use and when used in a power drive system. The frequency converter and drive system efficiencies are also included.

Operating point		Motor efficiency (%)		Switching frequency (Hz)	Converter efficiency (%)	Drive system efficiency (%)
f (Hz)	*T* (%)	Grid-connected	Converter-fed			
50	100	96.2	95.5	2544	98.1	93.7
50	75	96.4	95.8	2617	98.2	94.0
50	50	96.1	95.5	2588	98.2	93.7
50	25	94.1	93.3	2559	97.7	91.1
45	100	-	95.4	2636	98.1	93.5
45	75	-	95.5	2635	98.2	93.8
45	50	-	95.1	2631	98.2	93.4
45	25	-	92.8	2642	97.6	90.6

and the partial load test was carried out quickly after the thermal equilibrium was reached. In practice, the losses in Table 2.2 are higher than in normal use because the motor temperature is close to the rated load temperature, which is significantly higher than in normal use with partial loads. It should be noted that this motor, as most of the induction motors today, has been designed for sinusoidal supply, and it has a double cage structure in the rotor to enhance the DOL starting performance of the motor. A single cage structure would be more suitable and less susceptible to the high-frequency harmonics and the related increase in the losses with a converter supply. It is also worth remembering that the converter-fed motors should not be dimensioned so that they are continuously used in the 50 Hz operating point (or above). This is typically an unfavorable point because of the insufficient voltage level, which leads to increased losses and derating of the loading capability. In this case, the converter is driving a motor that is rated for 400 V at the 50 Hz operating point with the line-to-line voltage ranging from 378 V to 386 V corresponding to the load points from 100% to 25%.

When the motor is operated with a converter at the 50 Hz operating point, the motor efficiency is decreased by 0.6%–0.8% compared with the sinusoidal supply efficiency. The system efficiency is further decreased by the converter losses, which are around 2% of the total power flow. The system efficiency is thus decreasing from 96.2% to 93.7% at the rated operating point of the 75 kW motor when the motor is operated using a frequency converter.

The motor efficiencies are only slightly lower at the 45 Hz operating point than at the 50 Hz point. Although the converter can now produce less distorted voltage compared with the 50 Hz point, also the relative part of the losses increases because the magnetizing

current is increased. The converter efficiency remains at the same level as at the 50 Hz point, and the resulting drive system efficiency is only slightly lower compared with the 50 Hz point.

3 Measurement uncertainty

The input–output method is by far the easiest and fastest method to measure losses and efficiency in a power drive system. It is, however, also the method with the highest uncertainty for modern high-efficiency electric motors and frequency converters. In this chapter, the uncertainty of the input–output method in power drive system measurements is covered thoroughly. The methodology for determination of measurement uncertainty in electric and mechanical power measurements is presented, and the loss and efficiency uncertainties of three drive systems with different power ratings are analyzed comprehensively. The uncertainty analysis is made for the motors and converters separately as well as for the complete power drive systems. The measurement uncertainties of the other two relevant methods, the loss segregation method and the calorimetric method, were not in the scope of this dissertation. They cannot be, however, completely neglected in the bigger picture and are therefore discussed using previous studies from the literature and the practical experience from performing the measurements.

This chapter is arranged as follows: section 3.1 covers electric power measurement uncertainty, section 3.2 mechanical power measurement uncertainty, and section 3.3 loss and efficiency measurement uncertainty. The focus is naturally on the uncertainty of losses and efficiency, but in the case of the input–output method, the uncertainties of the loss and efficiency results are determined by the input and output power measurement uncertainties. Therefore, the electric and mechanical power measurement uncertainties are discussed first.

Measurement uncertainty is the main topic in Publications VI, VII, and VIII. Publication VI focuses on the converter losses, the type A and type B uncertainties, and their differences and significance in the overall uncertainty. Publication VII dissects the overall uncertainty determination of converter-fed motors starting from the accuracy specifications of the measurement instruments and ending with the overall uncertainty value of the motor losses. Publication VIII takes another perspective to the input–output loss uncertainty from the viewpoint of the testing facility: the analysis focuses on the expected measurement uncertainty when using readily available measurement instruments in testing motors from a wide range of different rated powers. Furthermore, the input–output uncertainty analysis was used in frequency converter efficiency classification measurements in Publication IX. The accuracy values used in the type B uncertainty analysis in all Publications were obtained from the datasheets of each of the instruments. The calibrated accuracies of individual instruments can be higher than the general model-specific accuracies given in datasheets. All the uncertainty values given in this chapter are presented at a coverage factor of $k = 2$ unless stated otherwise.

3.1 Electric power measurement uncertainty

The most accurate device to measure the electric power of frequency converters and electric machines is a power analyzer. As the current handling capability of power analyzers is limited, external current transformers or transducers are often required. The uncertainty of the electric power measurement is a function of voltage and current amplitudes, frequency, and power factor. In power drive systems, all these quantities vary depending on the operating point of the electric machine, that is, the load torque and the operating speed.

3.1.1 Power analyzer accuracy in different frequency ranges

The power analyzer measurement accuracy is given for certain frequency bands, and usually, the accuracy is best around the common grid frequencies of 50 and 60 Hz. However, outside this range, the accuracy decreases rapidly. Different aspects of this issue in power drive system measurements have been addressed in Publications VI, VII, and IX. In Publication IX, the input and output electric powers of a 160 kW frequency converter were analyzed in the frequency domain. A similar figure from the data of Publication I is provided in Figure 3.1. The reading and range accuracies of the power analyzer used in the measurements (Yokogawa WT1600) and the cumulative active powers with DOL and PWM supplies of the 15 kW induction motor at the 50 Hz operating frequency are given. It should be noted that the cumulative power curves were obtained

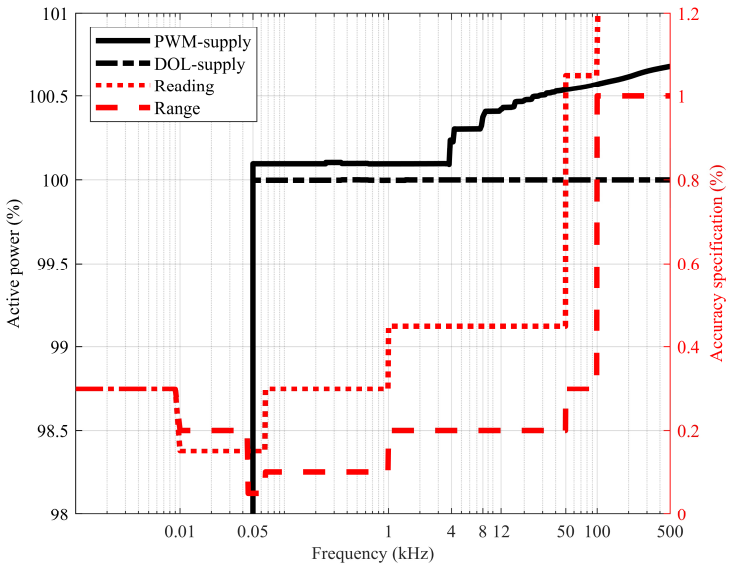

Figure 3.1. Active power of the 15 kW induction motor with the DOL and frequency converter supplies and the power analyzer reading and range accuracies as a function of frequency. 100% relative power is equal to the total active power with the direct-on-line supply. The switching frequency of the frequency converter was 4 kHz.

by processing one-second waveform data consisting of one million samples (1 MS/s) in MATLAB. The waveform data were recorded using another power analyzer (Yokogawa PX8000), which was used solely for this purpose during the measurements. From Fig. 3.1 it can be observed that the range accuracy and reading accuracy around 50 Hz are 0.05% and 0.15%, respectively, while at 25 Hz the corresponding values are 0.2% and 0.15%. At slightly higher frequencies above 66 Hz, the range and reading accuracies are 0.1% and 0.3%, respectively. The effect of the power analyzer accuracy ranges can be very clearly seen in the uncertainty maps provided later in this chapter: particularly in the electric power measurement uncertainty in Figure 3.2, but also in the loss and efficiency uncertainties presented for the frequency converter, motor, and power drive system measurements in section 3.3.

Another aspect illustrated by Figure 3.1 is the measurement accuracy of the highly distorted converter-fed motor input power. The cumulative motor power curve with the PWM supply shows that while the majority of the power, over 99%, is at the 50 Hz fundamental frequency, a relatively small part of the power is at the frequency range at and above 4 kHz. This can, however, be considered significant as the power is not used in torque production and can thus be regarded as losses. The 0.7% input power increase is equal to a 12% loss increase in the motor. The switching frequency was 4 kHz, and a relatively large part of the harmonic power is at the switching frequency band. Additionally, there is some harmonic power at the multiples of the switching frequency. As the reading and range accuracy curves in Figure 3.1 show, the accuracy of the power analyzer is significantly decreased above 1 kHz and even more above 50 kHz. In Publication VII, the uncertainty analysis of the frequency converter output power is investigated in more detail. It is shown that the impact of the high-frequency harmonics is negligible in the overall electric power measurement uncertainty. In practice, the motor input power measurement uncertainty is similar for DOL motors and converter-fed motors.

3.1.2 Measurements over wide operating range

The electric power measurement uncertainty over a wide operating range was investigated in Publications VI and VII. The measurements were made for three different-sized frequency converters supplying three different-sized induction motors: 15 kW, 37 kW, and 75 kW. The tests were carried out in a total of 16 operating points from 25% to 100% of the rated load of each motor and at the frequencies of 12.5 Hz, 25 Hz, 37.5 Hz, and 50 Hz. The electric power measurement uncertainty including type A and type B uncertainties was determined for all the three converters and motors in all the operating points, and the results were interpolated over the whole operating range at the motor rated operating point and below.

The input electric power uncertainty in the 15 kW, 37 kW, and 75 kW induction motor measurements is presented in Figure 3.2 in watts and in Figure 3.3 as a percentage of the power value. The distributions of the uncertainty values are quite similar, which is due to the fact that the same power analyzer and similar current transducers were used with all

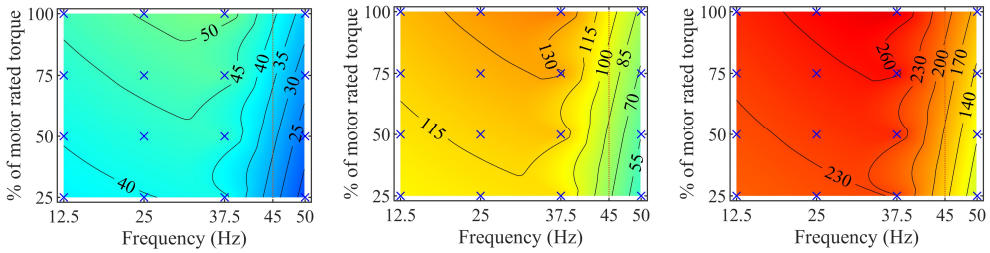

(a) 15 kW (b) 37 kW (c) 75 kW

Figure 3.2. Electric power uncertainty in watts (W) for the input electric power of the 15 kW, 37 kW, and 75 kW converter-fed induction motors. The uncertainties are interpolated over the measurement range of 25%–100% load torque and 12.5 Hz–50 Hz supply frequency. The values represent expanded uncertainty at the 95% level of confidence ($k = 2$).

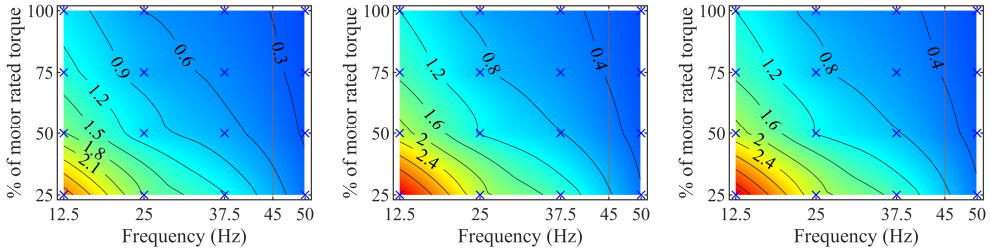

(a) 15 kW (b) 37 kW (c) 75 kW

Figure 3.3. Electric power relative uncertainty in percent (%) for the input electric power of the 15 kW, 37 kW, and 75 kW converter-fed induction motors. The uncertainties are interpolated over the measurement range of 25%–100% load torque and 12.5 Hz–50 Hz supply frequency. The values represent expanded uncertainty at the 95% level of confidence ($k = 2$).

the three motors. The significant change in Figure 3.2 between 37.5 and 50 Hz is caused by the range accuracy border of the power analyzer at 45 Hz. The effect of the accuracy ranges is not as obvious in Figure 3.3 as it is seen as the relative uncertainty becoming more operating frequency dependent around the 45 Hz mark. Some differences can also be noticed in Figure 3.3, where the relative values should be identical in an ideal situation. The relative uncertainty in the 15 kW motor measurements was slightly lower than with the two larger motors, which is the result of a better-matching power analyzer current range for the 15 kW motor.

3.2 Mechanical power measurement uncertainty

The mechanical power P_m is the product of the angular speed Ω and the torque T as

$$P_\mathrm{m} = \Omega T, \tag{3.1}$$

and modern torque measurement devices are usually able to record both.

The rotational speed is typically measured by magnetoresistive or optical means. The uncertainty in the speed measurement originates from the uncertainty of the speed measurement system itself, and the inherently digital nature of the speed measurement based on counting pulses, that is, the actual resolution of the speed data.

There are different methods to measure torque, but in practice, for loss and efficiency determination purposes, only direct methods relying on in-line torque sensors or transducers are viable. The accuracy of the in-line torque sensors attached on the shaft between the motor and the load is affected by several sources of uncertainty. Consequently, manufacturers usually specify several separate accuracy values in the transducer datasheets. The torque measurement uncertainty sources can be categorized by their behavior over the measurement range. As an example, the uncertainty components of a 500 Nm HBM T12 torque transducer are illustrated in Figure 3.4 as a function of the measured torque value. An uncertainty source can affect the torque value independently of load resulting in an equal uncertainty (in Nm) at any measurement point, or the uncertainty can be load dependent resulting in a higher uncertainty at a high torque. In Figure 3.4, parasitic loads, temperature influence on the zero value, and repeatability

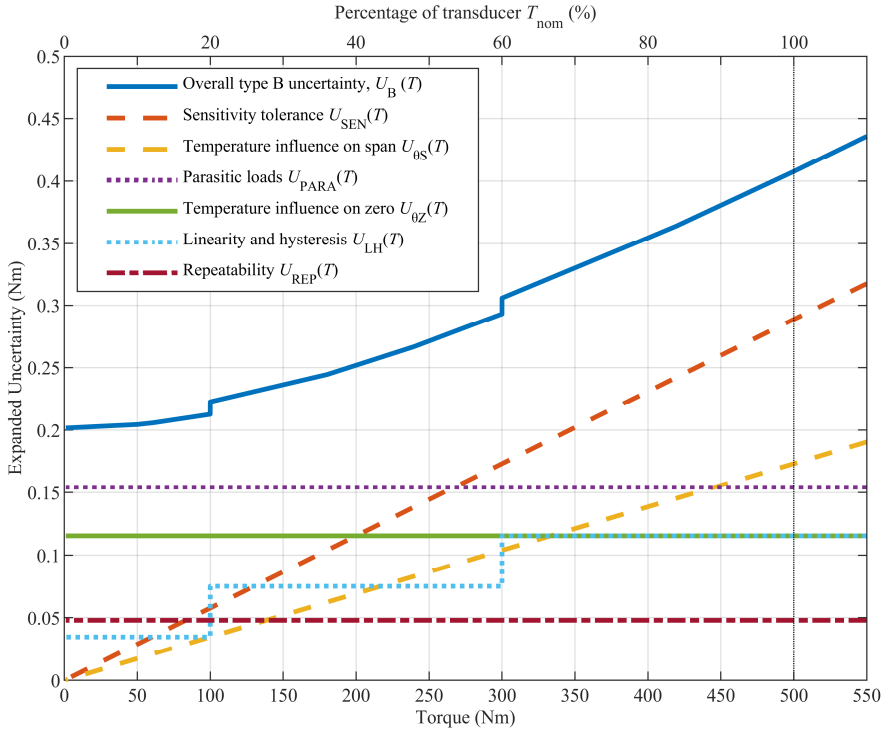

Figure 3.4. HBM T12 (500 Nm) torque measurement type B uncertainty components presented over the measurement range of the transducer in the 37 kW IM measurements. HBM T12 is guaranteed to fulfil the accuracy specifications up to 110% rated torque. The values represent the expanded uncertainties at the 95% level of confidence (coverage factor $k = 2$).

fall into the aforementioned category, while sensitivity tolerance and temperature influence on span are linearly load dependent. Linearity and hysteresis are a mix of both as they are given for different ranges of the torque being measured but defined as constant within each range. Most of the torque uncertainty sources are simple to take into account in the uncertainty analysis, but for example the parasitic loads are the forces taking place in a specific test bench, and estimating their influence requires detailed information from the alignment of the motor, support bearings and load machine. There are also sources of uncertainty that may not be covered by any of the datasheet values. For instance, as measuring torque from a rotating shaft is challenging, torque transducers are typically calibrated in standstill, and it is not clear if this difference is considered in any of the datasheet values. The torque and speed uncertainty components as well as the uncertainty analysis for rotational speed measurement and torque measurement are comprehensively explained in Publication VII.

The uncertainties of speed and torque do not correlate, and they are measured with separate sensors. Hence, the uncertainty contributions of both quantities can be analyzed individually and combined according to the realistic perturbation method similar to (1.4). Taking into account the sensitivity of the mechanical power to both speed and torque, the mechanical power uncertainty is (see Publication VII for details)

$$U(P_{\mathrm{m}})=\sqrt{|T\,|\cdot U(\Omega)+|\Omega|\cdot\ U(T)}\,, \tag{3.2}$$

where $U_{\mathrm{T}}(\Omega)$ and $U_{\Omega}(T)$ are the uncertainties of the speed and torque measurements, respectively. Figure 3.5 presents the mechanical power uncertainty in absolute values and Figure 3.6 in relative values for the 15 kW, 37 kW, and 75 kW induction motors. In absolute values (watts), the mechanical power uncertainty is mostly frequency—or speed—dependent. As some of the uncertainty sources are constant and some load and speed dependent, the relative uncertainty is somewhat higher when measuring at lower operating frequency and load values, but compared with the electric power relative

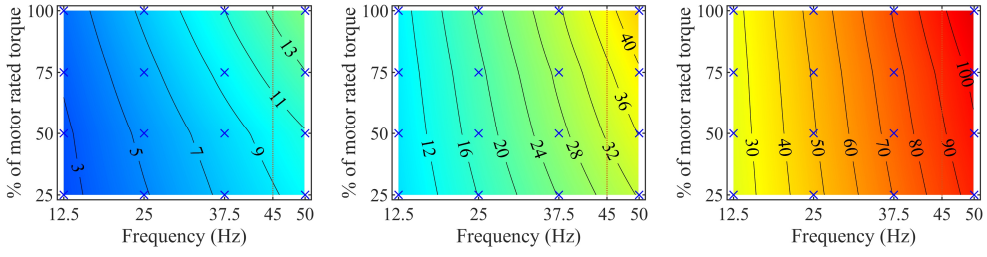

(a) 15 kW (b) 37 kW (c) 75 kW

Figure 3.5. Mechanical power uncertainty in watts (W) for the output mechanical power of the 15 kW, 37 kW, and 75 kW converter-fed induction motors. The uncertainties are interpolated over the measurement range of 25%–100% load torque and 12.5 Hz–50 Hz supply frequency. The values represent expanded uncertainty at the 95% level of confidence (k = 2).

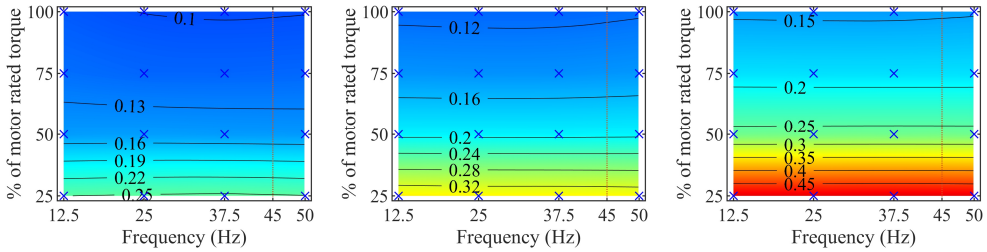

(a) 15 kW (b) 37 kW (c) 75 kW

Figure 3.6. Mechanical power relative uncertainty in percent (%) for the output mechanical power of the 15 kW, 37 kW, and 75 kW converter-fed induction motors. The uncertainties are interpolated over the measurement range of 25%–100% load torque and 12.5 Hz–50 Hz supply frequency. The values represent expanded uncertainty at the 95% level of confidence (k = 2).

uncertainty (Figure 3.3), the dependence is weaker. In fact, the relative uncertainty of mechanical power in Figure 3.6 is almost completely load dependent. The relative uncertainty also shows the reason for the low load dependence of the uncertainty in watts: from the 100% load to the 25% load, the relative uncertainty is increased three- to fourfold, while the mechanical power is reduced to one-fourth. Figure 3.6 also shows that the mechanical power uncertainty in these measurements was lowest for the 15 kW motor and highest for the 75 kW motor. This is partly due to a closer match of the rated value of the transducer and the measured torque with the 15 kW motor, but also due to some uncertainty sources being relatively higher with larger transducers. For example, the tolerance for parasitic loads is not increased in proportion to the transducer torque rating between 500 Nm and 1 kNm transducers, which were used with the 37 kW motor and the 75 kW motor, respectively.

3.3 Uncertainty of losses and efficiency

The final uncertainty values for the input–output losses and efficiency are calculated using the input and output power uncertainties. As the losses are the difference of the input and output power (1.3), and the uncertainties of the input and output powers do not correlate, the loss uncertainty is calculated combining them according to the realistic perturbation method similar to (1.4). The loss uncertainty is thus

$$U(P_{\text{loss}})=\sqrt{U(P_{\text{in}})^2+U(P_{\text{out}})^2}, \tag{3.3}$$

where $U(P_{\text{in}})$ and $U(P_{\text{out}})$ are the input and output power uncertainties, respectively.

The input–output efficiency is the ratio of the output power P_{out} to the input power P_{in} according to the first form of (1.2), and thus, the sensitivity of the efficiency to both the input and output power has to be taken into account. The equation for the input–output efficiency uncertainty is

$$U(\eta)=\sqrt{\left(\left|-\frac{P_{\text{out}}}{P_{\text{in}}^{2}}\right|U(P_{\text{in}})\right)^{2}+\left(\left|\frac{1}{P_{\text{in}}}\right|U(P_{\text{out}})\right)^{2}}, \tag{3.4}$$

which is derived in Appendix A.

The input–output measurement uncertainty is heavily dependent on the efficiency of the device being tested. Using the input–output method, the loss uncertainty approaches infinity when the efficiency approaches unity, which is explained mathematically in Publication III. This behavior is illustrated in Figure 3.7, where both the input power measurement uncertainty and the output power measurement uncertainty are set to 0.1%, 0.2%, and 0.5% and the loss uncertainty is calculated as a function of the efficiency of the device. For example, the input–output loss uncertainty for a device with 94% efficiency is slightly below 5% when both the input and output power uncertainties are 0.2%. When using indirect methods, such as loss segregation or calorimetric methods, the loss uncertainty is not dependent on the efficiency of the device.

In Figure 3.8 both the input power measurement uncertainty and the output power measurement uncertainty are set to 0.1%, 0.2%, and 0.5% and the efficiency uncertainty is calculated as a function of the efficiency of the device. Indirect method efficiency uncertainty, when the efficiency is calculated using the total losses and input power according to the second from of (1.2), is included in the figure with the loss uncertainty set to 1% and 5%. The input power uncertainty is 0.2% in both indirect cases. The input-output efficiency uncertainty only slightly increases with the efficiency of the device

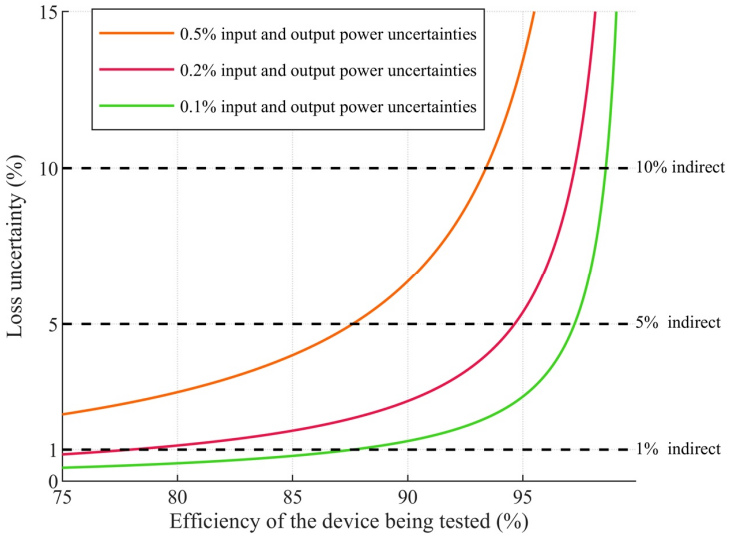

Figure 3.7. Input–output loss measurement uncertainty as a function of the efficiency of the device being measured when the uncertainty in both the input and output power measurements is 0.1%, 0.2% and 0.5%.

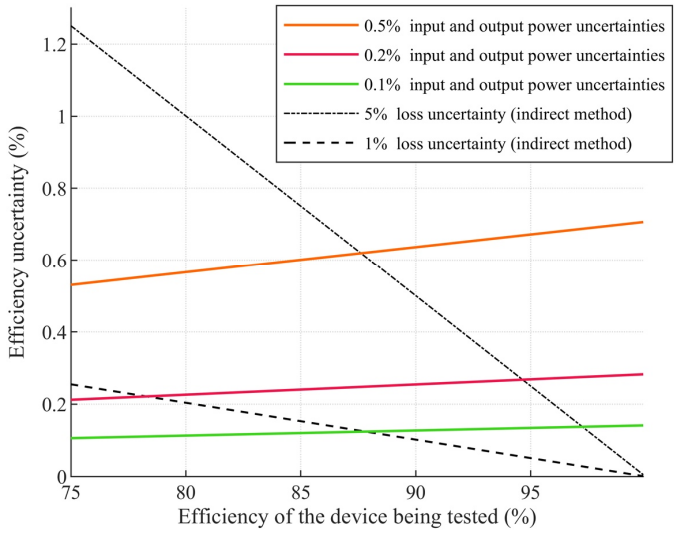

Figure 3.8. Input–output efficiency measurement uncertainty as a function of the efficiency of the device being measured when the uncertainty in both the input and output power measurements is 0.1%, 0.2% and 0.5%. The efficiency uncertainty when the losses are determined using an indirect method with loss uncertainty of 1% and 5%, and with input power uncertainty of 0.2%, is presented for comparison.

while the indirect efficiency uncertainty approaches zero as the losses approach zero. Determining the indirect efficiency uncertainty is presented in Appendix A.

Figures 3.7 and 3.8 illustrate well the strengths and weaknesses of the direct and indirect methods over the different device efficiency ranges. An indirect method with the loss uncertainty of 1% has lower loss and efficiency uncertainties than the input-output method with power measurement uncertainties of 0.1% when the device efficiency is higher than approximately 87%. If the efficiency of the device is lower, the input-output method is superior. When the efficiency of the device increases, the indirect uncertainty becomes more accurate even with significantly higher loss uncertainties, as the 5% and 10% lines in Figure 3.7 and the 5% line in Figure 3.8 illustrate. The point where the input-output and indirect efficiency curves cross depends on the indirect method and the measurement instruments used.

In the case of a power drive system, three different cases of input–output loss measurement must be considered. The losses of a frequency converter are the difference of two electric power values, while the motor losses and the power drive system losses are the difference of the electric power and the mechanical power. Frequency converters have typically a higher efficiency than motors, and as Figure 3.7 suggests, also the input–output loss uncertainty is generally higher for frequency converters than motors. In the case of a power drive system, however, the total losses of the system consist of both motor and converter losses. As the overall efficiency is lower than the motor efficiency alone,

also the uncertainty of the power drive system losses is lower than the motor loss uncertainty.

The electric input power uncertainties and mechanical power uncertainties for the 15 kW, 37 kW, and 75 kW induction motors were presented in Figure 3.2, Figure 3.3, Figure 3.5, and Figure 3.6. The loss uncertainties for the motors are shown as combined according to (3.3) in Figure 3.9 and Figure 3.10. Comparing with the behavior of the power uncertainties and the loss uncertainties, the electric power uncertainty clearly dominates the loss uncertainty behavior in these measurements. This is because the power analyzer used here has only average accuracy specifications, whereas the torque transducer has a very high accuracy. There are power analyzers with far better accuracy specifications available in the market, and thus, this behavior cannot be generalized.

Using (3.4), the measurement uncertainty was determined also for the 15 kW, 37 kW, and 75 kW induction motor efficiencies, Figure 3.11. Overall, the uncertainty of the efficiency results is acceptable over the range above the 50% rated load and the 25 Hz frequency. For reference, the efficiencies of the motors are plotted in Figure 3.12. Especially the

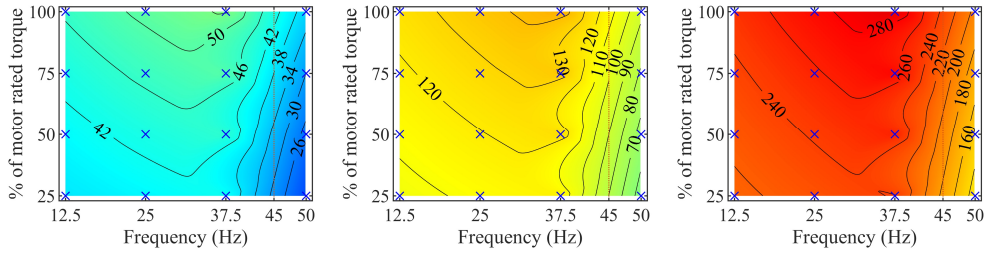

(a) 15 kW (b) 37 kW (c) 75 kW

Figure 3.9. Input–output loss uncertainty in watts (W) for the 15 kW, 37, kW and 75 kW converter-fed induction motors. The uncertainties are interpolated over the measurement range of 25%–100% load torque and 12.5 Hz–50 Hz supply frequency. The values represent expanded uncertainty at the 95% level of confidence ($k = 2$).

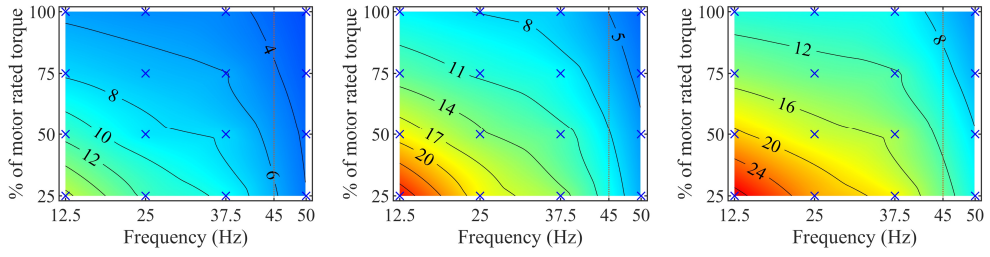

(a) 15 kW (b) 37 kW (c) 75 kW

Figure 3.10. Input–output loss relative uncertainty in percent (%) for the 15 kW, 37 kW, and 75 kW converter-fed induction motors. The uncertainties are interpolated over the measurement range of 25%–100% load torque and 12.5 Hz–50 Hz supply frequency. The values represent expanded uncertainty at the 95% level of confidence ($k = 2$).

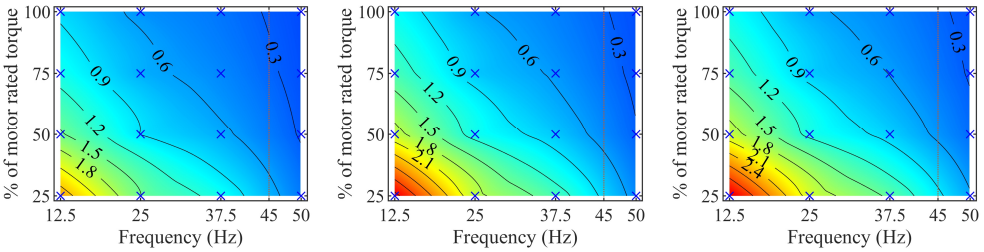

(a) 15 kW (b) 37 kW (c) 75 kW

Figure 3.11. Uncertainty of the input–output efficiency in %-units for the 15 kW, 37 kW, and 75 kW converter-fed induction motors. The uncertainties are interpolated over the measurement range of 25%–100% load torque and 12.5 Hz–50 Hz supply frequency. The values represent expanded uncertainty at the 95% level of confidence (k = 2).

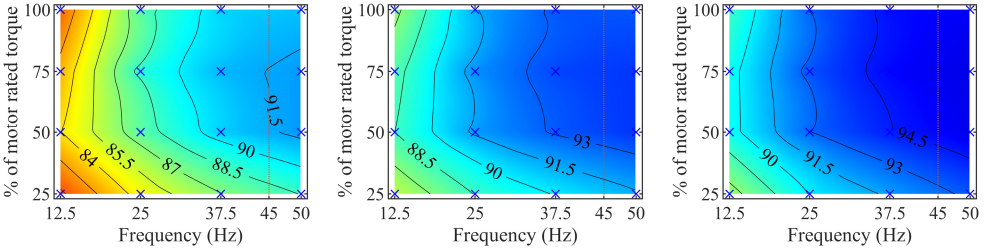

(a) 15 kW (b) 37 kW (c) 75 kW

Figure 3.12. Input–output efficiency in percent (%) for the 15 kW, 37 kW, and 75 kW converter-fed induction motors. The efficiencies are interpolated over the measurement range of 25%–100% load torque and 12.5 Hz–50 Hz supply frequency.

approximately 3 %-unit uncertainty of the 37 kW and 75 kW motor efficiencies with a low load and a low frequency is high compared with the efficiency values in Figure 3.12. There is one obvious reason for the high uncertainties in the low torque and frequency range. In these measurements, the power analyzer current and voltage measurement ranges were the same in all the test points. Although a high voltage range is required in all the test points because of the PWM voltage, the current range can be reduced for low load points.

3.4 Other factors related to measurement accuracy

Accurate measurement results can be obtained with low-uncertainty methods. The prerequisites for accurate results are: choosing the appropriate method, selecting the right measurement instruments, using and initializing the instruments correctly, and analyzing the data with judgment. All these requirements can incorporate human error. The influence of human error on results can be reduced with high-quality instructions, patient guidance, and effective training, but it cannot be removed entirely.

Understanding the origin and effect of the different uncertainty sources on the overall uncertainty result enables its control. The uncertainty analysis is a tool that can be used to examine and minimize the factors related to measurement uncertainty, and thus, it can be used to also reduce the human error.

Another important factor is the postprocessing of the raw measurement data. Considering the type A and type B uncertainties in power drive system input–output measurements, the type A uncertainty is significantly affected by the length of the test data. In Publication VI, the type A uncertainty was calculated as a function of the number of samples for the losses of three frequency converters with different power ratings as shown in Figure 3.13. The figure illustrates the importance of a sufficiently high number of samples regarding the type A uncertainty. Naturally, the length of each sample affects the variation between the samples; the data used for Figure 3.13 consists of 100 samples recorded over a time span of 100 seconds, which is also the data length used in all the input–output measurements of this doctoral dissertation. According to the results of Publication VI, the converter loss type A uncertainty can be easily reduced to an insignificant level considering the overall (combined) uncertainty, where the type B uncertainty becomes dominant. According to the results of Publications VII and VIII, the impact of the type A uncertainty is minimal also in the motor loss uncertainty when the data length is similar.

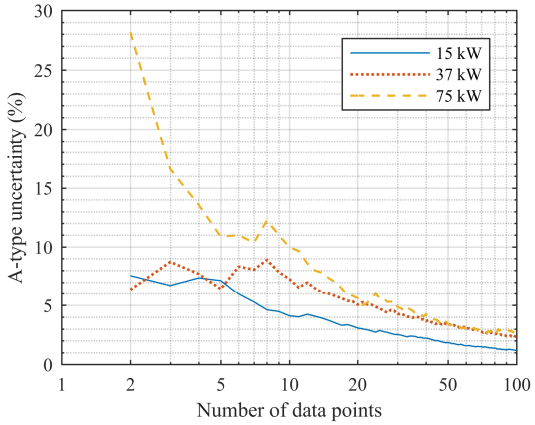

Figure 3.13. Type A uncertainties of the drive losses as a function of the number of the data points for the three different frequency converters supplying a 15 kW, 37 kW, and 75 kW induction motor in the rated operating point. The curves are plotted with the coverage factor $k = 2$ (95% level of confidence).

4 Summary and discussion

This chapter highlights the importance of this work, widens the scope of the results, explains how the results can be utilized in a broader scope, and discusses the harmonic losses in induction machines from the design point of view.

4.1 Importance of the work

The uncertainty analysis constitutes a major part of the scientific results of this work, but in the previous power drive system and motor research it has often been omitted. The development of the measurement instruments and the transformation of the devices from analog to digital ones with a high number of digits have created an impression that measurement results are accurate and correct. However, the increase in the efficiencies of the devices and the distorted waveforms as a result of switching power supplies have made the experimental measurements a more challenging task. The experimental method is typically the final proof; the analytical or numerical results are verified by an experimental method, and therefore, the reliability of the experiments is crucial in scientific work or in the R&D of electric devices.

Until now, there has not been a complete tool available for analyzing the measurement uncertainty of the tests that are used in the loss and efficiency determination of converters and electric machines. The uncertainty analysis can be used to control and minimize the measurement uncertainty. It also helps to choose and set up the measurement instruments correctly. Similarly, it can be used to analyze what kinds of measurement instruments are suitable for obtaining the required accuracy. The assessment of the measurement uncertainty was covered in this dissertation starting from the datasheet information and the statistical properties of the collected data without going into details of the internal operation of the measurement instruments or into the foundations of how the manufacturers obtain or define the accuracy specifications for the datasheets.

In the international standards, the measurement uncertainty is controlled by using minimum accuracy classes of specifications. These accuracy classes are ambiguous and cannot be used directly to estimate the reliability of the results. Most often, the same accuracy classes are used for all devices regardless of the efficiency. One step towards the control of the measurement uncertainty is taken in IEC 60034-2-3 (2020), where the accuracy specifications of the torque transducer are connected with the expected efficiency of the device.

In this dissertation, only the uncertainty of the input-output method was covered. The input-output method is the only method equally well suitable for all motor technologies and frequency converters, and it is also the only practical method for general use with these devices. Comparisons of uncertainty between the input-output method and loss segregation method have been presented in literature (Doppelbauer, 2015), (Yogal, et al., 2018). However, the loss segregation results of different motor technologies are not

directly comparable because of differences in the operation principles and loss components, which hinders its usability. Even comparing the loss segregation and input-output results of the same motor is not straightforward because of differences in the loss and efficiency determination principles of the methods.

At the moment, there is no guidance on the international standards, or more generally, how many samples should be taken from one measurement point. The type A uncertainty analysis shows that the uncertainty can be significantly reduced by using a large number of samples and/or long sample times. This will increase the repeatability and reliability of the results.

The harmonics are included in the active power value shown by the power analyzer. However, the subharmonics and interharmonics are not fully taken into account. In practice, if a high number of samples or long samples are used, this should not be a major problem, because the share of the power of the partial periods of the inter- and subharmonics decreases as a function of the examination period.

Measuring electric motor drives according to the efficiency standards set by the authorities is very challenging and gives rise to a concern that the skills to measure machines correctly may be lacking or insufficient. There are standard-compliant measurements on the one hand, and measurements suitable for scientific work on the other.

4.2 Extension of results

The power drive system losses or efficiency uncertainties have not been analyzed in this work. The converter input waveform in a typical voltage source converter is close to the sinusoidal supply, and it has only active power at the fundamental wave frequency as shown in Fig 3.1. The sinusoidal supply together with a lower system efficiency makes the determination of the efficiency or losses of the motor drive systems less demanding than in the case of a motor or a converter. The measurement uncertainty of a power drive system can be easily combined from the presented results.

Simultaneous use of the calorimetric and the input–output method is viable to calibrate the measurement systems. Based on the difference between the calorimetric and input–output measurement results, the systematic errors from absolute values can be eliminated. The input–output method is and will be the most commonly used method in the loss and efficiency determination, and in most of the cases it is the best choice. The undeniable advantages of the input–output method are its rapidity and ability to detect the trends.

In practice, multiple methods are required in the research work. The calorimetric method can only measure the total losses, whereas the loss segregation can give further information about the loss components. The electrical measurements contain additional information about the waveforms, such as phase shift and harmonic content.

For example, it is extremely challenging to obtain the losses of a sine filter or other output filters that are used to suppress the specific harmonics from the PWM waveform. The low power factor, near-unity efficiency, and harmonics over a wide frequency band are challenging for the input–output method, and a calorimeter is preferred to obtain the total losses, but the electrical measurements are required to analyze the harmonic contents.

4.3 Motor design and harmonic losses

One interesting question in the induction motor design is how well the motors are really adapted to the PWM supply. Traditionally, the induction motors have been designed primarily for DOL drives. Originally, at the beginning of the era of frequency converters, the idea was that any induction motor can be used in speed-controlled drives and can replace a DC motor drive in industrial applications.

So far, this thinking has been widely applied and all the potential benefits of a drive system have not been in use while the induction motors for DOL and converter applications have mainly had similar magnetic circuits and conductor designs especially on the rotor side. The only clear differences are found in reinforced insulation and possibly insulated bearings to avoid premature bearing failure in the PWM supply.

Because a converter-fed motor does not need to comply with the DOL start requirements defining a certain current value dictated by both the standard limitations and customer needs for DOL motors, the magnetic circuit and the rotor of a PWM-supplied motor should be optimized for the converter supply.

DOL motors frequently have a double cage to limit the starting current. Further, for manufacturing reasons, the rotor slots are closed thus creating a high-loss vulnerability from the viewpoint of the PWM supply. A double cage is not advantageous in a PWM supply. The rotor conductor could be larger resulting in a lower slip and improved efficiency in converter-supplied motor drives. The closed slot construction is also harmful as high rotor surface losses are produced in the thin lamination bridges closing the rotor slot. By choosing a single cage design and utilizing the surface available for the rotor conductors, and finally, by opening the rotor slots to break the eddy current paths on the rotor surface, we could have a special converter-fed motor that should have close to the same efficiency as the DOL counterpart but now in the PWM supply.

As the highest possible efficiency of the induction motor drives has been the target of both authorities and motor manufacturers, it is somewhat astonishing that dedicated rotor constructions are not frequently offered. Only in some special cases, motor manufacturers have optimized the rotor construction from the viewpoint of PWM loss minimization.

5 Conclusion

The number of converter-driven electric machines is increasing rapidly in various applications, and they consume a majority of the electric energy produced. Because the electric machines are at the end of the energy chain, all the energy efficiency improvements will have a follow-up effect and reduce the losses in all parts of the chain. The energy efficiency improvements must be verified by experimental methods. The accuracy of the measurements in the case of high-efficiency devices is a concern.

Different methods have their advantages and disadvantages, and the choice of the measurement methods depends on the usage of the results. The accuracy requirement can be different in field tests, in type testing, or in scientific research work.

In this work, the experimental methods used in the determination of efficiency and losses of an electric machine system and its parts, converter and motor were analyzed and discussed. The accuracy of the input–output method has been criticized, but the results presented in this work show that the input–output results match extremely well with calorimetric measurements, showing that carefully prepared and conducted input–output measurements using high-accuracy measurement instruments can give reliable and accurate results. It is also shown that the results obtained using the IEC loss segregation method are in good agreement when Joule losses are adjusted to a matching temperature.

The calorimeter is often thought to be a complex measurement system. One of the simplest calorimeter versions is the air-cooled, balance type calorimeter. However, one of the main disadvantages of the air-cooled calorimeter has been variation in the specific heat capacity of the air during the tests. To include these variations in the results requires extra hardware, thus making the measurement system more complex and costly. In addition, more complicated analysis is required, but the outcomes of this work confirm that humidity and barometric pressure sensors (and corrections in the analysis) are not crucial if the main test and the balance test are made in similar conditions (balance test immediately after the main test without major changes in the ambient environment between the tests).

The method used in this work is close to the best possible. When two independent methods were used simultaneously, the differences between the results could be accurately observed.

The uncertainty analysis confirms that the measurement uncertainty of the total active electric power is similar for a sinusoidal supply and a PWM supply. Therefore, the PWM supply measurement results can be considered as reliable as the sinusoidal supply results. It was shown that the converter-caused additional losses in an induction motor are dependent on both the operating frequency (speed) and the load contrary to several findings in the literature.

The load dependence was confirmed with the IEC/TS loss segregation method for converter-fed motors. However, this method is complex to apply and, in practice, not usable with commercial converters, but it can be used for scientific purposes for induction motors, and it can be usable for instance for comparing converter-caused losses between different motors and PWM waveforms.

The uncertainty analysis shows that the effect of the type A uncertainty on the combined uncertainty is negligible when a sufficient number of sample periods are used (long enough measurement).

The loss difference between consequent efficiency classes is around 20%. Based on the results of this work, the uncertainty of the input–output method is low enough for efficiency classification purposes. In addition, it can be concluded that the accuracy levels of the measurement instruments required by testing standards are high enough for the input–output method.

The uncertainty analysis is a tool for evaluating the reliability of measurement results, and it is not expected that the absolute values have true physical meaning. The choices made in the uncertainty analysis may have a substantial effect on the uncertainty results. If the distribution or the coverage factor are not given, the choice of the distribution and the coverage factor may have a significant effect on the final uncertainty value.

The bandwidth of a power analyzer is always limited, while a calorimeter has, in practice, an unlimited bandwidth because of conservation of energy. Electric power measurement uncertainty can be estimated based on the total power and fundamental frequency band accuracy specifications of the power analyzer. Uncertainty in converter-fed motor measurements is similar to DOL motor measurements.

The main purpose of the doctoral dissertation was not to study motor technologies in detail. However, the synchronous reluctance machine technology is advantageous from the perspective of efficiency improvement. In one of the measurement series, the SynRM and the IM were compared. It was verified that the loss and efficiency differences between the SynRM and the IM originate almost completely from the combination of the IM rotor losses and the power factor difference. The IM rotor losses are much higher than the SynRM rotor losses. However, the IM is better from the viewpoint of power factor.

References

Aarniovuori, L., 2010. "Induction Motor Drive Energy Efficiency - Simulation and Analysis". *Acta Universitatis Lappeenrantaensis*.

Aarniovuori, L., Kolehmainen, J., Kosonen, A., Niemelä, M., Huifeng, C., Cao,W. & Pyrhönen, J., 2016b. "Application of Calorimetric Method for Loss Measurement of a SynRM Drive System". *IEEE Transactions on Industrial Electronics,* pp. vol. 63, no. 4, pp. 2005-2015, April 2016..

Aarniovuori, L., Kärkkäinen, H., Niemelä, M.,, Cai, K., Pyrhönen, J. & Cao, W., 2019. "Experimental Investigation of the Losses and Efficiency of 75 kW Induction Motor Drive System,". *in IECON 2019 - 45th Annual Conference of the IEEE Industrial Electronics Society,* Lisbon, Portugal, Oct. 2019.

Aarniovuori, L., Kärkkäinen, H., Kosonen, A., Pyrhönen, J., Liu, Z. & Cao, W., 2017. "Overview of calorimetric systems used in loss determination of electric motors and drives". *in IECON 2017 - 43rd Annual Conference of the IEEE Industrial Electronics Society,* pp. 2110-2115, Beijing, China, Oct. 2017.

Aarniovuori, L., Musikka, T., Kosonen, A., Niemelä, M. & Pyrhönen, J., 2015. "Three alternative methods to determine voltage source converter losses". *in 17th European Conference on Power Electronics and Applications,* Geneve, Switzerland. Sept. 2015.

Aarniovuori, L., Niemelä, M., Pyrhönen, J., Cao, W. & Agamloh, E. B., 2018. "Loss Components and Performance of Modern Induction Motors". *in 2018 XIII International Conference on Electrical Machines (ICEM),* Alexandroupoli, Greece, Sept. 2018.

Aarniovuori, L., Rasilo, P., Niemelä, M. & Pyrhönen, J., 2016a. "Analysis of 37-kW Converter-Fed Induction Motor Losses". *IEEE Transactions on Industrial Electronics,* vol. 63, no. 9, pp. 5357-5365, Sept. 2016..

Boglietti, A., Cavagnino, T., Mthombeni, L. & Pillay, P., 2005. Comparison of lamination iron losses supplied by PWM voltages: US and European experiences. *in IEEE International Conference on Electric Machines and Drives,* San Antonio, Texas, May 2005.

Boldea, I. & Nasar, S. A., 2002. Airgap field space harmonics, parasitic torques, radial forces, and noise. Teoksessa: *The Induction Machine Handbook.* Boca Raton, FL: CRC Press, pp. 34-35.

de Almeida, A., Ferreira, F. & Baoming, G., 2014. "Beyond induction motors—Technology trends to move up efficiency". *IEEE Transactions on Industrial Applications,* Vol. 50, no. 3, pp. 2103–2114, May-June 2014.

Deusinger, B., Lehr, M. & Binder, A., 2014. Determination of efficiency of permanent magnet synchronous machines from summation of losses. *in 2014 International Symposium on Power Electronics, Electrical Drives, Automation and Motion,* Ischia, Italy, June 2014.

Doppelbauer, M., 2015. "Measurement uncertainty of direct and indirect efficiency testing of induction machines". *in 9th International Conference on Energy Efficiency in Motor Driven Systems (EEMODS'15),* Helsinki, Finland, Sept. 2015.

European Commission, 2009. Commission Regulation (EC) No 640/2009 of 22 July 2009 implementing Directive 2005/32/EC of the European Parliament and of the Council with regard to ecodesign requirements for electric motors. *Official Journal of the European Union,* Issue L 191, p. 26–34.

European Commission, 2019. *Energy efficiency – ecodesign requirements for electric motors.* [Online]
Available at:
https://ec.europa.eu/info/law/better-regulation/initiatives/ares-2018-5354258_en
[Accessed 26 November 2019].

Gamal Eldin, A. M., 2007. *Leakage and rotordynamic effects of pocket damper seals and see-through labyrinth seals.* Doctoral dissertation. College Station, Texas: Texas A&M University. Available at: http://hdl.handle.net/1969.1/ETD-TAMU-2084.

IEA, 2016. *World Energy Outlook 2016.* [Online]
Available at: https://doi.org/10.1787/weo-2016-en
[Accessed 26 November 2019].

IEC, 1974. Rotating electrical machines - Part 2: Methods for determining losses and efficiency of rotating electrical machinery from tests (excluding machines for traction vehicles) - Measurement of losses by the calorimetric method, First edition. *IEC 34-2A*.

IEC, 2010. Rotating electrical machines - Part 2-2: Specific methods for determining separate losses of large machines from tests - Supplement to IEC 60034-2-1. *60034-2-2*.

IEC, 2013. Rotating electrical machines - Part 2-3: Specific test methods for determining losses and efficiency of converter-fed AC induction motors, Edition 1. *IEC/TS 60034-2-3*.

IEC, 2014a. Rotating electrical machines - Part 30-1: Efficiency classes of line operated AC motors (IE code). *IEC 60034-30-1*.

IEC, 2014b. Rotating electrical machines - Part 2-1: Standard methods for determining losses and efficiency from tests (excluding machines for traction vehicles), Edition 2. *IEC 60034-2-1*.

IEC, 2016. Rotating electrical machines - Part 30-2: Efficiency classes of variable speed AC motors (IE-code). *IEC TS 60034-30-2*.

IEC, 2017. Adjustable speed electrical power drive systems - Part 9-2: Ecodesign for power drive systems, motor starters, power electronics and their driven applications - Energy efficiency indicators for power drive systems and motor starters. *IEC 61800-9-2*.

IEC, 2020. Rotating electrical machines - Part 2-3: Specific test methods for determining losses and efficiency of converter-fed AC motors, Edition 1. *IEC 60034-2-3*.

IEEE, 2017. IEEE Standard Test Procedure for Polyphase Induction Motors and Generators. *IEEE Std 112™-2017*.

JCGM, 2008. Evaluation of measurement data – Guide to the expression of uncertainty in measurement. *JCGM 100:2008*, September 2008.

Sander, J., 2016. "Efficient Motor Policy for Europe – view from CEMEP". *in Motor Summit 2016,* Zurich, Switzerland, Oct. 2016.

Yogal, N., Lehrmann, C. & Henke, M., 2018. "Determination of the Measurement Uncertainty of Direct and Indirect Efficiency Measurement Methods in Permanent Magnet Synchronous Machines". *in 2018 XIII International Conference on Electrical Machines (ICEM),* Alexandroupoli, Greece, Sept. 2018.

Appendix A: Deriving equations

Input-output efficiency uncertainty

Calculating the uncertainty for the efficiency result of the input–output method is not presented in any of the publications. The input–output efficiency is calculated from the input power P_{in} and the output power P_{out} as

$$\eta = \frac{P_{\text{out}}}{P_{\text{in}}} \tag{A.1}$$

The sensitivity coefficients of the efficiency for P_{in} and P_{out} are

$$c_{P_{\text{in}}} = \frac{\partial \eta}{P_{\text{in}}} = -\frac{P_{\text{out}}}{{P_{\text{in}}}^2} \quad \text{and} \quad c_{P_{\text{out}}} = \frac{\partial \eta}{\partial P_{\text{out}}} = \frac{1}{P_{\text{in}}}. \tag{A.2}$$

The uncertainty contribution that the input power has on the efficiency is

$$U(\eta)_{P_{\text{in}}} = \left|c_{P_{\text{in}}}\right| U(P_{\text{in}}) \tag{A.3}$$

and the contribution of the output power

$$U(\eta)_{P_{\text{out}}} = \left|c_{P_{\text{out}}}\right| U(P_{\text{out}}). \tag{A.4}$$

The uncertainty of the input–output efficiency is thus

$$U(\eta) = \sqrt{(U(\eta)_{P_{\text{in}}})^2 + (U(\eta)_{P_{\text{out}}})^2} \tag{A.5}$$

$$U(\eta) = \sqrt{\left(\left|-\frac{P_{\text{out}}}{{P_{\text{in}}}^2}\right| U(P_{\text{in}})\right)^2 + \left(\left|\frac{1}{P_{\text{in}}}\right| U(P_{\text{out}})\right)^2}. \tag{A.6}$$

Efficiency uncertainty when using an indirect method

When an indirect loss and efficiency determination method is used, the measured losses P_{loss} and either the input power P_{in} or the output power P_{out} are needed for calculating the efficiency. Using the indirect losses and the input power, the indirect efficiency is

$$\eta_{\text{indirect}}=\frac{P_{\text{in}}-P_{\text{loss}}}{P_{\text{in}}}=1-\frac{P_{\text{loss}}}{P_{\text{in}}} \tag{A.7}$$

The uncertainty of the indirect efficiency can be determined using the second form of (A.7). The sensitivity coefficients of the efficiency for P_{in} and P_{loss} are

$$c_{P_{\text{in}}}=\frac{\partial\eta_{\text{indirect}}}{P_{\text{in}}}=\frac{P_{\text{loss}}}{{P_{\text{in}}}^2} \quad \text{and} \quad c_{P_{\text{loss}}}=\frac{\partial\eta_{\text{indirect}}}{\partial P_{\text{loss}}}=-\frac{1}{P_{\text{in}}}. \tag{A.8}$$

The uncertainty contribution that the input power has on the efficiency is

$$U\left(\eta_{\text{indirect}}\right)_{P_{\text{in}}}=\left|c_{P_{\text{in}}}\right|U(P_{\text{in}}) \tag{A.9}$$

and the contribution of the losses

$$U\left(\eta_{\text{indirect}}\eta\right)_{P_{\text{loss}}}=\left|c_{P_{\text{loss}}}\right|U(P_{\text{loss}}). \tag{A.10}$$

The uncertainty of the indirect efficiency is thus

$$U\left(\eta_{\text{indirect}}\right)=\sqrt{\left(U\left(\eta_{\text{indirect}}\right)_{P_{\text{in}}}\right)^2+\left(U\left(\eta_{\text{indirect}}\right)_{P_{\text{loss}}}\right)^2} \tag{A.11}$$

$$U\left(\eta_{\text{indirect}}\right)=\sqrt{\left(\left|\frac{P_{\text{loss}}}{{P_{\text{in}}}^2}\right|U(P_{\text{in}})\right)^2+\left(\left|-\frac{1}{P_{\text{in}}}\right|U(P_{\text{loss}})\right)^2}. \tag{A.12}$$

Publication I

Kärkkäinen, H., Aarniovuori, L., Niemelä, M., and Pyrhönen, J.
Converter-fed induction motor losses in different operating points

18th European Conference on Power Electronics and Applications (EPE'16 ECCE Europe)
pp. 1-8, 2016

Converter-fed Induction Motor Losses in Different Operating Points

Hannu Kärkkäinen, Lassi Aarniovuori, Markku Niemelä and Juha Pyrhönen
LAPPEENRANTA UNIVERSITY OF TECHNOLOGY
P.O. Box 20, FI-53851
Lappeenranta, Finland
Fax: +358 5 621 6799
hannu.s.karkkainen@lut.fi
URL: http://www.lut.fi

Keywords

Adjustable speed drive, Induction motor, Measurement, Pulse Width Modulation

Abstract

The use of converters to feed the motors instead of the direct-on-line supply has increased the need to understand the losses of the induction machine in different operating points. Most of the earlier studies have focused on the losses with the nominal supply frequency while this study covers most of the frequency-torque plane below nominal values. A 15 kW standard squirrel-cage machine's losses are analyzed in 16 different operating points with torque values of 25 %, 50 %, 75 % and 100 % of motor rated torque and supply frequency values of 25 %, 50 %, 75 % and 100 % of rated motor frequency. Measurements in all 16 operating points are made with both sinusoidal generator supply and with frequency converter supply.

Introduction

The modern frequency converter allows precise control of motor speed and torque based on the application. With the usage of converters arises the need to understand the motor losses in different operating points. According to the widely used and investigated [1]–[8] standards IEC 60034-2-1 [11] and IEEE 112 [12], machine losses and efficiency are determined at the rated operating point(rated torque, rated speed, rated voltage). IEC methods for determining the losses and efficiency of converter-fed induction motors (IM) currently exist as technical specification IEC/TS 60034-2-3 [13], and also these methods aim for determining the losses and efficiency of IMs at rated motor conditions. The methodology of IEC/TS 60034-2-3 has been analyzed in some studies [8]–[10] and the complexity of the method, use of strictly specified converter waveform and the single rated operating point have been considered its main issues. IM losses and efficiency on converter supply and at different operating points have been inspected in [7], [8], [14] and [15]. However, none of these studies gives a wider perspective to the segregated motor loss components and converter-caused harmonic losses in relation to frequency and torque.

Induction motors are rated for the common grid frequencies of 50 Hz and 60 Hz. On frequency converter supply, the load torque and operating speed may vary on a wide operating range between 0 % and 100 % of their rated values and in some applications above the rated values, too. In addition, the fundamental voltage is adjusted depending on the operating point. All these three quantities also affect the motor losses and efficiency; hence, a single efficiency value is not enough to depict the efficiency of a converter-fed motor. In order to properly optimize the operation of a variable speed drive (VSD), the behavior of the motor losses over the full operating range needs to be determined.

In this paper, the losses and efficiency of a standard 15 kW four-pole squirrel-cage induction motor are determined on sinusoidal generator supply and on frequency converter supply at 16 different operating points. The motor plate values are listed in Table I. The motor loss components and loss difference between sinusoidal and pulse-width modulated (PWM) converter supply are calculated and analyzed at

Table I
Test motor nameplate values for 400 V, 50 Hz with Δ-connection

Variable	Value
Power	15 kW
Current	27.8 A
Voltage	400 V
Frequency	50 Hz
Speed	1474 r/min
Power factor	0.84
Efficiency	92.7 % (IE3)

each operating point in order to examine their dependence of torque and operating frequency. The aim is to clarify the behavior of the converter-caused additional harmonic losses over the frequency-torque plane.

Induction Motor Loss Components

Stator Joule losses are the resistive losses of the stator windings. They are often also called stator copper losses and are calculated by using the test resistance R_{H} and current I_{H} values

$$P_{\mathrm{s}} = 1.5 R_{\mathrm{H}} I_{\mathrm{H}}^2, \tag{1}$$

where I_{H} Is the stator phase current and R_{H} is the average winding line-to-line resistance. Stator copper losses are directly proportional to the stator resistance and proportional to the square of the stator winding current. Rotor Joule losses are the resistive losses of the rotor cage. They are produced by the current flowing in the rotor windings. The rotor winding losses are slip (s) related and are typically calculated with the well-known equation

$$P_{\mathrm{r}} = (P_1 - P_{\mathrm{s}} - P_{\mathrm{Fe}})s, \tag{2}$$

where $P_1$is the electric input power, P_{s} is the stator winding loss, P_{Fe} is the iron loss from the no-load test and s is the per-unit slip. Iron losses are the magnetic circuit losses occurring in the stator and rotor core. The iron losses are calculated from

$$P_{\mathrm{Fe}} = P_{\mathrm{c}} - P_{\mathrm{fw}}, \tag{3}$$

where P_{fw} are the friction and windage losses and the P_{c} is the constant loss that is defined by subtracting the stator resistive losses $P_{\mathrm{s},0}$ from the electric input power P_0 during the no-load test. The friction and windage losses include the motor mechanical losses caused by air resistance of the rotor fan and the rotor, and friction of the bearings. The friction losses are typically directly proportional to speed and the windage losses are typically proportional to the square of the speed. The friction and windage losses can be determined from the no-load test, but here it is more convenient to use the retardation test, which gives the result for each operating speed. Therefore, only a shorter no-load test is required at each operating frequency to determine the constant losses for iron loss calculation with (3).

Stray-load losses are the losses caused by non-idealities of the practical machine, e.g. air-gap space harmonics, and supply voltage time harmonics. The stray-load losses are typically considered proportional to the square of torque. In the loss segregation methods of [11] and [12], the stray-load losses P_{LL} are determined with the load curve test from the residual losses. The residual losses P_{Lr} are the difference between input-output losses and the stator and rotor copper losses, iron losses and friction and windage losses

$$P_{\mathrm{Lr}} = P_1 - P_2 - P_\mathrm{s} - P_\mathrm{r} - P_{\mathrm{Fe}} - P_{\mathrm{fw}}, \tag{4}$$

where P_2 is the output mechanical power. P_{Lr} is calculated for each load point and relationship of P_{Lr} as function of torque squared is smoothed by linear regression resulting in

$$P_{\mathrm{Lr}} = AT^2 + B, \tag{5}$$

where A and B are constants from the linear regression. The stray-load loss-curve

$$P_{\mathrm{LL}} = AT^2 \tag{6}$$

is formed from the P_{Lr}-curve by removing the constant B. [11]

Removing the constant B from (5) is based on the assumption that the stray-load losses only exist with load and that the constant B is result from measurement errors. However, by determining all torque measurement offset errors and taking them into account in the analysis, the value of B is reduced to near zero. Therefore, here the residual loss value calculated with (4) for each operating point is used to represent the stray-load losses directly. The total motor losses are the sum of the loss components

$$P_{\mathrm{tot}} = P_{\mathrm{LL}} + P_\mathrm{s} + P_\mathrm{r} + P_{\mathrm{Fe}} + P_{\mathrm{fw}} \tag{7}$$

and the motor efficiency

$$\eta = \frac{P_1 - P_{\mathrm{tot}}}{P_1}, \tag{8}$$

where P_1 is the electric input power. [11]

Frequency converter PWM-voltage contains high amount of time harmonics. The higher harmonic content of the PWM-voltage supply creates additional losses in the machine. The increased losses in the machine increase the machine temperature and have a follow-on effect increasing the temperature related loss components. The additional harmonic losses P_{HL} can be calculated as the difference of the total losses $P_{\mathrm{tot,Con}}$ with frequency converter supply and total losses with sinusoidal supply

$$P_{\mathrm{HL}} = P_{\mathrm{tot,Con}} - P_{\mathrm{tot}}. \tag{9}$$

However, using (9) requires that the motor fundamental voltage, fundamental frequency and load are matched properly when determining $P_{\mathrm{tot,Con}}$ and P_{tot}, since they all affect the motor losses. Harmonic loss ratio r_{HL} represents the amount of the harmonic losses of the total losses and is defined with

$$r_{\mathrm{HL}} = \frac{P_{\mathrm{HL}}}{P_{\mathrm{tot}}} \cdot 100\ \%, \tag{10}$$

where P_{tot} are the total losses with sinusoidal supply [13].

Experimental measurements

The measurements were performed on a standard 15 kW squirrel cage induction motor with frequency converter supply and with sinusoidal generator supply at 16 different operating points. The used load torque values were 25 %, 50 %, 75 % and 100 % of the motor rated torque. The supply fundamental frequencies used in the measurements were 25 %, 50 %, 75 % and 100 % of rated motor frequency. The measurements with frequency converter supply were made first and matching fundamental voltage and

frequency were then used at each of the 16 load point measurements with sinusoidal supply. In addition, no-load voltage curve tests were made with sinusoidal supply at each four operating frequencies to determine the iron losses. Several retardation tests were also made at different motor temperatures to determine the friction and windage losses for each load point.

Measurement setup

The measurement setup consisted of the 15 kW IM, a larger IM for mechanical load, instruments for measuring and recording data and the frequency converter or generator for power supply. The electric quantities, including voltage and current waveforms were measured with Yokogawa PX8000 power analyzer. PX8000 was equipped with Hitec Zero-Flux CURACC current measuring system. Winding resistance and temperatures were measured with Keithley Integra Series 2701 Ethernet multimeter systems. The stator winding resistance was measured using four-wire method. Ambient temperature was measured with four A-class Pt100 sensors approximately 20 cm behind the motor air inlet. Stator winding temperature was measured with a two-wire B-class Pt100 sensor from the winding end surface. HBM T12 digital torque measurement system with rated torque of 100 Nm was used for measuring the mechanical torque and operating speed. All measurement data was gathered with a LabVIEW™ interface on a PC. In the sinusoidal supply tests, the electric power was supplied by a converter-fed IM driven synchronous generator. The mechanical load was created with a line converter driven 37 kW induction machine. In the retardation tests, an optical incremental encoder was used for measuring the rotational speed.

The frequency converter used in the measurements was set to use classic space vector modulation and all feedback features and corrections including efficiency optimizations were disabled. Therefore, the measurements were made with constant U/f ratio, which does not represent the typical converter-fed motor operation, but is more relevant when examining behavior of the motor losses. The converter carrier frequency was set to 4 kHz. Also the switching frequency was 4 kHz in all measurements, which was confirmed by analyzing the waveform data recorded at the end of each load point measurement. The intermediate circuit DC voltage was adjusted to 623 V, which was high enough to avoid overmodulation in the most demanding 50 Hz point at rated motor load. The DC voltage was checked and readjusted every for each load point measurement and the measured value was 622 V – 624 V in all the 16 measurements.

Matching the load points with sinusoidal supply and converter supply

The fundamental voltage and fundamental frequency of the measurements with sinusoidal generator supply were adjusted to match the converter supply values as closely as possible: The fundamental voltage difference was less than 0.12 % and the fundamental frequency difference less than 0.04 % between the measured values at each 16 load points. Before taking recordings of each operating point, motor thermal equilibrium was established. The motor winding temperature change was less than 0.35 K during the last 30 min before each of the 32 measurements. The same load torque reference was used with both sinusoidal supply and converter supply and also the load torque match was very precise differences being less than 0.04 % in all 16 load points. The torque offset caused by axle support bearings and the torque transducer offset were determined and taken into account in calculations.

The motor loss components for each of the operating points were calculated with (1)–(4) and from the retardation test. The test resistance R_H was determined from the temperature-resistance curve for each load point temperature. The load torque altered slightly between different operating frequencies and therefore all calculated quantities were adjusted to match the target operating point torque (25 %, 50 %, 75 % or 100 % of rated motor load). The temperature dependent resistive loss components and the total losses were also corrected to 25 °C ambient temperature. The friction and windage losses were determined from the retardation test calculations according to each load point operating speed and the 25 °C ambient temperature corrected operating temperature. From the 16 measurement points, the loss data was interpolated over the frequency-torque (*f*-*T*) plane from 20–103 % rated motor torque and 10–51.5 Hz fundamental motor supply frequency.

Results

The segregated loss components, total losses, efficiency and the differences between converter supply and sinusoidal supply are presented with contour-plots in Fig. 1 – Fig. 6. The target operating points are marked with "x" in the charts. The stator and rotor Joule losses are presented in Fig. 1 and Fig. 2. As could be expected, the resistive winding losses depend almost purely on the load torque. Both stator and rotor Joule losses show some increase towards low operating frequencies especially at high loads. This is caused by the stator winding voltage drop becoming more prominent at low frequencies and voltages, which results in flux reduction and increase in stator and rotor currents. This behavior is typically compensated by converters increasing the fundamental voltage slightly above the U/f ratio to keep the flux level constant.

Plot c on the right-hand side in Fig. 1 and Fig. 2 shows the converter-caused loss increase as percentage. Both show mostly similar dependence on load and operating frequency. At high loads the loss increase is mainly load dependent. Below 70 – 80 % rated load, the frequency dependence is more prominent and the highest loss increases are around the 25 Hz frequency. However, it should be noted that the determined differences at low loads are only a few watts, although the frequency-dependent behavior spans over several measurement points.

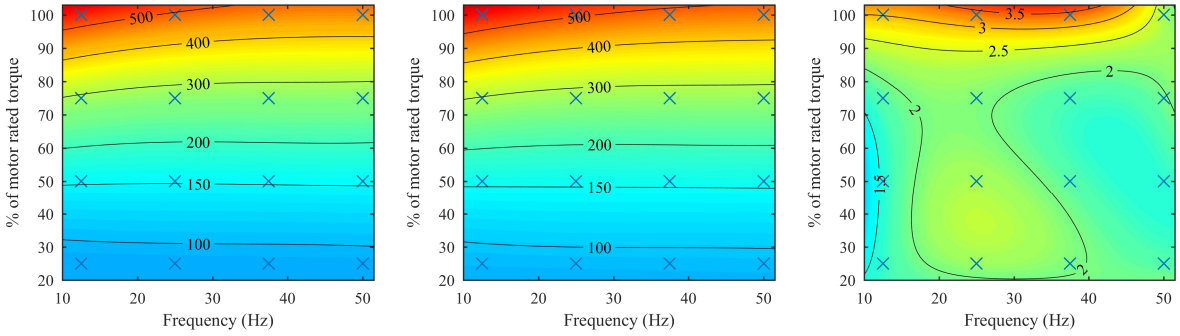

(a) P_s with sinusoidal supply (W) (b) P_s with converter supply (W) (c) P_s increase (%)

Fig. 1: Stator Joule losses P_s of the 15 kW IM with sinusoidal generator supply and with frequency converter supply over the *f*-*T*–plane. The third plot shows the percentage of the loss increase with converter supply in comparison to generator supply.

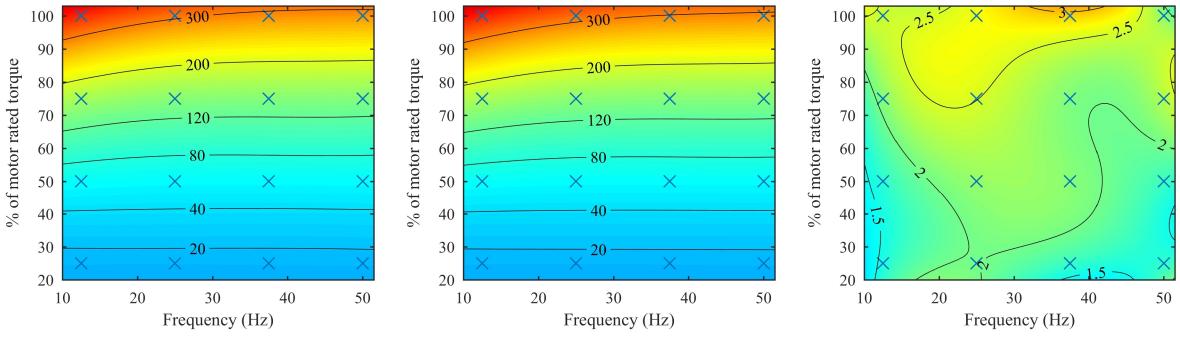

(a) P_r with sinusoidal supply (W) (b) P_r with converter supply (W) (c) P_r increase (%)

Fig. 2: Rotor Joule losses P_r of the 15 kW IM with sinusoidal generator supply and with frequency converter supply over the *f*-*T*–plane. The third plot shows the percentage of the loss increase with converter supply in comparison to generator supply.

The friction and windage losses, fundamental iron losses and stray-load losses are shown in Fig. 3. All these three loss components are shown only for sinusoidal supply. The friction and windage loss values at the converter supply test temperatures are used in calculations, but the differences are only fractions of a watt and therefore are presented with only one plot. Also, in reality, the PWM-caused vibrations may affect the friction losses, which cannot be determined with retardation test. The friction and windage losses, being dependent on the rotor speed, change only slightly with load (and slip).

The fundamental iron losses are also affected mainly by the operating frequency, although they too show some load dependence, which is caused by the stator winding resistance voltage drop. The harmonic iron losses with converter supply comprise a major part of the additional harmonic losses [16], but there are currently no practical means to segregate the iron losses from the friction and windage losses and rotor losses with measurements at sufficient accuracy.

The stray-load losses with sinusoidal supply depend from both load torque and operating frequency in approximately equal manner. The stray-load losses with frequency converter supply cannot be calculated since the iron losses with converter supply are not known. Also, the whole term stray-load loss is rather difficult in this context, since by definition the stray-load losses include all time harmonic losses.

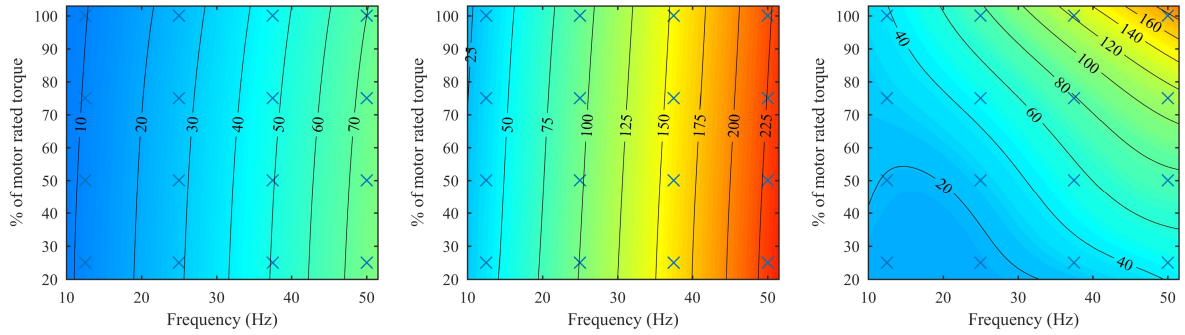

(a) P_{fw} with sinusoidal supply (W) (b) P_{Fe} with sinusoidal supply (W) (c) P_{LL} with sinusoidal supply (W)

Fig. 3: Friction and windage losses P_{fw}, iron losses P_{Fe} and stray-load losses P_{LL} of the 15 kW IM with sinusoidal generator supply over the *f*-*T*–plane.

The total losses on are shown in Fig. 4 and the distribution is very similar with both sinusoidal and converter supply. The additional harmonic losses presented in Fig. 5a are the difference of the total losses and the harmonic loss ratio in Fig. 5b depicts the relative proportion of the converter-caused motor loss increase.

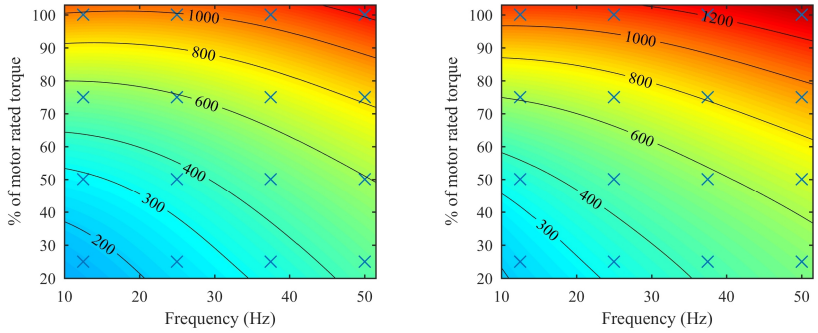

(a) Total losses with sinusoidal supply (W) (b) Total losses with converter supply (W)

Fig. 4: Total segregated losses of the 15 kW IM with sinusoidal generator supply and with frequency converter supply over the *f*-*T*–plane.

According to Fig. 5a, the additional harmonic losses (P_{HL}) are dependent on both load and operating frequency. P_{HL} seems to increase with load over the whole plotted operating frequency range. The highest P_{HL} values along the frequency-axle, on the contrary, are located at around 30 Hz at lower loads and at approximately 40 Hz at the rated motor load. Although the P_{HL} values are decreases with operating frequency, the relative proportion of the additional harmonic losses increases significantly towards lower loads and operating frequencies as shown in Fig. 5b.

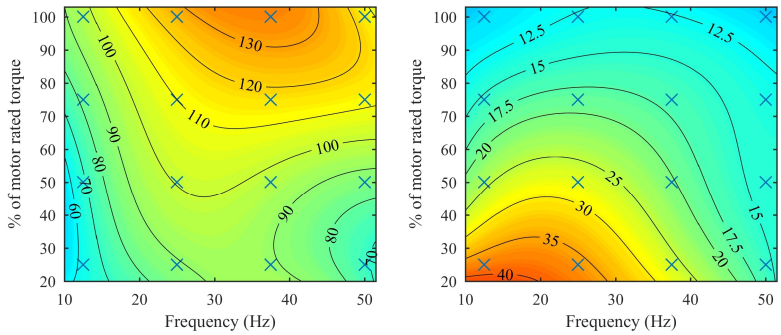

(a) Total additional harmonic losses (W) (b) Harmonic loss ratio (%)

Fig. 5: Total additional harmonic losses and harmonic loss ratio of the 15 kW IM determined from the difference of the total losses with converter supply and with sinusoidal supply.

The motor efficiency on sinusoidal supply and on frequency converter supply are presented in Fig. 6. The efficiency distributions are similar and the 15 kW IM reaches its highest efficiency at around 60 – 70 % load with 50 Hz and at around 50 % load with lower operating frequencies. The converter-caused efficiency drop shown in Fig. 6c is at lowest near the rated operating point and increases when the load or the operating frequency is reduced.

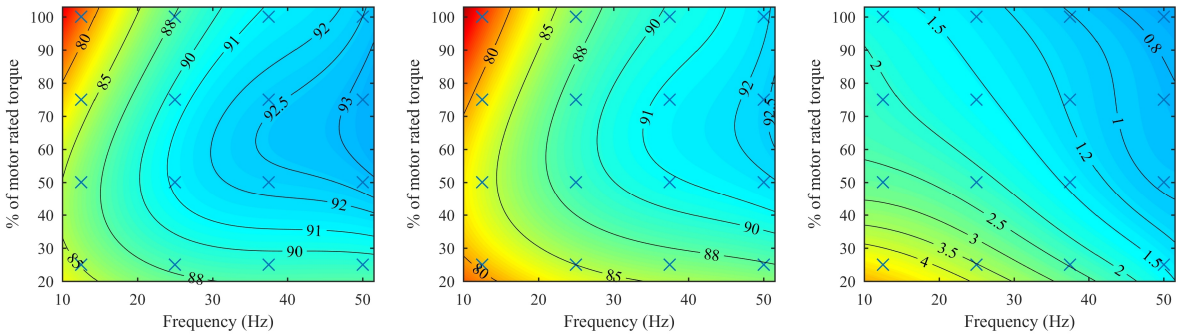

(a) Efficiency with sinusoidal supply (%) (b) Efficiency with converter supply (%) (c) Efficiency difference [%-unit]

Fig. 6: Efficiency of the 15 kW IM with sinusoidal generator supply and with frequency converter supply over the *f*-*T*–plane. The third plot shows the decrease of motor efficiency with converter supply in comparison to generator supply.

Discussion

The measurement results presented in this paper are aimed for clarifying the behavior of the induction motor loss components and the additional harmonic losses. The well-known U/f optimizations, for instance, are used to optimize the loss behavior. Typically, commercial frequency converters have also other methods to optimize the motor loss behavior over the operating range. All these feedback and correction features were specifically disabled for these measurements to avoid them from influencing the results.

The 15 kW TEFC IM used in the measurements has a typical cooling solution where the cooling fan is attached to the motor axle and therefore the cooling capacity depends on the operating speed. Since the motor losses are higher with frequency converter supply at the same load and operating speed, the motor temperature was approximately 3 – 6 K higher in the converter measurements. With external cooling, the loss results would be different. However, this type of motor used here is the most common type in the industry.

The iron losses, friction and windage losses and the additional load losses cannot be separated with measurements in any practical way. For determining the harmonic iron losses, simulations with finite element methods are probably the only viable solutions.

Conclusion

Understanding the behavior of the different motor loss components over the full operating range is beneficial when optimizing a variable speed drive. In case of a self-cooling motor, such as a typical totally enclosed fan-cooled induction motor, also the cooling power is dependent of the operating speed. The reduced cooling along with the knowledge of the motor loss components at low speeds can be taken into account in thermal design of a VSD duty cycle. In addition, the motor design is usually based on only sinusoidal supply at nominal 50 Hz or 60 Hz frequency. The results of this paper may help to take into account a wider operating range in the motor design stage also.

References

[1] W. Cao, "Comparison of IEEE 112 and New IEC Standard 60034-2-1", IEEE Trans. Energy Convers., vol. 24, no. 3, pp. 802–808, September 2009.

[2] A. Boglietti, A. Cavagnino, and S. Vaschetto, "Induction motor EU standards for efficiency evaluation: The scenario after IEC 60034-2-1", in Proc. 37th Conf. on IEEE Industrial Electronics Society, Melbourne, Australia, pp. 2786–2791, November 2011.

[3] C.S. Gajjar, J.M. Kinyua, M.A. Khan and P.S. Barendse, "Analysis of a Non-Intrusive Efficiency Estimation of Induction Machines Compared to the IEEE 112B and IEC 34-2-1 Standards", IEEE Trans. on Ind. Appl., early access, 2015.

[4] A. Boglietti, A. Cavagnino, M. Lazzari and M. Pastorelli, "International Standards for the Induction Motor Efficiency Evaluation: A Critical Analysis of the Stray-Load Loss Determination", IEEE Trans. on Ind. Appl., vol. 40, no. 5, pp. 1294-1301, September/October 2004.

[5] A. Boglietti, A. Cavagnino, L. Ferraris, and M. Lazzari, "Impact of the supply voltage on the stray-load losses in induction motors", IEEE Trans. Ind. Appl., vol. 46, no. 4, pp. 1374–1380, July/August 2010.

[6] W. Cao, "Assessment of induction machine efficiency with comments on new standard IEC 60034-2-1", in Proc. 18th Int. Conf. on Electrical Machines, Vilamoura, Portugal, pp. 1–6, September 2008.

[7] L. Aarniovuori, A. Kosonen, M. Niemelä, and J. Pyrhönen, "Frequency converter driven induction motor losses", in Proc. IECON 2013 - 39th Annual Conference of the IEEE Industrial Electronics Society, Nov. 2013, pp. 2881–2886.

[8] A. de Almeida, F. Ferreira, and A. Quintino Duarte, "Technical and economical considerations on super high-efficiency three-phase motors", IEEE Trans. Ind. Appl., vol. 50, no. 2, pp. 1274–1285, March 2014.

[9] R. Antonello, F. Tinazzi, M. Zigliotto, "Energy efficiency measurements in IM: The non-trivial application of the norm IEC 60034-2-3:2013", in Proc. 2015 IEEE Workshop on Electrical Machines Design, Control and Diagnosis (WEMDCD), Torino, Italy, pp. 248–253, March 2015.

[10] A. Boglietti, A. Cavagnino, M. Cossale, A. Tenconi, "Efficiency determination of converter-fed induction motors: Waiting for the IEC 60034–2–3 standard" Proc. 2013 IEEE Energy Conversion Congress and Exhibition, pp. 230–237, Denver, Colorado, USA, September 2013.

[11] Rotating electrical machines – Part 2-1: Standard methods for determining losses and efficiency from tests (excluding machines for traction vehicles), Ed. 2, IEC 60034-2-1, June 2014.

[12] IEEE standard test procedure for polyphase induction motors and generators, IEEE Std 112-2004, November 2004.

[13] Rotating electrical machines – Part 2-3: Specific test methods for determining losses and efficiency of converter-fed AC induction motors, Ed. 1, IEC 60034-2-3, November 2013.

[14] L. Aarniovuori, M. Niemelä and J. Pyrhönen, "PWM Effect on motor losses and temperature rise", in Proc. 8th Int. Conf. on Energy Eff. in Motor Driven Systems, pp. 23-33, Rio de Janeiro, Brazil, October 2013.

[15] M. Benhaddadi, F. Landry, R. Houde and G. Olivier, "Energy efficiency electric premium motor driven systems" in Proc. 2012 International symposium on power electronics, electrical drives, automation and motion, Sorrento, Italy, pp. 1235–1239, June 2012.

[16] Z. Gmyrek, A. Boglietti, A. Cavagnino, "Estimation of Iron Losses in Induction Motors: Calculation Method, Results, and Analysis," IEEE Trans. on Ind. Electron, vol. 57, no. 1, pp.161–171, January 2010.

Publication II

Kärkkäinen, H., Aarniovuori, L., Niemelä, M., and Pyrhönen, J.
Converter-Fed Induction Motor Efficiency: Practical Applicability of IEC Methods

IEEE Industrial Electronics Magazine
Vol. 11, pp. 45-57, 2017

Converter-fed Induction Motor Losses and Efficiency

Practical Applicability of IEC Methods

Hannu Kärkkäinen, Lassi Aarniovuori, Markku Niemelä, and Juha Pyrhönen
Lappeenranta University of Technology
LUT School of Energy Systems, Electical Drives Lab.
P.O. Box 20, FI-53851 Lappeenranta, Finland
hannu.s.karkkainen@lut.fi

Abstract— Electric motors consume a major proportion of the world's electric energy. Over the recent years, new regulations on the efficiency of electric motors have been introduced around the world. Reductions in the energy consumption of motors can be achieved by steering the industry to use more efficient motors but also by encouraging the application of frequency converters to supply motors. Related to this progress, International Electrotechnical Commission (IEC) is preparing standards for converter-fed motor efficiency measurements. Existing efficiency measurement standards cover only direct-on-line motors, and there is a strong demand for standardized classification measurements for converter-fed motor efficiency. The current IEC methods for determining losses and efficiency of converter-fed induction motors have been introduced as a technical specification while the standardization is still in process. Therefore, it is important to promote critical discussion about the issue in general. In this article, the IEC loss segregation methodology for converter-fed motors is described, executed in practice, and analyzed. Some features of the IEC main method, such as the strictly defined converter voltage waveform and the single motor rated determination point, have been criticized in previous articles and these issues are addressed in detail. Laboratory measurements are made with two frequency converters; the first converter is set to provide the IEC-defined voltage modulation, and the second converter represents a practical case, a commercial frequency converter for comparison. The IEC loss segregation for converter-fed motors is found to be usable for motor loss comparison purposes, but the method itself is complex to apply. Further, the method cannot be used to predict the losses of a variable speed drive system in an end user application.

***Index Terms*—Induction motors, variable speed drives, IEC standards, energy efficiency, loss measurement, pulse width modulation.**

Introduction

Energy efficiency is an important topic when considering the electric motor drives market. Electric motors consume a major proportion of the world's electric energy, and new regulations on the efficiency of motors have been introduced around the world over the recent years. Reductions in the energy consumption of motors can be achieved by steering the industry to use more efficient motors but also by encouraging the application of frequency converters to supply motors. Related to this

progress, the International Electrotechnical Commission (IEC) has revised standards for direct-on-line motor efficiency measurements and is also preparing corresponding standards for converter-fed motors. The recent developments and the current status of upcoming IEC motor standards were presented by the IEC technical committee chairman in Motor Summit 2016 [1]. For further insight into global standards, the worldwide industry requirements for electric motors are surveyed in [2].

Although there are more efficient electric motor types available, the induction motor (IM) remains by far the most common industrial motor type [3], and therefore, it is natural that IMs are first to receive new regulations and standards. The IEC [4] specifies four International Efficiency (IE) classes for single-speed (direct-on-line, DOL), three-phase, cage induction motors: IE4 – Super Premium, IE3 – Premium, IE2 – High, and IE1 – Standard Efficiency. In [4], also IE5 class is envisaged to be incorporated in the next edition of the standard and its goal is to further reduce the losses by some 20% from IE4 levels. The motor efficiency levels must be based on low uncertainty tests specified in [5]. The European Commission has defined that the efficiency classification of new induction motors with DOL supply must be IE3 or better [6]. The IE3 requirement has been put into action gradually, and from the 1st of January 2017 onwards, it covers all induction motors with a rated output power of 0.75 kW–375 kW. The EU regulation allows a lower IE2 classification for motors fed with a frequency converter, which is related to the lower total power consumption of the speed-controllable drive system in several applications in comparison with a DOL motor. When a motor is supplied by a frequency converter, additional losses are generated in the motor because of the supply harmonics, but the ability to adjust the motor speed according to the load often results in a lower overall energy consumption. The benefits of converter-fed motors are also reflected in the market; while the market share of motors with variable speed drives was 30% in 2014, it has been anticipated to rise to 50% by 2020 [7].

Converter-fed motors do not have IE classes of their own or final standards for efficiency determination yet. The rising popularity of variable speed drives has increased the demand for standardized motor efficiency measurements and classification also for nonsinusoidal, adjustable frequency supply. Furthermore, frequency converters – in tandem with the tightening efficiency requirements – enable newer, more efficient electric motor technologies, such as permanent magnet synchronous machines (PMSM) [8], [9] and synchronous reluctance machines (SynRM) [9], [10], to become potentially strong alternatives for the induction motor. PMSMs and SynRMs can be equipped with line start capabilities but for these machine types converter supply is the optimal solution

regarding the machine structure and efficiency. According to [9], only medium to large IMs (>30 kW) are likely to achieve the upcoming IE5 efficiency class, while PMSMs and SynRMs may reach it in also the low power range. In the case of PMSM, the machine cost has been a prohibiting factor for the popularity of the machine type, but taking the lifetime energy cost into account, a converter-fed PMSM may become a very cost effective solution. However, comparisons between different motor technologies are not straightforward without common efficiency standards.

The current IEC methods for loss and efficiency determination of converter-fed induction motors have recently been released as the technical specification IEC/TS 60034-2-3 [11]. The methodology of the technical specification is based on determining the additional converter-caused motor losses as the difference in test results between converter supply and sinusoidal supply at the motor rated fundamental voltage and frequency. The technical specification has been analyzed in [12]–[14], and determination of the motor losses at a single rated operating point with a strictly defined converter pulse width modulated (PWM) waveform has been seen as a weakness of the methodology. In [15] it is also pointed out that the 50 Hz rated voltage operating point is complicated for converter-fed motor analysis because, the motors often run in the field weakening with converter supply at this frequency. While standardization is still in process and the current test methods cover only IMs, in the future, all motor types will be included in the same efficiency standard. Therefore, it is important to encourage critical discussion about the issue in general.

The losses and efficiency of induction motors have been a frequent topic in IEEE journals [12], [15]–[21]. Although determination of high-efficiency motor losses is always challenging, converter-fed motors with PWM supply voltage add even more challenge to the motor efficiency determination. The loss distribution of a PWM inverter-fed and sinusoidal-fed three-phase IM is compared in [22], and time-stepped finite element analysis is used to segregate the motor loss components. The losses of the machine are a function of fundamental voltage waveform, load condition, and PWM switching conditions. In [22] it is also shown that the additional stray loss caused by PWM supply (when compared with sinusoidal supply) is a function of these factors. A measurement-based segregation and analysis of converter–fed IM loss components over a wide operating range is presented in [23], showing a significant dependence of the converter-caused harmonic losses on both the motor load and the operating frequency. A method for determining the harmonic losses of a converter-fed IM by both calculation and measurement is introduced in [24], and the dependence of the harmonic losses on the

pulse frequency is shown. The impact of PWM switching schemes on power losses in IMs is investigated in [15] and [25]–[28]. In [29], an analytical approach to predict the PWM supply eddy-current loss dependence on the modulation index is proposed. Experimental results shown in [30] and [31] confirm the dependence on the PWM iron loss modulation index, which can also be seen in the results of [23]. A careful analysis of iron losses under PWM supply is provided in [21]. The impact of overmodulation on inverter and motor losses in induction motor drives is analyzed in [32]. In addition, options for nonintrusive inverter-fed IM efficiency estimation with limited measurement values are considered and analyzed in [16].

In this article, the methodology of IEC/TS 60034-2-3 (IEC/TS) is investigated. Laboratory measurements are made on a standard 15 kW totally enclosed fan-cooled (TEFC) induction motor. To analyze the feasibility of the IEC/TS method with different frequency converters and nonfixed supply waveforms, two distinct frequency converters are used in the measurements. The first frequency converter is set to provide the IEC-pre-defined PWM-voltage waveform, and the second converter applies classical direct torque control (DTC) with a 25 μs minimum pulse width resulting in a completely different PWM voltage waveform compared to the standard waveform. The DTC may be regarded as a control method, but it results in a typical nondeterministic PWM waveform, however in practice, converging towards the space-vector-modulated output in the steady state. The tests according to the IEC/TS indirect method are run on both converters with artificially increased converter input voltage, resulting in the motor rated fundamental voltage at the motor rated frequency of 50 Hz as required by the IEC/TS. This feature of the method has justifiably been criticized as such operating points are typically available only in cases where the converter has an active DC voltage boosting rectifier. Therefore, for comparison and for practical interest, the tests are run with both converters also at the normal 400 V grid input voltage, which results in a lower motor fundamental voltage and a reduced flux level, but should be clearly more relevant from the practical point of view.

The IEC/TS main method requires indirect IEC measurements with sinusoidal supply. Therefore, the induction motor losses with the recently updated IEC 60034-2-1 [5] summation of losses method 2-1-1B are determined. The IEC 60034-2-1 loss segregation method 2-1-1B is similar to the corresponding IEEE 112 [33] method B, and these methods are widely used and investigated [12], [34]–[38]. In addition to the indirect results, direct input-output losses and efficiencies are calculated from all measurements with converter supply and with sinusoidal supply for comparison. The direct

losses and efficiency are of interest also because the input-output measurements are applicable to all machine technologies while the IEC/TS indirect methods can only be used with induction machines.

Technical specification IEC/TS 60034-2-3

The technical specification IEC/TS 60034-2-3 [11] defines four methods for determining losses and efficiency of converter-fed induction motors. The methods are listed in Table 1; the main interest lies in the first two indirect loss segregation methods 2-3-A and 2-3-B. The method 2-3-A requires an IEC-defined converter PWM waveform to make the results comparable between different frequency converter hardware. The term 'test converter' is used in the IEC/TS (and correspondingly, also in this article) to refer to the frequency converter producing this IEC/TS-defined, strictly fixed, PWM waveform. For the test converter operation and waveform, the frequency converter has to meet several requirements, including for instance the following:

- The frequency converter has to be a two-level voltage source converter.
- Fixed converter switching frequency is to be used (4 kHz if motor rated power ≤ 90 kW, 2 kHz if > 90 kW).
- Motor rated fundamental voltage and frequency are required at the converter output.
- Slip compensation and current feedback control must be deactivated.

The second indirect method, 2-3-B, is similar to the test converter method, but it is intended for determining motor losses with the frequency converter that will be used with the motor in the final application. The other two methods defined in the IEC/TS, the input-output method 2-3-C and the calorimetric method 2-3-D, are similar to the methods defined for line-fed motors in [5] and [39].

Loss segregation methodology

The IEC/TS indirect methods apply the procedures defined for line-fed motors in the IEC 60034-2-1 [5] method 2-1-1B, which is the IEC-recommended loss segregation method for line-fed three-phase induction motors. This referencing to the standard makes the procedures ambiguous at some points,

TABLE 1 - IEC/TS 60034-2-3 test methods.

Method	Description
2-3-A: Summation of losses with test converter supply	Loss segregation. Requires IEC-defined test converter supply and variable voltage sinusoidal supply.
2-3-B: Summation of losses with specific converter supply	Loss segregation. Similar to method 2-3-A but is used with the frequency converter for the final application.
2-3-C: Input-output method	Total losses are found as the difference between direct input and output power measurements.
2-3-D: Calorimetric method	Total losses are determined from the heat generated by the motor. Suitable for water cooled motors. Procedure according to IEC 60034-2-2 [39].

and in the previous articles [12]–[14] there have been differences in the interpretations. For this reason, the IEC/TS loss segregation methodology is explained at length in the following.

Figure 1 illustrates the full measurement procedure of the IEC/TS method 2-3-A. As shown in Figure 1, the method 2-3-A first includes the full loss segregation measurement procedure of the IEC method 2-1-1B with sinusoidal supply. After this, the measurements with frequency converter supply are made, and also these are performed according to the same tests defined in the method 2-1-1B.

The standard loss segregation with sinusoidal supply is based on three separate tests: rated load test (Step I), load curve test (Step II), and no-load test (Step III). In the rated load test, the motor is heated up to thermal equilibrium before recording data. The load curve test is performed with the hot motor immediately after the rated load test, or alternatively, the motor must be re-heated until the winding temperature is within 5 K of the rated load test temperature. The no-load test is performed immediately after the load curve test with the hot motor. Stator copper losses and rotor copper losses are determined from the rated load test (Step I); constant losses, friction and windage losses, and iron losses are calculated from the no-load test (Step III). The load curve test (Step II) is needed for determining the stray-load losses.

In the IEC/TS, the additional harmonic losses caused by the PWM converter supply are understood as the difference in the motor losses with frequency converter supply and with sinusoidal supply. Therefore, a full six-point load curve test (Step IV) and a single voltage point no-load test (Step V) are performed with converter supply at the motor rated fundamental voltage and frequency, as illustrated in Figure 1. From the load curve test (Step IV), the stray-load losses are determined for the converter-

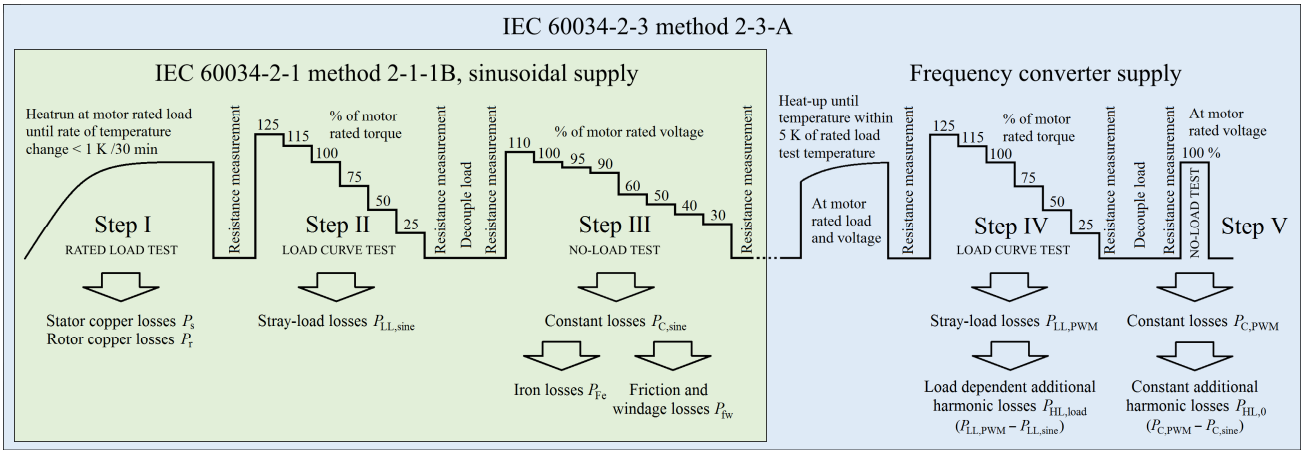

FIGURE 1 – The five-step measurement procedure of the IEC 60034-2-3 method 2-3-A for determining the segregated loss components of a converter-fed induction motor.

fed motor. The load-dependent part of the additional harmonic losses is the difference in the stray-load losses with converter supply and with sinusoidal supply (Steps IV and II). Similarly, the constant part of the additional harmonic losses is the constant loss difference at the rated voltage no-load test points with converter supply and with sinusoidal supply (Steps III and V).

The main equations needed in the calculations of the IEC/TS indirect method are listed in Table 2. The stator copper losses P_s are the resistive I^2R losses of the stator windings (1). The rotor copper losses P_r are calculated from the slip s and the air-gap power (2). For final rated load values, the copper losses are corrected to 25 °C ambient temperature with (21)–(23). The constant losses P_C are the sum

TABLE 2 - The main equations needed in the motor loss calculations of the IEC 60034-2-3 method 2-3-A [5], [11]. The variables are according to the IEC [5], [11], except in subscripts there are some additions, such as "sine" and "PWM", for clarity. The steps I–V refer to the tests required for each calculation, see Figure 1.

	Step	Sinusoidal supply		Frequency converter supply		Step
Stator copper losses	I	$P_s = I^2R$	(1)			
Rotor copper losses		$P_r = (P_1 - P_s - P_{Fe})s$	(2)			
Constant losses	II	$P_{C,sine} = P_{fw,0} + P_{Fe,0} = P_{1,0,sine} - P_{s,0,sine}$	(3)	$P_{C,PWM} = P_{1,0,PWM} - P_{s,0,PWM}$	(11)	IV
Friction and windage losses		$P_{fw,0} = P_C(0\,\mathrm{V})$	(4)			
Iron losses		$P_{Fe,0} = P_C - P_{fw,0}$	(5)			
Residual losses	III	$P_{Lr,sine} = P_{1,sine} - P_{2,sine} - P_s - P_r - P_{fw} - P_{Fe}$	(6)	$P_{Lr,PWM} = P_{1,PWM} - P_{2,PWM} - P_s - P_r - P_{fw} - P_{fe}$	(12)	
Linearized residual losses		$P_{Lr,sine} = A_{sine}T^2 + B_{sine}$	(7)	$P_{Lr,PWM} = A_{PWM}T^2 + B_{PWM}$	(13)	V
Stray-load losses		$P_{LL,sine,N} = A_{sine}T_N^2$	(8)	$P_{LL,PWM,N} = A_{PWM}T_N^2$	(14)	
Load dependent additional harmonic losses				$P_{HL,load} = P_{LL,PWM,N} - P_{LL,sine,N}$	(15)	II & IV
Constant additional harmonic losses				$P_{HL,0} = P_{C,PWM} - P_{C,sine}$	(16)	III & V
Total additional harmonic losses				$P_{HL} = P_{HL,0} + P_{HL,load}$	(17)	II–V
Total losses	I–III	$P_{tot,sine} = P_{s,N,\theta} + P_{r,N,\theta} + P_{fw,N} + P_{Fe,N} + P_{LL,sine,N}$	(9)	$P_{tot,PWM} = P_{tot,sine} + P_{HL}$	(18)	
Efficiency		$\eta_{sine} = \frac{P_{1,\theta} - P_{tot,sine}}{P_{1,\theta}}$	(10)	$\eta_{PWM} = \frac{P_{2,sine}}{P_{2,sine} + P_{tot,PWM}}$	(19)	I–V
Harmonic loss ratio				$r_{HL} = \frac{P_{HL}}{P_{tot,sine}} \cdot 100\,\%$	(20)	

Additional temperature and load corrections							
Copper loss correction to 25 °C ambient temperature	$P_{s,\theta} = k_\theta P_s$	(21)	$P_{r,\theta} = (P_1 - P_{s,\theta} - P_{Fe})k_\theta s$	(22)	$k_\theta = \frac{235 + \theta_w + 25 - \theta_{amb}}{235 + \theta_w}$	(23)
Input power correction to 25 °C ambient temperature			$P_{1,\theta} = P_1 - (P_s - P_{s,\theta}) - (P_r - P_{r,\theta})$	(24)		
Friction and windage loss correction with rotor speed			$P_{fw} = P_{fw,0}(1-s)^{2.5}$	(25)		
Iron loss correction with stator winding voltage drop	$P_{Fe} = P_{Fe,0}(U_i)$	(26)	$U_i = \sqrt{\left(U - \frac{\sqrt{3}}{2}IR\cos\varphi\right)^2 + \left(\frac{\sqrt{3}}{2}IR\sqrt{1-\cos^2\varphi}\right)^2}$	(27)	$\cos\varphi = \frac{P_1}{\sqrt{3}UI}$	(28)

Nomenclature

Variables		Subscripts			
A	Slope of residual losses	0	No-load	1	Input
B	Constant part of residual losses	2	Output	amb	Ambient/coolant
cos φ	Power factor	C	Constant	Fe	Iron/core
I	Stator line current	fw	Friction and windage	HL	Additional harmonic loss
k	Correction factor	i	Inner, after stator winding	load	Load dependent
P	Power loss	N	At rated load	PWM	With frequency converter supply
R	Stator winding line-to-line resistance	r	Rotor	s	Stator
s	Slip	sine	With sinusoidal supply	tot	Total
T	Torque	w	winding	θ	Temperature corrected
U	Line-to-line voltage				
θ	Temperature				

of no-load friction and windage losses and no-load iron losses, and can also be calculated as a difference between the no-load input power and the stator copper losses (3).

Figure 2 illustrates determination of the no-load friction and windage losses, the rated load iron losses, and the constant part of the additional harmonic losses. The values used for plotting Figure 2 are from actual measurements presented later in this article. First, the constant losses for the no-load test points with sinusoidal supply (Step III) and the single rated voltage point with converter supply (Step V) are calculated. In Figure 2, the constant losses are plotted as a function of the square of the fundamental voltage. The no-load friction and windage losses $P_{\mathrm{fw},0}$ are linearly extrapolated from the four lowest constant loss points at zero voltage (4). Since the load affects the IM rotor speed, the friction and windage losses of the loaded motor have to be corrected according to the slip (25). The four highest constant loss points are used for interpolating the rated load iron losses. The no-load iron loss curve $P_{\mathrm{Fe},0}(U_0)$ is the difference between the constant loss curve and the no-load friction and windage losses (5). The rated load iron losses $P_{\mathrm{Fe,N}}$ are calculated from the interpolated iron loss curve at the inner voltage U_{i}, which takes the stator winding voltage drop into account (26)–(28). The constant part of the additional harmonic losses $P_{\mathrm{HL},0}$ is the difference in the constant losses with converter supply (11) and with sinusoidal supply in the rated voltage point (16).

The stray-load losses and the load-dependent part of the additional harmonic losses are determined from the residual losses of the load curve test points (Steps II and IV). Figure 3 illustrates the calculation procedure. The values used for Figure 3 are from actual measurements presented later in this article. First, the residual losses $P_{\mathrm{Lr,sine}}$ (6) and $P_{\mathrm{Lr,PWM}}$ (12) are calculated for each of the six load

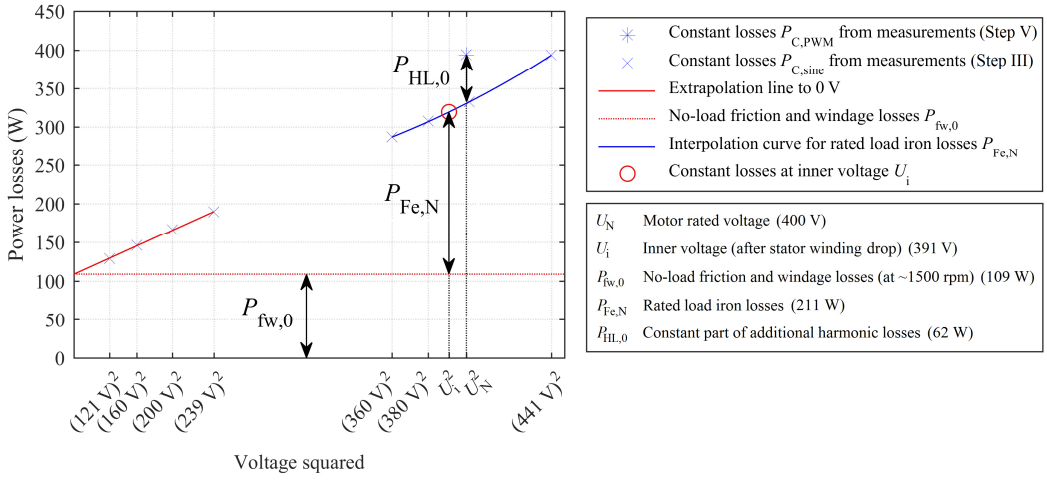

FIGURE 2 – Determination of the no-load friction and windage losses $P_{\mathrm{fw},0}$, the rated load iron losses $P_{\mathrm{Fe,N}}$, and the constant part of the additional harmonic losses $P_{\mathrm{HL},0}$.

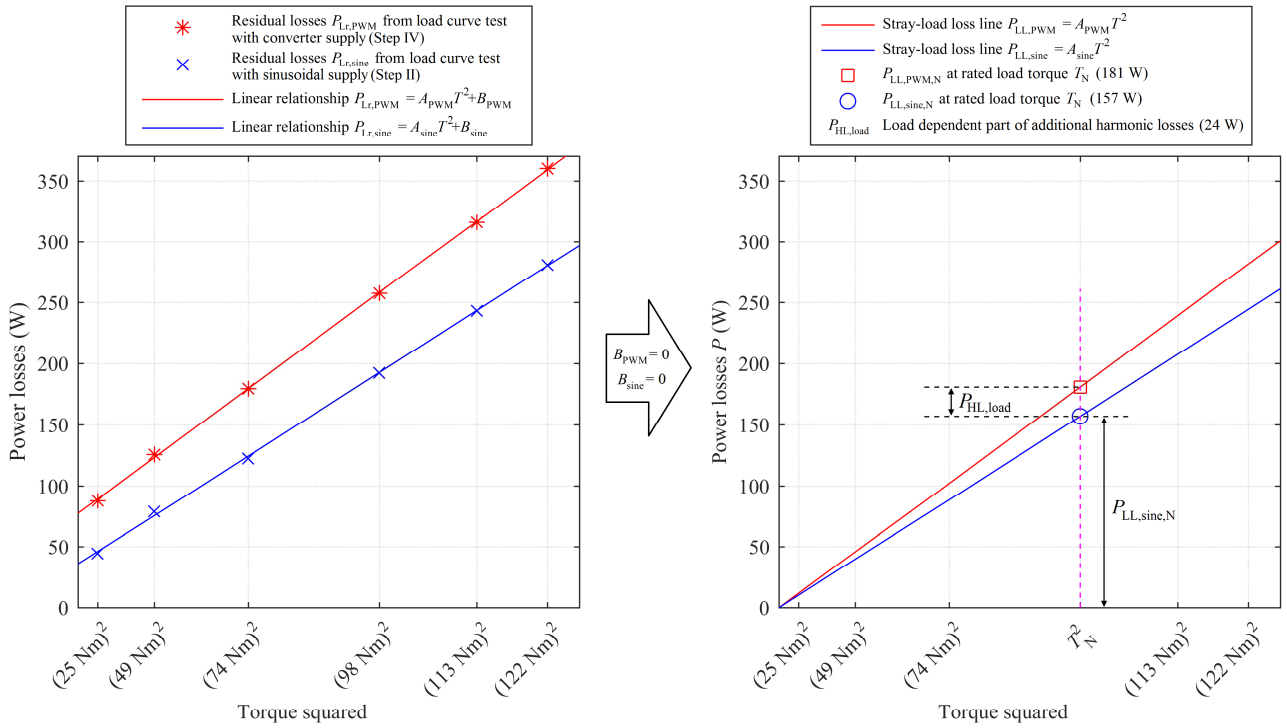

FIGURE 3 – Determination of stray-load losses $P_{LL,sine}$ and the load-dependent part of the additional harmonic losses $P_{HL,load}$.

curve points of both sinusoidal supply and test converter supply measurements, and a linear relationship as function of load torque is formed for both (Figure 3a). The linearization method for the residual losses (7) and (13) is given in [5]. To derive the stray-load losses, the constant parts of residual losses, B_{sine} and B_{PWM}, are removed, effectively shifting both lines to pass through origin (Figure 3b). The rated load stray-load losses $P_{LL,sine,N}$ are calculated from the sinusoidal supply $P_{LL,sine}$ line at the rated load test torque T_N (8). The rated load stray-load losses with converter supply are calculated similarly at T_N (14), but they are used only to determine the load-dependent part of the additional harmonic losses $P_{HL,load}$ as the stray-load loss difference between converter supply and sinusoidal supply (15).

The total motor losses are the sum of the segregated loss components. The total losses with sinusoidal supply $P_{tot,sine}$ are the sum of the loss components at rated load and at 25 °C ambient temperature (9). The total losses with converter supply $P_{tot,PWM}$ (18) are the sum of the total losses with sinusoidal supply and the total additional harmonic losses P_{HL} (17). Efficiency with sinusoidal supply is calculated from the temperature-corrected input power (24) and the total losses with sinusoidal supply (10). For calculating the efficiency with converter supply, the output power with sinusoidal supply and

the total losses with converter supply are used (19). Harmonic loss ratio (20) is used to represent the relative increase in motor losses with converter supply in comparison with losses with sinusoidal supply.

Laboratory measurements

The measurements were made in three test runs, as summarized in Table 3, to analyze the applicability of the IEC/TS method. Two frequency converters were used in the measurements. The first converter normally applies classical space vector modulation and was set to provide the IEC-defined "test converter" waveform with a 4 kHz switching frequency, and the second converter used DTC with automatic settings producing a very different PWM pulse pattern with a 1.5–2.5 kHz average switching frequency.

First, tests with sinusoidal supply and tests with both frequency converters were made at the motor rated fundamental voltage of 400 V. In order to produce the fundamental line-to-line voltage of 400 V, 50 Hz without overmodulation, the supply voltages of both converters had to be increased considerably above 400 V.

For the second run, the test converter was fed with a 400 V input voltage, and the motor voltage in the sinusoidal tests was reduced to match the test converter fundamental output voltage. Similarly, in the third test run, the DTC converter was supplied with a 400 V grid voltage, and the fundamental voltage with sinusoidal supply was matched with the DTC converter fundamental. As the IEC [5], [11] requires, all the measurements were made with the motor rated fundamental frequency of 50 Hz.

The measurement setup consisted of the motor under test, a larger machine for mechanical load, an electrical power supply, and instruments for measuring and recording data. Figure 4 shows the setup used in the frequency converter measurements, and the 15 kW induction motor nameplate values are listed in Table 4. The setup in the sinusoidal supply measurements was similar but without the frequency converter.

TABLE 3 – Summary of the test runs and the input voltages

Test run	Motor voltage (fundamental)	Test converter input voltage	DTC converter input voltage
Rated voltage run	**Rated voltage, 400 V, 50 Hz**	Increased voltage, 460 V, 50 Hz	Increased voltage, 433 V, 50 Hz
Reduced voltage run 1	Reduced voltage, 350 V, 50 Hz	**Grid voltage, 400 V, 50 Hz**	-
Reduced voltage run 2	Reduced voltage, 377 V, 50 Hz	-	**Grid voltage, 400 V, 50 Hz**

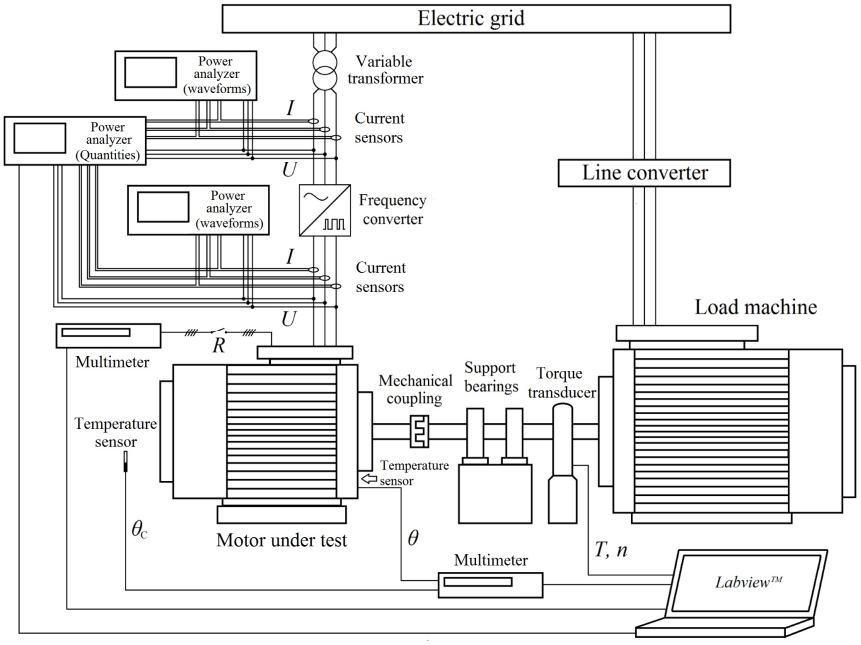

Power analyzer for electric quantities	Yokogawa WT1600
Power analyzers for waveforms and fundamental voltage	Yokogawa PZ4000
Current sensors	Hitec Zero-Flux CURACC
Multimeters	Keithley Integra 2701
Temperature sensor, ambient/coolant	Pt100 A-class
Temperature sensor, stator winding	Pt100 B-class
Torque transducer	HBM T12 (200 Nm rated)

FIGURE 4 – The setup used in the test converter measurements.

TABLE 4 – Nameplate values of the test motor for 400 V, 50 Hz with Δ-connection

Variable	Value
Power	15 kW
Current	27.8 A
Voltage	400 V
Frequency	50 Hz
Speed	1474 r/min
Power factor	0.84
Efficiency	92.7 % (IE3)

Indirect method with test converter supply with standard modulation

The frequency converter used in these measurements was set to provide the IEC/TS-defined test converter waveform as closely as possible. No overmodulation is allowed by the IEC/TS, and therefore, the modulation index M must be limited to $M \leq 0.907$ resulting in approx. 380 V RMS output with 400 V input and no voltage drop in the rectification [40]. However, the motor rated fundamental voltage and frequency of 400 V and 50 Hz are required. Therefore, the converter input voltage had to be increased even up to 460 V to keep the output at the motor rated 400 V, 50 Hz without

overmodulation during all tests. It should be noted that, in theory, about 420 V input should suffice to produce the 400 V output with $M = 0.907$.

The IEC/TS requires that the test converter waveform is carefully checked; all switchings shall take place, the pulse pattern must match the required switching frequency, and the voltage reference shape has to be correct. The recorded output line-to-line voltage waveform of the test converter used in the measurements is presented in Figure 5 (a and b). Figure 5a contains one fundamental wave period of the test converter line-to-line voltage, and Figure 5b shows an enlarged view between the 14–16 ms points of plot a. All pulses are present in the waveform showing no overmodulation. The line-to-line voltage waveform in Figure 5b contains eight pulses per millisecond (this was also checked for a longer period); hence, the switching frequency of one converter phase was 4 kHz, which is the IEC/TS requirement for motors with a rated power of 90 kW or less. The filtered waveform in Figure 5c was measured between one converter output phase and the negative intermediate circuit DC voltage with 2nd-order 500 Hz low-pass filtering. The filtered waveform has a correct shape containing third-order linearity extension as the IEC/TS defines.

The segregated loss results with test converter supply are presented in Figure 6. As typical for a small machine, almost two-thirds of the losses are resistive winding losses while friction and windage losses and stray-load losses are only 8% and 12% of the total losses, respectively. Because of the IEC methodology, the first five loss components determined with sinusoidal supply are the same also for the converter-fed motor, and the additional harmonic losses contain all additional motor losses caused

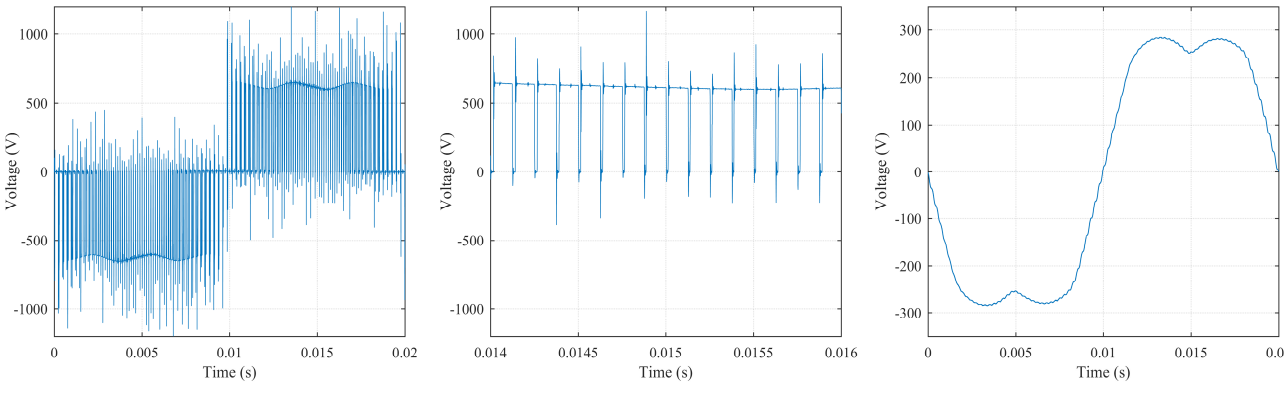

FIGURE 5 – The test converter output voltage waveform. Line-to-line voltage (a), enlarged view of the line-to-line voltage (b), and 500 Hz low-pass-filtered phase voltage (c). The fundamental voltage was 400 V, 50 Hz and the switching frequency 4 kHz. Space vector modulation was used.

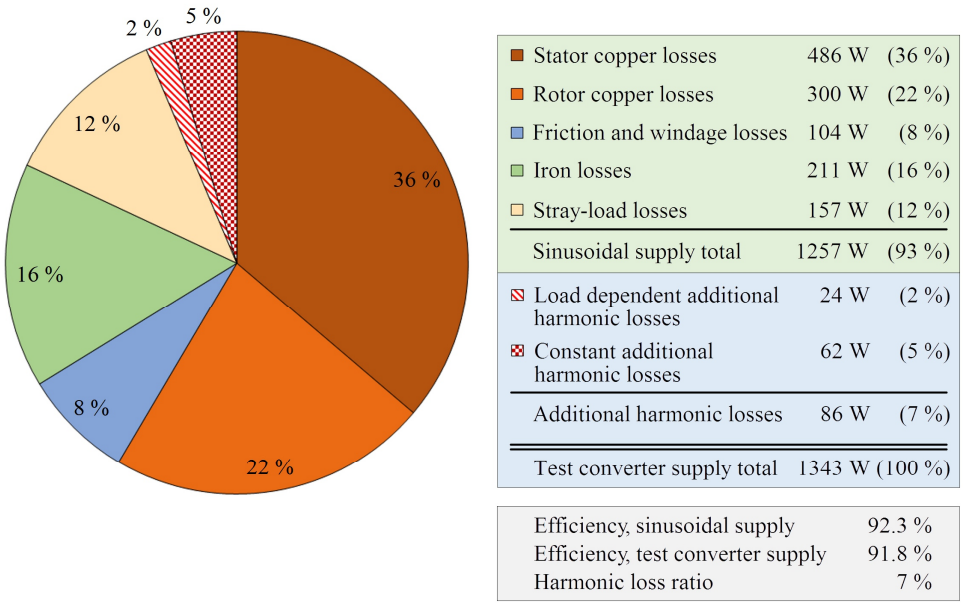

FIGURE 6 – Distribution of the 15 kW induction motor loss components determined with the IEC/TS 60034-2-3 indirect method at the motor fundamental voltage of 400 V, 50 Hz.

by the converter. For the 15 kW motor, the additional harmonic losses were relatively low, and the harmonic loss ratio was only 7%.

Indirect method with DTC converter supply

A frequency converter applying direct torque control (DTC) and the resulting DTC modulation deviating from the standard (test converter) modulation was used in these measurements. The IEC/TS defines that with a specific converter and motor combination for a final application, the final converter parameters shall be used. Therefore, the DTC converter used in the tests was running at its default and automatic settings with the 15 kW motor. However, to maintain the 50 Hz fundamental frequency, the slip compensation was ensured to be deactivated. The converter input voltage had to be increased to 433 V for the output fundamental voltage to reach the required 400 V, 50 Hz at the motor rated load.

The typical operation principle of the DTC converter differs markedly from the predefined and fixed test converter operation. With the DTC, the voltage switchings are made only when needed depending on the estimated motor state, and therefore, the width and frequency of the voltage PWM pulses are not constant. The differences between the test converter waveform and the DTC converter waveform are illustrated in Figure 7. The DTC waveform in Figure 7b shows variable length pulses characteristic of the classical DTC as opposed to the even-spaced pulse pattern of the test converter waveform in Figure 7a. The average switching frequency of the DTC converter was approx. 1.5 kHz with the motor

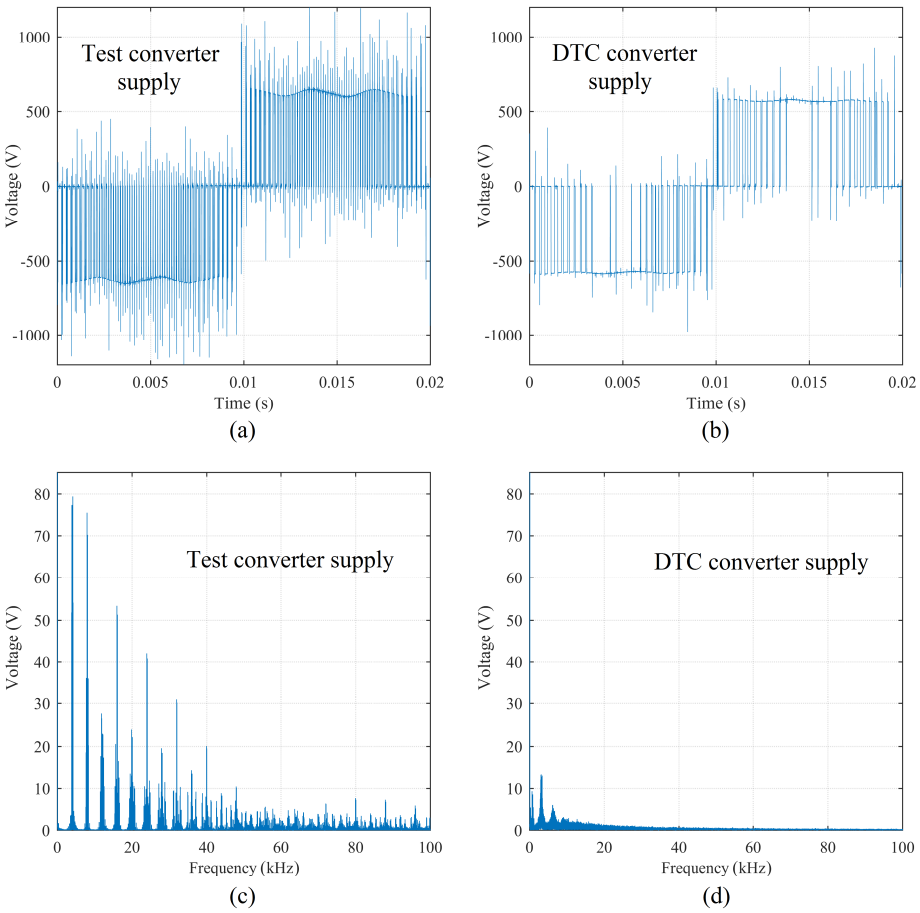

FIGURE 7 – Comparison of the motor input voltage waveforms and spectra with the test converter supply (SVM) and the DTC converter supply at the motor rated load and the 400 V, 50 Hz fundamental voltage. The fundamental voltage is scaled outside the plots c and d.

rated load while the test converter had a fixed 4 kHz switching frequency. The test converter voltage harmonics shown in Figure 7c are concentrated around the multiples of the switching frequency, while the DTC harmonics in Figure 7d are distributed more evenly along the spectrum down to the frequency range of below 1 kHz. As there are no restrictions for the pulse frequency or length, the DTC converter is able to produce the 400 V, 50 Hz fundamental voltage at the lower input voltage of 433 V in comparison with the 460 V input required for the test converter. This difference is mainly due to the test converter restrictions, and for most commercial frequency converters, an input voltage level closer to the DTC converters 433 V should suffice for the 400 V, 50 Hz fundamental output. It should be noted, however, that there is always variation in the fundamental voltage production capability of frequency converters as a result of structural and electrical differences between manufacturers and products.

The measurements were made successfully, but some issues concerning the suitability of the method for DTC were noticed. The motor fundamental voltage was adjusted to 400 V at rated load, but during

the measurements, it varied between 396 V at no load and 404 V at 115% and 125% of rated load. This behavior is caused by the operation principle of the DTC. The DTC estimates and adjusts the motor flux directly, thus compensating for the stator winding voltage drop at the same time. However, for the IEC/TS indirect method to be accurate, the motor rated fundamental voltage has to be maintained in all tests and test points with converter supply. A mismatch of fundamental voltages in corresponding points with sinusoidal supply and with converter supply causes error in the results. Moreover, because of the dynamic and random nature of the DTC, the average switching frequency and the harmonic content of the motor voltage were load-dependent. At the 100% load, the average switching frequency was only 1.5 kHz, but for instance at the 25% load it was 2.0 kHz. Because of both the changing fundamental voltage and the varying average switching frequency, the DTC results with the indirect method cannot be considered valid, and therefore, are not presented here. The direct input-output calculations, however, only require the rated load measurements and are thus fully usable. The input-output results with the 400 V, 50 Hz DTC converter supply are included in Figure 8.

Measurements with 400 V converter input voltage (reduced motor voltage)

In these measurements, both the converters were fed with normal 400 V mains voltage to investigate the more common situation in a final application, where no increased supply voltage is available. The 50 Hz fundamental frequency was used also in these measurements. The motor fundamental voltage with the test converter directly connected to the 400 V network was only 350 V and with the corresponding DTC converter arrangement 377 V. The motor voltage with sinusoidal supply was adjusted to match the motor fundamental voltage of the corresponding converter measurement. To keep the loss results comparable, the motor rated load of 15 kW was used also in the reduced voltage tests. Otherwise, the measurements were performed according to the IEC/TS indirect method.

Usually, the motor loadability is considered lower when the motor fundamental voltage is below the rated value and higher current is needed for delivering the same power. Therefore, as a considerable increase in the resistive losses and the motor temperature was expected, the stator winding temperature readings were observed during the heat runs to avoid the motor reaching excessively high temperatures.

The fundamental output voltage was load dependent with both converters, which causes error in the indirect loss segregation as already discussed. Thus, for the grid-fed converters, only the direct input-output results are used in further analysis and are presented in Figure 8.

Comparison of results

The main results from all measurements are collected in Figure 8. Because the loss segregation could not be adequately applied with the DTC converter supply or the grid-fed test converter supply, only the input-output results of these measurements are included. The additional harmonic losses in the input-output results are calculated as the difference in the total losses between converter supply and sinusoidal supply.

The IEC/TS loss segregation method and the direct input-output results were in good agreement, and the total motor losses were within 1 W according to both methods with the test converter supply. However, there was a 19 W difference in the motor losses between the two methods with sinusoidal supply, which is relatively small considering the measured input and output powers of the 15 kW

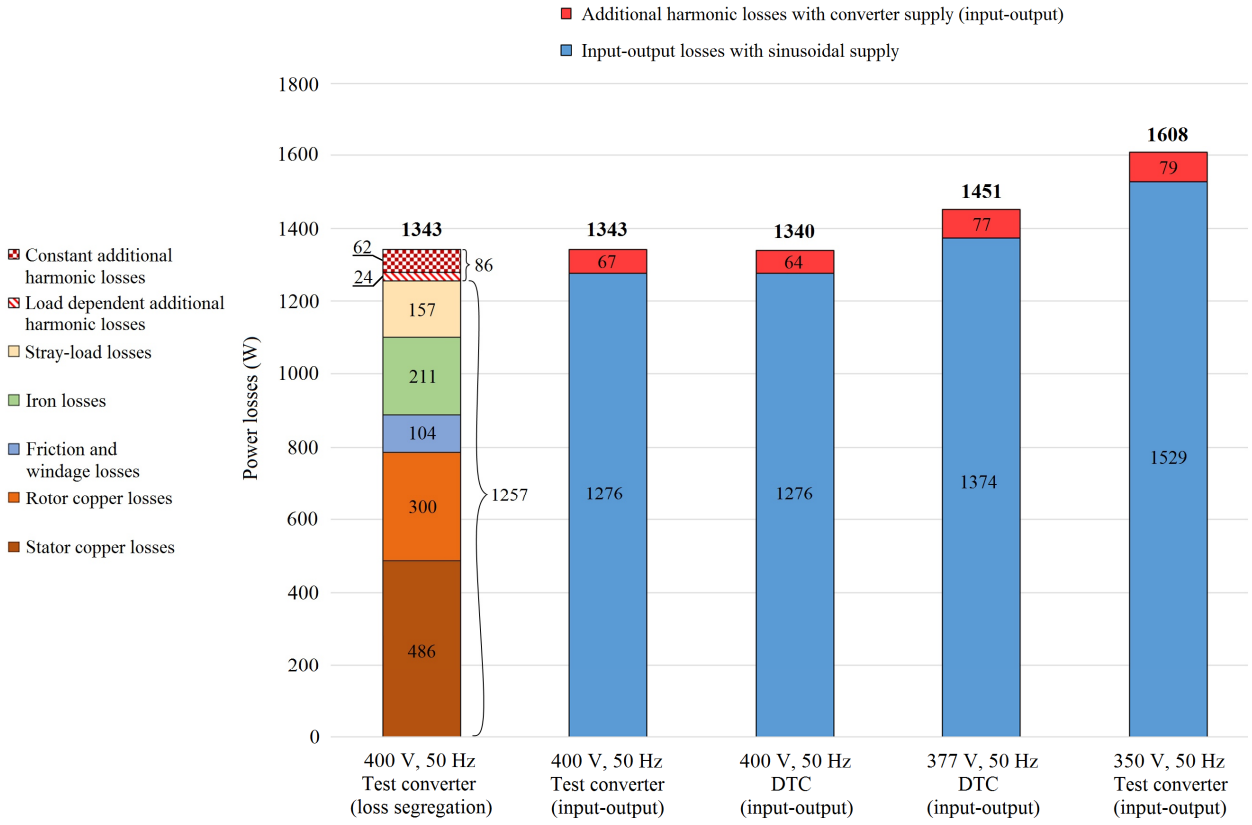

FIGURE 8 – The indirect loss segregation results and the direct input-output loss results for the 15 kW induction motor with sinusoidal supply and two frequency converter supplies at the motor rated torque. The motor voltages of 400 V were reached with increased input voltages of 460 V (test converter) and 433 V (DTC converter). The motor voltages of 377 V and 350 V were the output fundamental voltages when the converters were supplied directly with the 400 V grid voltage.

range. Still, it translates into a 28% difference in the additional harmonic losses determined with the two methods, thus making this a demonstrative example of the challenge of determining the additional harmonic losses even at some level of accuracy.

When comparing the results with the two different converters and modulations, the motor losses were approximately the same with both converters at the 400 V, 50 Hz motor fundamental voltage, even though the switching patterns were significantly different as illustrated in Figure 7. This result is in line with [15], where only small differences were detected between motor losses with three distinct converters and modulation methods.

As expected, the motor losses at the lower fundamental voltages of the grid-fed converters were considerably higher than with the fixed 400 V motor fundamental voltage. The reduced fundamental voltage results in lower iron losses, but as the losses of a small motor are dominated by the copper losses, the total losses were increased. The additional harmonic losses also increased with the total losses, and the harmonic loss factor was 5.0%–5.6 % according to all four input-output results, which is also lower than the 7% harmonic loss factor determined with the indirect method.

Discussion

The IEC indirect loss-determination method 2-3-A with test converter supply gave promising results. The basic principle of determining the additional harmonic losses from the differences between the results with test converter supply and with sinusoidal supply is simple and useful. However, the method is rather complex to apply, because the loss segregation consists of separate tests, which have to be performed with both converter and sinusoidal supply.

The test converter seemed to work as expected, and the measurement results of the converter-fed motor were very stable. However, the method requires a clean and stable sinusoidal supply to yield accurate results. Moreover, because the measurements are made in two parts with sinusoidal supply and with test converter supply, the test conditions during both measurements have to be similar. The requirement for similar test conditions applies, naturally, also to the input-output method, if it is used for determining the additional harmonic losses from the difference between PWM supply and sinusoidal supply, as was done in this study.

The total motor losses with the test converter supply were the same when determined either with the IEC/TS indirect method or the direct input-output method, but there was a difference in the amount of

additional harmonic losses. With sinusoidal supply, the standard loss segregation has a lower uncertainty than the input-output method [41], [42]. The IEC/TS loss segregation with PWM supply may have a higher uncertainty than the indirect method with sinusoidal supply, as only a single no-load measurement with converter supply (Step V in Figure 1) is used for calculating the constant part of the additional harmonic losses, see Figure 2 and (16), but it is still probably lower than the input-output uncertainty. Moreover, with modern high-accuracy torque and speed measuring equipment, the input-output measurement uncertainty approaches the indirect uncertainty [41], [42], and the direct method can easily be recommended as a simpler alternative especially for determining the total losses and efficiency of a variable speed drive (VSD) system. Besides, the direct input-output measurement is suitable for any electric machine type while the IEC/TS indirect method is only applicable to induction motors.

The significant problem with the IEC/TS indirect method is that the results do not give a realistic estimate of the motor losses with a specific converter supply in a final application as the motor voltage, load, and frequency cannot reach their rated values simultaneously when considering a practical VSD application with 400 V supply unless a step-up rectifier is used. However, the ability to compare the losses and efficiencies of different motors is often more important than determination of the actual losses, and this is also what the method is intended for. Nevertheless, using a single operating point in the loss determination is by no means optimal when considering a typical VSD application, and motors intended for use in the VSD should be optimized for a wider operating range than a single rated point.

Although the motor losses at the motor rated fundamental voltage with the two different converters used in these measurements were similar, it does not mean that modulation would not affect the motor losses. Only one motor was used, and the measurements were made only once. In addition, the accuracy of the direct input-output measurement used for the comparison may not be sufficient. Although small changes in the input electrical power and the output mechanical power can be measured successfully when the setup is not altered, comparing the motor losses with two different converters is a more complicated situation, because for instance the dissimilar harmonic content may affect the accuracy of the electric input power measurement.

The DTC converter fundamental output voltage is load-dependent, which causes error in the indirect method. To determine the motor losses and efficiency accurately with the indirect method, the motor fundamental voltage and the voltage waveform have to be stable. With a specific frequency converter

with a manufacturer-specific control method, such as DTC, the operation may vary depending on the motor load, and it seems that based on these results, the indirect method with a specific converter cannot be recommended for determining the motor losses. The most reliable methods for determining motor losses with a specific frequency converter would be direct methods, where only one operating point is measured for each calculation.

Determining converter-fed motor losses at the 50 Hz fundamental frequency without an increased converter input voltage seems to be suitable only for direct input-output measurement for final application purposes. For comparable results between motors, the motor fundamental voltage and the voltage waveform have to be similar. Using a lower fundamental frequency of for instance 45 Hz, the problematic field weakening operation at the 50 Hz motor fundamental frequency with the 400 V converter input could be avoided, and the indirect method would also be feasible. However, 45 Hz sinusoidal supply would be required in such a case.

When measuring electric motors, it should also be noted that the motor losses themselves are not constant. The losses depend, for example, on the ambient temperature, and some of the loss components, such as friction and windage losses, also vary over time. Further, the iron losses may decrease as a new motor gathers operating hours and lamination-punching-caused stresses are relieved. Also bearings run smoother and with lower losses after an adaptation period.

Conclusion

The IEC/TS 60034-2-3 indirect method and the test converter supply seem to be feasible for comparing losses and efficiencies of different induction motors with the IEC-defined test converter supply at the operating point of rated voltage, rated frequency, and rated load. The results, however, do not provide any prediction of the motor losses in the final application, and thus, for adequate determination of converter-fed motor losses and efficiency, measurements in a wide operating range would be required. Moreover, the IEC/TS indirect method is rather complex to apply, and since the input-output results were in good agreement with the indirect results, the direct method can be considered a simpler alternative if the facilities are adequate for accurate input and output power measurements. The IEC/TS offers also a variation of the indirect method to be used with a specific frequency converter in a final application, which, however, cannot be considered reliable according to the results obtained in this study. Therefore, only the direct methods can be recommended for

determining converter-fed motor losses in a final application. In addition, the requirement of rated motor fundamental frequency and voltage restricts the opportunities to apply the IEC/TS methods. Obviously, the release of the IEC 60034-2-3 as a technical specification instead of a final standard for now was justified. Alternative approaches for determining converter-fed motor losses are being explored, and the development of the standard IEC 60034-2-3 may actually take another direction after all.

References

[1] M. Doppelbauer, "Update on IEC Motor and Converter Standards", in *Proc. Motor Summit 2016*, Zurich, Switzerland, October 2016.

[2] G. Arce, M. Campbell, M. Fisher and R. Turner, "Global Standards for Rotating Machinery: Navigating Worldwide Industry Requirements for Electric Motors", *IEEE Industry Applications Magazine*, vol. 23, no. 1, pp. 58–69, Jan./Feb. 2017.

[3] A. de Almeida, H. Falkner, J. Fong, K. Jugdoyal, EuP Lot 30: Electric motors and drives. Task 1: Product definition, standards and legislation. *ENER/C3/413-2010*, Final, April 2014.

[4] Rotating electrical machines – Part 30-1: Efficiency classes of line operated AC motors (IE code), Ed. 1, *IEC 60034-30-1*, March 2014.

[5] Rotating electrical machines – Part 2-1: Standard methods for determining losses and efficiency from tests (excluding machines for traction vehicles), Ed. 2, *IEC 60034-2-1*, June 2014.

[6] Commission Regulation (EC) No 640/2009 of 22 July 2009 implementing Directive 2005/32/EC of the European Parliament and of the Council with regard to ecodesign requirements for electric motor). *Off. Jour. of the EU*, L 191, pp. 26–34, 23 July 2009.

[7] J. Sander, "Efficient Motor Policy for Europe – view from CEMEP", in *Proc. Motor Summit 2016*, Zurich, Switzerland, October 2016.

[8] A. de Almeida, F. Ferreira and J. Fong, "Standards for Efficiency of Electric Motors", *IEEE Industry Applications Magazine*, vol. 17, no. 1, pp. 12–19, Jan./Feb. 2011.

[9] A. de Almeida, F. Ferreira, and G. Baoming, "Beyond induction motors—Technology trends to move up efficiency," *IEEE Trans. Ind. Appl*., vol. 50, no. 3, pp. 2103–2114, May/Jun. 2014.

[10] L. Aarniovuori, J. Kolehmainen, A. Kosonen, M. Niemelä, H. Chen, W. Cao and J. Pyrhönen, "Application of Calorimetric Method for Loss Measurement of a SynRM Drive System", *IEEE Transactions on Industrial Electronics*, vol. 63, no. 6, pp. 3942–3953, April 2016.

[11] Rotating electrical machines – Part 2-3: Specific test methods for determining losses and efficiency of converter-fed AC induction motors, Ed. 1, *IEC/TS 60034-2-3*, November 2013.

[12] A. de Almeida, F. Ferreira, and A. Quintino Duarte, "Technical and economical considerations on super high-efficiency three-phase motors", *IEEE Trans. Ind. Appl*., vol. 50, no. 2, pp. 1274–1285, March 2014.

[13] R. Antonello, F. Tinazzi, M. Zigliotto, "Energy efficiency measurements in IM: The non-trivial application of the norm IEC 60034-2-3:2013", in *Proc. 2015 IEEE Workshop on Electrical Machines Design, Control and Diagnosis (WEMDCD)*, Torino, Italy, pp. 248–253, March 2015.

[14] A. Boglietti, A. Cavagnino, M. Cossale, A. Tenconi, "Efficiency determination of converter-fed induction motors: Waiting for the IEC 60034–2–3 standard" in *Proc. 2013 IEEE Energy Conversion Congress and Exhibition*, Denver, Colorado, USA, pp. 230–237, September 2013.

[15] L. Aarniovuori, P. Rasilo, M. Niemelä and J. Pyrhönen, "Analysis of 37 kW Converter-Fed Induction Motor Losses," *IEEE Trans. Ind. Electron.,* vol. 63, no. 9, pp. 5357–5365, September 2016.

[16] M. Chirindo, M. A. Khan and P. S. Barendse, "Considerations for Nonintrusive Efficiency Estimation of Inverter-Fed Induction Motors*", IEEE Trans. Ind. Electron.*, vol. 63, no. 2, pp. 741-749, February 2016.

[17] P. Pillay, M. Al-BBadri, P. Angers and C. Desai, "A New Stray-Load Loss Formula for Small and Medium-Sized Induction Motors", *IEEE Trans. En. Conv.*, vol. 31, no. 3, pp. 1221–1227, September 2016.

[18] S. A. Odhano, R. Bojoi, A. Boglietti, S.G. Rosu and G. Griva, "Maximum Efficiency per Torque Direct Flux Vector Control of Induction Motor Drives", *IEEE Trans. Ind. Appl.*, vol. 51, no. 6, pp. 4415–4424, November–December 2015.

[19] J. Rivera Dominguez, C. Mora-Soto, S. Ortega-Cisneros, J. J. Raygoza Panduro, and A. V. Loukianov, "Copper and Core Loss Minimization for Induction Motors Using High-order Sliding-mode Control," *IEEE Trans. Ind. Electron.*, vol. 59, no. 7, pp. 2877–2889, July 2012.

[20] L. Aarniovuori, L. Laurila, M. Niemelä, and J. Pyrhönen, "Measurements and simulations of DTC voltage source converter and induction motor losses," *IEEE Trans. Ind. Electron.*, vol. 59, no. 5, pp. 2277–2287, May 2012.
[21] Z. Gmyrek, A. Boglietti, and A. Cavagnino, "Estimation of iron losses in induction motors: Calculation method, results, and analysis," *IEEE Trans. Ind. Electron*., vol. 57, no. 1, pp. 161–171, January 2010.
[22] A. Boglietti, A. Cavagino, A.M. Knight, and Y. Zhan, "Factors affecting losses in induction motors with non-sinusoidal supply," in *Conf. Rec. 2007 IEEE Industry Applications Conf. 42nd IAS Annu. Meeting*, vol. 1, New Orleans, LA, USA, pp. 1193–1199, September 2007.
[23] H. Kärkkäinen, L. Aarniovuori, M. Niemelä, J. Pyrhönen, "Converter-fed Induction Motor Losses in Different Operating Points", in *18th Eur. Conf. on Power el. and appl. (EPE'16 ECCE-Europe),* Karlsruhe, Germany, pp. 1–8, September 2016.
[24] E.N. Hildebrand and H. Roehrdanz, "Losses in three-phase induction machines fed by PWM converter," *IEEE Trans. Energy Convers.*, vol. 16, no. 3, pp. 228–233, September 2001.
[25] A. Boglietti, A. Cavagnino, and A. M. Knight, "Isolating the impact of PWM Modulation on Motor Iron Loss," in *Proc. IEEE Industry Application Society Annu. Meeting*, Edmonton, Alberta, Canada, pp. 1–7, October 2008.
[26] J.-J. Lee, Y.-K. Kim, H. Nam, K.-H. Ha, J.-P. Hong, and D.-H. Hwang, "Loss distribution of three-phase induction machines fed by pulsewidth-modulated inverter," *IEEE Trans. Magn.*, vol. 40, no. 2, pp. 762–765, March 2004.
[27] Y. Wu, R.A. McMahon, Y. Zhan, and A.M. Knight, "Impact of PWM schemes on induction motor losses," in *Conf. Rec. 2006 IEEE Industry Applications Conf. 41st IAS Annu. Meeting*, vol. 2, Tampa, FL, USA, pp. 813–818, October 2006.
[28] Y. Zhan, A.M. Knight, Y. Wu, and R.A. McMahon, "Investigation and comparison of inverter-fed induction machine loss," in *Proc. IEEE Industry Applications Society Annu. Meeting*, Edmonton, Alberta, Canada, pp. 1–6, October 2008.
[29] A. Ruderman and R. Welch, "Electrical machine PWM loss evaluation basics," in *Proc. Int. Conf. Energy Eff. in Motor Driven Systems* (EEMODS), Heidelberg, Germany, September 2005.
[30] K. Yamazaki and N. Fukushima, "Iron Loss Model for Rotating Machines Using Direct Eddy Current Analysis in Electrical Steel Sheets", *IEEE Trans. on Energy Convers.*, vol. 25, no. 3, pp. 633–641, September 2010.
[31] M. Schweizer, T. Friedli and J. W. Kolar, "Comparative Evaluation of Advanced Three-Phase Three-Level Inverter/Converter Topologies Against Two-Level Systems", *IEEE Trans. Ind. Electron*., vol. 60, no. 12, pp. 5515–5527, December 2013.
[32] H. Mahlfeld, T. Schuhmann, R. Döbler and B. Cebulski, "Impact of overmodulation methods on inverter and machine losses in voltage-fed induction motor drives", in *Proc. 2016 XXII International Conference on Electrical Machines (ICEM)*, Lausanne, Switzerland, pp. 1064–1070, November 2016.
[33] IEEE standard test procedure for polyphase induction motors and generators, *IEEE Std 112-2004*, November 2004.
[34] W. Cao, "Comparison of IEEE 112 and New IEC Standard 60034-2-1", *IEEE Trans. Energy Convers*., vol. 24, no. 3, pp. 802–808, September 2009.
[35] W. Cao, "Assessment of induction machine efficiency with comments on new standard IEC 60034-2-1", in *Proc. 18th Int. Conf. on Electrical Machines*, Vilamoura, Portugal, pp. 1–6, September 2008.
[36] A. Boglietti, A. Cavagnino, M. Lazzari and M. Pastorelli, "International Standards for the Induction Motor Efficiency Evaluation: A Critical Analysis of the Stray-Load Loss Determination", *IEEE Trans. on Ind. Appl*., vol. 40, no. 5, pp. 1294-1301, September/October 2004.
[37] A. Boglietti, A. Cavagnino, and S. Vaschetto, "Induction motor EU standards for efficiency evaluation: The scenario after IEC 60034-2-1", in *Proc. 37th Conf. on IEEE Industrial Electronics Society*, Melbourne, Australia, pp. 2786–2791, November 2011.
[38] A. Boglietti, A. Cavagnino, L. Ferraris, and M. Lazzari, "Impact of the supply voltage on the stray-load losses in induction motors", *IEEE Trans. Ind. Appl*., vol. 46, no. 4, pp. 1374–1380, July/August 2010.
[39] Rotating electrical machines – Part 2-2: Specific methods for determining separate losses of large machines from tests – Supplement to IEC 60034-2-1, Ed. 1, IEC 60034-2-2, March 2010.
[40] J. Pyrhönen, V. Hrabovcová and R. S. Semken, "DC and AC power electronic topologies – modulation for the control of rotating-field motors", in *Electrical Machine Drives Control: An Introduction*, Chichester, United Kingdom: John Wiley & Sons, Inc., 2016, pp. 147–190.
[41] L. Aarniovuori, J. Kolehmainen, A. Kosonen, M. Niemelä and J. Pyrhönen, "Uncertainty in motor efficiency measurements", in *Proc. 2014 International Conference on Electrical Machines (ICEM)*, Berlin, Germany, pp. 323 - 329, September 2014.
[42] G. Bucci, F. Ciancetta, E. Fiorucci and A. Ometto, "Uncertainty Issues in Direct and Indirect Efficiency Determination for Three-Phase Induction Motors: Remarks About the IEC 60034-2-1 Standard", *IEEE Trans. on Instr. and Meas*., in press, 2016.

Publication III

Kärkkäinen, H., Aarniovuori, L., Niemelä, M., Pyrhönen, J., and Kolehmainen, J.
Technology comparison of induction motor and synchronous reluctance motor

43rd Annual Conference of the IEEE Industrial Electronics Society, IECON 2017
pp. 2207-2012, 2017

Technology Comparison of Induction Motor and Synchronous Reluctance Motor

Hannu Kärkkäinen, Lassi Aarniovuori, Markku Niemelä, and Juha Pyrhönen
Lappeenranta University of Technology
LUT School of Energy Systems, Electrical Drives Tech.
P.O. Box 20, FI-53851 Lappeenranta, Finland
hannu.s.karkkainen@lut.fi

Jere Kolehmainen
ABB Oy
Motors and Generators
Strömbergin puistotie, 65101 Vaasa, Finland

***Abstract*—Electric motors play an important role in global efforts to reduce energy consumption as they account for almost half of the total electrical energy usage in the world. The energy consumption of electric motors can be reduced by using more efficient motors and by applying frequency converters to feed the motors, thereby enabling accurate control according to the load. The induction motor has been – and still is – the dominant motor technology in the industry, but also more efficient motor technologies are available in the market. Considering industrial motors, the two most important competing technologies are probably permanent magnet synchronous motors and synchronous reluctance motors. This papers provides a comparison between the induction motor and synchronous reluctance motor technologies. The main differences between the two are covered and measurements are made with a frequency converter supply to compare the efficiencies over a wide operating range of 10–100% of rated torque and 10–140% of rated operating frequency.**

Keywords—AC motors; induction motors; synchronous reluctance motors; variable speed drives; efficiency measurement; PWM converters

I. INTRODUCTION

Electric motors consume a large share of electrical energy in the world; it has been estimated that electric motors account for 44–46% of the global electricity consumption [1]. Over the past few decades, global awareness of environmental issues has increased, and reflecting this, new regulations on the efficiency of electric motors have been introduced around the world. Reductions in the energy consumption of electric motors can be achieved by using more efficient motors and by applying frequency converters to supply the motors according to load demand. The motor efficiency regulations are based on efficiency classifications; the International Electrotechnical Commission (IEC) [2] specifies four International Efficiency (IE) classes for single-speed (direct-on-line, DOL), three-phase, cage induction motors:

- IE1 – Standard Efficiency,
- IE2 – High Efficiency,
- IE3 – Premium Efficiency, and
- IE4 – Super Premium Efficiency.

Under the Commission Regulation (EC) No 640/2009, new induction motors with a DOL supply shall not be less efficient than the IE3 efficiency level [3], and from the 1st of January 2017 onwards, the requirement covers all induction motors with a rated output power of 0.75 kW–375 kW. As new, higher-efficiency motors become available, the next IE5 class will be introduced [2], and the efficiency regulations are expected to tighten even further in the future.

The induction motor (IM) has been the workhorse of the industry for decades, and it still remains by far the most common industrial motor type [4]. However, more efficient motor technologies, such as synchronous reluctance motors (SynRM) [5], [6] and permanent magnet synchronous motors (PMSM) [5], [7], are available in the market. According to [5], only medium to large IMs (>30 kW) are likely to achieve the upcoming IE5 efficiency class, while PMSMs and SynRMs may be able to reach the IE5 efficiency level also in lower power levels [5]. Both PMSMs and SynRMs can be equipped with line start capabilities, but a frequency converter supply is the natural solution for these motors as no efficiency compromising structures optimized for DOL starting are needed. Comparison between converter-driven motors of different technologies, however, is not a trivial task. Typically, manufacturers give only the rated operating point efficiency and sometimes additionally a couple of partial load values for rated speed operation. For a frequency-converter-driven motor, the rated frequency information is not sufficient as different motors, and especially different motor technologies, do not behave similarly over a wide operating range. For adequate comparability, standardization is needed, and to this end, the IEC standard 60034-2-3 with its intended release in spring 2018 will finally provide the efficiency determination of converter-fed motors. Closely related to this, the IEC standard 61800-9-2 [8] covering the energy efficiency on the power drive system level (converter + motor), was released already in March 2017. The new standards should facilitate the task of the end user to choose the best motor and converter for each application.

In this paper, differences between the dominant IM technology and its present-day contender, the SynRM technology, are analyzed with a frequency converter supply. Efficiency measurements are performed over a wide operating range for a 15 kW IM and a 15 kW SynRM. In addition to the same power rating, both motors are from the same

manufacturer and have exactly the same frame size. The measurements are performed using the same 35 A frequency converter with both motors. The measurements are made in 49 operating points (IM) and 48 operating points (SynRM) over a supply frequency range from 5 Hz to 70 Hz (10%–140% of the motor rated frequency of 50 Hz) and a torque range from 10% to 100% of the IM rated torque. The efficiency results are interpolated over the measurement range and presented as contour maps of the motor efficiencies and the efficiency difference between the two motors. The converter efficiency is also measured and the differences between the SynRM and IM tests are shown. In addition, combined (complete drive system) efficiency differences are presented, and the IES efficiency classes introduced in [8] are determined for both the IM and SynRM drive systems.

II. Motor Technologies

For the IM, its line start capability, low initial cost, rugged structure, and simple maintenance are the main reasons for its popularity. For the highly efficient PMSM, the motor cost has been a prohibiting factor for the popularity of the motor type, but taking the lifetime energy cost into account, a converter-fed PMSM can also become a cost effective solution. A converter-driven SynRM, however, features most of the same benefits as a converter-fed IM with efficiency closer to a PMSM, and the structure of a SynRM is as simple as that of an IM. While the focus of this paper is on comparing SynRM and IM technologies, the PMSMs have been covered extensively in [7].

A. Differences between induction motors and synchronous reluctance motors

Although a SynRM and an IM can be identical excluding the rotor, they represent very different motor technologies in terms of the operating principle. The torque production of an IM is based on the interaction of the rotating mutual air-gap magnetic field and the rotor currents. Because a varying magnetic field is needed to produce the rotor current, there is a torque-proportional speed difference, commonly known as slip, between the air-gap field and the rotor of the IM. The SynRM torque production, in contrast, is based on the tendency of the mutual flux to take the route in the rotor iron circuit through the minimum reluctance path, which is often called the direct axis (d-axis) in electric machines featuring reluctance torque. The higher the motor torque is, the wider is the angle between the stator flux and the d-axis of the SynRM. As increasing the torque only affects the angle, the SynRM operates always at the synchronous speed. In addition to the different torque production principles, also the torque production capability is different between IMs and SynRMs; while a 300% breakdown torque is typical for industrial IMs, SynRMs are usually only capable of about 150% overload torque.

The losses occurring in an electric machine are commonly divided into four main components: stator copper losses, rotor copper losses, iron losses, and friction and windage losses. The copper losses are load (current) dependent, while iron losses depend on the supply frequency and the peak voltage. The friction and windage losses are dependent on the speed, and thus, naturally also on the supply frequency. In addition to the aforementioned losses, in frequency-converter-driven motors, the pulse-width-modulated voltage causes additional harmonic losses. The losses of converter-fed induction motors have been covered for instance in [9]–[11].

As a SynRM has no rotor current, the rotor copper losses are absent, which is one of the main reasons for the better efficiency of the SynRM compared with a similar-sized IM. All other motor loss components are present also in the SynRM. As the total losses of the SynRM are lower, a smaller cooling fan is required, and thus, the windage losses can also be lower. However, because of the lower power factor of the SynRM, the stator current and stator copper losses can be slightly higher than in an IM with identical windings.

As the operating principles of the SynRM and the IM are fundamentally different, comparisons between the motors are not straightforward. First, a choice has to be made whether to match the supply frequency or the motor speed, as the induction motor speed is lower at the matching frequency because of the slip. From a practical perspective, matching the motor speed could be useful, as the output powers of the motors would also match. When considering the losses, however, the fundamental frequency matching can be more relevant, as the frequency converter losses and the iron losses of the motors are proportional to the supply frequency rather than the speed. In addition, the SynRM and the IM require different control algorithms, but, the effects of control differences can be minimized by applying the same frequency converter designed for both motor types.

III. Losses in frequency converters

The losses of a frequency converter, or more precisely, a voltage source converter (VSC), can be divided into seven main loss components; output bridge semiconductor losses, input bridge semiconductor losses, DC link losses, input choke losses, busbar losses, cooling losses, and control losses [12]. Furthermore, the semiconductor losses can be separated into switching and conduction losses. Assuming a fixed network voltage supply for the VSC, the dependences of the converter loss components are explained in brief in the following. Usually, the majority of the VSC losses are generated in the inverter bridge semiconductors. The conduction losses are proportional to current, power factor, and modulation index. The switching losses naturally increase with the converter switching frequency. The DC link losses are mainly caused by resistors used to share the voltage equally among the series-connected DC capacitors and by the internal series resistances of the DC capacitors. The former one is load independent, whereas the latter component depends on load. The choke losses depend on the current flowing through the choke. The busbar losses are resistive losses, and therefore, relative to the square of the current. The cooling losses depend on the heat production of the converter, that is, the sum of the other converter loss components. The control losses are, in principle, independent of the converter operation [12].

IV. Laboratory measurements

Direct input-output efficiency measurements were performed for a standard 15 kW squirrel cage IM and for a 15 kW SynRM using the same 35 A frequency converter with

both motors. In addition to the motor measurements, the frequency converter input power was measured to determine the efficiency of the converter and the complete drive system efficiency. In former studies [13], the input-output measurement system used here has been verified to give similar results as a calorimetric measurement system.

A. Measurement setup

The measurement setup consisted of the motor under test, a larger machine for mechanical load, a frequency converter, and instruments for measuring and recording data, Fig. 1. The nameplate values of the motors used in the measurements are listed in Table I. Apart from the power and frequency ratings, the nominal values of the IM and the SynRM are completely different: While the IM is obviously rated for network supply, the SynRM can only be run with a converter and a specific control strategy, which is taken into account as a lower voltage rating of 370 V. The SynRM voltage rating, however, is set somewhat low, as most frequency converters can provide more than 370 V fundamental RMS output with a 400 V network supply. The lower voltage is also partly responsible for the significantly higher current rating of the SynRM; nevertheless, most of the current difference comes from the lower power factor of the SynRM. The rated power factor is not given in the nameplate, but calculation from the other rated parameters gives 0.74, which is markedly lower than the IM power factor of 0.84. Because of the current requirements of the SynRM, a frequency converter with 35 A current rating was required, while a 30 A converter would have sufficed for the 15 kW IM.

In addition to the nameplate values and the technological differences, for instance the winding resistance, the cooling fan size, and the selected electrical steel can affect the motor performance and should thus be taken into consideration. In the SynRM under test, lower-loss steel sheets are used (M270, M400 in the IM), but the stator winding resistance is almost identical for both motors, and the cooling fans are exactly the same.

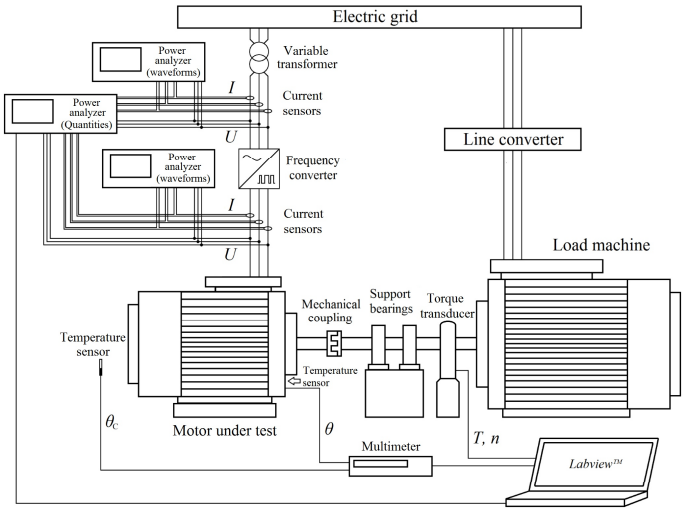

Power analyzer for electric quantities	Yokogawa WT1600
Power analyzers for waveforms and fundamental voltage	Yokogawa PX8000
Current sensors	Hitec Zero-Flux CURACC
Multimeters	Keithley Integra 2701
Temperature sensors	Pt100
Torque transducer	HBM T12 (200 Nm rated)

Fig 1. Measurement setup.

TABLE I. NAMEPLATE (RATED) VALUES FOR THE MOTORS USED IN THE MEASUREMENTS

	Induction motor	**Synchronous reluctance motor**
Power	15 kW	15 kW
Current	27.8 A	33.5 A
Voltage	400 V	370 V
Frequency	50 Hz	50 Hz
Speed	1474 r/min	1500 r/min
Power factor	0.84	(0.74)
Efficiency	92.7% (IE3)	94.2%

In the measurements with both motors, the frequency converter was supplied with the 400 V network voltage, which is usually the case also in industrial environments. Direct torque control (DTC) was used with both motors, and all energy efficiency optimizations were activated in both cases.

B. Test procedure

The measurements were made in 49 operating points with the IM and in 48 operating points with the SynRM. The operating points are indicated in Fig. 2. The point numbers denote the order in which the points were applied. The measurements were made in two parts. Part I consisted of the operating points at the rated operating frequency of 50 Hz and below, whereas Part II covered the operating points of 55 Hz and above. The operating points 1–30 were the same with both motors. The high-frequency operating points were somewhat different for these two motors as the SynRM loadability was restricted by the current handling capability of the converter, while the IM rated power could be maintained also in the highest load points at each frequency. The measurement points 1–30 are based on [14], except for the 45 Hz (90%) frequency point, which was added to these measurements. The order of the measurement points was adopted from a draft version of [14], but the order in the final version is different from that. The high-frequency points (i1–i19 with the IM and s1–s18 with the SynRM) were run simply in the order of the torque and frequency values from the highest to the lowest ones as shown in Fig. 2.

Before starting each of the four measurement runs (Part I and Part II with both motors), the motor under test was loaded at the rated operating point (point no. 1) until thermal stability was reached. The measurement procedure was fully automated and data were recorded for 100 s at each operating point. The load points with the same operating frequency were applied and recorded in a row without any delay. However, after each frequency change (e.g. in points 6, 11, 16, 21, and 26), the motor was operated for 30 minutes for the motor temperature to stabilize before taking the recordings.

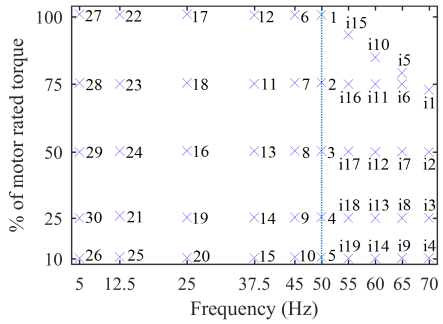

(a) Operating points with induction motor

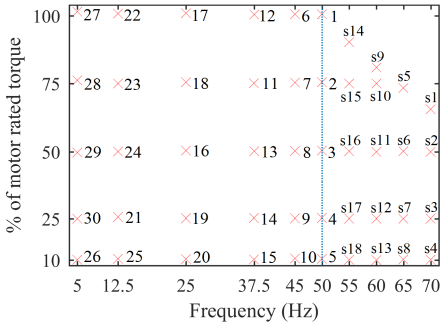

(b) Operating points with SynRM

Fig. 2. Operating point matrices used in the measurements. Points 1–30 were the same for both motors.

C. *Analysis procedure*

In order to compare the results from tests performed for two separate motors with different properties, the basis of the comparison has to established. There is a difference in speed between the induction motor and the synchronous reluctance motor, which is due to the slip of the IM when both motors are driven at the same supply frequency. This results in some difference in the output power at the same torque, but as the converter losses and also the motor losses are dependent on the supply frequency rather than on the rotor speed, a comparison based on frequency and torque is more relevant from the efficiency point of view.

To match the measurement data over the frequency–torque (*f*-*T*) plane, the data were interpolated over the measurement range. To best illustrate the plotted results, hertz (Hz) was used as the unit for frequency whereas torque was converted into a percentage of the IM rated torque. The interpolation was performed with the Matlab griddata function with the natural neighbor interpolation method and with a grid density of 0.1 (Hz, torque-%). All calculations for the efficiency determination were performed with the interpolated data.

D. *Efficiency determination*

The motor efficiency, the converter efficiency, and the complete drive system efficiency were calculated from the interpolated measurement results. The motor efficiency is

$$\eta_{\mathrm{mot}} = \frac{P_{\mathrm{mech}}}{P_{\mathrm{in}}} \cdot 100\% \,, \tag{1}$$

where P_{in} is the electrical input power of the motor obtained with the power analyzer, and P_{mech} is the output power of the motor

$$P_{\mathrm{mech}} = 2\pi \frac{n}{60} T \,, \tag{2}$$

where n is the operating speed in r/min and T is the torque. The converter efficiency is

$$\eta_{\mathrm{con}} = \frac{P_{\mathrm{in}}}{P_{\mathrm{con}}} \cdot 100\% \,, \tag{3}$$

where P_{con} is the input power of the converter from the power analyzer. The drive system efficiency is

$$\eta_{\mathrm{drvs}} = \frac{P_{\mathrm{mech}}}{P_{\mathrm{con}}} \cdot 100\% \,. \tag{4}$$

E. *Efficiency results*

The interpolated efficiency results and efficiency differences are presented as contour plots in Figs. 3 and 4. The differences between the measurements with the SynRM and the IM were calculated by directly subtracting the IM efficiency percentages from the corresponding SynRM results. The measurement points are indicated by × in the figures. In the efficiency difference plots (Fig. 3(c) and Fig. 4), × is used to denote the points common to both motors while asterisks and crosses denote the IM-only and SynRM-only points, respectively, at

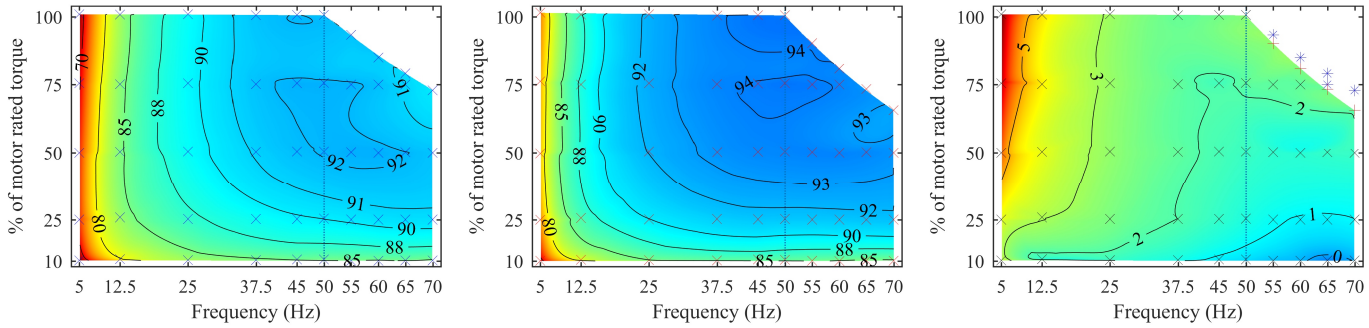

(a) Induction motor efficiency (%) (b) SynRM efficiency (%) (c) Motor efficiency difference (%-unit)

Fig. 3. Induction motor (IM) and synchronous reluctance motor (SynRM) efficiencies over the tested frequency–torque range, and the difference between the motor efficiencies.

the highest torque points over the field weakening range.

The efficiency maps calculated for the tested motors are presented in Fig. 3. Plots (a) and (b) in Fig. 3 show that the overall efficiency behaviors of the IM and of the SynRM are similar, the highest efficiency being found around the motor rated frequency of 50 Hz and at around 75% of the rated torque. Plot 3(c), however, shows that there are signifigant differences in the efficiency values in certain areas of the measurement range. The efficiency difference between the IM and the SynRM is largest at low frequencies (low speeds) and high torques, whereas the difference is lowest at high frequencies (high speeds) and low torques. This is expected, as the IM rotor losses increase at higher loads, and at higher frequencies, the relative speed difference caused by the slip of the IM becomes less significant.

The difference in the efficiency of the frequency converter used with both the IM and the SynRM is shown in Fig. 4(a). The converter efficiency when driving the SynRM is lower than when used with the IM over most of the measured range; only at low loads below 10–20% the converter efficiency is slightly higher with the SynRM. The lower converter efficiency at higher loads with the SynRM is due to the lower power factor, and thereby a higher stator current, of the SynRM compared with a similar IM.

The total efficiencies of the complete drive systems are compared in Fig. 4(b), showing very similar results to Fig. 3(c). This is no surprise as the converter efficiency difference in Fig. 4(a) is small compared with the motor efficiency difference in Fig. 3(c).

F. Efficiency ratings for the tested drive systems (IEC 61800-9-2)

The new standard IEC 61800-9-2 [8] defines the type testing of power drive systems (PDS) for IES efficiency ratings. The measurements performed at the rated operating points meet the standard requirements, and thus, the IES ratings could be determined for both the IM drive system and the SynRM drive system. The IES rating is based on a comparison of the total losses of the tested drive system with the IEC-defined reference drive system. For a 15 kW reference drive system, the relative reference losses are 19.94%; in other words, the reference losses are 2.99 kW. According to [8], the total losses of the tested drive system are calculated as

$$P_{\mathrm{L,PDS}} = P_{\mathrm{L,PDS,determined}} + \Delta P_{\mathrm{L,PDS}}\,, \tag{5}$$

where $P_{\mathrm{L,PDS,determined}}$ are the drive system total losses determined at the rated operating point and $\Delta P_{\mathrm{L,PDS}}$ is the total loss uncertainty. The values for the above quantities for both drive systems are shown in Table II. For the IM drive system, the total losses are 1813 W and for the SynRM drive system 1397 W, and with the uncertainty added, the total loss values are 1861 W and 1445 W, respectively. The IEC [8] defines three IES classes; the drive system efficiency rating is IES1 if the losses are within 80–120% of the reference losses, IES0 if over 120%, and IES2 if less than 80% of the reference losses. For the tested IM drive system, the drive system total losses are 62% and for the SynRM drive system 48% of the reference losses. Thus, the efficiency rating for both drive systems is IES2.

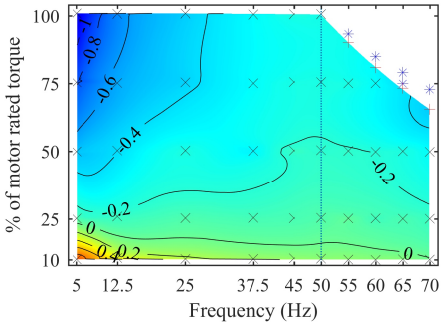

(a) Converter efficiency difference (%-unit)

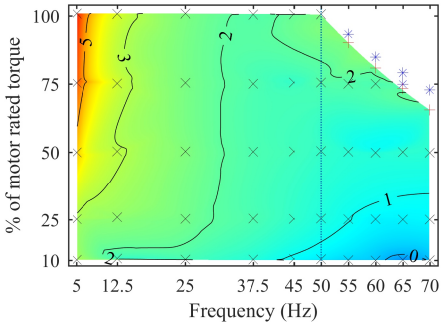

(b) Drive system efficiency difference (%-unit)

Fig. 4. Difference in the frequency converter efficiency between the IM and the SynRM measurements (a), and difference in the complete drive system efficiency between the IM and the SynRM measurements (b).

V. Discussion

Several aspects have to be considered when comparing two electric motors of different technologies. Here, even though the power rating is equal for the compared IM and SynRM, the test results show a totally different behavior for the motors over the measurement range. The difference in the rated efficiencies of the motors is 1.5% in favor of the SynRM, but in practice, according to the results, the efficiency difference varies substantially over the operating range from negligible at high

TABLE II. Determining the IES class for the tested drive systems

Variable	Induction motor	Synchronous reluctance motor
Determined total losses, $P_{\mathrm{L,PDS,determined}}$	1813 W	1397 W
Total loss uncertainty, $\Delta P_{\mathrm{L,PDS}}$	48 W	48 W
Rated power, P_{N}	15 kW	15 kW
Total losses with uncertainty, $P_{\mathrm{L,PDS}}$	1861 W	1445 W
Reference losses[a], $P_{\mathrm{L,REF}}$	2.99 kW	2.99 kW
$\frac{P_{\mathrm{L,PDS}}}{P_{\mathrm{L,REF}}}$	62%	48%
IES rating[a,b]	IES2	IES2

Values are for the drive system rated operating point used in the IES classification.
[a.] Defined in [8].
[b.] IES2 class is defined as losses less than 80% of the reference losses [8].

speeds and low loads up to over 5% at low speeds and high loads. The larger difference in the low-speed and high-load area is related to the per-unit slip of the IM, which is 2% in the rated operating point for the 15 kW IM used in the tests, but rises up to over 10% at low speeds. Further, the measured efficiency difference in the rated operating point is over 2%, which is more than the 1.5% difference given in the manufacturer's rated efficiencies. This discrepancy is due to the motor voltage ratings; the SynRM can only be used with a frequency converter and it is rated for 370 V, while the IM is rated for a nominal 400 V grid voltage. In these measurements, both motors were driven with a frequency converter, and thus, the IM voltage was lower than rated, which degrades the efficiency. Moreover, because of the SynRM and IM differences, the output power differs slightly between the two as the torque and frequency were matched in the measurements. The mechanical output power is the product of torque and rotational speed, and as the IM speed is slightly lower because of the slip, in reality, the SynRM produces slightly more power over the whole measurement range. The difference is largest at low speeds with high loads, further widening the efficiency gap between the two motors in this operating range. As slip is typically higher in small IMs, the benefits of the SynRM, and naturally also of the PMSM, are more significant in small motors.

The difference in the frequency converter efficiency was small when used with the two motors. The difference can be explained by the lower power factor and higher current requirement of the SynRM in the same conditions compared with a similar IM. The power factor difference between the SynRM and the IM increases with the motor size further reducing the benefits of the SynRM in large motors. It is emphasized that the power factor of a PMSM, on the other hand, is typically higher than the power factor of the IM of the same size. The efficiency difference of the converter part, however, had only a slight impact on the total drive system efficiency distribution, and the differences between the IM and SynRM drive system efficiencies were similar to the motor efficiency differences.

Both the IM and the SynRM drive systems achieved the IES2 rating [8], which is the highest IES rating. The SynRM drive system, or probably both systems, would actually be rated as IES3 if such a class was defined with the same principles as with the other IEC motor efficiency classifications. With the motor IE classes [2], each higher efficiency class reduces the losses by 20% from the previous class, which would result in the IES3 rating for drive systems with relative losses less than 64% of the reference losses. As the IE3 induction motor was capable of achieving the highest IES class by such a wide margin, the IES efficiency requirements seem rather loose, and at least the next IES3 level would already be needed.

All in all, although the SynRM used in these tests had a few extra advantages, such as the lower voltage rating and lower-loss electrical sheets, the results show that in certain applications, a SynRM drive system can be a viable alternative in terms of efficiency. On the other hand, the IM still has some obvious benefits, such as higher overloadability, and should not be counted out as an option at least in more demanding usage scenarios. Torque and current ripple have sometimes been considered as possible issues for SynRMs for instance in automotive or other applications requiring smooth torque, but these aspects were not addressed in this paper.

VI. Conclusion

The synchronous reluctance motor can provide a more efficient alternative to an induction motor at least in variable speed systems of low to medium power ratings. However, the different behavior of the motor compared with an induction motor should be kept in mind. According to the results of this paper, the efficiency difference is highest at low speeds with high torque, and correspondingly, lowest at high speeds with low torque.

References

[1] P. Waide and C. U. Brunner, Energy-Efficiency Policy Opportunities for Electric Motor-Drive Systems, International Energy Agency, 2011.

[2] Rotating electrical machines – Part 30-1: Efficiency classes of line operated AC motors (IE code), Ed. 1, *IEC 60034-30-1*, March 2014.

[3] Commission Regulation (EC) No 640/2009 of 22 July 2009 implementing Directive 2005/32/EC of the European Parliament and of the Council with regard to ecodesign requirements for electric motor). *Off. Jour. of the EU*, L 191, pp. 26–34, 23 July 2009.

[4] A. de Almeida, H. Falkner, J. Fong, K. Jugdoyal, EuP Lot 30: Electric motors and drives. Task 1: Product definition, standards and legislation. *ENER/C3/413-2010*, Final, April 2014.

[5] A. de Almeida, F. Ferreira, and G. Baoming, "Beyond induction motors—Technology trends to move up efficiency," *IEEE Trans. Ind. Appl*., vol. 50, no. 3, pp. 2103–2114, May/Jun. 2014.

[6] L. Aarniovuori, J. Kolehmainen, A. Kosonen, M. Niemelä, H. Chen, W. Cao and J. Pyrhönen, "Application of Calorimetric Method for Loss Measurement of a SynRM Drive System", *IEEE Transactions on Industrial Electronics*, vol. 63, no. 6, pp. 3942–3953, April 2016.

[7] A. de Almeida, F. Ferreira and J. Fong, "Standards for Efficiency of Electric Motors", *IEEE Industry Applications Magazine*, vol. 17, no. 1, pp. 12–19, Jan./Feb. 2011.

[8] Adjustable speed electrical power drive systems – Part 9-2: Ecodesign for power drive systems, motor starters, power electronics and their driven application – Energy efficiency indicators for power drive systems and motor starters, Ed. 1, *IEC 61800-9-2*, March 2017.

[9] L. Aarniovuori, P. Rasilo, M. Niemelä and J. Pyrhönen, "Analysis of 37 kW Converter-Fed Induction Motor Losses," *IEEE Trans. Ind. Electron.,* vol. 63, no. 9, pp. 5357–5365, September 2016.

[10] A. Boglietti, A. Cavagnino, M. Cossale, A. Tenconi, "Efficiency determination of converter-fed induction motors: Waiting for the IEC 60034–2–3 standard" in *Proc. 2013 IEEE Energy Conversion Congress and Exhibition*, Denver, Colorado, USA, pp. 230–237, September 2013.

[11] A. de Almeida, F. Ferreira, and A. Quintino Duarte, "Technical and economical considerations on super high-efficiency three-phase motors", *IEEE Trans. Ind. Appl*., vol. 50, no. 2, pp. 1274–1285, March 2014.

[12] L. Aarniovuori, T. Musikka, A. Kosonen, M. Niemelä and J. Pyrhönen, "Three alternative methods to determine voltage source converter losses", in *Proc. 17th Eur. Conf. on Power el. and Appl*., Geneva, Switzerland, Sept. 2015.

[13] R. Kanchan, L. Aarniovuori, M. Niemelä, R. Chitroju, F. Gyllensten,"Loss Measurements Analysis of VSD Motors Using Both Direct Input-Output and Calorimetric Methods," in *proc. Energy Efficiency in Motor Driven Systems 2015 (EEMODS'15)*, 15–17 Sept. 2015. Helsinki, Finland

[14] Energy efficiency test methods for three-phase variable frequency drive systems, Ed. 1, *CSA C838*, March 2013.

Publication IV

Kärkkäinen, H., Aarniovuori, L., Niemelä, M., Pyrhönen, J., Kolehmainen, J., Känsäkangas, T., and Ikäheimo, J.

Direct-On-Line Synchronous Reluctance Motor Efficiency Verification with Calorimetric Measurements

XIII International Conference on Electrical Machines (ICEM)
pp. 171-177, 2018

Direct-On-Line Synchronous Reluctance Motor Efficiency Verification with Calorimetric Measurements

H. Kärkkäinen, L. Aarniovuori, M. Niemelä, J. Pyrhönen, J. Kolehmainen, T. Känsäkangas, J. Ikäheimo.

***Abstract* – Direct-on-line motors are in the majority despite that an increasing number of new motor installations are equipped with frequency converter. However, regulations and environmental awareness are pushing the efficiency demands, and the dominant induction motor technology is approaching its practical efficiency limits. Direct-on-line synchronous reluctance motor technology provides an alternative to the induction motor technology with the capability to reach higher efficiency levels especially in low power range. This paper presents efficiency verification measurements using calorimetric method for two 45 kW direct-on-line synchronous reluctance motor prototypes. The results are compared with high-efficiency induction motors available in the market.**

***Index Terms*—AC motors, electric motors, energy efficiency, loss measurement, measurement techniques.**

I. Introduction

NOWADAYS, an increasing number of new electric motor installations are equipped with frequency converters [1]. There are, however, a variety of applications where speed control is not needed and optimal operation can be achieved with direct-on-line (DOL) motors. While this has been the natural playground for induction motors (IM), it seems that IM may not be able to keep up with the higher and higher efficiency requirements [2]. Permanent magnet synchronous motors (PMSM) and synchronous reluctance motors (SynRM) have better efficiency characteristics [2]-[5], but these motors are optimally suited for frequency converter supply as they inherently lack DOL-start capabilities. The DOL-capabilities can, however, be implemented by adding damper windings in the rotor construction.

This paper presents efficiency verification measurements for two 200-frame size direct-on-line SynRM (DOL SynRM) prototypes: a 2-pole and a 4-pole 45 kW motors. The performance characteristics are compared to high efficiency DOL induction motors with similar power ratings.

This work was supported in part by the European Union through Marie Sklodowska-curie actions under Grant ID 746900.

Hannu Kärkkäinen, Markku Niemelä and Juha Pyrhönen are with the LUT School of Energy Systems, Lappeenranta University of Technology, Lappeenranta, Finland, (e-mail: hannu.s.karkkainen@lut.fi, markku.niemela@lut.fi, juha.pyrhonen@lut.fi).

Lassi Aarniovuori is with the School of Engineering and Applied Sciences, Aston University, Birmingham, UK (e-mail: l.aarniovuori@aston.ac.uk).

Jere Kolehmainen is with School of Technology and Innovations, University of Vaasa, Finland (e-mail:jere.kolehmainen@univaasa.fi.

Tero Känsäkangas and Jouni Ikäheimo are with ABB Motors and Generators, Vaasa, Finland (e-mail: tero.kansakangas@fi.abb.com, jouni.ikaheimo@fi.abb.com).

II. Direct-on-line synchronous reluctance motor

The operation principle of a synchronous reluctance motor is based on reluctance torque and the rotor of a SynRM is designed with saliency maximized. Ideally, the SynRM rotor consists only of the reluctance path optimized stack built on the rotor shaft and the rotor structure is therefore even simpler than the one of an induction motor rotor. However, such a structure is not able to start from standstill without control. Therefore, a direct-on-line SynRM requires some additional properties. The simplest way to implement line start capabilities is to add a damper winding (short-circuit cage) in the rotor. The damper winding produces additional torque when the rotor speed differs from the synchronous speed exactly in the same manner as in a typical cage induction motor. Ideally, when the synchronous speed is reached, the cage winding should be currentless, but in reality fluctuations in the speed induce current – and cause resistive losses – to some extent in the cage winding.

In recent studies, two different types of line-start SynRM topologies have been considered: the one that is investigated here has a die-casted aluminum cage inside the rotor flux barriers [5] and another topology with a completely separate cage winding [6].

The nameplate values of the DOL SynRMs tested in this paper are shown in Table I. Both of the DOL SynRM prototypes are initially rated for 400 V, 50 Hz and 45 kW but one of the motors is a 2-pole machine with a rated speed of 3000 rpm, and the other one is a 4-pole machine running at 1500 rpm with the rated supply frequency. The DOL SynRM technology is a direct rival for the induction motor. Therefore,

TABLE I
THE NAMEPLATE DATA FOR THE DOL SYNRM PROTOTYPES AND FOR CORRESPONDING HIGH EFFICIENCY INDUCTION MOTORS FOR COMPARISON

	2-pole DOL SynRM	2-pole IM	4-pole DOL SynRM	4-pole IM	4-pole IM
Frame size (mm)	200	200	200	**225**	200
Rated efficiency (%)	96.3	94.0 (IE3)	94.7	94.2 (IE3)	93.9 (IE3)
Number of pole pairs	1	1	2	2	2
Rated voltage (V)	400	400	400	400	400
Connection	D	D	D	D	D
Rated frequency (Hz)	50	50	50	50	50
Rated power (kW)	45	45	45	45	**37**
Rated speed (rpm)	3000	2955	1500	1482	1480
Rated current (A)	81.4	77.6	86.7	80.2	69.3
Power factor	0.83*	0.89	0.79*	0.85	0.82

* Calculated based on the nameplate data

the measured losses and efficiencies are compared against industrial high efficiency IMs. For the 2-pole machine, a perfect competitor can be found from [7] but for the 4-pole version, there is no motor with the same frame size and rated power. Thus, we compare the results to both an IM with a matching power rating but a bigger frame size and to another IM with the same frame size but a lower rated power of 37 kW. The DOL SynRM measurements are performed also with 37 kW load in addition to the rated 45 kW, hence, the comparison with the 37 kW IM is straightforward. The nameplate data for the IM counterparts are included in Table I.

It has to be noted, that as the DOL SynRMs are prototypes the nameplate data are not final, but rather based on the machine design. However, some of the main differences of DOL SynRM and IM can already be seen in Table I: The DOL SynRMs run at synchronous speed while the speed ratings of the IMs are a slip value lower than the synchronous speed. When the power rating is the same, a difference in the rated speed also leads to a difference in the rated torque, i.e. the DOL SynRMs have slightly lower torque ratings. In addition, the DOL SynRMs power factor values are lower – and therefore the rated current values are higher – compared to the IM counterparts.

III. Determining the Losses and Efficiency of High-Efficiency Motors

The simplest method to determine the efficiency of an electric motor is the input-output method (also known as the direct method). The input-output method is based on direct measurements of the input electrical power P_e and output mechanical power P_m. The efficiency is calculated as a fraction P_m/P_e and total machine losses P_l are the difference between the mechanical and electrical power

$$P_l = P_e - P_m. \tag{1}$$

However, when measuring higher efficiency motors, this method begins to suffer of inaccuracy, since the small amount of losses is a difference of two large power values. The maximum absolute machine loss uncertainty U when calculated with (1) can be written as

$$U(P_l)_{max} = |\Delta P_e| + |\Delta P_m| \tag{2}$$

with ΔP_e and ΔP_m being errors in the corresponding measurement values. The efficiency η, mechanical power and electrical power have the following relationships

$$\eta = \frac{P_m}{P_e} \leftrightarrow P_e = \frac{P_m}{\eta} \leftrightarrow P_m = \eta P_e. \tag{3}$$

Substituting P_e and P_m from the second and the third form of (3) to (2), we get

$$U(P_l)_{max} = \frac{1}{\eta}|\Delta P_m| + \eta|\Delta P_e|, \tag{4}$$

which shows that the absolute machine loss uncertainty is a function of efficiency. However, commonly the uncertainties are given as relative values. We get the relative loss uncertainty by dividing (4) with the losses

$$U(P_l)_{max,rel} = \frac{1}{\eta P_l}|\Delta P_m| + \frac{\eta}{P_l}|\Delta P_e| \tag{5}$$

By reordering (5) we get the form

$$U(P_l)_{max,rel} = \frac{1}{1-\eta}\left|\frac{\Delta P_m}{P_m}\right| + \frac{\eta}{1-\eta}\left|\frac{\Delta P_e}{P_e}\right|, \tag{6}$$

which leads to the conclusion that the relative loss uncertainty $U(P_l)_{max,rel}$ is approaching infinity when the efficiency is approaching unity

$$\lim_{\eta \to 1} U(P_l)_{max,rel} = \infty. \tag{7}$$

Therefore, we have to examine other approaches than the one based on input and output powers such as segregation of losses method, which has been widely used for IMs and is also applied for PMSMs [8], and calorimetric methods to verify the high efficiency machine losses. Calorimetric methods are based on determining the machine losses directly from the heat dissipation of the machine and the loss uncertainty is therefore independent of the efficiency of the tested machine.

An open and balance type calorimeter is used in the measurements presented in this paper. According to previous studies [9], [10], this calorimeter type is considered one of the most accurate calorimetric systems in practice because only the differences between the two successful tests are deteriorating the accuracy of the acquired loss results. A detailed description of this calorimetric method has been presented in [11].

IV. Laboratory Measurements

Efficiency measurements using an open and balance type calorimeter were made for two 45 kW DOL SynRM prototypes. Input and output powers are measured during the calorimetric tests and the direct input-output results are presented for comparison. In addition, the mechanical losses of the tested motor are needed in the calorimetric analysis as explained later and therefore, retardation tests were performed for both motors.

The measurements were made for four different operating points listed in Table II. The first two points were 45 kW and 37 kW load points measured using the rated 400 V, 50 Hz input. The third operating point was 45 kW, 50 Hz using the optimal voltage resulting in the best efficiency, which was 420 V for both 2-pole and 4-pole motors. The fourth and the last point was 45 kW load at 60 Hz supply frequency at the optimal voltage of 480 V. The optimal voltage for 37 kW, 50 Hz was 400 V, i.e. the same as the second measurement point. The optimal voltage values resulting in the best efficiency were found using the direct input and output power measurements. Although the overall uncertainty of the input-

TABLE II
The Measurement Operating Points for Both Motors

Test point	Point 1	Point 2	Point 3	Point 4
Voltage (V)	400	400	420	480
Frequency (Hz)	50	50	50	60
Load (kW)	45	37	45	45

output method is high, the method is well suitable for finding the optimal voltage as even small differences can be measured reliably when the test setup and test conditions remain the same and each compared point is measured for long enough. Here, the voltage was altered at 2 V steps at 60 second intervals and the optimal voltage value was rounded down to the closest 10 V.

A. Test setup

The measurement setup (Fig. 1) consisted of the motor under test, a larger machine for adjustable load, instruments for measuring and recording electric and mechanical quantities, the calorimetric measurement system, and a synchronous generator for adjustable sinusoidal power supply. The electric quantities were measured with Yokogawa PX8000 power analyzer equipped with Hitec CURACC current measurement system. The torque and speed were measured with HBM T12 torque transducer. In the retardation test, an optical speed sensor was used for speed measurement. Temperature sensors were read with Keithley 2701 multimeter. The calorimetric measurement system was a medium-sized open- and balance type calorimeter equipped with hardware capable of measuring losses up to 3 kW.

B. Measurement and analysis procedure

The calorimetric method consists of two tests: the main test and the balance test. Here, the measurement procedure is explained using the rated point measurements with the 4-pole DOL SynRM as an example: the calorimetric data are presented in Table III, and the input-output data during the main test in Table IV. In the open and balance type calorimeter, determining the heat loss is based on first establishing a thermal equilibrium with the device under test as the heat source (main test), and after that a DC heater is used to find the same thermal conditions (balance test). During the measurement, chamber inlet and outlet temperatures are controlled: in the example case of Table III, the inlet temperature reference value was 23°C and outlet temperature reference value 40°C in both main test and balance test. A pre-heater controls the chamber inlet temperature during both

TABLE III
CALORIMETRIC DATA FOR THE 4-POLE DOL SYNRM AT THE RATED OPERATING POINT (45 KW, 400 V, 50 HZ)

Calorimetric data	Main test	Balance test
Ambient temp. (°C)	21.50	21.23
Chamber average temp. (°C)	36.28	42.89
Chamber inlet temp. (°C)	23.00	23.00
Chamber outlet temp. (°C)	39.99	40.04
Temp. difference (°C)	16.99	17.03
Pressure (mbar)	1002.0	1001.7
Humidity (RH)	23.68	24.33
Resistor power (W)	0	2654.5
Exhaust blower speed (rpm)	1552.3	1552.7
Motor cooling air temp. (°C)	35.4	44.8
Motor winding temp. (°C)	100.7	48.3
Mechanical losses (W)	N/A	89*

* Determined with a separately performed retardation test

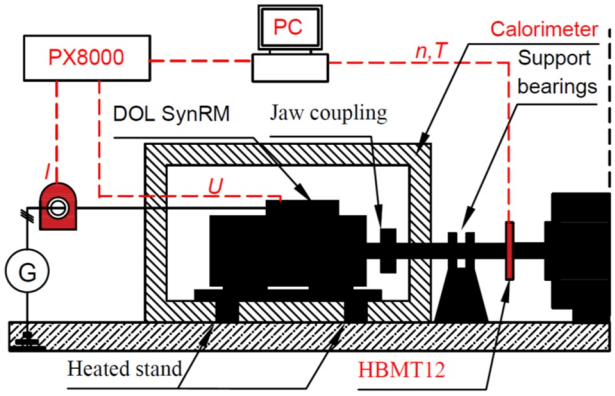

Fig. 1. The measurement setup for calorimetric- and input-output measurements.

tests. In the main test, the chamber exhaust blower controls the outlet temperature and in the balance test, the DC heater controls the outlet temperature. When the thermal equilibrium is established in the main test and the outlet blower speed has stabilized, the blower speed is fixed to the final value. After confirming that the thermal equilibrium is maintained without the blower control, the main test data are recorded. Next, the motor is stopped and the balance test is started. During the balance test, the air circulation has to be kept identical as in the main test and to achieve this, the tested motor is rotated at the same speed as in the main test using the load machine. Rotating the motor externally also naturally keeps up the cooling of the motor and reduces settling time of the motor temperature. When the motor temperature has settled down and the DC heater power has stabilized, the heater power is fixed to the final value. After confirming that the thermal equilibrium is maintained, the balance test data are recorded. Here, in both main test and balance test, the sampling interval was 20 seconds, and the data length for each test was 100 samples (2000 s). Ideally, if the conditions during main test and balance test were identical, the loss result for the tested motor would simply be the sum of the DC heater power and the mechanical losses of the motor. However, as the recordings for the main test and balance test are taken several hours apart, the air properties – such as air pressure and humidity – may vary significantly. As the humidity and pressure affect the specific heat of the air, these quantities are recorded and their effects are taken into account in the final analysis. In addition, although inlet and outlet temperature are

TABLE IV
MAIN TEST INPUT-OUTPUT DATA FOR THE 4-POLE DOL SYNRM AT THE RATED OPERATING POINT (45 KW, 400 V, 50 HZ)

Input-output data	Main test
Electric Power (W)	47695
Current (A)	87.79
Voltage (V)	400.5
frequency (Hz)	50.00
cos(φ)	0.783
Shaft power (W)	45019
Speed (rpm)	1500.1
Torque (Nm)	286.58

controlled, slight differences often occur in the final data, and these deviations are also taken into account in the analysis. In the example case (Table III), the differences between the main test and the balance test were modest: humidity had changed by 0.65 %-units, the air pressure by 0.3 mbar, and inlet-outlet temperature difference by 0.04°C. Especially the changes in humidity and air pressure can be significantly higher between the tests.

As the motor is rotated during the balance test, it acts as an additional heat source with heating power equal to the mechanical losses of the motor. In order to take the mechanical losses into account in the calorimetric analysis, a retardation test is performed separately. The retardation test was performed in open test bench after the calorimetric measurements. The friction in the bearings is temperature dependent, and therefore the retardation test was made with the motor heated to approximately the same temperature as during the balance test. In the test, the motor was accelerated up to slightly above the 60 Hz speed (~1850 rpm for the 4-pole motor) and after this, the power supply was cut off, leaving the motor rotated only by its own inertia without excitation. The speed of the freely decelerating motor was measured at one second intervals using an optical speed sensor. From the instantaneous decrease-rate of the speed, the mechanical losses P_{fw} (friction and windage) can determined as [12]

$$P_{\mathrm{fw}} = -Cn\frac{\mathrm{d}n}{\mathrm{d}t}, \tag{8}$$

where t is time, n is the speed in rpm, and C is the retardation constant, which depends on the total inertia J according to [12]

$$C = \frac{4\pi^2}{60}J. \tag{9}$$

A second order polynomial fit for the speed $n(t)$ was made and the mechanical loss curve $P_{\mathrm{fw}}(n)$ was calculated using (8). The mechanical losses for the 4-pole machine were 89 W at 50 Hz (1500 rpm) and 140 W at 60 Hz (1800 rpm). For the 2-pole machine the values were significantly higher, 425 W at 50 Hz (3000 rpm) and 625 W at 60 Hz (3600 rpm).

The calorimetric results for the example case with the 4-pole DOL SynRM are shown in Table V. The first column contains the results in the actual cooling air temperature inside the calorimeter (35.4°C), which however is notably higher than the reference coolant temperature of 25°C given in the motor efficiency standards [13]. In the case of a synchronous reluctance motor, only the stator Joule losses P_{s} are significantly temperature dependent. The stator losses can be determined from the stator winding resistance R_{s} and current I

$$P_{\mathrm{s}} = 1.5R_{\mathrm{s}}I^2. \tag{10}$$

Furthermore, the stator losses can be corrected to the reference coolant temperature. According to [13], the stator Joule losses in the 25°C temperature are

$$P_{\mathrm{s,25°C}} = k_\theta P_{\mathrm{s}}, \tag{11}$$

where the temperature correction factor

$$k_\theta = \frac{235 - \theta_{\mathrm{w}} + 25 - \theta_{\mathrm{c}}}{235 + \theta_{\mathrm{w}}}, \tag{12}$$

in which 235 is the temperature constant for copper, 25 is the reference coolant temperature, θ_{w} is the motor winding temperature, and θ_{c} is the coolant air temperature. In the example case (Tables III-V), the winding temperature θ_{w}=100.7°C and the coolant air temperature θ_{c} = 35.4°C. The calorimetric results corrected to 25°C are shown in the second column of Table V. Correcting the stator losses naturally affects the electric power draw as shown in Table V. Here, the shaft power is calculated from the electric power and the calorimetric losses as the electric power measurement can usually be considered more accurate than the measured shaft power. However, the measured shaft power value from Table IV could be used as well, because when the loss value is accurate, the effect of the power measurement inaccuracy on the efficiency result is small. For example, 1% (450 W) error in the shaft power value would only cause a 0.06%-unit error in the efficiency result in this case.

The input-output losses and efficiency were corrected to 25°C in similar manner as the calorimetric results.

TABLE V
CALORIMETRIC RESULTS FOR THE 4-POLE DOL SYNRM AT THE RATED OPERATING POINT (45 KW, 400 V, 50 HZ) IN CALORIMETER TEMPERATURE AND CORRECTED TO STANDARD REFERENCE TEMPERATURE OF 25°C

	Coolant temperature	
	35.4°C	**25°C**
Calorimetric losses, $P_{\mathrm{l,cal}}$ (W)	2691	2650
Electric power, P_{e} (W)	47695	47654
Shaft power, $P_{\mathrm{m}} = P_{\mathrm{e}} - P_{\mathrm{l,cal}}$ (W)	45004	45004
Efficiency, $\eta = \frac{P_{\mathrm{m}}}{P_{\mathrm{m}}+P_{\mathrm{l,cal}}}$ (%)	94.36	94.44

V. RESULTS AND COMPARISONS

The measurement results are compared here to the efficiency levels given in international standard [14], and to the induction motor counterparts. Additionally, the stator and rotor loss differences between IMs and DOL SynRMs are analyzed.

A. Efficiency comparison

The results from the calorimetric measurements and the input-output measurements in all four test points with both motors are shown in Fig. 2. The calorimetric method and the direct method are in very good agreement, although it has to be noted that the instruments used here for the input-output power measurements are state-of-the-art and the torque transducer reading offset is checked carefully before and after each set of measurements. Considering the loss values, the 2-pole DOL SynRM has approximately 10% lower losses than the 4-pole machine in each of the measurement points. The difference between 400 V and the optimal voltage of 420 V at 45 kW was small but clear for both motors.

The determined efficiencies and IE-classes for the tested motors are presented in Tables VI and VII. The 2-pole DOL SynRM is able to reach IE4-efficiency in every test point– although only barely at the nameplate rated point. The

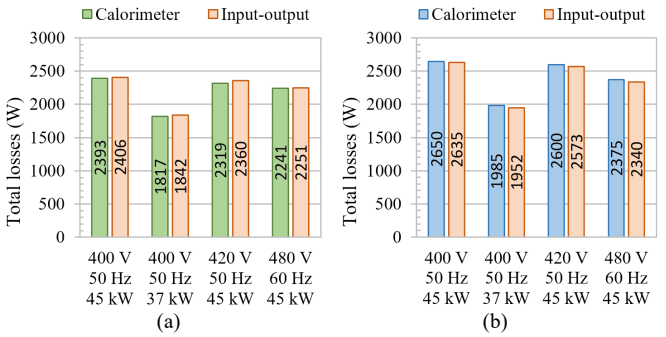

Fig. 2. The losses of the 2-pole (a) and 4-pole (b) DOL SynRM determined with the calorimetric method and with the direct method. The loss values are corrected to the reference coolant temperature of 25°C.

4-pole motor in turn, reaches only IE3 level at all points, being however closer to IE4-level (≥ 95.2%) at 37 kW, but falling to the bare minimum of the IE3-level at the 60 Hz point. The 2-pole motor does not seem to benefit as much as the 4-pole motor from a lower load: the efficiency of the 2-pole DOL SynRM is only 0.3%-units higher at 37 kW than at 45 kW, while the corresponding number for the 4-pole DOL SynRM is 0.5%-units.

In Fig. 3 and Table VIII, the test results are compared against the three IM rivals introduced in Table I. Each of the IMs are rated at exactly the limit of the IE3-class and DOL SynRMs seem to have efficiency advantage against all three IM counterparts. The 2-pole DOL SynRM has one %-unit – and one IE-class – advantage over the corresponding IM. The 4-pole DOL SynRM is compared against a larger frame (225 vs. 200) IM at 45 kW, and against the same frame size IM at 37 kW. At 45 kW, there is only a slight efficiency advantage for the DOL SynRM. Against a matching frame size at 37 kW, the advantage of the 4-pole DOL SynRM widens to one %-unit in similar manner to the 2-pole motors, still however coming short by 0.3%-unit from the IE4-classification.

Table VIII compares the measurement results against the IM nameplate data and the initial nameplate data of the DOL SynRMs (from Table I). Although performing well compared to the corresponding IM, the measured values of the 2-pole DOL SynRM are quite far from the initial nameplate data: The measured efficiency and power factor are considerably lower and as a result, the measured current is correspondingly higher, than the nameplate would indicate.

TABLE VI
THE LOSSES, EFFICIENCY AND IE-CLASS OF THE 2-POLE DOL SYNRM PROTOTYPE IN THE DIFFERENT OPERATING POINTS DETERMINED WITH THE CALORIMETRIC METHOD

Rating point	Total losses (W)	Efficiency (%)	IE-class
45 kW, 400 V, 50 Hz	2393	95.0	IE4 (≥95.0)
37 kW, 400 V, 50 Hz	1817	95.3	IE4 (≥94.8)
45 kW, 420 V, 50 Hz	2319	95.1	IE4 (≥95.0)
45 kW, 480 V, 60 Hz	2241	95.3	IE4 (≥94.5)

The IE-classes are according to IEC 60034-30-1 [14].

TABLE VII
THE LOSSES, EFFICIENCY AND IE-CLASS OF THE 4-POLE DOL SYNRM PROTOTYPE IN THE DIFFERENT OPERATING POINTS DETERMINED WITH THE CALORIMETRIC METHOD

Measurement point	Total losses (W)	Efficiency (%)	IE-class
45 kW, 400 V, 50 Hz	2650	94.4	IE3 (≥94.2)
37 kW, 400 V, 50 Hz	1985	94.9	IE3 (≥93.9)
45 kW, 420 V, 50 Hz	2600	94.5	IE3 (≥94.2)
45 kW, 480 V, 60 Hz	2375	95.0	IE3 (≥95.0)

The IE-classes are according to IEC 60034-30-1 [14].

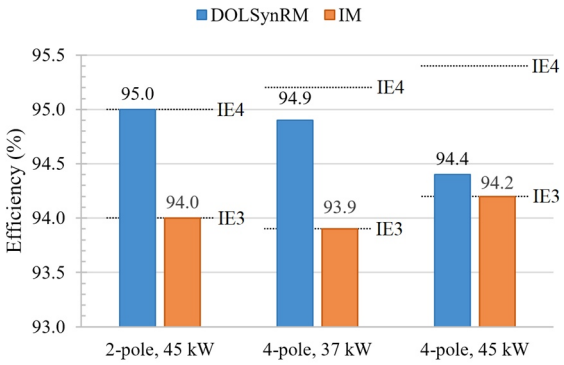

Fig. 3. Comparison of the efficiencies of the DOL SynRMs and the IM competitors. The 4-pole DOL SynRM is compared with an IM having same power rating but larger frame size, and also also with a 37 kW IM, which in turn has the same frame size.

The measured values for 4-pole DOL SynRM are, however, a lot closer to the nameplate data, although coming a bit short of the nameplate values as well. The induction motors have better power factor than the DOL SynRMs in all three cases, but especially the 0.89 vs. 0.77 power factor difference for the 2-pole motors is quite high.

TABLE VIII
THE MEASUREMENT RESULTS COMPARED WITH THE NAMEPLATE DATA

	2-pole, 45 kW			4-pole, 45 kW			4-pole, 37 kW	
	DOL SynRM		IM	DOL SynRM		IM	DOL SynRM	IM
	Nameplate	Measured	Nameplate	Nameplate	Measured	Nameplate	Measured	Nameplate
Efficiency (%)	96.3	**95.0**	94.0	94.7	**94.4**	94.2	94.9	93.9
Voltage (V)	400	400.4	400	400	400.5	400	400.2	400
Frequency (Hz)	50	50.00	50	50	50.00	50	50.00	50
Power (kW)	45	45.1	45	45	45.0	45	37.0	37
Speed (rpm)	3000	3000	2955	1500	1500	1482	1500	1480
Current (A)	81.4	**89.6**	77.6	86.7	**87.8**	80.2	73.0	69.3
Power factor	0.83*	**0.77**	0.89	0.79*	**0.78**	0.85	0.77	0.82

* Calculated based on the nameplate data

B. Joule losses

In a SynRM, the Joule losses in the rotor are practically zero, while in an induction motor the rotor Joule losses are

$$P_{\mathrm{r}} = (P_1 - P_{\mathrm{s}} - P_{\mathrm{Fe}})s, \tag{13}$$

where P_1 is the electric input power, P_{s} is the stator Joule loss, P_{Fe} is the iron loss, and s is the slip. Since $P_1 \gg |P_{\mathrm{s}} + P_{\mathrm{Fe}}|$, the rotor Joule losses can be estimated as

$$P_{\mathrm{r}} = P_1 s. \tag{14}$$

Using the induction motor rated power, efficiency and slip values from Table I we can try to estimate the losses of the corresponding DOL SynRM from the IM values. On the other hand, the stator Joule losses are higher for DOL SynRMs due to lower power factor. A change ΔP_{s} in stator losses affects the input power draw P_1, but as $P_1 \gg \Delta P_{\mathrm{s}}$, we can estimate the DOL SynRM current at a matching power factor with

$$I = \frac{P_1}{1.5 U \cos\varphi}, \tag{15}$$

using the measured DOL SynRM input power as P_1 and the induction motor power factor as $\cos\varphi$. Now, the stator losses can be recalculated with (10) using the lower current value from (15).

Table IX shows the calculated effects of the IM rotor losses and DOL SynRM power factor. For the 2-pole 45 kW motors and the 4-pole 37 kW motors, the adjusted total losses of the DOL SynRM and IM match almost perfectly. For the 4-pole 45 kW results, the difference is smaller without the adjustments. With the adjustments, there is a considerable difference in favor of the IM. This is in line with the efficiency difference, which was similar (1%-unit) between 2-pole motors and 4-pole 37 kW motors but much smaller (0.2%-unit) between the 4-pole 45 kW motors. The similarities indicate that the 4-pole DOL SynRM has more in common with the similar frame-sized 37 kW IM than with the larger 45 kW IM. According to this analysis, by neglecting the rotor losses of an IM and with an estimate for the SynRM power factor, the efficiency of a corresponding (DOL) SynRM can be predicted. The lower power factor of the SynRM increases the stator losses, but its efficiency deterioration effect is much lower than the improving effect of removing the IM rotor losses as shown in Table IX.

TABLE IX
COMPARISON BETWEEN DOL SYNRM LOSSES WITH A POWER FACTOR MATCHING WITH IM, AND IM LOSSES WITHOUT ROTOR LOSSES

Losses	2-pole 45 kW	4-pole 45 kW	4-pole 37 kW
DOL SynRM	2393 W	2650 W	1985 W
P_{s}	1032 W	1301 W	854 W
$P_{\mathrm{s,PF\text{-}match}}$	764 W	1105 W	752 W
ΔP_{s}	268 W	196 W	102 W
DOL SynRM$-\Delta P_{\mathrm{s}}$	2125 W	2454 W	1883 W
IM	2872 W	2771 W	2404 W
P_{r}	718 W	573 W	525 W
IM -P_{r}	2154 W	2197 W	1878 W
$\Delta P_{\mathrm{actual}}$	-479 W	-120 W	-419 W
$\Delta P_{\mathrm{adjusted}}$	**-29 W**	**257 W**	**5 W**

The 4-pole DOL SynRM has obvious similarities with the 37 kW IM and in practice, the lower losses of the DOL SynRM allow the motor to be rated for 45 kW. All the compared motors here are temperature rise class B motors with class F insulation. The temperature rise of the 4-pole DOL SynRM windings was only 48 K at 37 kW, and at 45 kW still reasonable 65 K, while 80 K would be the allowed for a temperature rise class B motor. The 2-pole DOL SynRM was closer to the class B limit with a temperature rise of 75 K despite its lower losses.

VI. DISCUSSION

The SynRM with DOL starting capability via die-casted aluminum cage inside the rotor flux barriers is a highly interesting motor design due to low manufacturing costs and it can be a real alternative for induction motors in the fixed speed applications. The lower rotor losses also end up in the lower bearing temperatures, which will increase the lifetime of the bearings. The SynRM technology has been criticized for needing larger currents to provide the same output power due to low power factor, but the rated current differences are actually rather small as shown here.

Although the results presented here show distinctly, that DOL SynRM has an efficiency advantage over IM, the differences in the motor technologies and in the basic operation have to be kept in mind. The operating speed difference in all compared cases here is larger than the efficiency difference, which leads to a situation, where the higher efficiency motor with higher speed actually consumes more energy if the higher operating speed cannot be utilized by the application efficiently.

VII. CONCLUSION

The 2-pole and 4-pole DOL SynRM experimental efficiency verification with a calorimetric method was performed and the results were compared to the IM counterparts. The two DOL SynRM prototypes had higher efficiency against all three IM counterparts. The 2-pole DOL SynRM had a full IE-class advantage over the IM rival. The 4-pole DOL SynRM had only slightly higher efficiency compared to the IM rival with matching 45 kW power rating but larger frame size. At partial load of 37 kW against a similar frame size 37 kW-rated IM, the 4-pole DOL SynRM had 1%-unit higher efficiency. In addition, the results were analyzed further by matching the power factors, and neglecting the IM rotor losses. It appears that the efficiency of a corresponding (DOL) SynRM can be estimated by subtracting the rotor losses from the IM total losses and adjusting the stator losses according to the power factor difference between IM and SynRM. Overall, the results show, that the DOL SynRM technology has an evident advantage over IM in efficiency, at least up to the 45 kW power range rather. Larger DOL SynRMs will see diminishing benefits compared to corresponding IMs, but in lower power range, the advantage of the DOL SynRM is even higher.

VIII. REFERENCES

[1] J. Sander, “Efficient Motor Policy for Europe – view from CEMEP”, in *Proc. Motor Summit 2016*, Zurich, Switzerland, October 2016.

[2] A. de Almeida, F. Ferreira, and G. Baoming, “Beyond induction motors—Technology trends to move up efficiency,” *IEEE Trans. Ind. Appl*., vol. 50, no. 3, pp. 2103–2114, May/Jun. 2014.

[3] H. Kärkkäinen, L. Aarniovuori, J. Kolehmainen, M. Niemelä, and J. Pyrhönen, ”Technology Comparison of Induction Motor and Synchronous Reluctance Motor,” *IECON 2017 - 43rd Annual Conference of the IEEE Industrial Electronics Society*, Beijing, 2017, pp. 2207-2212.

[4] A. de Almeida, F. Ferreira and J. Fong, “Standards for Efficiency of Electric Motors”, *IEEE Industry Applications Magazine*, vol. 17, no. 1, pp. 12–19, Jan./Feb. 2011.

[5] M. Gamba, G. Pellegrino, A. Vagati and F. Villata, "Design of a line-start synchronous reluctance motor," *2013 International Electric Machines & Drives Conference*, Chicago, IL, 2013, pp. 648-655.

[6] H. C. Liu and J. Lee, "Optimum Design of an IE4 Line-Start Synchronous Reluctance Motor Considering Manufacturing Process Loss Effect," in *IEEE Transactions on Industrial Electronics*, vol. 65, no. 4, pp. 3104-3114, April 2018.

[7] ABB Motors and Generators, “Catalog – Low Voltage Process Performance Motors,” Dec. 2017. [Online]. Available: ‘http://www.abb.com/abblibrary/DownloadCenter/’

[8] B. Deusinger, M. Lehr and A. Binder, "Determination of efficiency of permanent magnet synchronous machines from summation of losses," *2014 International Symposium on Power Electronics, Electrical Drives, Automation and Motion*, Ischia, 2014, pp. 619-624.

[9] L. Aarniovuori, J. Kolehmainen, A. Kosonen, M. Niemelä, H. Chen, W. Cao, and J. Pyrhönen, "Application of Calorimetric Method for Loss Measurement of a SynRM Drive System," in *IEEE Transactions on Industrial Electronics*, vol. 63, no. 4, pp. 2005-2015, April 2016.

[10] L. Aarniovuori, H. Kärkkäinen, A. Kosonen, J. Pyrhönen, Z. Liu and W. Cao, "Overview of calorimetric systems used in loss determination of electric motors and drives," *IECON 2017 - 43rd Annual Conference of the IEEE Industrial Electronics Society*, Beijing, 2017, pp. 2110-2115.

[11] A. Kosonen, L. Aarniovuori, J. Ahola, J. Backman, J. Pyrhönen and M. Niemelä, “Loss Definition of Electric Drives by a Calorimetric System With Data Processing,” *IEEE Transactions on Industrial Electronics*, vol. 61, no. 8, pp. 4432-4442, Aug. 2014.

[12] Rotating electrical machines – Part 2-2: Specific methods for determining separate losses of large machines from tests – Supplement to IEC 60034-2-1, Ed. 1, IEC 60034-2-2, March 2010.

[13] Rotating electrical machines – Part 2-1: Standard methods for determining losses and efficiency from tests (excluding machines for traction vehicles), Ed. 2, *IEC 60034-2-1*, June 2014.

[14] Rotating electrical machines – Part 30-1: Efficiency classes of line operated AC motors (IE code), Ed. 1, *IEC 60034-30-1*, March 2014.

IX. BIOGRAPHIES

Hannu Kärkkäinen was born in Imatra, Finland, in 1980. He received the M.Sc. degree in electrical engineering from Lappeenranta University of Technology (LUT), Lappeenranta, Finland, in 2015. He is currently a Junior Researcher with the Department of Electrical Engineering, LUT. His research interests include electric drive systems, particularly loss and efficiency measurements of motors and drives.

Lassi Aarniovuori received M.Sc. and D.Sc. degrees in electrical engineering from Lappeenranta University of Technology (LUT), Lappeenranta, Finland, in 2005 and 2010, respectively.

Dr. Aarniovuori is currently a Marie Curie Fellow with the School of Engineering and Applied Science, Aston University, UK. His current research interests include the field of electric motor drives, especially wide band-gap power switches, modulation methods, simulation of electric drives, efficiency measurements, and calorimetric measurement systems.

Markku Niemelä was born in Mäntyharju, Finland, in 1968. He received the B.Sc. degree in electrical engineering from Helsinki Institute of Technology in 1990, and the M.Sc. and D.Sc. (technology) degrees from Lappeenranta University of Technology (LUT), Lappeenranta, Finland, in 1995 and 1999, respectively.

He is currently a Senior Researcher with the Carelian Drives and Motor Centre in LUT. His current research interests include motion control, control of line converters, and energy efficiency of electric drives.

Juha Pyrhönen born in 1957 in Kuusankoski, Finland, received the Doctor of Science (D.Sc.) degree from Lappeenranta University of Technology (LUT), Finland in 1991. He became Professor of Electrical Machines and Drives in 1997 at LUT.

He is engaged in research and development of electric motors and power-electronic-controlled drives. Prof. Pyrhönen has wide experience in the research and development of special electric drives for distributed power production, traction and highspeed applications. Permanent magnet materials and applying them in machines have an important role in his research. Currently he is also studying possibilities of using carbon-based materials in electrical machines.

Jere Kolehmainen received the M.Sc. and Ph.D. degrees in theoretical physics from the University of Jyväskylä, Finland, in 1996 and 2000, respectively, and the D.Sc. degree in electrical engineering from Aalto University, Helsinki, Finland, in 2012.

He is currently with the University of Vaasa, Vaasa, Finland. His research interests include synchronous and induction machines, and electromagnetic modeling

Tero Känsäkangas received the B.Sc. and M.Sc. degrees in electrical engineering from the University of Vaasa, Vaasa, Finland, in 2011 and 2012, respectively, where he is currently working toward the D.Sc. degree in electrical engineering.

He is currently a Senior Research and Development Engineer with ABB Oy Motors and Generators, Vaasa, and a part time Teacher with the Department of Electrical Engineering, University of Vaasa. His research interests include synchronous reluctance and induction ac machines.

Jouni Ikäheimo received the M. Sc. and Ph.D. degrees in theoretical physics from the Helsinki University of Technology, Espoo, Finland, in 1992 and 1996, respectively. He is currently the Manager of Future Technologies with ABB Oy Motors and Generators, Vaasa, Finland.

Publication V

Kärkkäinen, H., Aarniovuori, L., Niemelä, M., and Pyrhönen, J.
Induction Motor Efficiency Verification Using a Balance-Type Calorimeter Equipped with a Mass Flow Meter

20th European Conference on Power Electronics and Applications (EPE'18 ECCE Europe)
pp. 1-10, 2018

Induction Motor Efficiency Verification Using a Balance-Type Calorimeter Equipped with a Mass Flow Meter

Hannu Kärkkäinen, Lassi Aarniovuori, Markku Niemelä and Juha Pyrhönen
LAPPEENRANTA UNIVERSITY OF TECHNOLOGY
P.O. Box 20, FI-53851
Lappeenranta, Finland
hannu.s.karkkainen@lut.fi
URL: http://www.lut.fi

Keywords; Experimental testing, Calorimetry, Induction Motor, Measurement, Standards, Uncertainty.

Abstract

Determination of losses accurately is challenging for today's high-efficiency power electronics and motors. Due to the limitations of the typically used input-output method, other loss measurement methods have been designed. Here, the efficiency of a direct-on-line induction motor prototype is determined using the IEC loss segregation method, the input-output method, and with a balance type calorimeter. The calorimetric results are further analyzed with the help of a mass flow meter that is used to verify the loss results obtained using the balance test.

Introduction

The ability to verify the energy efficiency improvements in motors and drives is becoming more and more challenging because distorted waveforms make accurate electric measurements difficult and because of the very small difference of the input and output power as a result of high efficiency. High energy efficiency is one of the key trends in the electric drives and motors industry. When using loss determination based on input and output powers, the loss uncertainty is approaching infinity when the device efficiency is approaching unity. One solution to this problem is to measure the dissipated heat directly using a calorimeter [1]. The calorimetric measurement method has been an official measurement method to determine the electric motor losses [2], but it has been removed as unnecessary from the latest IEC standard editions due to accuracy improvements in power analyzers and torque transducers. Therefore, the calorimetric method is nowadays not an official measurement method for electric motors. However, calorimeters have been introduced recently as a standard method in IEC 61800-9-2 [3] to overcome the problems in the experimental determination of frequency converter losses and they have been used in motor efficiency evaluation [4],[5]. One of the promising calorimetric approaches is the balance-type calorimeter with air as coolant [6]. The balance-type calorimeter relies on calibrating the measurement system with reference power at the very specific loss measurement point after a successful test with the device under test (DUT) rather than using the mass or volume flow measurement [7]. Here, the induction machine losses are measured with the IEC segregation of losses method, the input-output method, and compared with calorimetric results obtained with reference power tests and with an accurate mass flow meter. The effect of the air specific heat variation during the measurements due to barometric pressure and air humidity deviation is analyzed. The mass flow meter is used to examine the actual mass flow changes during the main and balance tests and to estimate the amount of the total heat leakage during the measurement.

Experimental measurements

In the mass production of industrial motors, it is common that that same physical construction is sold with different nameplate values but naturally, it has to fulfill all the requirements that have been set in the regulations and legislation. The motivation of these measurements was to verify the efficiency of 132 frame-sized prototype totally enclosed fan-cooled induction motor (TEFC IM) in three different operating points, Table I. All these measurement points can be considered nominal operating points for

this motor. Two heat run tests in all operating points were performed, one as part of IEC segregation of losses method and another inside the calorimetric chamber as well as several other runs to obtain all loss components accurately. The mechanical losses of the motor were measured with the no-load test and with a retardation test.

Table I: Operating points for efficiency verification

Quantity	Nominal Point I	Nominal Point II	Nominal Point III
Frequency	50 Hz	50 Hz	60 Hz
Voltage	380 V	380 V	440 V
Output power	5.5 kW	7.5 kW	6.3 kW

Measurement setup

The measurement setup consisted of the test object–132 frame-sized TEFC IM, a larger IM for adjustable mechanical load, instruments for measuring and recording data and a generator for power supply. The electric quantities, including voltage and current waveforms, were measured with Yokogawa PX8000 power analyzer. HBM T12 torque transducer was used to measure the mechanical load and speed. Keithley 2701 multimeter was used to read the temperature sensors. An open and balance-type calorimetric system with air as a coolant was used to verify the losses.

Segregation of losses according to IEC 60034-2-1

In all three nominal operating points, the losses were segregated according to IEC 60034-2-1 [8]. The loss segregation is based on three tests: rated load heat run test, load curve test and no-load test. The stator Joule losses P_s and rotor Joule losses P_r are determined from the rated load heat run test results listed in Table II. According to [8], the stator and rotor Joule losses are calculated from

$$P_s = 1.5\, I^2 R \tag{1}$$

and

$$P_r = (P_1 - P_s - P_{Fe})s, \tag{2}$$

where I is the stator phase current, R is the stator line-to-line resistance, P_1 is the electric power, P_{Fe} is the iron loss (determined with the no-load test), and s is the per-unit slip. The no-load test is used to determine the mechanical losses and the iron losses. The no-load mechanical loss value is extrapolated at zero voltage and adjusted for load points according to speed (slip). The actual iron loss value is interpolated from the iron loss curve taking the stator winding voltage drop into account. The additional load losses are determined from the load curve test using the load dependent residual loss, which is the difference between the input-output loss value and other four loss components at each load point. The IEC loss segregation procedure is explained in detail in [8] and [9].

The results of the IEC loss segregation analysis are shown in Figure 1. When examining 5.5 kW and

Table II: IEC Measurement results, rated load heat run test

	Nominal Point I	Nominal Point II	Nominal Point III
Frequency (Hz)	50.0	50.0	60.0
Voltage (V)	380.7	380.2	440.7
Current (A)	10.4	14.1	10.21
cos (φ)	0.90	0.92	0.90
Electric power (kW)	6.211	8.545	7.032
Speed (rpm)	2917	2864	3518
Torque (Nm)	18.3	25.1	17.2
Shaft power (kW)	5.595	7.528	6.302
Ambient temperature (°C)	27.2	27.0	24.7
Winding temperature* (°C)	59.3	78.8	53.8
Test resistance (Ω)	1.06	1.13	1.04

*Winding temperature is estimated from stator resistance.

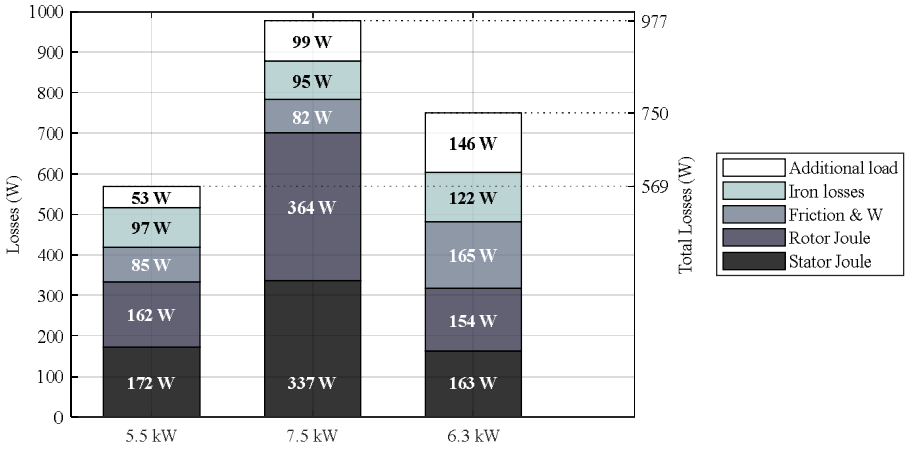

Fig. 1: Shares of motor losses in different operating points according to IEC – segregation of losses method.

7.5 kW point results, it is obvious that the mechanical losses and iron losses remain roughly on the same level while the load is increased and the load dependent copper losses increase in the stator and rotor. Both the friction and windage losses increase with speed and we see a slightly lower mechanical loss value at 7.5 kW point because of the lower speed due to the higher slip. The iron losses also see a slight reduction at the 7.5 kW point, which, in turn, is caused by the larger voltage drop in the stator resistance, and hence slightly lower flux linkage, than at the 5.5 kW operating point. The stator and rotor copper losses at the 7.5 kW point are approximately twice as high as at the 5.5 kW point, because of the higher current and increased resistance due to the higher temperature rise. In addition, as the nomenclature indicates, the additional load losses are notably higher at the 7.5 kW point. Due to the increased resistive losses, the measured power factor is higher with 7.5 kW load (Table II).

At the 6.3 kW, 60 Hz point, the mechanical losses are naturally significantly higher than at the two 50 Hz points as the operating speed is also higher. An increase in the iron losses is caused by the higher supply frequency, but this is slightly compensated by the fact that the air-gap flux linkage is actually slightly lower at 440 V/60Hz than at 380 V/50 Hz. The current is slightly lower and because of increased cooling the winding temperature is lower, which can be seen as lower copper losses in the stator and the rotor. The increase in the additional load losses compared with the 50 Hz, 5.5 kW point is expected, but the amount is rather high.

Retardation tests

The correct value for the mechanical losses of the motor is important for the calorimetric analysis. This is because the motor is rotated by the load machine during the balance test to keep the air circulation similar between the main test and the balance test. Therefore, the reference power during the balance test, which is the basis of the balance type calorimetric analysis, is the sum of the DC-resistor power P_{heater} and the mechanical losses P_{mech} of the tested motor

$$P_{\mathrm{ref}} = P_{\mathrm{heater}} + P_{\mathrm{mech}}. \tag{3}$$

The mechanical losses (friction and windage losses) were determined in the IEC loss segregation from the no-load voltage curve test. Another means for determining the mechanical losses is from a retardation test. In a retardation test, the tested motor is first heated to the operating temperature, and then accelerated up to a high speed and the power supply is disconnected leaving the motor rotated by its own inertia and decelerated by the mechanical losses. Based on the inertia and deceleration, the mechanical losses can be determined for the whole speed range from the initial speed to (almost) standstill.

In these measurements, the jaw coupling attached to the motor shaft was large-sized, and to make sure the results were correct, separate retardation tests were made with and without the coupling. To be able

to remove the jaw coupling, the motor had to be moved from the load test position, therefore this comparison was made with a cool motor only warmed up by running it at no-load until the measured input power and the temperature of the motor were stabilized.

The results from the retardation tests are shown in Table III. We can see that the mechanical losses of the hot motor with the jaw coupling attached are consistent with the IEC friction and windage loss results in Figure 1. The cool motor results, however, show that the jaw coupling (JC) causes the additional loss increase and that the actual mechanical loss value is lower. The difference P_{JC} was consistently seen also in the no-load power, indicating that it is due to the air resistance of the jaw. When the jaw is coupled during load tests, the jaw teeth causing the air resistance are filled by the coupling counterpart, hence the corrected value for hot motor mechanical losses $P_{\mathrm{mech,r}}$ can be considered more accurate.

Table III: Retardation test results

	50 Hz 5.5 kW	**50 Hz 7.5 kW**	**60 Hz 6.3 kW**
Mech. losses of cool motor with jaw coupling attached (W)	92.7	87.0	170
Mech. losses of cool motor without jaw coupling (W)	67.4	63.6	122.2
Effect of the jaw coupling, P_{JC} (W)	**25.3**	**23.4**	**47.8**
Mech. losses of hot motor with jaw coupling attached, $P_{\mathrm{mech,r,JC}}$ (W)	**84.3**	**79.0**	**156.2**
Mech. losses of hot motor, $P_{\mathrm{mech,r}} = P_{\mathrm{mech,r,JC}} - P_{\mathrm{JC}}$ (W)	**59.0**	**55.6**	**108.4**

Calorimetric tests

The principle of an open and balance type calorimeter is presented in Figure 2. Ideally, if the conditions during the main test and the balance test were identical, the reference power during balance test would give directly the loss result. However, as the conditions usually variate, several quantities affecting the heat transfer from the chamber are measured, and the data is used to correct the effects of the different conditions to obtain an accurate loss result.

The calorimetric loss results $P_{\mathrm{tl,cal}}$ can be written as

$$P_{\mathrm{tl,cal}} = \bar{c}_{\mathrm{p,M}} q_{\mathrm{m,M}} \Delta T_{\mathrm{air,M}} + U_{\mathrm{wall,M}} S_{\mathrm{wall,M}} \Delta T_{\mathrm{wall,M}}, \quad (4)$$

where the first part of the equation describes the losses transferred by air flow and the second part the total heat leakage. The subscript 'M' denotes the values during the main test. In equation (4), $\bar{c}_{\mathrm{p}}$ is the specific heat capacity of the moist air (J/(kg·K)) calculated with the average temperatures of the inlet and outlet air, q_{m} is the mass flow rate (kg/s), and ΔT_{air} is the temperature difference of the moist air between the inlet and outlet tubes (K). U_{wall} is the overall heat transfer coefficient of the chamber (W/(m^2·K)), S_{wall} the total area of the chamber walls (m^2), and ΔT_{wall} is the temperature gradient across the chamber walls (K).

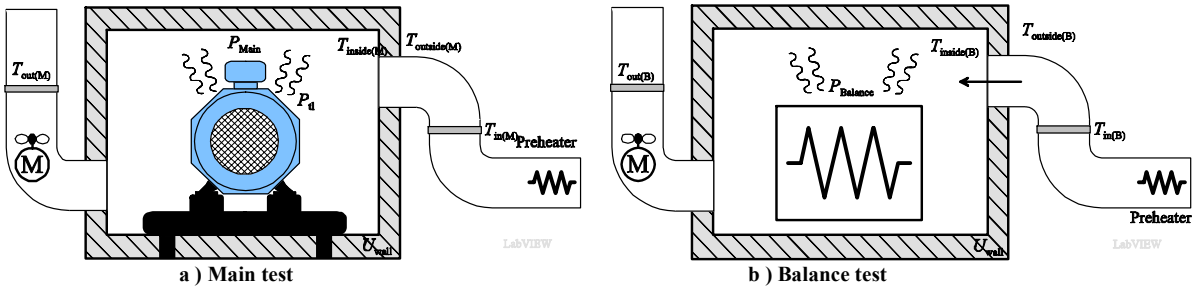

Fig. 2: Principle of the open and balance-type calorimeter. In the main test, the tested motor is running inside the calorimeter. The test is continued until a thermal equilibrium is reached. In the balance test, the resistor is used to reproduce the motor losses when the air flow through the chamber is fixed. If the conditions remain the same in both tests, the resistor power is equal to the motor loss power.

In a balance-type calorimeter, the mass flow is not measured but it can be estimated based on the reference power test (the balance test). The estimated mass flow rate $\hat{q}_{\mathrm{m}}$ can be computed based on

$$\hat{q}_{\mathrm{m}} = \frac{P_{\mathrm{ref}} - U_{\mathrm{wall,B}} S_{\mathrm{wall,B}} \Delta T_{\mathrm{wall,B}}}{\bar{c}_{\mathrm{p,B}} \Delta T_{\mathrm{air,B}}}. \tag{5}$$

where P_{ref} is the reference power (W) and the subscript 'B' denotes the values during balance test. The mass flow estimate is equal to real mass flow if the calorimetric chamber and fluid flow conditions are the same during both tests. Practically, in the air-cooled calorimeter the problem arises from the specific heat capacity of air $\bar{c}_{\mathrm{p,B(AIR)}}(p, T, \varphi)$, which is a function of the barometric pressure(p), temperature (T) and humidity (φ). A parallel chamber calorimeter is introduced in [10] to overcome the variation of fluid properties during the measurement. Another approach is to measure the barometric pressure and humidity and to use data processing methods to improve the accuracy of the result as proposed in [11]. In addition, the air properties will have an effect on the mass flow produced by the blower, however, this can be taken into account by fitting the mass flow to different air properties as follows

$$q_{\mathrm{mx}} = q_{\mathrm{m0}} \frac{p_{\mathrm{x}}}{p_0} \sqrt{\frac{T_0 R_0}{T_{\mathrm{x}} R_{\mathrm{x}}}} \tag{6}$$

where R is the gas constant for moist air. The subscripts 'x' and '0' denote the fitted and known point, respectively. The air temperatures T_0 and T_{x} are the outlet temperatures. In [11], this procedure of taking the fluid properties variation in specific heat and in the mass flow production of the blower into account is denoted as a 'mass flow correction'. Here, we examine the two parts of the correction procedure separately. The adjustment due to air specific heat difference is denoted as 'Specific Heat Correction', SHC and the blower mass flow production correction simply as 'Blower Flow Correction', BFC. The temperature correction (TC) is the product of known power and the ratio of the steady state temperature differences in the main and balance tests. The calorimetric data and the effect of the corrections to the results are given in Table IV. The uncorrected result in Table IV is the calorimetric motor loss result without applying SHC and BFC, that is, using the same mass flow and specific heat values in (4) and (5).

Table IV: Calorimetric measurement results

	50 Hz / 5.5 kW		**50 Hz /7.5 kW**		**60 Hz / 6.3 kW**	
Quantity	Main	Balance	Main	Balance	Main	Balance
p (hPa)	996.6	991.7	985.4	986.8	988.7	992.0
φ (%)	27.4	31.6	35.2	34.3	36.0	29.5
t_{ambient} (°C)	24.67	24.16	24.48	24.04	24.96	24.6
t_{chamber} (°C)	40.56	42.60	39.21	42.99	40.28	42.53
t_{in} (°C)	25.16	24.59	25.00	24.99	24.94	25.01
t_{out} (°C)	40.10	39.94	39.98	39.99	40.03	40.04
$\bar{c}_{\mathrm{p}}$ (J/(kg·K))*	1009.4	1010.0	1010.8	1010.6	1010.9	1009.7
R (J/(kg·K))	287.96	288.08	288.242	288.208	288.26	288.03
$q_{\mathrm{m,meas}}$(kg/s)	0.0609	0.0606	0.0896	0.0899	0.0689	0.0680
P_{heater} (W)	500	1050.7	500	1484.7	500	1085.9
P_{mech}	-	61.5	-	58.0	-	112.5
P_{ref} (W)	-	1112.2	-	1542.7	-	1198.4
Result (uncorrected**) (W)	**568.9**		**1013.8**		**685.4**	
SHC(W)	-0.5		+0.2		1.2	
BFC(W)	+4.6		-2.2		-4.0	
Result (SHC & BFC) (W)	**573.0**		**1011.8**		**682.6**	
RMC (W)	+3.7		-4.2		+13.6	
Result (RMC) (W)	**572.6**		**1009.6**		**699.0**	

*Calculated based on measured barometric pressure, relative humidity and average air temperature.
**(before applying SHC and BFC, or RMC)

Here, ABB Sensyflow FMT500-IG Thermal Mass Flowmeter for gases is installed in the calorimetric system's outlet tube. A weld-on adapter is used to obtain a firm installation. The meter uses a hot-film anemometer as a measuring principle that allows the direct determination of the mass flow and gas temperature. The sensor is calibrated with normal air and it gives the standard volume flow rate directly without any additional pressure and temperature compensation. The measurement accuracy is better than 0.9% and reproducibility better than 0.2% of the measured value [12]. Since the real mass flow is measured from the end of the outlet tube of the calorimetric system and the calorimeter exhaust blower is located in the pipeline before the mass flow measurement, a slight increase in the air temperature is expected due to the losses of the blower. However, the measured values can be used to detect and correct any changes in the real mass flow during the measurement. The correction according to the real mass flow measurement (RMC) is included in Table IV.

The calculated specific heat (SHC) and blower flow correction (BFC) values are low and the effect on the result is minimal. The real mass flow corrections (RMC) values are also low, although the RMC value for 60 Hz, 6.3 kW test point is notably higher than the other two. The effect of these corrections on the final efficiency value is negligible and the uncorrected results would be just as usable.

Heat balance analysis during calorimetric measurement

The results from the normal calorimetric analysis are shown in Table V. The normal calorimetric loss analysis is based on the known reference heat power during balance test $P_{\mathrm{ref,B}}$ and the pre-determined chamber wall heat transfer coefficient U_{wall}. In the following equations, and Tables V and VI, the subscripts M and B refer to Main test and Balance test, respectively. The total heat leakage during the balance test $P_{\mathrm{wall,B}}$ is the second part of the numerator in (5)

$$P_{\mathrm{wall,B}} = U_{\mathrm{wall}} S_{\mathrm{wall.B}} \Delta T_{\mathrm{wall,B}}. \tag{7}$$

and subtracting it from the reference power yields the heat transfer by air flow

$$P_{\mathrm{air,B}} = P_{\mathrm{ref}} - P_{\mathrm{wall,B}}. \tag{8}$$

Estimate for the mass flow during the balance test $q_{\mathrm{m,B}}$ is calculated from (5) and the estimated mass flow during the main test is determined with (6). The calorimetric total loss result $P_{\mathrm{tl,cal}}$ is calculated from (4), where the second part is the total heat leakage during the main test $P_{\mathrm{wall,M}}$. Here, $P_{\mathrm{tl,cal}}$ includes additional heater power $P_{\mathrm{heater,M}}$ (see Table IV), hence, the motor loss result is

$$P_{\mathrm{cal}} = P_{\mathrm{tl,cal}} - P_{\mathrm{heater,M}}. \tag{9}$$

The heater was used during the main test to increase the loss power as the calorimeter is designed for losses up to 3 kW, and the measurement accuracy may decrease when measuring very low losses.

Table V: Calorimetric analysis based on pre-estimated chamber heat transfer coefficient

	50 Hz / 5.5 kW	**50 Hz /7.5 kW**	**60 Hz / 6.3 kW**
Total heat leakage, balance test, $P_{\mathrm{wall,B}}$ (W)	123	126	119
Heat transfer by air flow, balance test, $P_{\mathrm{air,B}}$ (W)	989	1416	1079
Total heat leakage, main test, $P_{\mathrm{wall,M}}$ (W)	106	98	102
Total loss result for the motor, P_{cal} (W)	**573.0**	**1011.8**	**682.6**

Here, the mass flow was also measured during the balance test. Utilizing the measured mass flow, we can use the balance test to determine the total heat leakage directly as

$$P_{\mathrm{wall,B,mf}} = P_{\mathrm{ref}} - P_{\mathrm{air,B,mf}}, \tag{10}$$

where

$$P_{\mathrm{air,B,mf}} = \bar{c}_{\mathrm{p,B}} q_{\mathrm{m,B,meas}} \Delta T_{\mathrm{air,B}}, \tag{11}$$

and the subscript mf refers to the value being determined based on the measured mass flow $q_{\mathrm{m,meas}}$. From (7), we solve the heat transfer coefficient as

$$U_{\mathrm{wall,mf}} = \frac{P_{\mathrm{wall,B,mf}}}{S_{\mathrm{wall.B}} \Delta T_{\mathrm{wall,B}}}. \tag{12}$$

and use this value in the main test analysis. $U_{\mathrm{wall,mf}}$ can be considered as a more accurate estimate for the heat transfer coefficient than the pre-determined U_{wall}, because it is determined in more similar conditions with the main test and with the same motor running inside the chamber at the same speed resulting also in similar air circulation inside the chamber as during the main test. The results, where the mass flow meter is used to determine the heat leakage coefficient are presented in Table VI.

Table VI: Calorimetric analysis using mass flow meter to determine the chamber heat transfer coefficient

	50 Hz / 5.5 kW	**50 Hz /7.5 kW**	**60 Hz / 6.3 kW**
Heat transfer by air flow, balance test, $P_{\mathrm{air,B,mf}}$ (W)	940	1362	1032
Total heat leakage, balance test, $P_{\mathrm{wall,B,mf}}$ (W)	172	180	166
Total heat leakage, main test, $P_{\mathrm{wall,M,mf}}$ (W)	148	140	142
Total loss result for the motor, $P_{\mathrm{cal,mf}}$ (W)	**567**	**997**	**693**
Difference of the results, $P_{\mathrm{cal,mf}} - P_{\mathrm{cal}}$ (W)	**-6**	**-15**	**+10**

The difference between the total losses $P_{\mathrm{cal,mf}}$, where the heat transfer coefficient is determined from balance test data using the real mass flow, and the normal analysis result P_{cal}, which is obtained using a pre-determined heat transfer coefficient (Table V), is calculated in the last row of Table VI. The difference of the results is very low, less than 2% of the loss value in all three test points. When comparing the total heat leakage values between Tables V and VI, we notice that P_{wall} values in Table VI are significantly higher than in Table V. This would indicate, that the pre-determined U_{wall} value is underestimated. However, the loss result differences are relatively low, because U_{wall} and P_{wall} affect only the heat transfer corrections between the main test and the balance test. Based on this comparison, the balance test is accurate enough to be used for estimating the mass flow, even without exact value for the chamber heat transfer coefficient.

Comparison of the loss results using temperature correction

The motor's input and output power are measured during the rated load test of the IEC loss segregation method and both electrical and mechanical power were measured also during the calorimetric tests. Therefore, we have obtained two input-output loss measurement results in two different ambient conditions; at around 25°C in the open test bench and at approximately 40°C inside the calorimetric chamber. The consistency of these loss results can be analyzed using the temperature correction of the resistive losses. In order to correct the total losses to different temperature, the sum of stator and rotor Joule losses, and the corresponding ambient temperature need to be known. Here, we have determined the Joule losses in the IEC loss segregation test. In the IEC loss segregation analysis [8], the Joule losses are corrected to 25°C reference temperature by multiplying with temperature correction factor

$$k_\theta = \frac{235 + \theta + 25 - \theta_c}{235 + \theta}, \tag{13}$$

where 235 is the temperature constant for copper, θ is the winding temperature, θ_c is the coolant temperature, and 25 refers to the desired coolant temperature after the correction.

The temperature correction analysis, where the input-output losses measured inside the calorimeter $P_{\mathrm{IO,Cal}}$ are corrected to IEC test ambient temperature is presented in Table VII. In Table VII, the Joule losses from IEC tests are adjusted to the chamber temperature (using t_{chamber} instead of θ_c in (13)), and then the amount of the correction is subtracted from the $P_{\mathrm{IO,Cal}}$ value. The corrected $P_{\mathrm{IO,Cal}}$ values seem to be somewhat consistently lower than the $P_{\mathrm{IO,IEC}}$ values. The loss difference in matching temperature can be caused by several factors. The friction losses of the motor may be a bit lower when the motor runs hotter, but the most probable cause is the torque reading and its correction to take account support bearings located between the tested motor and the torque transducer. The torque offset caused by the support bearings is measured by rotating the decoupled shaft with the load machine, which cannot be considered very accurate. Additionally, the friction of the bearings may be different when the shaft is coupled to the tested motor.

Table VII: Using temperature correction of Joule losses to adjust the input-output losses from IEC tests and calorimetric tests to a matching ambient temperature (t_{IEC})

	50 Hz / 5.5 kW	50 Hz /7.5 kW	60 Hz / 6.3 kW
Input-output losses, IEC-test, $P_{\mathrm{IO,IEC}}$ (W)	**616**	**1016**	**729**
Input-output losses, calorimetric test, $P_{\mathrm{IO,Cal}}$ (W)	**606**	**1034**	**716**
IEC-test ambient temperature, t_{IEC} (°C)	27.2	27.0	24.7
Calorimetric chamber temperature, t_{chamber} (°C)	40.6	38.2	40.3
Temperature correction factor, k_θ	1.053	1.045	1.053
Joule losses in t_{IEC}, $P_{\mathrm{Cu,IEC}}$ (W)	336	706	317
Joule losses in t_{chamber}, $P_{\mathrm{Cu,Cal}}$ (W)	354	738	334
Amount of correction, $P_{\mathrm{Cu,corr}}$ (W)	18	32	17
$P_{\mathrm{IO,Cal}}$ corrected to t_{IEC} (W)	**588**	**1002**	**699**
IO-loss difference in matching temperature t_{IEC} (W)	**28**	**14**	**30**

In similar manner, the actual calorimetric loss results can be adjusted to the reference coolant temperature of 25°C. The temperature correction of the calorimetric losses is shown in Table VIII, where the results are compared with the IEC loss segregation results. When corrected to a matching ambient temperature, the results show very good consistency. The difference is the largest with the 60 Hz results, where the additional loss results of the IEC-method seemed high compared to the other test points (Figure 1), and this comparison would support that observation.

Table VIII: Using temperature correction of Joule losses to adjust the calorimetric results to the reference coolant temperature of 25°C

	50 Hz 5.5 kW	50 Hz 7.5 kW	60 Hz 6.3 kW
Calorimetric results in chamber temperature, $P_{\mathrm{cal,mf}}$ (W)	567	997	693
Amount of correction, $P_{\mathrm{Cu,corr,25°C}}$ (W)	20	37	16
Calorimetric results in 25°C ambient temp. (W)	**547**	**960**	**677**
IEC results corrected with P_{JC}, see Table III (W)	**543**	**951**	**693**
Difference of IEC and calorimetric results after corrections (W)	**4**	**9**	**-16**

Efficiency

As given in [13], the efficiency of a four-pole induction motor with 5.5 kW rated power must be 88.8% to be labeled as IE1, 89.1% for IE2 and 90.1% for IE3, respectively. Similarly, we obtain the limit values for a 7.5 kW motor. However, there are no official limits for 6.3 kW with 60 Hz excitation frequency since it is not an official IEC power rating. The measured efficiencies are compared with IEC limits in Figure 3. The efficiency is

$$\eta = \frac{P_{\mathrm{mech}}}{P_{\mathrm{electric}}} = \frac{P_{\mathrm{electric}} - P_{\mathrm{loss}}}{P_{\mathrm{electric}}} = \frac{P_{\mathrm{mech}}}{P_{\mathrm{mech.}} + P_{\mathrm{loss}}}. \tag{14}$$

The first part of the equation is used for the input-output method and the second part for the IEC loss segregation method. The second and the third part are suitable for the calorimetric method. The mechanical loss-corrected IEC-results from Table VIII were used in calculating the IEC efficiencies. The calorimetric loss results corrected with mass flow measurement (Table VI) were used in calculating the calorimetric efficiency results. The input output efficiency was calculated from the input and output powers of the IEC rated load heat run test (Table II).

At the first operating point 50 Hz/5.5 kW, the motor efficiency is higher than the IE3 level limit. The input-output method gives 1.1%-units and calorimetric measurement 0.3%-units lower efficiencies than

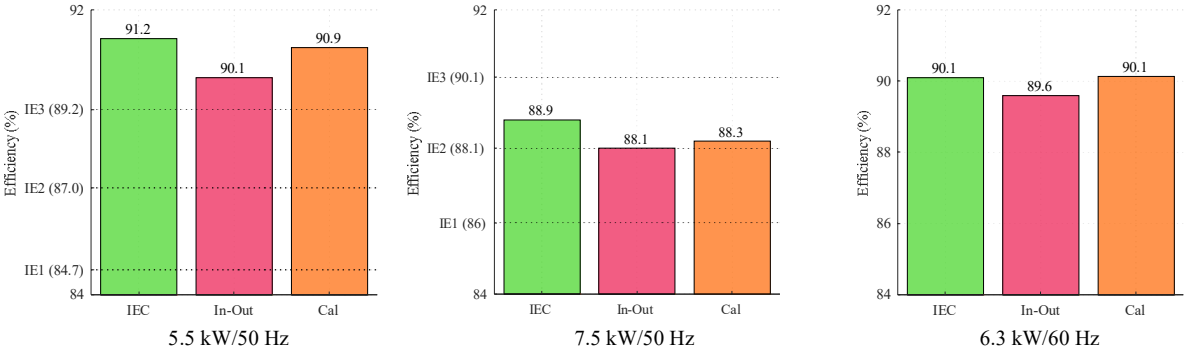

Fig. 3. Experimentally determined motor efficiency and IEC classification limits. 6.3 kW is not an official IEC power class and no limits exist.

the indirect IEC-method. In the second test point 50 Hz / 7.5 kW, the IEC method gives, again, the best efficiency that is well over IE2 classification limit while the input-output and calorimetric methods give 0.8%-units and 0.6%-units lower efficiency results that are barely worth IE2-rating. At the third test point, the calorimetric method and the IEC-method yielded the same result and the input-output method gave 0.5%-units lower result.

The differences in the efficiency originate from several sources. As shown in Table VIII, the IEC and calorimetric loss results are very consistent when corrected to the same temperature; hence, the efficiency difference between the IEC- and the calorimetric results in 5.5 kW and 7.5 kW points is mainly caused by the higher motor temperature during the calorimetric measurement. The input-output efficiency is the lowest in all three test points, and this difference is most likely due to torque measurement offset; there are support bearings located between the motor and the torque transducer in the measurement setup. Their effect is measured by rotating the uncoupled shaft with the load machine, which may not give the exact correct value.

Discussion

Accurate determination of the losses of high efficiency devices is complicated regardless of the method. The aim here was to verify the efficiency of a 5.5 kW motor in three operating points and that task was well accomplished. The test bench used was designed for larger motors and therefore the shaft coupling used was relatively big due to the high power load machine. The coupling effect on the no-load test and retardation test results would have been almost meaningless in the case of a four-pole machine, but the effect was relatively high with a two-pole machine.

The overall heat transfer coefficient (U_{wall}) in equation (7) describes not only the heat leakage through the insulation but also through the motor shaft and basement, as well as air leakage through seals (if any), therefore the calorimetric result obtained with the balance test is not critically affected even if the coefficient value is not absolutely correct. The key element to obtain accurate results with the balance-type calorimeter is to ensure exactly similar conditions during both tests – the load test and the balance test. In here, the overall heat transfer coefficient was determined using two resistor tests. However, the heat transfer through the system is higher when the motor fan is circulating the air inside the chamber, this might have a minor effect on the loss result.

The mass flow meter can be used to observe the flow through the system and to correct the result obtained with the balance test, which was done here. However, if it is used to directly determine the loss result, more advanced heat leakage control or higher insulation thickness are required to obtain accuracy in the range of a few watts. The usage of the mass flow meter cannot be justified in the typical applications, since adding an accurate mass flow meter in the system doubles the calorimetric measurement system price and it is a more economical solution to use a mass flow correction based on measured barometric pressure and humidity.

Conclusion

The losses of the induction motor have been determined experimentally with several different methods and discrepancy between the results can be found. At the efficiency level of the measured induction motor, no major discrepancy of the methods was expected. The open and balance-type calorimetric loss result is studied with direct mass flow measurement and relatively small variations due to mass flow deviation during the measurement can be examined in the total losses. According to this study, the air properties variation during the calorimetric measurement sequence is not a major problem in the efficiency verification of electric motors. The humidity and barometric pressure sensors are not crucial instruments in the open and balance-type calorimeter.

References

[1] F. W. Fuchs, J. Schröder and B. Wittig, "State of the technology of power loss determination in power converters," *2013 15th European Conference on Power Electronics and Applications (EPE)*, Lille, 2013, pp. 1-10.

[2] Rotating electrical machines – Part 34-2A, "Methods for determining losses and efficiency of rotating electrical machinery from tests (excluding machines for traction vehicles) Measurement of losses by the calorimetric method," IEC 34-2A, Genève, Switzerland, 1974.

[3] Adjustable speed electrical power drive systems – Part 9-2: Ecodesign for power drive systems, motor starters, power electronics nad their driven applications – Energy efficiency indicators for power drive systems and motor starters. Ed. 1. IEC 61800-9-2, March 2017.

[4] P. McLeod, K.J. Bradley, A. Ferrah, R. Magill, J.C. Clare, P. Wheeler, and P. Sewell, "High precision calorimetry for the measurement of the efficiency of induction motors," in Conf. Rec. 1998 IEEE Industry Applications Conf. 33rd IAS Annu. Meeting, vol. 1, St. Louis, MO, USA, Oct. 1998, pp. 304–311.

[5] B. Szabados and A. Mihalcea, "Design and implementation of a calorimetric measurement facility for determining losses in electrical machines," IEEE Trans. Instrum. Meas., vol. 51, no. 5, Oct. 2002, pp. 902–907.

[6] A. Kosonen, L. Aarniovuori, J. Pyrhönen, M. Niemelä and J. Backman, "Calorimetric concept for measurement of power losses up to 2 kW in electric drives," in *IET Electric Power Applications*, vol. 7, no. 6, pp. 453-461, July 2013.

[7] W. Cao, G.M. Asher, X. Huang, H. Zhang, I. French, J. Zhang, and M. Short, "Calorimeters and techniques used for power loss measurements in electrical machines," IEEE Instrum. Meas. Mag., vol. 13, no. 6, pp. 26–33, Dec. 2010.

[8] Rotating electrical machines – Part 2-1: Standard methods for determining losses and efficiency from tests (excluding machines for traction vehicles), Ed. 2, IEC 60034-2-1, June 2014.

[9] H. Kärkkäinen, L. Aarniovuori, M. Niemela and J. Pyrhonen, "Converter-Fed Induction Motor Efficiency: Practical Applicability of IEC Methods," in *IEEE Industrial Electronics Magazine*, vol. 11, no. 2, pp. 45-57, June 2017.

[10] L. Aarniovuori, A. Kosonen, M. Niemelä and J. Pyrhönen, "Parallel chamber calorimetric concept," *15th European Conference on Power Electronics and Applications (EPE)*, Lille, 2013, pp. 1-9.

[11] A. Kosonen, L. Aarniovuori, J. Ahola, J. Backman, J. Pyrhönen and M. Niemelä, "Loss Definition of Electric Drives by a Calorimetric System With Data Processing," in *IEEE Transactions on Industrial Electronics*, vol. 61, no. 8, pp. 4432-4442, Aug. 2014.

[12] ABB Ltd Measurement & Analytics, Operating Instruction Thermal Mass Flowmeter Sensyflow FMT500-IG (OI/FMT500-IG-EN), June 2017.

[13] Rotating electrical machines – Part 30-1: Efficiency classes of line operated AC motors (IE code), Ed. 1, IEC 60034-30-1, March 2014.

Publication VI

Kärkkäinen, H., Aarniovuori, L., Niemelä, M., and Pyrhönen, J.
Advanced Uncertainty Calculation Method for Frequency Converter Loss Determination

20th European Conference on Power Electronics and Applications (EPE'18 ECCE Europe)
pp. 1-10, 2018

Advanced Uncertainty Calculation Method for Frequency Converter Loss Determination

Hannu Kärkkäinen, Lassi Aarniovuori, Markku Niemelä and Juha Pyrhönen
LAPPEENRANTA UNIVERSITY OF TECHNOLOGY
P.O. Box 20, FI-53851
Lappeenranta, Finland
hannu.s.karkkainen@lut.fi
URL: http://www.lut.fi

Keywords

Experimental testing, Measurement, Standards, Uncertainty, Variable Speed Drives.

Abstract

The loss determination based on input and output powers is the most commonly used method in electrical drives. However, the accuracy of the measurement results can be strongly questioned. Here, a workflow starting from measurement instruments' data sheet information to final measurement uncertainty result is presented for three different frequency converters.

Introduction

The measurement uncertainty assessment has always been part of the experimental physical sciences. In classical physical science, the result is commonly thought to be useless without the knowledge of measurement uncertainty. However, in applied sciences, such as electrical engineering, the measurement uncertainty is commonly just omitted. The word 'uncertainty' is used to represent the doubt about the validity of the measurement result. The narrower the uncertainty band is the stronger the weight of the result is and correspondingly the broader the uncertainty band the weaker the result is. The terms uncertainty and error should not be mixed. An error is the part of the result that we can correct but uncertainty is always present also in the correct value. However, the measurement uncertainty can be estimated and the amount of the uncertainty can be controlled. The basic uncertainty analysis presented in this paper is based on the work in [1].

Joint Committee for Guides in Metrology (JCGM) [2] defines the measurement uncertainty: It is expressed as a number that describes the amount the true value of the quantity being measured can deviate from the result, i.e.

$$Y = y \pm U, \tag{1}$$

where Y is the quantity being measured, y the measurement result, and U the measurement uncertainty. A measurement uncertainty is divided into type A and type B uncertainties, which are associated with uncertainties related to the variation of the quantity being measured and uncertainties associated with the measurement instruments respectively. The information of all the individual components contributing to the measurement uncertainty is also referred to as the uncertainty budget [2].

Here, the guidelines to perform the measurement uncertainty analysis for frequency converters' losses measurement are given. The input-output method is an official method to determine the losses of electric drives as given in IEC standard 61800-9-2 [3]. The IEC segregation of losses -method for induction motors and the motor testing has been a topic of numerous scientific publications. In [4], the efficiency of induction machines and measurement uncertainties arising from various input-output testing methods used in industry is assessed. The different IEC -standard versions are compared in [5] using 10 industrial induction motors from 4 kW up to 70.5 kW with pole numbers equal to 2, 4, or 6 and the results are analyzed and discussed. The European (IEC), Japanese (JEC) and American (IEEE) motor measurement standards in efficiency determination are compared in [6]. The IEC testing standard, nowadays, shares similar testing methods with IEEE 112-B. One comparative analysis of the methods is presented in [8]

using six general-purpose four-pole three-phase induction machines with rated powers from 5.5 kW to 150 kW as examples. The efficiency measurement uncertainty is analyzed using realistic perturbation-perturbation estimation (RPBE) -method in [8] and the influence of the measurement error on the uncertainty of the determination of the efficiency by the indirect procedure (summation of losses methods, stray load losses determined from residual loss) is analyzed using Monte Carlo simulations in [9]. The induction motor direct and indirect efficiency measurement method comparison from a collection of test data using Bland-Altman procedure is presented in [10]. In [11] the results of five induction motor efficiency measurements according IEC 60034-2-1 are presented. The uncertainty of the measurements is analyzed using scientific and numerical methods. Most of the previous studies consider only uncertainty issues related to the losses and efficiency of electric motors. The main reason is that IEC 61800-9-2, released in 2017, was the first international standard to define loss and efficiency determination methods for frequency converters.

Type A uncertainty

Type A uncertainty is the standard deviation of the mean [2]. With common words, it is related to the repetition of measurements and describes how much the average of this set of repetitions can fluctuate. Type A uncertainty is calculated with the help of statistics and involves a mathematical function model, and the calculation of averages and standard deviations. The calculation in [2] is based on the assumption that individual data points distribute around the mean randomly. JCGM suggests that when an output quantity Y is a function of input quantities X_i

$$Y = y \pm U, \tag{2}$$

the result of the measurement y estimates the output quantity Y and the measured quantities x_i represent estimates of the input quantities. Therefore

$$Y \approx y = f(x_1, x_2, x_3, \dots, x_N), \tag{3}$$

where N is the number of input quantities (for example in the case of electric power, input quantities include current, voltage, and power factor). The best estimates of the input quantities are calculated as averages x_i from sets of measurement data

$$x_i = \bar{x}_{i,j} = \frac{1}{n}\sum_{j=1}^{n} x_{i,j}, \tag{4}$$

where n is the number of data points in the set and j denotes the indices of these points. The dispersion of the measurement points from the average is indicated by experimental standard deviation s, which is given by

$$s(x_{i,j}) = \pm\sqrt{\frac{1}{n-1}\sum_{j=1}^{n}(x_{i,j} - x_i)^2}, \tag{5}$$

The experimental standard uncertainty u refers to the standard deviation of the mean and is calculated with equation

$$u(x_i) = s(x_i) = \frac{s(x_{i,j})}{\sqrt{n}}, \tag{6}$$

The uncertainty contribution of an input to the uncertainty of the output quantity describes the effect the variation of the input quantity has on the output quantity i.e. the result. It is received by multiplying the standard uncertainty of the input quantity with the sensitivity coefficient c_i i.e. the partial derivative of the function with respect to the input quantity localized at the measured average

$$u(y_i) = c_i u(x_i) = \left.\frac{\partial f}{\partial x_i}\right|_{x_i = \bar{x}_{i,j}} u(x_i), \tag{7}$$

JCGM suggests that the uncertainty contribution of an input to the uncertainty of the output quantity can also be calculated numerically without determining the partial derivative with

$$u(y_i) = \frac{1}{2}\{f(x_1, \dots, x_i + u(x_i), \dots x_N) - f(x_1, \dots, x_i - u(x_i), \dots x_N)\}, \tag{8}$$

Type B uncertainty

Type B uncertainty is associated with the instruments used in the measurement. JCGM lists the following sources for determining type B uncertainty; 1) Previous measurement data, 2) Experience with or general knowledge of the behaviour and properties of relevant materials and instruments, 3) Manufacturer's specifications, 4) Data provided in calibration, 5) Uncertainties assigned to reference data taken from handbooks. The numbers given in sources stated above such as the manufacturer's specifications follow certain probability distributions. An estimate for standard uncertainty is received by converting the given uncertainty value U to standard uncertainty u by dividing with a distribution related coverage factor k

$$u = \frac{U}{k}, \tag{9}$$

The coverage factor is chosen based on a statistical distribution such as the normal distribution and a desired level of confidence. The confidence level describes the incidence that the true value of the quantity being measured will be within the confidence interval i.e. within the interval defined by the given uncertainty value U and the measurement result y

$$y - U \leq Y \leq y + U, \tag{10}$$

For instance a coverage factor $k = 2$ yields roughly a 95 % level of confidence for a normally distributed estimate. This suggests that the true value of the quantity being measured will be within the interval (10) defined by the measurement result with a 95 % incidence rate. Figure 1 illustrates the coverage factors k and the corresponding levels of confidence.

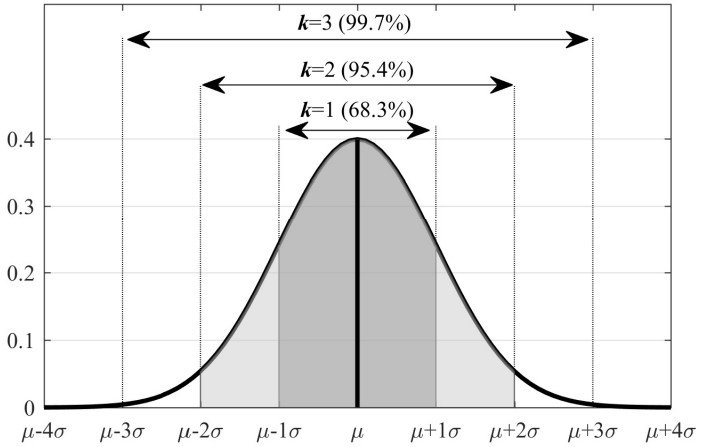

Fig. 1: Probability density curve for a normally distributed quantity with average μ and standard deviation of the mean σ. For example, coverage factor $k = 1$ corresponds to uncertainty value $U = \sigma$, signifying that the measured quantity is within the confidence interval $\mu \pm U$ with a 68.3% incidence rate. For higher coverage factors k values, $U = k\sigma$.

Expression of measurement uncertainty

The combined standard uncertainty u_c is intended for representing the total uncertainty of measurements with multiple sources of uncertainty. It represents the total standard uncertainty in the measurement result by combining the standard uncertainty contributions of all the input quantities. JCGM suggests using the Realistic Perturbation Method (RPM) for combining the individual uncertainties i.e. to combine the uncertainties in root-sum-square. Provided the input quantities are uncorrelated the combined standard uncertainty can be obtained with equation

$$u_c(y) = \pm\sqrt{\sum_{i=1}^{N} u^2(y_i)} = \pm\sqrt{\sum_{i=1}^{N} \left(\frac{\partial f}{\partial x_i}\Big|_{x_i=\overline{x_{1,j}}}\right)^2 u^2(x_i)}, \tag{11}$$

the combined uncertainty can also be calculated as a sum of absolute values of individual uncertainty contributions

$$u_c(y) = \pm \sum_{i=1}^{N} |u(y_i)|, \quad (12)$$

which results in a Worst Case (WC) uncertainty value. The worst-case uncertainty has been criticized for overestimating the measurement uncertainty, which is why the RPM is becoming more commonplace for combining uncertainties [12].

Measurement uncertainty is commonly expressed as expanded uncertainty U

$$U = k u_C. \quad (13)$$

The coverage factor is chosen based on a statistical distribution and a desired level of confidence. Typically, the coverage factor is chosen between 2 and 3 [2]. The levels of confidence for $k = 1...4$ are listed in Table I.

Table I: Levels of confidence for different coverage factor *k* values (normal distribution)

Coverage factor	Level of confidence
$k = 1$	68.3%
$k = 2$	95.4%
$k = 3$	99.7%
$k = 4$	99.99%

Uncertainty analysis workflow

Both type A and B uncertainty are analyzed here. Type A uncertainty is analyzed as a function of the number of the samples. The uncertainty analysis workflow for type B uncertainty can be segregated in five different sections:

1. Obtain measurement accuracy or uncertainty from manufacturers' specifications.
2. Choose (or use if given) statistical distribution for all quantities.
3. Combine the contribution of all partial results.
4. Choose the confidence level.
5. Calculate the extended uncertainty.

Experimental measurements

Electric drive loss measurements were performed using 16 measurement points in the frequency – torque plane. Three four-pole induction motors were used as a load for three different voltage source converters. The test setup details are given in Table II. The motor nominal powers were 15 kW, 37 kW and 75 kW all rated with IE3 efficiency level. The motor load values were used instead of output current values in these measurements, since the target of these measurements was to obtain total system losses and efficiency. Digital power analyzers were used to perform the converter input and output power measurements. This kind of a digital meter takes simultaneous samples of currents and voltages, digitizes these values, and provides arithmetic multiplication and averaging by applying digital techniques to obtain the power measurement.

Table II: Measurement setups

Rated mechanical output of the setup	15 kW	37 kW	75 kW
Converter (I_{max} continuous)	34 A	103 A	202 A
Motor	15 kW IM (IE3)	37 kW IM (IE3)	75 kW IM (IE3)
Power analyzer	Yokogawa WT1600	Yokogawa WT1600	Yokogawa WT1600
Current transducers	Hitec CURACC (100 A)	Hitec CURACC (300 A)	Hitec CURACC (300 A)

In the power analyser, the active input power (P) is calculated as

$$P = \frac{1}{n}\sum_{k=1}^{n} u(k)i(k), \quad (1)$$

where $u(k)$ and $i(k)$ are the corresponding phase voltage and current values at time instants (k). It is obvious that the power measurement accuracy depends on the voltage, current and power factor values. The power factor uncertainty is the time difference between the voltage and current values at time instant (k). The delay between the voltage and the current channels in the power analyser will generate an uncertainty source in the power factor that depends on the signal frequency. Since the active power includes also all the harmonic power, the power value also depends on the bandwidth of the current and voltage measurement channels. The bandwidth of the voltage and current channels gives the maximum electric power bandwidth that the measurement system is capable of including in the power value. Here, the current measurement system small signal bandwidth is 500 kHz and the power analyser measurement bandwidth reaches up to 1 MHz with both the current and voltage channels. However, the power analyser sampling frequency is 200 kS/s and this is setting the limit for the maximum signal frequency that is included in the power value. The uncertainty for the electric power can be calculated using the measurement instrument manufacturer's specifications.

The basic power measurement uncertainty of the power analyzers is given for sinusoidal signals with a unity power factor in the given frequency range. Additional uncertainties arise from the leading or lagging power factors and common-mode voltages in the measurement system, and the distortion of the voltage and current signals.

At maximum, direct input ranges of the digital power analyzers are up to 50 A, and therefore, the currents of power converters and motor drives are measured by current transducers that add their own uncertainty to the measurement system. Here, the power analyser input range is only 5 A and the current measurement system and power analyser are not calibrated together and they must be analysed independently. Though, the uncertainties can be considered not to correlate and they can be added using the sum of the square. Therefore, it is a complex task to define exact uncertainty bounds for the power measurement of pulse-width-modulated (PWM) signals that contain multiple frequencies. The used Zero-Flux current sensor outputs a 1 A signal with nominal load values of 100 A and 300 A (peak).

Type A uncertainty analysis

The type A uncertainty analysis for the converter losses in the rated measurement point of each setup is shown in Table III. In the measurements, each of the test points were measured for 100 seconds and readings were recorded once a second, hence the number of data points is $n = 100$. First, the input power and output power uncertainties are determined according to equations (4)–(6). The converter loss extended uncertainty is obtained by combining the input and output power standard uncertainties

Table III: Type A uncertainty analysis for the converter losses in the rated test point of each setup (100% motor load torque, 50 Hz)

	Rated mechanical output of the setup	15 kW	37 kW	75 kW
	Number of data points	100	100	100
Input	Converter input power average, P_{in} (W)	16968	40833	80099
	P_{in} standard deviation (W)	20.1	97.4	149
	P_{in} standard uncertainty (W)	2.0	9.7	14.9
Output	Converter output power average, P_{out} (W)	16508	39708	78546
	P_{out} standard deviation (W)	18.3	91.4	143
	P_{out} standard uncertainty (W)	1.8	9.1	14.3
Losses	Converter losses, P_{loss} (P_{in} - P_{out}) (W)	459	1125	1554
	P_{loss} type A extended uncertainty (W), $k = 2$	5.4	26.7	41.3
	P_{loss} type A extended uncertainty (%), $k = 2$	1.2	2.4	2.7

according to (11) and multiplying the result with the coverage factor k (13). Coverage factor was chosen as $k = 2$ resulting in 95% level of confidence.

The absolute converter loss type A uncertainty values increase with the setup's power rating, which is expected. There are also differences between the setups' relative type A uncertainties: The 15 kW setup's converter loss type A uncertainty being notably lower than the 37 kW and 75 kW setup's values. In practice, this means that the relative variation between individual data points is smaller in the 15 kW measurements. The stability (or amount of variation in the recorded data point values) of the power measurement can be affected by several factors. For example, mechanical vibrations or the load machine's control may cause motor power fluctuations and increase type A uncertainty. In addition, measurement instruments' analog-to-digital conversion may affect the variations in measurement data due to the limited number of quantization steps, which can have an effect on the type A uncertainty result.

The significance of the used number of data points regarding the type A uncertainty is illustrated in Figure 2. The curves are obtained by using only the indicated number of data points (2–100) and repeating the analysis for each number of points in similar manner as in Table III. Figure 2 shows clearly, that the benefits of prolonging the measurement start to diminish after approximately 50 data points – or in other words – 100 data points is well enough for this measurement.

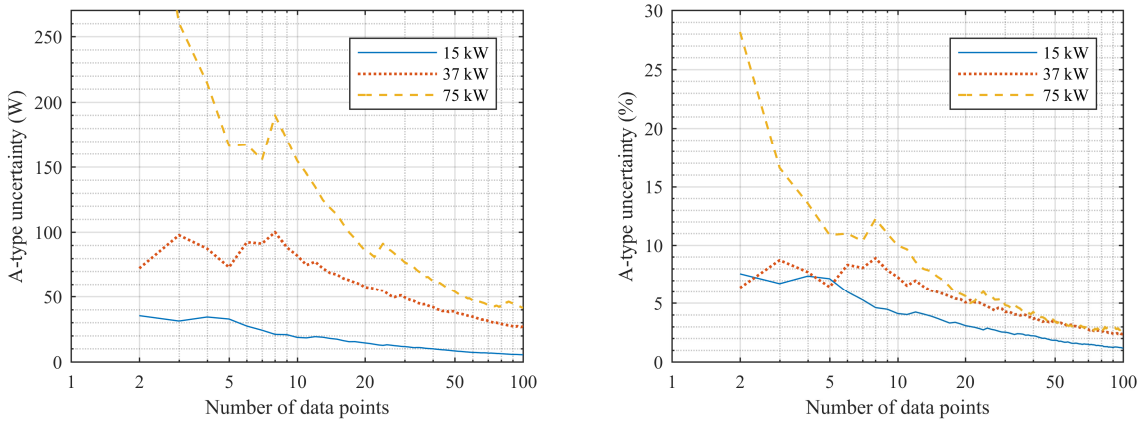

a) Absolute values (W)

b) Relative values (%)

Fig. 2: The type A uncertainties of the drive losses as the function of the number of the data points for the three different drives supplying a 15 kW, a 37 kW, and a 75 kW induction motor at the rated operating point. The curves are plotted with coverage factor $k = 2$ (95% level of confidence). The 75 kW setup's uncertainty value in Watts with two data points was 440 W, which is scaled outside the figure.

Type B uncertainty analysis

Determining the type B uncertainty requires information about the measurement instruments' accuracies. The accuracy data for Yokogawa WT1600 power analyzer and Hitec CURACC current tranducers are presented in Table IV [13], [14]. The fundamental frequency used in the measurements varies from 12.5 Hz to 50 Hz, hence the accuracy data for the corresponding ranges of the power analyzer are included in the table. In here, we assume that the majority of the electric power is transferred by the fundamental frequency components and we can omit the power of the harmonics. Specifications show that the accuracy of the current transducers exceeds the power analyzer accuracy by more than tenfold, and we can safely neglect the current transducer uncertainty in the analysis. For instance, in the rated operating point of the 75 kW setup, the output current measurement type B uncertainty without the transducer uncertainty taken into account is 0.3212 A, and when the current transducer uncertainty is combined with the power analyzer current accuracy, the uncertainty value is 0.3217 A, showing an insignificant influence on the result. In the frequency range below 45 Hz, the influence is even smaller

Table IV: Accuracy specifications of the measurement instruments [13], [14]

Device / uncertainty source	Specification
WT1600 power accuracy, 45 Hz $\leq f <$ 60 Hz	0.15% of reading + 0.05% of range
WT1600 power accuracy, 10 Hz $\leq f <$ 45 Hz	0.15% of reading + 0.2% of range
WT1600 power factor influence, 45 Hz $\leq f <$ 60 Hz	power reading × tan φ × 0.15%
WT1600 power factor influence, $f <$ 45 Hz, $f >$ 60Hz	power reading × tan φ × (0.15% + 0.05 × f(kHz))
Hitec CURACC current accuracy	0.01% of reading + 0.002% of range

as the CURACC system maintains its accuracy while the WT1600's accuracy is decreased in the range below 45 Hz.

Table V shows the type B uncertainty analysis for the converter losses in the rated measurement point of each setup. In Table V the input and output total error values are calculated according to the Yokogawa WT1600 specifications and these values are converted to standard uncertainty values by dividing with the coverage factor value. However, Yokogawa does not give a level of confidence for the accuracy specifications and states that they are guaranteed specification limits. The guaranteed specification limits can be considered to have 100% level of confidence. However, here we have used a coverage factor of $k = 4$, which results in 99.99% level of confidence, to convert the WT1600 accuracy values to standard uncertainty values, since there is no 100% level of confidence in statistics.

The total measurement uncertainty values for the rated operating points of each setup were calculated by combining the type A and type B uncertainties in root-sum-square (11) and the results are included in Table V. Comparing the combined uncertainty values with type B uncertainty values it becomes obvious that the type B uncertainty dictates the combined uncertainty and that the effect of the type A uncertainty is insignificant here when using 100 data points.

Table V: Type B uncertainty analysis and combined uncertainty for the converter losses in the rated test point of each setup (100% motor load torque, 50 Hz)

	Rated mechanical output of the setup	15 kW	37 kW	75 kW
Converter input	Converter input power, P_{in} (W)	16968	40833	80099
	Converter input power factor	0.93	0.88	0.90
	Power range (W)	31820	95459	190919
	P_{in} range error (W)	16	48	95
	P_{in} additional reading error due to power factor (%)	0.06	0.08	0.07
	P_{in} reading error (W)	35	94	180
	P_{in} total error, U_{Pin} (W), $k = 4$ assumed	51	141	275
	P_{in} standard uncertainty, u_{Pin} (W)	13	35	69
Converter output	Converter output power, P_{out} (W)	16508	39708	78546
	Converter output current, I_{out} (A)	30.3	65.9	127.1
	Converter output power factor	0.72	0.76	0.75
	Power range (W)	31820	95459	190919
	P_{out} range error (W)	16	48	95
	P_{out} additional reading error due to power factor (%)	0.15	0.13	0.13
	P_{out} total reading error (W)	49	111	221
	P_{out} total error, U_{Pout} (W), $k = 4$ assumed	65	159	316
	P_{out} standard uncertainty, u_{Pout} (W)	16	40	79
Losses	Converter losses, P_{loss} (W)	459	1125	1554
	P_{loss} type B uncertainty (W), $k = 2$	41.3	106.3	209.5
	P_{loss} type B uncertainty (%), $k = 2$	9.0	9.5	13.5
	P_{loss} combined uncertainty (W), $k = 2$	**41.7**	**109.6**	**213.5**
	P_{loss} combined uncertainty (%), $k = 2$	**9.1**	**9.7**	**13.7**

Converter loss uncertainty distribution over the frequency–torque plane

The converter losses, and the type B uncertainty results from the 16 operating points of 25% – 100% of motor rated torque and 12.5 Hz – 50 Hz output frequency are shown in Figures 3–5 for each of the three setups. The calculated loss and uncertainty data was interpolated over the measurement range and the results are presented with contour plots. The 16 test points are marked with × in the plots. The uncertainty values in Figures 4 and 5 represent the extended type B uncertainty with coverage factor k = 2 (95% level of confidence). The color scales are different between subplots a, b and c in Figures 3 and 4, which present absolute power values. In Figure 5, the color scale is the same in subplots a, b and c to ease the comparison between the relative uncertainties of the three converters.

The converter losses shown in Figure 3 are as expected and the converter losses increase with both load and frequency, the influence of load being higher on the loss value. The difference in the converter losses between 37 kW and 75 kW measurements is relatively low while the difference between 15 kW and 37 kW setups is more clearly in direct proportion with load. The loss values in the rated operating points of the motors (100% torque, 50 Hz) are listed in Table V.

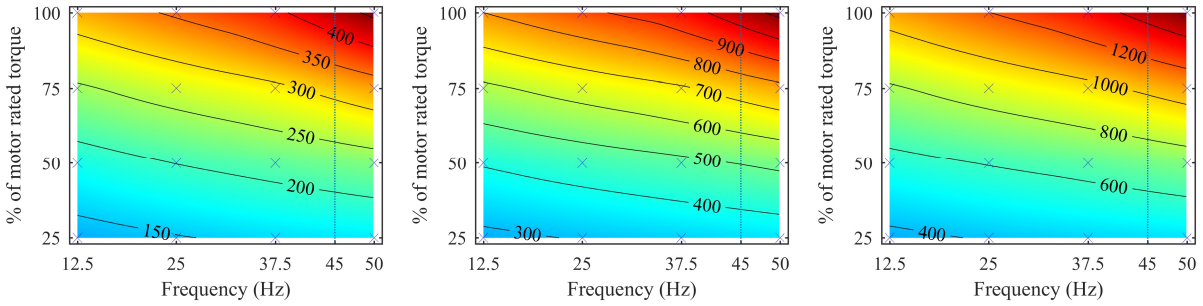

a) With 15 kW IM b) With 37 kW IM c) With 75 kW IM

Fig. 3: The converter losses (W) of the 15 kW (a), 37 kW (b), and 75 kW (c) setups interpolated over the motor operating ranges of 25% – 100% load torque and 12.5 Hz – 50 Hz supply frequency.

Figure 4 shows the converter losses' uncertainty distributions in Watts. In the operating range below 37.5 Hz, the absolute uncertainty rises with both load and frequency. Around the 45 Hz border, where the power analyzer accuracy range changes, the uncertainty values naturally decrease towards 50 Hz as the power analyzer accuracy is optimal in the range between 45 Hz and 66 Hz (see Table IV).

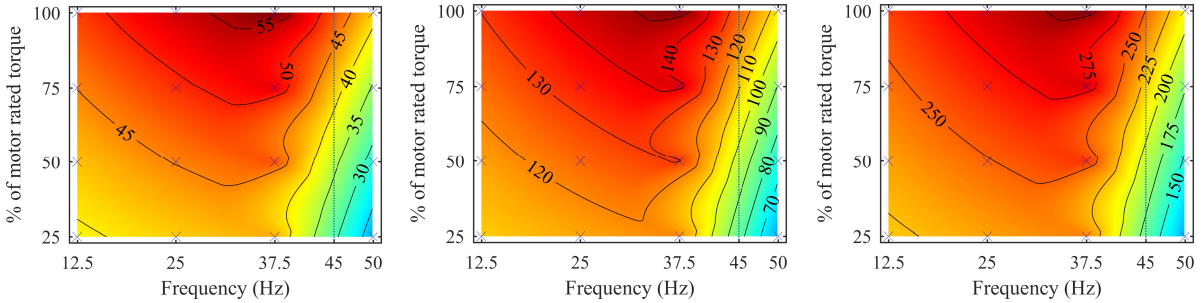

a) With 15 kW IM b) With 37 kW IM c) With 75 kW IM

Fig. 4: Absolute converter loss uncertainties in Watts (W). The converter loss extended uncertainties for the 15 kW (a), 37 kW (b), and 75 kW (c) setups interpolated over the motor operating ranges of 25% – 100% load torque and 12.5 Hz – 50 Hz supply frequency. The uncertainty values are presented at 95% level of confidence (coverage factor k = 2).

Figure 5, in turn, shows that the relative uncertainty improves in the lower frequency range when the load increases, but stays mostly constant with frequency until the 45 Hz area, where the relative uncertainty improves significantly and rapidly towards 50 Hz frequency. Using a more dense measurement point matrix we would see a steep, step-like behavior around the 45 Hz mark.

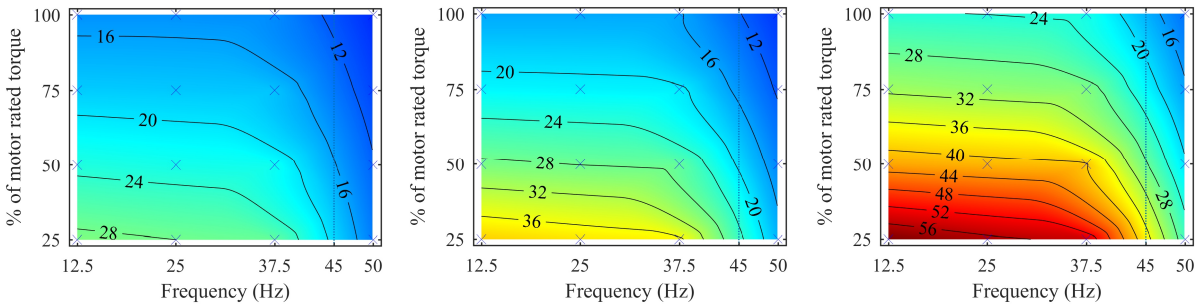

a) With 15 kW IM b) With 37 kW IM c) With 75 kW IM

Fig. 5: Relative converter loss uncertainties. The converter loss extended uncertainties as percentage units (%) for the 15 kW (a), 37 kW (b), and 75 kW (c) setups interpolated over the motor operating ranges of 25% – 100% load torque and 12.5 Hz – 50 Hz supply frequency. The uncertainty values are presented at 95% level of confidence (coverage factor $k = 2$).

The relative extended uncertainties in the low load and low frequency range are rather poor, although a modest coverage factor of $k = 2$ was used. In the low end of the measurement range, the converter loss uncertainties are over three times as high as in each setup's rated point, exceeding 50% for the 75 kW setup. The reason for this is that for partial loads, the instruments' ratings are far from optimal and the measurement range uncertainties together with the additional reading uncertainties due to low power factor have a significant effect on the overall uncertainty.

When comparing the results of the three different setups in Figure 5, we notice that the converter losses' relative uncertainty rises along the setup's power rating, the difference being modest between the 15 kW and the 37 kW setups, and notably higher between the 37 kW and the 75 kW setups. There are two main factors behind this behavior between the setups. The most obvious contributor to the much higher relative loss uncertainty of the 75 kW setup is the efficiency of the converter. In Figure 3 it can be easily seen, that while the loss values increase roughly in proportion to the motor power between Figures 3a and 3b, the proportional increase is much lower between Figures 3b and 3c. As the loss uncertainty in watts is calculated from the input and output power uncertainties, the relative amount of uncertainty is higher when the losses are lower. This is also the reason why the input and output power measurement is not well suitable for determining losses and efficiency of high efficiency devices. Here, the converter efficiency values calculated from Table V data for the rated operating point of each motor were 97.3%, 97.2%, and 98.1% for the 15 kW, 37 kW, and 75 kW setups respectively. However, as the efficiency values indicate, the difference in the converter losses' relative uncertainty between 15 kW and 37 kW setups arises from another source: The power measurement range (see Table V) is less optimal for the larger setups, which increases the power measurement uncertainty.

Discussion

The uncertainty determination was presented here for one kind of measurement system used with different setups and some simplifications could be made. Since the measurement period here was long enough, the type A uncertainty became insignificant compared to the type B uncertainty. In addition, the current transducers used here are state of the art and their uncertainty contribution was almost nonexistent. A measurement period of 100 seconds should usually be long enough for this kind of measurement and modern current transducers are usually very accurate. However, this cannot be generalized and the contribution of type A uncertainty and the uncertainties of all components of the measurement instrumentation should be checked in each case – as was done here.

Conclusion

The uncertainty analysis is a tool to control the uncertainty in measurements. The uncertainty budget is easy to create and can be built to examine different aspects' contribution to total measurement uncertainty. It should be kept in mind that the basic accuracy values given in the measurement

instruments marketing can only be met in special circumstances. The power analyzer's accuracy is typically highest in the frequency band near the grid frequency (45 Hz to 60 Hz) and decreases rapidly when the measured quantities are outside this band. By recording enough data points, the type A uncertainty can be reduced to insignificant levels. By choosing the correct measurement instruments with suitable rated values, also the type B uncertainty can be kept at a reasonable level. Determining losses of high-efficiency devices as the difference of input and output power measurements is especially sensitive to measurement instruments' accuracy and a low power factor together with overrated instruments can easily rise the uncertainty at partial load points to considerable level.

References

[1] M.-M. Kepsu, "Uncertainty of efficiency measurements in electric drives", Master's thesis of Electrical Engineering, Lappeenranta University of Technology, Faculty of Technology, 2015.

[2] Evaluation of measurement data – Guide to the expression of uncertainty in measurement, Ed. 1, JCGM 100:2008, September 2008, pp. 1–134.

[3] Adjustable speed electrical power drive systems – Part 9-2: Ecodesign for power drive systems, motor starters, power electronics and their driven applications – Energy efficiency indicators for power drive systems and motor starters. Ed. 1. IEC 61800-9-2, March 2017.

[4] W. Cao, "Assessment of induction machine efficiency with comments on new standard IEC 60034-2-1," in Proc. Int. Conf. on Electric Machines, Vilamoura, Portugal, September 2008, pp. 1–6.

[5] A. Boglietti, A. Cavagnino, and S. Vaschetto, "Induction motor EU standards for efficiency evaluation: The scenario after IEC 60034-2-1," in Proc. 37th Annu. Conf. on IEEE Industrial Electronics Society, *Melbourne*, *Australia*, November 2011, pp. 2786–2791.

[6] A. Boglietti, A. Cavagnino, M. Lazarri, and M. Pastorelli, "Induction motor efficiency measurements in accordance to IEEE 112-B, IEC 34-2 and JEC 37 international standards," in Proc. IEEE Int. Electric Machines and Drives Conference 2003, vol. 3, Madison, USA, June 2003, pp. 1599–1605.

[7] A. Baghurst, P. Angers, and M. Doppelbauer, "A standard algorithm for the calculation of induction motor efficiency based on International Standard IEC 60034-2-1," in Proc. 7th Int. Conf. on Energy Efficiency in Motor Driven Systems, Alexandria, USA, September 2011, pp. xx–xx.

[8] W. Cao,"Comparison of IEEE 112 and New IEC Standard 60034-2-1," IEEE Trans. Energy Conversion, vol. 24, no. 3, pp. 802–808, September 2009.

[9] M. Doppelbauer, "Accuracy of the determination of losses and energy efficiency of induction motors by the indirect test procedure", in Proc. 7th Int. Conf. on Energy Efficiency in Motor Driven Systems, Alexandria, USA, September 2011, pp. 457–469.

[10] E.B. Agamloh, "A Comparison of direct and indirect measurement of induction motor efficiency," in Proc. IEEE Int. Electric Machines and Drives Conference, Miami, USA, May 2009, pp. 36–42.

[11] L. Aarniovuori, J. Kolehmainen, A. Kosonen, M. Niemelä and J. Pyrhönen, "Uncertainty in motor efficiency measurements," 2014 International Conference on Electrical Machines (ICEM), Berlin, 2014, pp. 323-329.

[12] Cao, W et al. 2006. Experimental Uncertainty in Estimation of the Losses and Efficiency of Induction Motors. Conf. Rec. Industrial Applications, Tampa, USA, Oct. 8-12, p. 441 – 447.

[13] *WT1600 Digital Power Meter User's Manual (4th Edition)*, Yokogawa Electric Corporation, Tokyo, Japan, 2004, Accessed on: June, 4, 2018 [Online]. Available: https://web-material3.yokogawa.com/IM760101-01E.pdf?_ga=2.105844352.2062736829.1528097117-1553882151.1527243875

[14] *Zero-flux™ Current Sensors & Precision Power Meters: Hitec & Yokogawa – A perfect ACCURACY match*, Yokogawa Europe, Amersfoot, The Netherlands, 2009.

Publication VII

Kärkkäinen, H., Aarniovuori, L., Niemelä, M., and Pyrhönen, J.
Advanced Uncertainty Calculation Method for Converter-Fed Motor Loss Determining

IEEE International Electric Machines and Drives Conference (IEMDC)
pp. 1-10, 2019

Advanced Uncertainty Calculation Method for Converter-Fed Motor Loss Determining

Hannu Kärkkäinen
Laboratory of Electric Drives Technology
LUT University
Lappeenranta, Finland
hannu.s.karkkainen@lut.fi

Lassi Aarniovuori
Power Electronics, Machines and Power System Group
Aston University
Birmingham, UK
l.aarniovuori@aston.ac.uk

Markku Niemelä
Laboratory of Electric Drives Technology
LUT University
Lappeenranta, Finland
markku.niemela@lut.fi

Juha Pyrhönen
Laboratory of Electric Drives Technology
LUT University
Lappeenranta, Finland
juha.pyrhonen@lut.fi

***Abstract*— There is only a single practical method to determine the losses of converted-fed electrical machines. The method is based on mechanical output and electrical input power measurements. When this method is used, the loss measurement uncertainty is a function of the efficiency. The electrical motor efficiency increases non-linearly with increasing rated power. Therefore, the higher the rated power of the motor is the more care should be laid in the analysis of the efficiency measurement results. Here, a workflow starting from measurement instruments' data sheet information to final measurement uncertainty result is presented for three converted-fed induction motors with different rated power of 15 kW, 37 kW and 75 kW. The results are applicable for all rotating field machines regardless of technology.**

Keywords*— *electric power, efficiency, induction motor, measurement uncertainty, mechanical power.

I. Introduction

The nominal efficiencies of direct-on-line (DOL) electrical machines have been regulated for a long time and the efficiencies have been labelled and standardized using various approaches. Nowadays, the efficiency limits are more harmonized and the IEC and NEMA efficiency limits for 50 Hz machines are equivalent. There is an increased need to standardize the efficiencies of the converter-fed machines and IEC has split the IEC 60034-30, which specified the energy-efficiency classes for the single-speed, continuous duty cage-induction motors with 2, 4 or 6 poles, into two standards. The first part IEC 60034-30-1 [1] is dedicated for all motor technologies that are capable of DOL-starting and the second part IEC 60034-30-2 is for converter-fed machines regardless of technology [2] but excluding switched reluctance machines. The IEC efficiency limits for converter-fed machines are given for different rated rotational speed ranges. This differs from the DOL machine standard that is based on the number of pole pairs. The efficiency limits for converter-fed machines are adjusted by an allowance recognizing the converter-caused additional harmonic losses and the reduced efficiency due to using partial speed (90 %) in the measurements. The efficiency limits for converter-fed machines are obtained with

$$\eta_{\mathrm{n}} = \frac{1}{1 + (1 + r_{\mathrm{HL}})\left(\frac{1}{\eta_{\mathrm{ref}}} - 1\right)}, \tag{1}$$

where r_{HL} is the additional harmonic loss factor that is 0.15 (15%) for machines with rated power up to and including 90 kW and 0.25 (25%) for machines with rated powers higher than 90 kW. In (1), $(1/\eta_{\mathrm{ref}}\text{-}1)$ represents DOL motor losses and $(1+r_{\mathrm{HL}})(1/\eta_{\mathrm{ref}}\text{-}1)$ converter-fed motor losses. η_{ref} is the corresponding reference efficiency limit table value that is equal to DOL efficiency limit for IE1 to IE4 classes. In [2], also new target values for 'IE5 – ultra premium efficiency' are introduced. The rated efficiency limits of the converter-fed machines with rotating speeds from 1201 to 1800 rpm are presented in Fig. 1 taking (1) into account. Therefore, the efficiency values obtained by measurements should follow the values of Fig. 1 directly without adjustments.

When using the efficiency determination method based on output and input power measurements, the loss measurement uncertainty increases with increasing efficiency. However, the input-output method is the only practically applicable method for all converter-fed machines' efficiency determination and it is offered by IEC in [3]. The only other viable method would be to measure losses directly with calorimetric methods [4] that can be very precise, but complexity of the measurement systems and long duration of the measurements restrict the practical usage of calorimeters. For converter-fed machines, the uncertainty in losses $U(P_{\mathrm{l}})$ can be obtained by combining the electric power measurement uncertainty $U(P_{\mathrm{e}})$ and the mechanical power measurement uncertainty $U(P_{\mathrm{m}})$ using the square root of the sum of squares method by assuming that the uncertainties of the powers do not correlate. That is

$$U(P_{\mathrm{l}}) = \sqrt{U(P_{\mathrm{e}})^2 + U(P_{\mathrm{m}})^2}. \tag{2}$$

Assuming that the input and output measurement uncertainties are even, $U(P_{\mathrm{e}}) = U(P_{\mathrm{m}})$, and using the efficiency limits of the converter-fed machines from [2], we can create curves that present the minimum measurement uncertainty of the input and output powers as a function of the machine rated power required to obtain a specific loss tolerance. Fig. 2 shows for each of the IE-efficiency classes the measurement uncertainties required to achieve a 5% loss tolerance. For example, for 200 kW IE5 the measurement uncertainties of the input and the output power must be below 0.11% to obtain 5% loss tolerance, while for 1.1 kW IE5 power measurement uncertainties of 0.45% are sufficient to achieve the 5% loss tolerance.

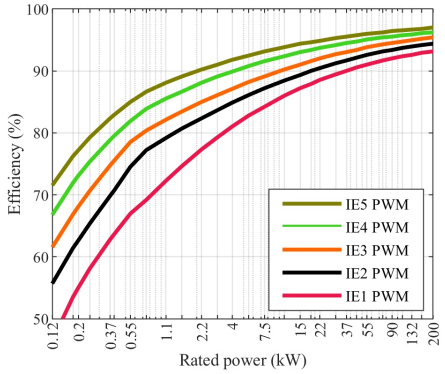

Fig. 1. The efficiency limits of the converter-fed machines with rated speeds of 1201 to 1800 rpm based on IEC 60034-30-1 and (1).

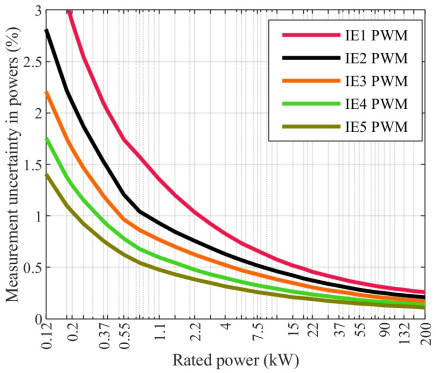

Fig. 2. The allowed measurement uncertainty limits to obtain a motor loss uncertainty of 5% with the input-output -method when assuming that the input and output power measurement uncertainties are even.

The uncertainty in electric motor loss measurements has been the topic of several publications. The efficiency of induction machines (IM) and measurement uncertainties in input-output testing methods used in industry are assessed in [5]. In [6], the efficiency measurement results of five induction motors with different rated powers according IEC 60034-2-1 are presented and the uncertainty of the measurements is analyzed using scientific and numerical methods. The influence of the measurement error on the uncertainty of the efficiency determination by the indirect summation of losses methods is analyzed using Monte Carlo simulations in [7] and in [8], the efficiency measurement uncertainty is analyzed using realistic perturbation-perturbation estimation (RPBE) –method. The uncertainty of IEC 60034-2-1 direct and indirect three-phase IM efficiency determination methods has been analyzed in [9] with suggestions for future standards. In [10], the uncertainty of direct and indirect efficiency determination methods in permanent magnet synchronous machines is investigated.

In the indirect summation of losses methods, the losses and efficiency are determined based of separate tests and human error can be considered as a potentially significant source of uncertainty [5], [8]. The input-output method, however, requires only static measurements of input and output power and the human errors are limited to setting up the measurement setup and instrumentation. Here, the input-output method with automated data recording was used; hence, the possibilities of human errors are minimized.

II. Electrical Power Measurement

The electrical power of the converted-fed electrical machines is usually measured using a power analyzer. The uncertainty of the electrical power measurement is a function of the voltage and current amplitudes, frequency and the power factor. The power analyzer measurement accuracy is given for certain frequency bands. To estimate the electrical power measurement uncertainty of the converter-fed electrical machines where the electrical power contains multiple signals with different frequencies, the active power must be split in these different frequency domains. This can be performed using the discrete Fourier transformation (DFT).

A. Electrical power in the frequency domain

The frequency distribution of the electric input power of converter-fed electric machines is a function of the switching frequency, DC-link voltage level and modulation method. Fig. 3 shows the cumulative power of a converter-fed 37 kW induction motor up to 500 kHz obtained with DFT from

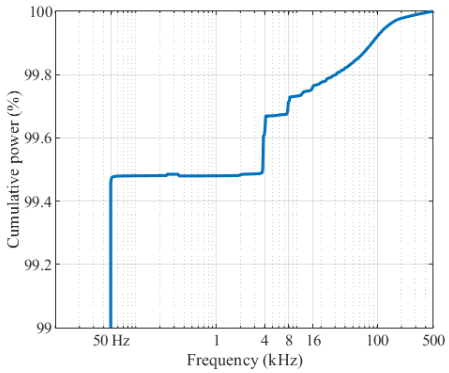

Fig. 3. A PWM-power cumulative function measured at increased converter terminal voltage and 50 Hz output frequency with 4 kHz carrier frequency that is equal to switching frequency in this case since there were no missing pulses in the corresponding time domain waveform.

one-second long waveform sample recorded with a power analyzer at a sample rate of 1 MS/s. Because the vast majority of power – approximately 99.5% – is at the fundamental frequency, the plot is scaled to show the topmost percent of the power.

The active electric power can be calculated in the frequency domain using the DFT results

$$P = \sum_{k=1}^{k=\mathrm{MAX}} U(k)I(k)\cos(\varphi(k)), \qquad (3)$$

where $U(k)$ and $I(k)$ are the frequency components of the voltage and current obtained with the DFT and $\cos(\varphi(k))$ is the power factor of the corresponding k^{th} frequency component. This can be applied to obtain the power content of each of the power analyzer accuracy bands. The motor input power measurement was performed with Yokogawa WT1600 power analyzer and its accuracy values for the different frequency bands given in the manufacturer's specifications [11] are listed in Table I. The third column of Table I shows the distribution of the PWM power data shown in Fig. 3 split into the different frequency bands. Most of the power is naturally in the band around the fundamental frequency and the PWM-caused harmonic power is distributed over the three highest bands between 1 kHz and 500 kHz. The frequency

TABLE I. The Accuracy Specifications of Yokogawa WT1600 Power Analyzer for Different Frequency Bands and 37 kW IM Power and Power Uncertainty at Each Band

Frequency band	Accuracy rdg + rng (%)[1]	Power (W)	Uncertainty (W) (k=2)
DC	0.15 + 0.2	0	0
0.5 Hz < f ≤ 10 Hz	0.3 + 0.3	0	0
10 Hz < f ≤ 45 Hz	0.15 + 0.2	1	0
45 Hz < f ≤ 66 Hz	**0.15 + 0.05**	**39660**	**79.4**
66 Hz < f ≤ 1 kHz	0.3 + 0.1	0	0
1 kHz < f ≤ 50 kHz	0.45 + 0.2	143	0.41
50 kHz < f ≤ 100 kHz	1.05 + 0.3	33	0.40
100 kHz < f ≤ 500 kHz	6 + 1	22	0.68
Total		**39859**	**80.9**
Using only the total power value and the fundamental frequency band accuracy		**39859**	**79.7**

[1]In addition, power factor has an influence on the accuracy:
- When 45 Hz ≤ f < 60 Hz: power reading × tan φ × 0.15%
- When f < 45 Hz, f > 60Hz: power reading × tan φ × (0.15 + 0.05 × f(kHz))%
For the example data, the total RMS power factor was 0.756 and outside the fundamental frequency band, $\varphi = \frac{\pi}{4}$ was assumed when calculating the uncertainties.

band from 66 Hz to 1 kHz shows zero power, but actually, both the fifth and the seventh harmonic are present. The fifth harmonic is transferring power to the motor while the seventh harmonic is transferring power back to the converter, which results in approximately zero contribution over this frequency band. This can be seen in Fig. 3 between 50 Hz and 1 kHz as a small increase in the cumulative power that returns to the level before the increase at a slightly higher frequency.

The fourth column of Table I contains the power expanded uncertainty calculated for the frequency bands separately. For comparison, the uncertainty calculated using only the total active power value and the accuracy values of the fundamental frequency band (45 Hz…66 Hz). An example calculation is presented in section IV. The coverage factor for the uncertainty values is k = 2 which results in 95% level of confidence. From Table I it can be clearly seen that the electrical power uncertainty is almost completely dominated by the fundamental frequency band and the total electric power uncertainty can be evaluated using only the total power value and the fundamental frequency band accuracy.

III. Mechanical power measurement

The mechanical power P_m is the product of angular velocity Ω and torque T, but usually the rotational speed n in revolutions per minute is used instead of the angular velocity

$$P_\mathrm{m} = \Omega T = \frac{2\pi n}{60} T. \tag{4}$$

The uncertainties of speed and torque do not correlate and they are measured with separate sensors, hence the uncertainty contributions of both quantities can be analyzed individually and combined in root-sum-square similar to (2). However, as mechanical power is the product of speed and torque, its sensitivity to both Ω and T has to be taken into account. The uncertainty contribution that an input quantity has on an output quantity is obtained as the product of the uncertainty of the input quantity and its sensitivity coefficient c, that is, the partial differential of the output quantity in respect to the input quantity. The sensitivity coefficients of the mechanical power for speed and torque are therefore

$$c_\Omega = \frac{\partial P_\mathrm{m}}{\partial \Omega} = T \quad \text{and} \quad c_T = \frac{\partial P_\mathrm{m}}{\partial T} = \Omega. \tag{5}$$

The uncertainty contribution the speed has on the mechanical power is

$$U(P_\mathrm{m})_\Omega = |c_\Omega| U(\Omega) \tag{6}$$

and similarly the contribution of torque uncertainty on P_m is

$$U(P_\mathrm{m})_T = |c_T| U(T) \tag{7}$$

Finally, the mechanical power uncertainty is

$$U(P_\mathrm{m}) = \sqrt{(U(P_\mathrm{m})_\Omega)^2 + (U(P_\mathrm{m})_T)^2}. \tag{8}$$

A. Rotational speed measurement

The rotational speed is typically measured using magnetoresistive or optical means. As the typical speed measurement technologies are based on counting pulses, the resolution of the digital speed signal may have an effect on the speed measurement accuracy especially on low speeds. A signal resolution δx causes a uniform uncertainty distribution between $x - \delta x/2$ and $x + \delta x/2$. The standard uncertainty for a quantity with uniform distribution between $x - a$ and $x + a$ is $a/\sqrt{3}$ [12], thus, the uncertainty contribution $u_{\delta x}$ of a digital instrument resolution δx can be expressed as

$$u_{\delta x} = \frac{\delta x}{2} \cdot \frac{1}{\sqrt{3}}. \tag{9}$$

B. Torque measurement

Different methods to measure torque exist but in practice for loss and efficiency determination purposes, only direct methods relying on in-line torque sensors or transducers are viable. The accuracy of in-line torque sensors attached in the shaft between the motor and the load is affected by several sources of uncertainty those can be categorized by their behavior over the measurement range. An uncertainty source can affect the torque value independently of load resulting in equal uncertainty (in Nm) at any measurement point, or the uncertainty can be load-dependent resulting in higher uncertainty at high torque. The uncertainty sources are discussed in detail using example data in section IV.

IV. Experimental results and analysis

The loss uncertainty analysis and results are presented here for three different converter-fed induction motors. The measurement data used in this analysis is from a series of input-output efficiency measurements over a wide operating range, consisting of a matrix of 16 operating points at 12.5 Hz, 25 Hz, 37.5 Hz and 50 Hz operating frequency and at 25%, 50%, 75% and 100% of the rated torque. Each load point in these measurements was measured for 100 s and recordings were taken once a second. The aim in these measurements was to obtain the loss distribution over the whole frequency–torque plane, which is essential when studying the energy efficiency of different motor driven applications. However, the operating point of 90% of the rated operating frequency and 100% of the rated torque is used for IEC- energy efficiency classification [2].

The measurement setup details are given in Table II. The motors tested in the measurements were rated for 15 kW, 37 kW and 75 kW powers and they all have IE3 efficiency classification. Each of the motors was supplied with a frequency converter of the same model but with different current rating matching the power of the motor. The same power analyzer was used for all three motors and the voltage levels for all motors are the same but the current sensors have different ratings and the ratio of the current sensor rating to motor rated current is different. At the partial load points, also the actual measured current of the machine is influencing the results. All the torque transducers are of the same model but with different ratings suitable for each motor. Similarly as the current sensors ratings, the ratio of the torque transducer rating to the measured torque has an influence on the results.

TABLE II. The measurement setups

Rated mechanical output power of the setup	**15 kW**	**37 kW**	**75 kW**
Motor	15 kW IM (IE3)	37 kW IM (IE3)	75 kW IM (IE3)
Converter (I_max continuous)	34 A	103 A	202 A
Power analyzer	Yokogawa WT1600		
Current transducers	Hitec CURACC (100 A)	Hitec CURACC (300 A)	Hitec CURACC (300 A)
Torque transducer	HBM T12 (100 Nm)	HBM T12 (500 Nm)	HBM T12 (1000 Nm)

In the following, the uncertainty analysis procedure is presented with example calculations using the measurement data from the rated operating point of the 37 kW IM (Table III). The power value in Table III is the average of 100 s while the value in Table I is from the analysis of one-second waveform data, hence there is a slight difference in the values. All uncertainty values are converted to normal distribution and calculated and presented for coverage factor $k = 2$, which corresponds to a 95% level of confidence. Both type A uncertainty and type B uncertainty have been taken into account in the calculations. Type A uncertainty is related to variations in repetition of measurements and describes how much the average of a set of measurements can fluctuate. Type B uncertainty, in turn, relates directly to the accuracy of the measurement instruments. Both type A and type B uncertainty have been covered in detail in [13].

A. Electrical power measurement uncertainty

The accuracy specifications for the power analyzer and uncertainty calculations for each frequency band were presented in Table I. According to the comparison included in Table I, we can evaluate the electric power uncertainty using only the total power and the accuracy values of the fundamental frequency band.

Yokogawa states that the accuracy specifications in Table I are guaranteed specification limits. The guaranteed limits can be considered to have 100% level of confidence but here we have assumed a coverage factor of $k_\mathrm{P} = 4$ that results in 99.99% confidence level. For the example operating point in Table III, the electrical power type B uncertainty can now be calculated as

$$\begin{aligned} U_\mathrm{B}(P_\mathrm{e}) &= \frac{k}{k_\mathrm{P}} \cdot (P_\mathrm{e} \cdot rdg + P_{\mathrm{e}_\mathrm{range}} \cdot rng + P_\mathrm{e} \cdot \tan(\varphi) \cdot 0.15\%) \\ &= \tfrac{2}{4} \cdot (39708\ \mathrm{W} \cdot 0.0015 + 95459\ \mathrm{W} \cdot 0.0005 + \\ &\quad 39708\ \mathrm{W} \cdot \tan(0.714) \cdot 0.0015) = 79.5\ \mathrm{W}, \end{aligned} \tag{10}$$

where dividing by k_P returns the Yokogawa expanded uncertainty to standard uncertainty, and multiplying by k gives our desired coverage factor and confidence interval.

Type A uncertainty is calculated from the standard deviation of the 100 samples long measurement data

$$U_\mathrm{A}(P_\mathrm{e}) = k \cdot \frac{s(P_\mathrm{e})}{\sqrt{N}} = 2 \cdot \frac{91.4\ \mathrm{W}}{\sqrt{100}} = 18.3\ \mathrm{W} \tag{11}$$

and the overall electrical power uncertainty $U(P_\mathrm{e})$ is obtained by combining the type A and type B uncertainties [12]

$$\begin{aligned} U(P_\mathrm{e}) &= \sqrt{\left(U_\mathrm{A}(P_\mathrm{e})\right)^2 + \left(U_\mathrm{B}(P_\mathrm{e})\right)^2} \\ &= \sqrt{(18.3)^2 + (79.5)^2}\ \mathrm{W} = 81.6\ \mathrm{W}. \end{aligned} \tag{12}$$

The type A uncertainty is very low when using as much samples as here (100) and it has very little effect on the combined uncertainty. In practice, $U(P_\mathrm{e})$ consists almost completely of the type B uncertainty, which is obvious comparing the results of (10)–(12).

B. Speed measurement uncertainty

The HBM T12 torque transducers used here include optical speed measurement system using infrared light and a metallic slotted disc. The speed measurement uncertainty of HBM T12 is affected by the speed measurement system accuracy of n_acc=150 ppm and the resolution of δn=0.1 rpm [14]. n_acc is related to the speed reading and is defined for a uniform distribution. For the example operating point (Table III), the type B expanded uncertainty (at $k = 2$, that is, 95% level of confidence) of the measurement system is

$$\begin{aligned} U_\mathrm{sys}(n) &= k \cdot n \cdot n_\mathrm{acc} \cdot \frac{1}{\sqrt{3}} \\ &= 2 \cdot 1473.9\ \mathrm{rpm} \cdot 0.00015 \cdot \tfrac{1}{\sqrt{3}} = 0.255\ \mathrm{rpm}, \end{aligned} \tag{13}$$

and the resolution-caused uncertainty is

$$U_{\delta n}(n) = k \cdot \frac{\delta n}{2} \cdot \frac{1}{\sqrt{3}} = \frac{0.1\ \mathrm{rpm}}{2} \cdot \frac{1}{\sqrt{3}} = 0.058\ \mathrm{rpm}. \tag{14}$$

U_sys and $U_{\delta n}$ do not correlate, thus the overall type B expanded uncertainty can be combined as

$$\begin{aligned} U_\mathrm{B}(n) &= \sqrt{\left(U_\mathrm{sys}(n)\right)^2 + \left(U_{\delta n}(n)\right)^2} \\ &= \sqrt{(0.255)^2 + (0.058)^2}\ \mathrm{rpm} = 0.262\ \mathrm{rpm}. \end{aligned} \tag{15}$$

For speed, the type A uncertainty and the combined uncertainty are calculated similarly as in (11) and (12) for the electric power: The type A expanded uncertainty is

$$U_\mathrm{A}(n) = k \cdot \frac{s(n)}{\sqrt{N}} = 2 \cdot \frac{0.737\ \mathrm{rpm}}{\sqrt{100}} = 0.147\ \mathrm{rpm}, \tag{16}$$

the combined expanded uncertainty is

$$\begin{aligned} U(n) &= \sqrt{\left(U_\mathrm{A}(n)\right)^2 + \left(U_\mathrm{B}(n)\right)^2} \\ &= \sqrt{(0.147)^2 + (0.262)^2}\ \mathrm{rpm} = 0.300\ \mathrm{rpm}. \end{aligned} \tag{17}$$

and the relative expanded uncertainty is

$$U_\mathrm{rel}(n) = \frac{U(n)}{n} = \frac{0.300\ \mathrm{rpm}}{1473.9\ \mathrm{rpm}} = 0.020\%. \tag{18}$$

TABLE III. THE MEASUREMENT DATA FOR THE 37 KW IM RATED OPERATING POINT AND OTHER PARAMETERS REQUIRED IN THE EXAMPLE CALCULATIONS.

Electric power (RMS), P_e (W)	39708
Standard deviation of electric power data (W)	91.4
Number of measurement data samples, N	100
Power factor, $\cos(\varphi)$	0.756
φ (rad)	0.714
Fundamental supply frequency, f_fund (Hz)	50
Speed, n (rpm)	1473.9
Standard deviation of speed data, $s(n)$ (rpm)	0.737
Torque, T (Nm)	239.7
Standard deviation of torque data, $s(T)$ (Nm)	0.380
Mechanical power, P_m (W)	36997
WT1600 power measurement range, $P_\mathrm{e,range}$ (W)	95459
WT1600 power measurement accuracy coverage factor,	4
Transducer nominal torque rating, T_nom (Nm)	500
Transducer temperature deviation from 23°C, $\Delta\theta$ (K)	10
Coverage factor k for expanded uncertainty	2
Level of confidence at $k = 2$	95%

C. Torque measurement uncertainty

The accuracy of the torque measurement is affected by various different sources of uncertainty and here the accuracy values and uncertainty sources are covered according to HBM specifications from [14] and [15]. Other torque transducer manufacturers may define the accuracies

differently, although same principles will apply. The calculation procedure followed here is based on [16] and examples provided by HBM.

The accuracy specifications and their distributions for HBM T12 are listed by each uncertainty source in Table IV. The values given in the table are the same for all transducer sizes of the same model. The transducer temperature has two separate effects on the torque accuracy that are defined per 10 K deviation from the reference temperature of 23°C. The *temperature influence on zero value* (θZ) causes an equal uncertainty over the torque range as it is related to the nominal torque of the transducer T_{nom}, while the *temperature influence on span* (θS) has an effect relative to the actual torque reading. For the example case of Table III, the torque uncertainty contributions of the temperature effects are

$$U_{\theta Z}(T) = k\left(T_{\mathrm{nom}} \cdot \frac{\theta Z}{10\ \mathrm{K}} \cdot \Delta\theta \cdot \frac{1}{\sqrt{3}}\right) = 2 \cdot \left(500\ \mathrm{Nm} \cdot \frac{0.0002}{10\ \mathrm{K}} \cdot 10\ \mathrm{K} \cdot \frac{1}{\sqrt{3}}\right) = 0.12\ \mathrm{Nm}, \text{ and} \quad (19)$$

$$U_{\theta S}(T) = k\left(T_{\mathrm{act}} \cdot \frac{\theta S}{10\ \mathrm{K}} \cdot \Delta\theta \cdot \frac{1}{\sqrt{3}}\right) = 2 \cdot \left(239.7\ \mathrm{Nm} \cdot \frac{0.0003}{10\ \mathrm{K}} \cdot 10\ \mathrm{K} \cdot \frac{1}{\sqrt{3}}\right) = 0.083\ \mathrm{Nm}. \quad (20)$$

Linearity and hysteresis (*LH*) is given as a percentage of the nominal torque value but it is dependent on the transducer's measurement range. This value includes deviations of the actual output signal from linear torque to signal relationship (linearity), and the effects of hysteresis, that is, the same load torque being measured slightly differently when approached with increasing or decreasing load. For the example case, the torque value of 239.7 Nm is approximately 48% of T_{nom} where *LH* is 0.013% and the torque uncertainty contribution due to linearity and hysteresis is therefore

$$U_{LH}(T) = k\left(T_{\mathrm{nom}} \cdot LH \cdot \frac{1}{\sqrt{3}}\right) = 2 \cdot \left(500\ \mathrm{Nm} \cdot 0.00013 \cdot \frac{1}{\sqrt{3}}\right) = 0.075\ \mathrm{Nm} \quad (21)$$

Repeatability (*REP*), in turn, takes into account variations in measured torque value when no changes in the measurement setup are made between two separate measurements of the exact same load situation. *REP* is related to the difference between the highest and the lowest (or highest negative) torque values occurring in the system. Here, the torque varies between zero and the rated torque of the motor and torque uncertainty contribution of repeatability is therefore

$$U_{REP}(T) = k(\Delta T \cdot REP \cdot 1) = 2 \cdot (239.7\ \mathrm{Nm} \cdot 0.0001 \cdot 1) = 0.048\ \mathrm{Nm}, \quad (22)$$

where the distribution factor is 1 instead of $1/\sqrt{3}$ as *REP* is given as a standard uncertainty (normal distribution instead of uniform distribution with the other accuracies).

Sensitivity tolerance (*SEN*) is defined as a percentage of the nominal sensitivity of the transducer. The sensitivity of HBM transducers defines the span of the output signal between zero torque and nominal torque [15]. As the sensitivity tolerance is given as the permissible deviation of the actual sensitivity at rated load from the nominal sensitivity, the uncertainty caused by sensitivity tolerance is relative to the actual torque being measured [15]. For the example case, the sensitivity tolerance is

$$U_{SEN}(T) = k\left(T \cdot SEN \cdot \frac{1}{\sqrt{3}}\right) = 2 \cdot \left(239.7\ \mathrm{Nm} \cdot 0.0005 \cdot \frac{1}{\sqrt{3}}\right) = 0.14\ \mathrm{Nm}. \quad (23)$$

The last source of uncertainty defined in Table IV is the group of different *parasitic loads* (*PARA*) that cover the mechanical stresses other than the actual load torque subjected to the torque transducer. Fig. 4 illustrates the different parasitic load components that are axial force, lateral force, and bending moment. The axial force is the component affecting in the shaft direction that can be caused by inaccurate positioning of the transducer in the direction of the shaft, but also by the thermal expansion of the shaft. The lateral force, in turn, is the component in the radial direction that can naturally originate from inaccurate positioning in the perpendicular direction. The bending moment, as the name suggests, is the parasitic load component twisting the transducer shaft and is caused by inaccuracies in the angle of the transducer mounting. The limits for the parasitic loads are given in Table V for the three transducers used in these measurements. Table V contains also the estimated values for the parasitic load components in the test setups and their relative proportions of each component's limit. The maximum allowed sum of the three relative values (*PARA%*) is 100%, which is also the reference point for the <0.3% accuracy value given in Table IV. For the example case, the uncertainty contribution of the parasitic load components is

$$U_{PARA}(T) = k\left(T_{\mathrm{nom}} \cdot Para\% \cdot PARA \cdot \frac{1}{\sqrt{3}}\right) = 2 \cdot \left(500\ \mathrm{Nm} \cdot 0.085 \cdot 0.003 \cdot \frac{1}{\sqrt{3}}\right) = 0.15\ \mathrm{Nm} \quad (24)$$

The overall type B uncertainty is obtained by combining all the uncertainty components

TABLE IV. THE TORQUE UNCERTAINTY SOURCES AND THE CORRESPONDING ACCURACIES OF HBM T12 TORQUE TRANSDUCERS [14]

Specification (accuracy related to)		Accuracy	Distribution
Temperature infl. on zero per 10 K, θZ (T_{nom})		0.02%	Uniform
Temperature infl. on span per 10 K, θS (T_{act})		0.03%	Uniform
Linearity and hysteresis, *LH* (torque range) Depends on torque ranges defined as percentages from the transducer nominal Torque T_{nom}	0…20% T_{nom}	0.006%	Uniform
	20…60% T_{nom}	0.013%	
	60…100% T_{nom}	0.02%	
Repeatability, *REP* (ΔT)		0.01%	Normal
Sensitivity tolerance, *SEN* (T_{act})		0.05%	Uniform
Parasitic loads, *PARA* (T_{nom})[1]		< 0.3%	Uniform

[1] The accuracy value corresponds to the maximum sum of permissible parasitic loads and it is downscaled according to the actual sum of parasitic loads in the measurement setup.

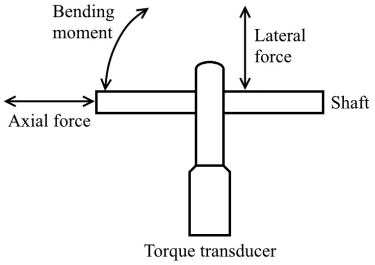

Fig. 4. Parasitic load components that can affect torque transducer output. The axial forces affect in the shaft direction, lateral forces in the radial direction, and bending moments are the force components trying to twist the shaft from the correct axial direction causing stress to the transducer.

TABLE V. THE PARASITIC LOAD LIMITS FOR THE HBM T12 TRANSDUCERS [14] AND THE ESTIMATED PARASITIC LOAD VALUES FOR THE TEST SETUPS

Transducer		Axial force	Lateral force	Bending moment	Sum (*Para%*) (Max. 100%)
100 Nm	Limit	5 kN	1 kN	50 N	
	Estimated	50 N	50 N	4 N	
	Est./Lim.	1%	5%	8%	**14%**
500 Nm	Limit	16 kN	4 kN	200 N	
	Estimated	125 N	125 N	10 N	
	Est./Limit	0.8%	3.1%	5%	**8.9%**
1000 Nm	Limit	19 kN	5 kN	220 N	
	Estimated	250 N	250 N	20 N	
	Est./Limit	1.3%	5%	9.1%	**15.4%**

$$U_{\mathrm{B}}(T) = \sqrt{{U_{\theta Z}}^2 + {U_{\theta S}}^2 + {U_{LH}}^2 + {U_{REP}}^2 + {U_{SEN}}^2 + {U_{PARA}}^2} = \sqrt{0.12^2 + 0.083^2 + 0.075^2 + 0.048^2 + 0.14^2 + 0.15^2}\ \mathrm{Nm} = 0.267\ \mathrm{Nm}. \quad (25)$$

The type A uncertainty and the combined uncertainty are calculated similarly as in (11) and (12) for the electric power: The type A expanded uncertainty is

$$U_{\mathrm{A}}(T) = k \cdot \frac{s(T)}{\sqrt{\mathrm{N}}} = 2 \cdot \frac{0.380\ \mathrm{Nm}}{\sqrt{100}} = 0.076\ \mathrm{Nm}, \quad (26)$$

the total combined expanded uncertainty is

$$U(T) = \sqrt{\left(U_{\mathrm{A}}(T)\right)^2 + \left(U_{\mathrm{B}}(T)\right)^2} = \sqrt{(0.076)^2 + (0.267)^2}\ \mathrm{Nm} = 0.278\ \mathrm{Nm}, \quad (27)$$

and the corresponding relative uncertainty is

$$U_{\mathrm{rel}}(T) = \frac{U(T)}{T} = \frac{0.278\ \mathrm{Nm}}{239.7\ \mathrm{Nm}} = 0.12\%. \quad (28)$$

The torque type B uncertainty components as the function of torque for the 37 kW IM are presented in Fig. 5. In the actual measurement range below 50% T_{nom}, the contributions of the uncertainty components with constant values, especially U_{PARA} and $U_{\theta Z}$ are quite significant, while their relative share is a lot lower in the upper end of the transducer measurement range.

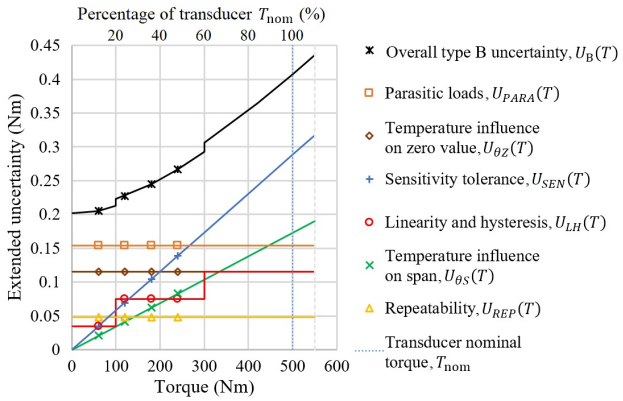

Fig. 5. HBM T12 (500 Nm) torque measurement type B uncertainty components presented over the measurement range of the transducer in the 37 kW IM measurements. HBM T12 is quaranteed to fulfill the accuracy specifications up to 110% nominal torque (grey dashed line). The values represent the expanded uncertainties at 95% level of confidence (coverage factor k = 2). The measured operating points are indicated with markers in the plots.

D. Mechanical power uncertainty

Now that we have the speed and torque uncertainties determined, we can calculate the mechanical power P_{m} uncertainty according to (5)–(9). From (5) and (7), we can calculate the speed uncertainty contribution to P_{m} uncertainty

$$U(P_{\mathrm{m}})_{\Omega} = |c_{\Omega}| \cdot U(\Omega) = T \cdot \frac{2\pi \cdot U(n)}{60}. \quad (29)$$

For the example case, this results in

$$U(P_{\mathrm{m}})_{\Omega} = T\,\frac{2\pi U(n)}{60} = 239.7\ \mathrm{Nm} \cdot \frac{2\pi \cdot 0.300\ \mathrm{rpm}}{60} = 7.5\ \mathrm{W}. \quad (30)$$

Similarly, using (6) and (8), the torque uncertainty contribution to $U(P_{\mathrm{m}})$

$$U(P_{\mathrm{m}})_T = |c_T| U(T) = \Omega \cdot U(T) = \frac{2\pi n}{60} U(T) \quad (31)$$

and for the example case this gives

$$U(P_{\mathrm{m}})_T = \frac{2\pi n}{60} U(T) = \frac{2\pi \cdot 1473.9\ \mathrm{rpm}}{60} \cdot 0.278\ \mathrm{Nm} = 42.9\ \mathrm{W}. \quad (32)$$

The mechanical power uncertainty can be calculated combining the speed and torque contributions according to (9)

$$U(P_{\mathrm{m}}) = \sqrt{(U(P_{\mathrm{m}})_{\Omega})^2 + (U(P_{\mathrm{m}})_T)^2} = \sqrt{7.5^2 + 42.9^2}\ \mathrm{W} = 43.6\ \mathrm{W} \quad (33)$$

E. Input-output loss uncertainty and relative uncertainties

As both the electrical and mechanical power uncertainties are now calculated, we can combine them according to (2) to find the uncertainty for the losses that are determined as the difference of the input electric power and output mechanical power. For the example case the motor loss uncertainty is

$$U(P_{\mathrm{l}}) = \sqrt{U(P_{\mathrm{e}})^2 + U(P_{\mathrm{m}})^2} = \sqrt{81.6^2 + 43.6^2}\ \mathrm{W} = 92.5\ \mathrm{W}. \quad (34)$$

The relative uncertainties of the electric power, mechanical power, and the losses can be calculated as

$$U_{\mathrm{rel}}(P_{\mathrm{e}}) = \frac{U(P_{\mathrm{e}})}{P_{\mathrm{e}}} = \frac{81.6\ \mathrm{W}}{39708\ W} = 0.21\%, \quad (35)$$

$$U_{\mathrm{rel}}(P_{\mathrm{m}}) = \frac{U(P_{\mathrm{m}})}{P_{\mathrm{m}}} = \frac{43.6\ \mathrm{W}}{36997\ \mathrm{W}} = 0.12\%, \text{ and} \quad (36)$$

$$U_{\mathrm{rel}}(P_{\mathrm{l}}) = \frac{U(P_{\mathrm{l}})}{P_{\mathrm{l}}} = \frac{U(P_{\mathrm{l}})}{P_{\mathrm{e}} - P_{\mathrm{m}}} = \frac{92.5\ \mathrm{W}}{2711\ \mathrm{W}} = 3.4\%. \quad (37)$$

The input and output power uncertainties, and the loss uncertainty for all three motors in the rated operating point are listed in Table VI. The electric power relative uncertainty is approximately equal for all three motors but there is difference in the mechanical power uncertainty. This is due to two separate factors: The torque transducer used with the 15 kW motor is an almost perfect match, the nominal torque of the motor being 98% of transducer T_{nom} while both the 37 kW and 75 kW motor's nominal torque values are only 48% of transducer T_{nom}. The parasitic loads affect the uncertainty increasingly with setup size, as the limits do not increase in

TABLE VI. UNCERTAINTY IN THE RATED OPERATING POINTS

Motor	15 kW	37 kW	75 kW
Electric power uncertainty	0.20%	0.21%	0.20%
Mechanical power uncertainty	0.10%	0.12%	0.15%
Loss uncertainty	2.4%	3.4%	5.2%

proportion with transducer size: the 1000 Nm transducer has only 10-20% higher limits for parasitic loads than the 500 Nm transducer, but the 1000 Nm test bench is estimated to have twice the parasitic loads compared to the 500 Nm test bench. The loss uncertainty rises with the motor size, which for a small part is due to the mechanical power uncertainty rising but mostly the uncertainty rises because of the higher efficiency of the larger motors as two large power values are used in calculating a relatively small loss value. In these measurements, the efficiencies at the rated operating point of 50 Hz, 100% rated torque were 91.0%, 93.2% and 95.2% for the 15 kW, 37 kW and 75 kW motors, respectively.

F. Loss uncertainty in frequency-torque plane

The uncertainties for all 16 operating points were calculated similarly as in (10)–(37) and here the results are interpolated over the measurement range and presented as contour plots in Figs. 6, 8 and 9. The input electric power uncertainty $U(P_e)$ and output mechanical power uncertainty $U(P_m)$ are shown in Fig. 6. Both $U(P_e)$ and $U(P_m)$ show some increase with load, but over the frequency-axis, the behavior is completely different as $U(P_m)$ increases in almost direct proportion to frequency, while $U(P_e)$ increases only slightly with operating frequency below 37.5 Hz but decreases rapidly near the nominal frequency of 50 Hz. The steep change is naturally due to the power analyzer range border at the 45 Hz mark (Table I).

The motor losses are more load-dependent than operating frequency-dependent, Fig. 7. The losses naturally increase with increasing motor rated power but not even nearly in direct proportion to the motor power, showing the higher efficiency of the higher-output motors. Fig. 8 shows the motor loss uncertainties in Watts (W). When comparing to Fig. 6 it is obvious that the loss uncertainty – and its behavior over the measurement range – is mostly governed by the power analyzer uncertainty in these tests. According to Fig. 9, the relative uncertainty improves with both load and frequency

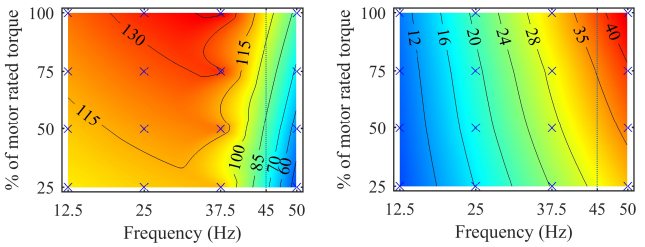

(a) Electric power uncertainty (b) Mechanical power uncertainty

Fig. 6. The 37 kW IM input and output power uncertainties in Watts (W). The expanded uncertainties for the input electric power and output mechanical power interpolated over the measurement range of 25% – 100% load torque and 12.5 Hz – 50 Hz supply frequency. The uncertainty values are presented at 95% level of confidence ($k = 2$).

and the power analyzer range border can be clearly seen also here as the uncertainty improves rapidly when approaching 50 Hz. The relative uncertainty, however, increases with motor size, which is partly due to the mechanical power uncertainty being higher in the larger setups but more significantly due to the efficiency rising with motor size as already discussed above.

V. Discussion

The results shown here represent only the measurement setups and instrumentation used in these specific measurements. Here, a high accuracy torque transducer was used, while the power analyzer accuracy is modest by today's standards. This shows in the results, as the electric power uncertainty at the 37 kW IM nominal point was twice higher than the mechanical power uncertainty, and in the lower operating speeds, the difference is even higher (Fig. 6). However, in the original purpose of this measurement series, which was loss and efficiency analysis over a wide operating range, WT1600 is accurate enough, as differences far smaller than the analytically calculated measurement uncertainty can be reliably measured when no changes are made to the test setup between measurement points. This shows also in very

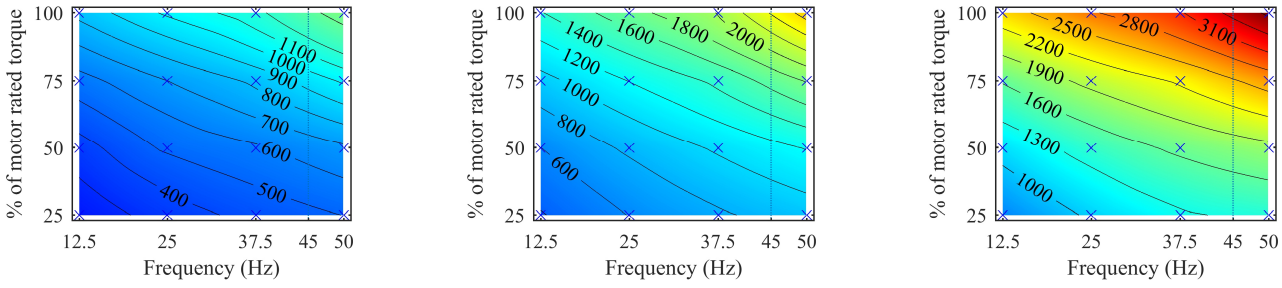

(a) 15 kW IM losses (b) 37 kW IM losses (c) 75 kW IM losses

Fig. 7. Total losses (W) of the 15 kW (a), 37 kW (b), and 75 kW (c) induction motors interpolated over the operating ranges of 25% – 100% load torque and 12.5 Hz – 50 Hz supply frequency.

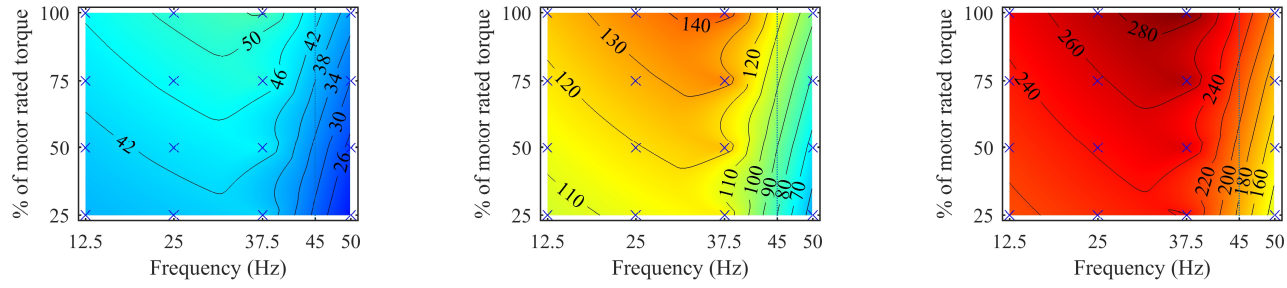

(a) 15 kW IM (b) 37 kW IM (c) 75 kW IM

Fig. 8. The motor loss uncertainties in Watts (W). The expanded uncertainties for the total losses of the 15 kW (a), 37 kW (b), and 75 kW (c) induction motors interpolated over the operating ranges of 25% – 100% load torque and 12.5 Hz – 50 Hz supply frequency. The uncertainty values are presented at 95% level of confidence ($k = 2$).

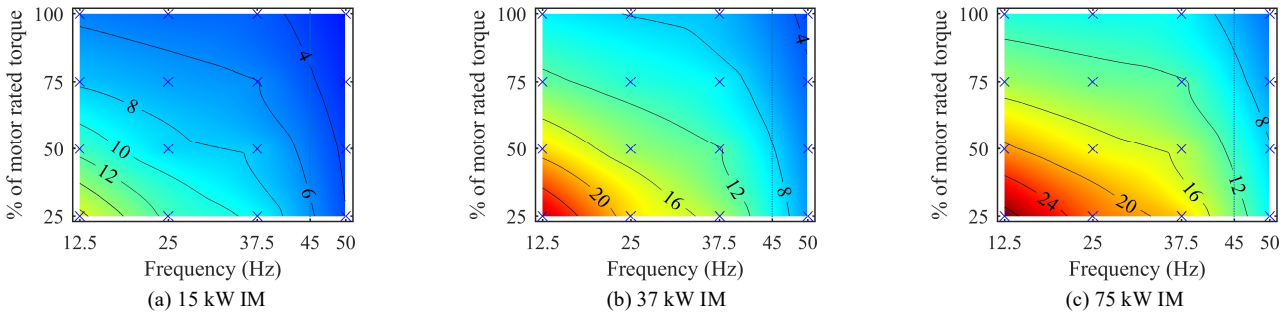

(a) 15 kW IM (b) 37 kW IM (c) 75 kW IM

Fig. 9. The relative motor loss uncertainties. The expanded uncertainty as percentage (%) of total losses for the 15 kW (a), 37 kW (b), and 75 kW (c) induction motors interpolated over the operating ranges of 25% – 100% load torque and 12.5 Hz – 50 Hz supply frequency. The uncertainty values are presented at 95% level of confidence ($k = 2$).

practical manner, that a good accuracy is required from both electrical and mechanical power to achieve decent loss uncertainty when using the input-output method.

Torque measurement is affected by several uncertainty sources, of which the parasitic loads are the most difficult to assess. Here, the details of the measurement setups were used to estimate the possible parasitic loads. The test setups are carefully built and checked with laser alignment system. Although the estimations for the parasitic load values here were quite small, their contribution to the torque – and to the mechanical power measurement as a whole – was the highest of all separate uncertainty sources in the low torque range.

In the case of converter-fed motors, the sizing of current transducers is straightforward, as only the current of the highest measured load point needs to be considered. For DOL motors, however, the startup current is typically 6-8 times higher than the rated current. If, for example, a variable transformer is not available for soft starting, or if the DOL startup transient is specifically of interest in the measurements, the current transducers have to be sized accordingly.

Conclusion

The uncertainty of the converter-fed motor measurements is similar to the one with direct-on-line machines. The modern power analyzers can easily capture the power transferred by the high-frequency harmonic components when equipped with high bandwidth current sensors. The uncertainty analysis shows two important factors that influence the uncertainty of the motor loss determination: The first one is how well the measured quantity matches with the rated value of the measurement instrument. When the measurement instruments are chosen according to the rated current and torque values, the accuracy at lower load points suffers. The second one is the efficiency of the motor under testing. The higher the efficiency, the higher the loss uncertainty if the input and output power uncertainties stay the same. Here, the uncertainty of electrical power was twice the mechanical power uncertainty in rated operating points and in lower load and speed range the difference was even higher. The optimal measurement range of power analyzers is typically around 50 and 60 Hz – here 45Hz–66 Hz – which affects the uncertainty of converter-fed motor measurements significantly when the operating frequency is outside this range.

References

[1] Rotating electrical machines – Part 30-1: Efficiency classes of line operated AC motors (IE code), Ed. 1, *IEC 60034-30-1*, March 2014.

[2] Rotating electrical machines – Part 30-2: Efficiency classes of variable speed AC motors (IE-code) Ed. 1, *IEC TS 60034-30-2*, Dec. 2016.

[3] Rotating electrical machines – Part 2-3: Rotating electrical machines - Part 2-3: Specific test methods for determining losses and efficiency of converter-fed AC induction motors", *IEC TS 60034-2-3*, Nov. 2013.

[4] L. Aarniovuori, H. Kärkkäinen, A. Kosonen, J. Pyrhönen, Z. Liu and W. Cao, "Overview of calorimetric systems used in loss determination of electric motors and drives," *IECON 2017 - 43rd Annual Conference of the IEEE Industrial Electronics Society*, Beijing, 2017, pp. 2110-2115.

[5] W. Cao, "Assessment of induction machine efficiency with comments on new standard IEC 60034-2-1," in *Proc. Int. Conf. on Electric Machines*, Vilamoura, Portugal, September 2008, pp. 1–6.

[6] L. Aarniovuori, J. Kolehmainen, A. Kosonen, M. Niemelä and J. Pyrhönen, "Uncertainty in motor efficiency measurements," *2014 International Conference on Electrical Machines (ICEM)*, Berlin, 2014, pp. 323-329.

[7] M. Doppelbauer, "Accuracy of the determination of losses and energy efficiency of induction motors by the indirect test procedure", in *Proc. 7th Int. Conf. on Energy Efficiency in Motor Driven Systems*, Alexandria, USA, September 2011, pp. 457–469.

[8] W. Cao,"Comparison of IEEE 112 and New IEC Standard 60034-2-1," *IEEE Trans. Energy Conversion*, vol. 24, no. 3, pp. 802–808, September 2009.

[9] G. Bucci, F. Ciancetta, E. Fiorucci and A. Ometto, "Uncertainty Issues in Direct and Indirect Efficiency Determination for Three-Phase Induction Motors: Remarks About the IEC 60034-2-1 Standard," in *IEEE Transactions on Instrumentation and Measurement*, vol. 65, no. 12, pp. 2701-2716, Dec. 2016.

[10] N. Yogal, C. Lehrmann and M. Henke, "Determination of the Measurement Uncertainty of Direct and Indirect Efficiency Measurement Methods in Permanent Magnet Synchronous Machines," *2018 XIII International Conference on Electrical Machines (ICEM)*, Alexandroupoli, 2018, pp. 1149-1156.

[11] *WT1600 Digital Power Meter User's Manual (4th Edition)*, Yokogawa Electric Corporation, Tokyo, Japan, 2004, Accessed on: June, 4, 2018 [Online]. Available: https://web-material3.yokogawa.com/IM760101-01E.pdf?_ga=2.105844352.2062736829.1528097117-1553882151.1527243875

[12] Committee Guides Metrology, Joint. (2008). *Evaluation of measurement data – Guide to the Expression of Uncertainty in Measurement* (GUM 2008).

[13] H. Kärkkäinen, L. Aarniovuori, M. Niemela and J. Pyrhonen, "Advanced Uncertainty Calculation Method for Frequency Converter Loss Determination," *2018 20th European Conference on Power Electronics and Applications (EPE'18 ECCE Europe)*, Riga, 2018, pp. P.1-P.10.

[14] *T12 Digital Torque Transducer Data Sheet (B1941-10.0 en)*, Hottinger Baldwin Messtechnik Gmbh, Darmstadt, Germany.

[15] R. Schicker, G. Wegener, "Selection criteria and application environment for torque transducers," in *Measuring Torque Correctly*, Hottinger Baldwin Messtechnik Gmbh, Darmstadt, Germany.

[16] G. Wegener and J. Andrae, "Measurement uncertainty of torque measurements with rotating torque transducers in power test stands," Measurement, vol. 40, no. 7/8, pp. 803–810, Aug.–Oct. 20

Publication VIII

Kärkkäinen, H., Aarniovuori, L., Niemelä, M., and Pyrhönen, J.
The Instrumentation Influence on the Motor Loss Determination Uncertainty

45th Annual Conference of the IEEE Industrial Electronics Society, IECON
pp. 1387-1392, 2019

The Instrumentation Influence on the Motor Loss Determination Uncertainty

Hannu Kärkkäinen
Laboratory of Electric Drives Technology
LUT University
Lappeenranta, Finland
hannu.s.karkkainen@lut.fi

Lassi Aarniovuori
Power Electronics, Machines and Power System Group
Aston University
Birmingham, UK
l.aarniovuori@aston.ac.uk

Markku Niemelä
Laboratory of Electric Drives Technology
LUT University
Lappeenranta, Finland
markku.niemela@lut.fi

Juha Pyrhönen
Laboratory of Electric Drives Technology
LUT University
Lappeenranta, Finland
juha.pyrhonen@lut.fi

***Abstract*—The input-output method is the most frequently used and, in practice, the only viable alternative to determine the losses of all electrical machines regardless of the supply type or motor technology. However, the losses obtained with the input-output method are sensitive to power measurement uncertainties of the input and output powers. The power measurement uncertainty is formed by two parts: type A uncertainty is related to the variations in the measurement data and type B uncertainty is related to measurement instruments. The variations in the data can be controlled using data processing techniques and the type B uncertainty can be controlled using accurate measurement devices and choosing correctly rated measurement instruments for each task. In practice, the range of the instruments is limited and it is not always possible to perfectly match the instruments to the measured values. In here, the effect of the ratings of the instruments on the loss measurement uncertainty when using the input-output method is studied using a set of induction motors with rated powers from 7.5 kW to 355 kW. The specifications of the measurement instruments available at Electric Drives laboratory at LUT-University are used to derive the theoretical loss measurement uncertainty for the motors. The detailed uncertainty analysis includes the electric and mechanical powers, and as a result, loss measurement uncertainty is given. The results can be used to get an overview about the level of the expected measurement uncertainty for motors with different power ratings and its effect on the determination of efficiency.**

Keywords—electric power, efficiency, induction motor, measurement uncertainty, mechanical power

I. Introduction

A method of determining losses and efficiency based on direct measurements of input electrical power and output mechanical power is widely used. The method is also simple and fast, and in principle, applicable to all motor types regardless of technology. The method, however, is highly sensitive to the accuracies of the electric power and mechanical power measurements – especially when testing modern high-efficiency machines. This is because when efficiency approaches unity, the relative uncertainty of losses approaches infinity [1].

Measurement uncertainty consists of type A uncertainty and type B uncertainty. Type A uncertainty value is based on the standard deviation of the mean of repeated measurement results. Type B uncertainty covers the (in)accuracies of the measurement instruments. Type A and type B uncertainty have been covered in detail in [2], where electric power measurement uncertainty in frequency converter loss determination is studied. The electrical machine loss uncertainty and its determination have been investigated in several previous publications. The uncertainty of the losses determined with the input-output method is analyzed for three different induction motors over a wide operating range in [3]. The uncertainties of input-output methods used in industry for induction motor measurements are assessed in [4]. The uncertainties of the input-output method and the indirect loss segregation method are analyzed with scientific and numerical methods in [5]. In [6], realistic perturbation-based estimation (RPBE) –method is used for analyzing the efficiency measurement uncertainty. The influence of the measurement error on the uncertainty of the indirect loss segregation method is analyzed using Monte Carlo simulations in [7]. In [8], the uncertainties of the input-output and loss segregation methods of the standard IEC 60034-2-1 are analyzed and suggestions for future standards are given. The uncertainties of the input-output and loss segregation methods in permanent magnet synchronous machine measurements are investigated in [9].

According to the results shown in [1], the efficiency of the measured motor (or any other device under test) is one of the two most important factors affecting the uncertainty of the input-output losses. The second one is how well the ratings of the measurement instruments match with the measured values. The latter one is further investigated in this paper. Uncertainty analysis for the theoretical input-output efficiency measurements of twelve induction motors with different power ratings is performed. A set of measurement instruments with rated values in the range suitable for the motors is used in the analysis. The main goal is to clarify the importance of matching the ratings of the instruments with the measured quantities, as it is not always possible to use perfectly matched instruments for every tested motor. Three cases are analyzed: The first analysis includes only the measurement instrument uncertainties (type B uncertainty). The second analysis includes type A uncertainty that is estimated based on previous work. In the third analysis, the number of instruments with different ratings is reduced to simulate a case where no optimally rated instruments are available. The analysis is carried out using the nameplate data of the motors and the accuracy specifications of the measurement instruments. Only the rated operating point is considered here because it is used for energy efficiency classification. For reference, motor loss uncertainty behavior in partial operating points has been analyzed and discussed in [3].

II. Uncertainty analysis

The purpose of the analysis presented in this paper was to find out the input-output loss measurement uncertainty for the

instruments available at Electrical Drives laboratory at LUT-University when measuring direct-on-line (DOL) motors with different power ratings. Several different motors with different ratings have naturally been tested in the laboratory. For this analysis, all common power ratings that are within the normal capability of the laboratory are taken into account. This results in a total number of twelve 4-pole 50 Hz induction motors from 7.5 kW to 355 kW rated power. Instead of actual measurements, the electrical and mechanical data for the motors are based on the nameplate values, Table I. When analyzing type B uncertainty, there is no need for actual measurement data as long as the (approximate) values that would be measured are known: The rated power (mechanical output power), rated current, rated speed, rated power factor, and rated efficiency are directly given as motor nameplate values. The electric input power is calculated from the rated power P_m and the rated efficiency η simply as

$$P_\mathrm{e} = \frac{P_\mathrm{m}}{\eta} \tag{1}$$

The rated torque is calculated from the rated power and the rated speed n

$$T = \frac{60 \cdot P_\mathrm{m}}{2\pi n}. \tag{2}$$

The specifications of the measurement instruments available in the laboratory are used to calculate the theoretical loss uncertainty for each of the motors. Yokogawa WT1600 power analyzer has been used in most of the motor measurements at LUT, and it is suitable for all the 12 motors when equipped with appropriate current transducers. All the current transducers currently used in the laboratory are Hitec CURACC -series and torque transducers are HBM T12 -series. In Table II, the measured quantities of the 12 motors are matched with the current and torque transducers that would be used in actual measurements in the laboratory. In addition to the ratings, the rated current and torque values of each motor are compared with the transducer ratings in Table II. The relative values ($\%I_\mathrm{nom}$ and $\%T_\mathrm{nom}$) illustrate well the need for this analysis: the percentage varies from a very good transducer match in the range of 80% to over 90% in several cases, down to as low as 22% for the current transducers' match with 7.5 kW motor. Overall, the match of the torque transducers with the motor torque values is better compared to the match of the current transducers. This is expected, because the number of available torque transducers

TABLE I. RATED VALUES FOR THE MOTORS.

Frame size	Rated power (kW)	Input power* (kW)	Current (A)	Speed (rpm)	Torque* (Nm)	Power factor	Efficiency (%)
132	7.5	8.3	15.7	1462	49.0	0.76	90.4
160	15	16.3	28.5	1477	97.0	0.82	92.1
225	37	39.4	68.9	1482	238	0.83	93.9
280	75	78.9	133	1485	482	0.86	95.0
280	90	94.5	158	1485	579	0.86	95.2
315	110	115	198	1489	705	0.84	95.4
315	132	138	231	1488	847	0.86	95.6
315	160	167	282	1488	1030	0.85	95.8
315	200	208	351	1487	1280	0.86	96.0
355	250	260	435	1491	1600	0.86	96.0
355	315	328	550	1491	2020	0.85	96.0
355	355	370	616	1490	2280	0.86	96.0

Common for all motors: 4 poles, 400 V, 50 Hz, IE3 efficiency class
*Calculated from nameplate values.

TABLE II. THE CURRENT AND TORQUE RATINGS FOR THE MOTORS AND FOR THE BEST MATCHING MEASUREMENT INSTRUMENTS AVAILABLE.

Rated Power (kW)	Rated current (A)	Current transducers* (A)	$\%I_\mathrm{nom}$ (%)	Rated torque (Nm)	Torque transducer (Nm)	$\%T_\mathrm{nom}$ (%)
7.5	15.7	100	22	49.0	100	49
15	28.5	100	40	97.0	100	97
37	68.9	300	32	238	500	48
75	133	300	63	482	500	96
90	158	300	74	579	1000	58
110	198	300	93	705	1000	71
132	231	600	54	847	1000	85
160	282	600	66	1030	2000	51
200	351	600	83	1280	2000	64
250	435	2000	31	1600	2000	80
315	550	2000	39	2020	5000**	40
355	616	2000	44	2280	5000**	46

*Rated with peak current value.
**Currently not available at LUT's lab.

with different ratings is five, while the current transducers are with only four different ratings.

The power analyzer measurement accuracy is given in percentages of the reading and range values in the specifications. The power analyzer input current range affects the effective current measurement range of the power analyzer (Table III) and the related range error. The output signal of CURACC system is 1 A (peak) when measuring the rated current of the transducer. Therefore, the power analyzer input range selection provides flexibility when the measured currents are far below the transducer rating. The motor rated current to power analyzer current measurement range ratio ($I_\mathrm{N} / I_\mathrm{range}$) is included in Table III. After the power analyzer input range selection, only 7.5 kW motor has a I_N to I_range –ratio of less than 50%. A more suitable range for 7.5 kW motor is not available, as the next smaller range would be 200 mA, which would cause $I_\mathrm{N} / I_\mathrm{range}$ to exceed 100%. Here, in practice, the power analyzer input range match is much more important in the uncertainty point of view than the current transducer match because the current range accuracy of the CURACC system is 25 times as high as the power analyzer current range accuracy (see specifications in Table V).

A. Type A uncertainty

Type A uncertainty arises from the variations in the measured values. Typically, motor measurements are performed taking several readings of the same operating point. The standard deviation of the mean value of these readings is the type

TABLE III. YOKOGAWA WT1600 CURRENT MEASUREMENT RANGE.

Rated Power (kW)	Rated current, I_N (A)	WT1600 input range (A)	Measurement range, I_range (A)	$I_\mathrm{N} / I_\mathrm{range}$ (%)
7.5 kW	15.7 A	0.5	35.4	44
15 kW	28.5 A	0.5	35.4	81
37 kW	68.9 A	0.5	106	65
75 kW	133 A	1	212	63
90 kW	158 A	1	212	75
110 kW	198 A	1	212	93
132 kW	231 A	1	424	54
160 kW	282 A	1	424	66
200 kW	351 A	1	424	83
250 kW	435 A	0.5	707	62
315 kW	550 A	0.5	707	78
355 kW	616 A	0.5	707	87

A standard uncertainty. The type A uncertainty analysis is covered in detail in [2].

Here, the type A uncertainty is estimated based on average relative type A uncertainty values from previous measurements, Table IV. In previous measurements, the relative type A uncertainties have been rather consistent regardless of the measured motor. Therefore, we can assume that using similar measurement instruments, the type A uncertainty values are at a similar level as in the previous analyses. In addition, the effect of the type A uncertainty on the overall uncertainty has been very small in LUT measurements. This is mainly because of a high number of recordings (typically 100) taken for each test point, which reduces the type A uncertainty [2], [3]. Hence, using the average values from previous measurements is well sufficient for the purpose of this analysis.

B. Type B uncertainty

The type B uncertainty analysis is performed similarly as in [3], where the full analysis procedure is covered thoroughly with example calculations. Type B uncertainty covers the uncertainty contribution of the measurement instruments. The accuracy specifications for the power analyzer and the current and torque transducers are given in Table V. As we are considering DOL measurements in this analysis, only the accuracy specifications for the band around 50 Hz grid-frequency are included for the power analyzer. Typically, the accuracy of the power analyzers is lower when operating at frequencies below or above the optimum range. The accuracy values for the power analyzer and the current transducers are given as percentages of reading and range. The HBM T12 speed sensor has a system accuracy of 150 ppm of the speed, and as the resolution of the speed signal is a rather modest 0.1 rpm, the effect of the resolution is taken into account in the uncertainty analysis.

The torque accuracy specifications, however, are a much more complex case where several different sources of inaccuracy exist. The torque accuracies are given related to either the transducer nominal torque T_{nom}, the torque being measured T_{act} (torque reading), or the torque span in the measurements ΔT. In this case, where each motor is measured at rated load, ΔT is equal to the rated torque value as in standstill before the test, torque value is zero and the maximum measured value is the rated torque value of each motor. The accuracy value of parasitic loads is related to the stresses other than torque that are affecting the transducer in an actual measurement setup. The parasitic loads are compensated in the transducer [10] and they do not therefore directly affect the torque reading. However, the parasitic loads have an effect on the uncertainty of the measurement [10]. The accuracy value of 0.3% corresponds to the maximum limit of total parasitic loads. Here, based on the previous work, the parasitic loads for each transducer are assumed as 25% of the limit in a setup where the transducer rated torque is measured. This value is further scaled down by the motor rated torque to transducer rating –ratio (%T_{nom}) given in Table II, because in smaller motor setups also the parasitic stresses can be considered to be lower. Therefore, the effect of the parasitic loads on the torque accuracy is assumed here as

$$\text{Parasitic loads accuracy} = 0.3\% \times 25\% \times \%T_{\mathrm{nom}}. \quad (3)$$

TABLE IV. TYPE A RELATIVE UNCERTAINTY VALUES USED IN THIS ANALYSIS. THE VALUES ARE BASED ON PREVIOUS MEASUREMENTS.

Quantity	Type A relative uncertainty
Electric power	0.035%
Speed	0.009%
Torque	0.031%

TABLE V. ACCURACY SPECIFICATIONS FOR THE MEASUREMENT INSTRUMENTS.

Device / Specification		Accuracy
Yokogawa WT1600		
Power accuracy, 45 Hz ≤ f < 66 Hz		0.15% of reading + 0.05% of range
Power factor influence, 45 Hz ≤ f < 66 Hz		power reading × tan φ × 0.15%
Hitec CURACC		
Current accuracy		0.01% of reading + 0.002% of range
HBM T12 torque accuracy		
Temperature influence on zero value, per 10 degree deviation from 23°C		0.02% T_{nom}*
Temperature influence on span, per 10 degree deviation from 23°C		0.03% T_{act}**
Linearity and hysteresis	0…20% T_{nom}	0.006% T_{nom}
	20…60% T_{nom}	0.013% T_{nom}
	60…100% T_{nom}	0.02% T_{nom}
Repeatability		0.01% ΔT***
Sensitivity tolerance		0.05% T_{act}
Parasitic loads		< 0.3% T_{nom}
HBM T12 speed accuracy		
Measurement system accuracy		0.015% (reading)
Resolution		0.1 rpm

* Transducer nominal torque
** Active torque being measured
*** Difference between the highest and lowest (or negative) torque values being measured in the system

C. Combined uncertainty, mechanical power uncertainty, and loss uncertainty

For the final electrical power, mechanical power, and motor loss uncertainty values, the uncertainty sources are combined. As type A and type B uncertainties do not correlate, the combined uncertainty can be calculated as the square root of the sum of squares

$$U = \sqrt{{U_{\mathrm{A}}}^2 + {U_{\mathrm{B}}}^2} \quad (4)$$

where U_{A} is type A uncertainty and U_{B} is type B uncertainty. To combine the speed and torque uncertainties into mechanical power uncertainty, the method of partial differentials has to be applied. This is presented with example calculations in [3]. The loss uncertainty, in turn is calculated from the input and output power uncertainties as the square root of the sum of squares assuming that the power uncertainties do not correlate:

$$U(P_{\mathrm{l}}) = \sqrt{U(P_{\mathrm{e}})^2 + U(P_{\mathrm{m}})^2} \quad (5)$$

where $U(P_{\mathrm{e}})$ and $U(P_{\mathrm{m}})$ are the electric power uncertainty and mechanical power uncertainty, respectively.

III. UNCERTAINTY RESULTS

The results are divided into three sections: First, only type B uncertainty is taken into account. Second, type A uncertainty is

included and the combined uncertainty results are presented and discussed. Third, the number of the current and torque transducers available is reduced to find the bare minimum amount of transducers with different ratings required to get usable results with the input-output method. All the uncertainty results are presented as expanded uncertainties at coverage factor $k = 2$, which corresponds to 95% level of confidence.

A. *Type B uncertainties of the input and output powers*

The electrical power type B relative expanded uncertainty values at the rated operating points of all 12 motors are shown in Fig. 1 together with motor rated current to current measurement range ratio (I_N / I_{range}). The uncertainty values show a clear inversely proportional dependence of the I_N to I_{range}-ratio, which is expected as the power analyzer range accuracy is higher when the match of the range is better. The uncertainty values – except 7.5 kW motor value – are over a quite narrow range between 0.16% and 0.19%. The uncertainty value of 7.5 kW motor being notably higher at approximately 0.24% shows illustratively how quickly the uncertainty starts to rise when the I_N to I_{range}-ratio falls.

The mechanical power type B relative expanded uncertainty values at the rated operating points of all 12 motors are shown in Fig. 2 together with motor rated torque to transducer nominal torque ratio (T_N / T_{nom}). Inversely proportional dependence of the torque uncertainty from the T_N to T_{nom} –ratio is clear, and the mechanical power uncertainty values vary only on a rather narrow range between 0.105% and 0.125%.

B. *Motor loss type B and combined uncertainty*

When combining the electric power and mechanical power uncertainty values illustrated in Figs. 1 and 2, the motor loss uncertainty can be calculated using (5). First, this is done only for the type B uncertainty values to obtain the motor loss type B uncertainty. Second, the type B uncertainties of electric power, torque, and speed are combined with the type A uncertainty values from the previous work (Table IV) to get the combined uncertainties. The motor loss type B relative uncertainty, the motor loss combined uncertainty, and the motor efficiency are presented in Fig. 3. The difference between the type B uncertainty curve and the combined uncertainty curve shows that the type A uncertainty is practically insignificant here. Fig. 3 shows in a practical manner, how the loss uncertainty rises

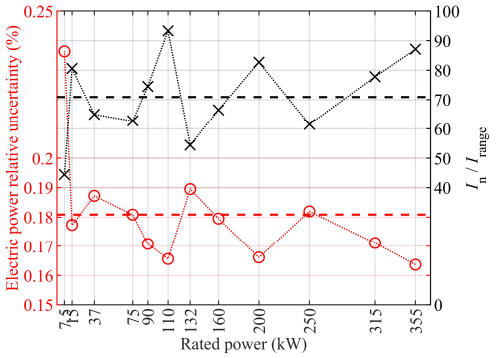

Fig. 1. The electric power type B relative uncertainty for the 12 motors in rated operating points (red), and the motor rated current to current measurement range ratio (black). The 12 motor average values are indicated with dashed lines. The uncertainty values are presented at coverage factor $k = 2$ which corresponds to 95% level of confidence.

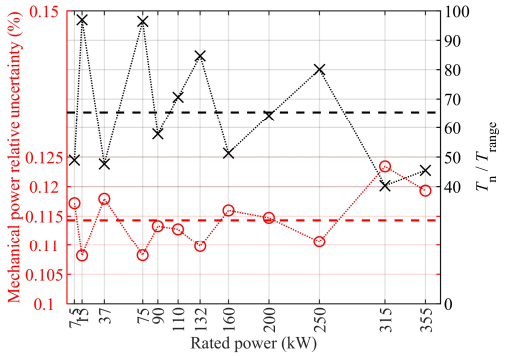

Fig. 2. The mechanical power type B relative uncertainty for the 12 motors in rated operating points (red), and the motor rated torque to the transducer nominal torque ratio (black). The 12 motor average values are indicated with dashed lines. The uncertainty values are presented at coverage factor $k = 2$ which corresponds to 95% level of confidence.

with the motor efficiency. The loss uncertainty values are in general at a very good level; from a bit below 3% for small motors up to slightly over 5% for motors with higher power ratings. Both the current and torque range mismatches show only as slight variations in the loss uncertainty curves because of a much wider scale of the uncertainty shown in the plot. It is notable, that although the electric power uncertainty was significantly higher with 7.5 kW motor compared to other motors – and also the mechanical power uncertainty was one of the highest with it – the lower motor efficiency mitigates the difference. As a result, 7.5 kW motor loss uncertainty is actually the second lowest of all the 12 motors.

It can be concluded from the results shown in Fig. 3 that even when we have almost perfectly matched high accuracy measurement instruments, the loss measurement uncertainty rises above 5% with the high power ratings. This shows how significant the influence of the efficiency is in the loss measurement uncertainty value. All motors considered here are rated for IE3 efficiency class, which is currently the minimum requirement by EU commission [11]. It should be kept in mind that for motors with higher efficiency classifications type B uncertainty is even higher. Motor efficiencies are continuously rising; IE4 motors are well available and IE5 motors are in the market.

C. *Uncertainty when using a limited number of current and torque transducers*

It is not always possible to acquire the best matching current and torque transducers for the measurements of every motor. Here, the lowest possible number of transducers with different ratings from Hitec CURACC and HBM T12 series were selected in such a way that usable loss and efficiency results could still be achieved. Therefore, the following uncertainty results show a hypothetical situation, where only a single set of 2 kA-rated CURACC transducers, and only two HBM T12 transducers rated for 500 Nm and 5 kNm would be used to measure all 12 motors from 7.5 kW to 355 kW. Table VI shows the transducers used for each motor and the ratios of motor ratings to transducer ratings. The rated current of 7.5 kW motor is only approximately one percent of 2 kA CURACC current rating. The rated torque to transducer nominal torque ratios are down to around 10% in the worst matching cases. For the largest motors, the transducers are naturally the same as before.

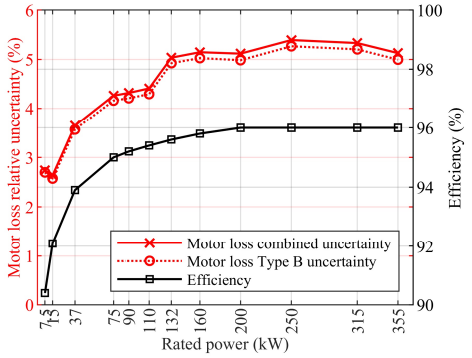

Fig. 3. The motor loss type B relative uncertainty and combined relative uncertainty for the 12 motors in rated operating points (red curves), and the rated efficiencies of the motors (black curve). The uncertainties are presented at coverage factor $k = 2$ which corresponds to 95% level of confidence.

When only a single set of current transducers is used, the power analyzer input range can, however, be adjusted according to the output level of the current transducers when motors with different current ratings are measured, Table VII. This results in very good effective measurement ranges for the WT1600 across all 12 motors.

In Fig. 4, the electric power type B uncertainties when using only 2 kA current sensors are compared with the uncertainty results obtained using all the current transducers with different ratings. According to the comparison, the uncertainty rises notably with some motors, but with two motors the uncertainty is even lower. The lower uncertainties with 75 kW and 132 kW motors are explained by considerably better matching with the power analyzer current ranges, which improves the uncertainty more than using the larger transducer deteriorates the uncertainty. For the three largest motors, the results are naturally equal as the 2 kA transducers are used in both cases.

The mechanical power uncertainties when using only the 500 Nm and 5 kNm transducers are compared with the uncertainty results obtained using all torque transducers with different ratings in Fig. 5. The comparison shows that the torque uncertainty increases more rapidly the further the transducer match is from optimal. Using two transducers for the whole range of motors, the uncertainty rise is limited to approximately twice the uncertainty level compared to when the whole T12-series is utilized (red curve).

TABLE VI. THE RATIOS OF THE MOTOR CURRENT AND TORQUE RATINGS TO THE TRANSDUCER RATINGS WHEN USING ONLY 2 KA CURRENT TRANSDUCER AND TWO TORQUE TRANSDUCERS.

Rated Power (kW)	Rated Current (A)	Current transducers* (A)	$\%I_{nom}$ (%)	Rated Torque (Nm)	Torque Transducer (Nm)	$\%T_{nom}$ (%)
7.5	15.7	**2000**	**1**	49.0	**500**	**10**
15	28.5	**2000**	**2**	97.0	**500**	**19**
37	68.9	**2000**	**5**	238	500	48
75	133	**2000**	**9**	482	500	96
90	158	**2000**	**11**	579	**5000**	**12**
110	198	**2000**	**14**	705	**5000**	**14**
132	231	**2000**	**16**	847	**5000**	**17**
160	282	**2000**	**20**	1030	**5000**	**21**
200	351	**2000**	**25**	1280	**5000**	**26**
250	435	2000	31	1600	5000	32
315	550	2000	39	2020	5000	40
355	616	2000	44	2280	5000	46

*Rated with peak current value.

TABLE VII. YOKOGAWA WT1600 CURRENT MEASUREMENT RANGE WHEN USING 2 KA CURRENT TRANSDUCERS WITH ALL MOTORS.

Rated Power (kW)	Rated current, I_N (A)	WT1600 input range (mA)	Measurement range, I_{range} (A)	I_N / I_{range} (%)
7.5	15.7	**20**	28.3	**56**
15	28.5	**50**	70.7	**40**
37	68.9	**100**	141	**49**
75	133	**100**	141	**94**
90	158	**200**	283	**56**
110	198	**200**	283	**70**
132	231	**200**	283	**82**
160	282	**500**	707	**40**
200	351	**500**	707	**50**
250	435	500	707	62
315	550	500	707	78
355	616	500	707	87

The motor loss uncertainties when using only 2 kA current transducers and 500 Nm and 5 kNm torque transducers are compared with the uncertainty results obtained using all torque and current transducers with different ratings in Fig. 6. The comparison shows a surprisingly modest increase in the loss uncertainty, although the uncertainty behavior with motor power rating and efficiency is not as predictable as it was the case in Fig. 3. At the most unfavorable cases, the loss uncertainty is approximately 1/3 to 1/4 higher for the 90 kW and 160 kW motors compared to situation when all the transducers are utilized.

The uncertainty penalty for using fewer transducers is naturally higher with the lower rated motors as the transducers selected are the suitable ones for the higher rated end of the motor scale. The torque uncertainty starts to rise very rapidly when the measured values are below 10% of the transducer rating and for that reason the whole range from 7.5 kW motor to 355 kW motor cannot practically be measured using a single torque transducer. Either 100 Nm or 500 Nm transducer had to be included in addition to the 5 kNm transducer to limit the torque uncertainty with 7.5 kW and 15 kW motors to sensible levels. Selecting the 100 Nm transducer as the second choice for this analysis instead of the 500 Nm transducer would have meant that the 5 kNm transducer would have been used for the 37 kW motor, and its loss uncertainty would have risen to 9%, hence the 500 Nm transducer was a better choice.

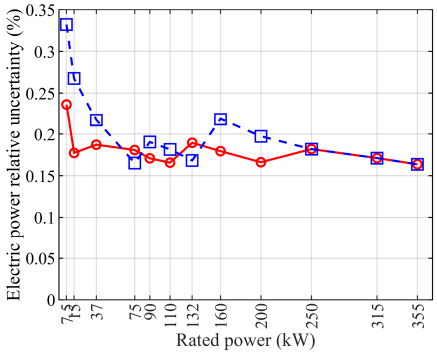

Fig. 4. The electric power type B relative uncertainties for the 12 motors in rated operating points. The red curve with circles shows the original situation, where all current transducers with different ratings are used with matching motors. The blue curve with squares shows the situation, where 2 kA current sensors are used with all motors. The uncertainty values are presented at coverage factor $k = 2$ which corresponds to 95% level of confidence.

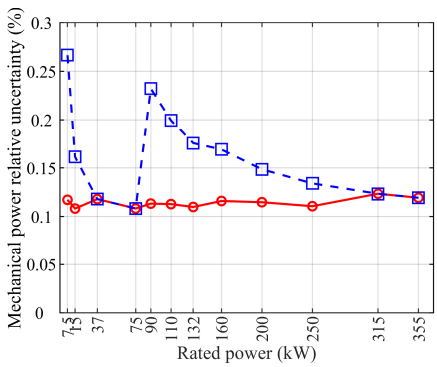

Fig. 5. The mechanical power type B relative uncertainties for the 12 motors in rated operating points. The red curve with circles shows the original situation, where all torque transducers with different ratings are used with matching motors. The blue curve with squares shows the situation, where only the 500 Nm and 5 kNm transducers are used. The uncertainties are presented at coverage factor $k = 2$ which corresponds to 95% level of confidence.

IV. Discussion and Conclusions

The proper selection of the measurement instruments has an effect on loss measurement uncertainty. Here, the average total measurement uncertainty of the electrical power was around 0.18% and the average total measurement uncertainty of the mechanical power was around 0.11%. The measurement uncertainty was considered here only at the rated load point and when operating with partial loads, the measurement uncertainty would be increased. However, the measurement uncertainty does not depend linearly from the ratio of the measurement instrument's rating to measured value, since part of the uncertainties are related directly to a measured value rather than to the rated value of an instrument. The selection of the rating of the current measurement device is less important than the torque transducer: there is a wide choice of current ranges available in power analyzers that can be used to match the effective current measurement range to the measured current in order to minimize the measurement uncertainty. In here, it is assumed that data are collected using a digital communication protocol without any voltage and/or frequency conversion. Each A/D conversion or level adjustment will increase the measurement uncertainty. Type A uncertainty is not a problem when enough data samples are used in the analysis and the most dominating factor in the total measurement uncertainty are the instruments and their accuracies. The losses of large induction motors are more demanding to be measured accurately, as they are typically operating with higher efficiency. However, the power factor is increasing as a function of the motor rated power and increased power factor decreases the active power measurement uncertainty (reading value). The power analyzer used here is not a state-of-the-art device but it is equipped with current transducers that are the most accurate ones on the market. With a high-end power analyzer, the total electrical power uncertainty would be much smaller. Based on the analysis here, the input-output method can be used to reliably measure the losses of direct-on-line induction motors if proper instrumentation is used. In practice, only a limited number of instruments are available in laboratories and some mismatch between the measured value and the rated value of the instrument must be accepted. However, if the rated value of the instrument is not far away from the measured value, it should not cause significant problems.

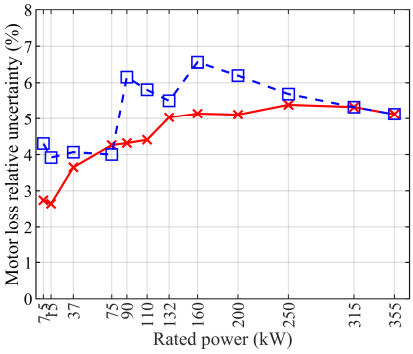

Fig. 6. The motor loss relative combined uncertainties for the 12 motors in rated operating points. The red curve shows the original situation, where all torque and current transducers with different ratings are used with matching motors. The blue curve shows the situation where only the 2 kA current transducers, and 500 Nm and 5 kNm torque transducers are used. The uncertainties are presented at coverage factor $k = 2$ (95% level of confidence).

References

[1] H. Kärkkäinen L. Aarniovuori, M. Niemelä, J. Pyrhönen, J. Kolehmainen, T. Känsäkangas and J. Ikäheimo., "Direct-On-Line Synchronous Reluctance Motor Efficiency Verification with Calorimetric Measurements," *2018 XIII International Conference on Electrical Machines (ICEM)*, Alexandroupoli, 2018, pp. 171-177.

[2] H. Kärkkäinen, L. Aarniovuori, M. Niemelä and J. Pyrhönen, "Advanced Uncertainty Calculation Method for Frequency Converter Loss Determination," *2018 20th European Conference on Power Electronics and Applications (EPE'18 ECCE Europe)*, Riga, 2018, pp. 1-10.

[3] H. Kärkkäinen, L. Aarniovuori, M. Niemelä and J. Pyrhönen, "Advanced Uncertainty Calculation Method for Converter-Fed Motor Loss Determining," *2019 IEEE International Electric Machines and Drives Conference (IEMDC)*, San Diego, CA, 2019.

[4] W. Cao, "Assessment of induction machine efficiency with comments on new standard IEC 60034-2-1," in *Proc. Int. Conf. on Electric Machines*, Vilamoura, Portugal, September 2008, pp. 1–6.

[5] L. Aarniovuori, J. Kolehmainen, A. Kosonen, M. Niemelä and J. Pyrhönen, "Uncertainty in motor efficiency measurements," *2014 International Conference on Electrical Machines (ICEM)*, Berlin, 2014, pp. 323-329.

[6] W. Cao,"Comparison of IEEE 112 and New IEC Standard 60034-2-1," *IEEE Trans. Energy Conversion*, vol. 24, no. 3, pp. 802–808, September 2009.

[7] M. Doppelbauer, "Accuracy of the determination of losses and energy efficiency of induction motors by the indirect test procedure", in *Proc. 7th Int. Conf. on Energy Efficiency in Motor Driven Systems*, Alexandria, USA, September 2011, pp. 457–469.

[8] G. Bucci, F. Ciancetta, E. Fiorucci and A. Ometto, "Uncertainty Issues in Direct and Indirect Efficiency Determination for Three-Phase Induction Motors: Remarks About the IEC 60034-2-1 Standard," in *IEEE Transactions on Instrumentation and Measurement*, vol. 65, no. 12, pp. 2701-2716, Dec. 2016.

[9] N. Yogal, C. Lehrmann and M. Henke, "Determination of the Measurement Uncertainty of Direct and Indirect Efficiency Measurement Methods in Permanent Magnet Synchronous Machines," *2018 XIII International Conference on Electrical Machines (ICEM)*, Alexandroupoli, 2018, pp. 1149-1156.

[10] R. Schicker, G. Wegener, "Selection criteria and application environment for torque transducers," in *Measuring Torque Correctly*, Hottinger Baldwin Messtechnik Gmbh, Darmstadt, Germany.

[11] Commission Regulation (EC) No 640/2009 of 22 July 2009 implementing Directive 2005/32/EC of the European Parliament and of the Council with regard to ecodesign requirements for electric motor). *Off. Jour. of the EU*, L 191, pp. 26–34, 23 July 2009.

Publication IX

L. Aarniovuori, H. Kärkkäinen, A. Anuchin, J. J. Pyrhönen, P. Lindh and W. Cao
Voltage-Source Converter Energy Efficiency Classification in Accordance With IEC 61800-9-2

IEEE Transactions on Industrial Electronics
Vol. 67, pp. 8242-8251, 2020

Voltage Source Converter Energy Efficiency Classification in Accordance with IEC 61800-9-2

Lassi Aarniovuori, *IEEE Member*, Hannu Kärkkäinen, *IEEE Student Member*, Alecksey Anuchin, *IEEE Senior Member,* Juha Pyrhönen, *IEEE Senior Member*, Pia Lindh, *IEEE Senior Member*, Wenping Cao, *IEEE Senior Member*

***Abstract*— New global energy efficiency classification standard IEC 61800-9-2 for frequency converters and motor systems has been recently launched. It classifies the energy efficiency of the converters and motor-drive systems and introduces three different methods to determine a voltage source converter (VSC) losses for the classification. In here, experimental tests are carried out using the input-output method and the calorimetric method to determine the losses and efficiency of a 160 kW commercial voltage source converter (VSC). The measurement results with these two independent methods are compared and the uncertainty of the methods are analyzed. The converter electric input and output power distributions are analyzed in the frequency domain and are used further to estimate the electric power measurement uncertainty. The measurement uncertainty related to losses obtained with the input-output method is compared with the loss difference between the two methods. This is the first research work to accurately evaluate the experimental methods for the determination of the power losses and examine the validity of the energy efficiency classes of the frequency converters according to new IEC61800-9-2. An urgent need to update the loss boundaries of the IE-classes has been found and the measurement uncertainty effect on the IE-classification is discussed.**

Index Terms*——AC Machines, Calorimetry, Energy Efficiency, Insulated Gate Bipolar Transistors, Loss measurement, Measurement Uncertainty, Power measurement, Pulse width modulated converters, Standards, Variable speed drives.

I. Introduction

Electric motors and drive systems form the largest end-user of electricity, consuming more than twice as much as lighting, which is the second largest end-user of electricity. It is estimated that motor drives account for between 43% and 46% of all global electricity consumption [1]. Most of the new industrial electric motors are supplied by frequency converters and therefore the amount of the frequency converters that are used to control electric motors is rapidly increasing. Converters provide accurate speed and torque control of AC-machines by realizing the desired voltage references using pulse-width-modulation (PWM) technique. Controlling the speed and torque allows the usage of a motor at partial speeds, flux levels and loads which reduces the energy drawn by the application. This can lead to significant energy savings in many applications, especially where a fluid flow control is involved. However, the converter also consumes some energy and creates additional harmonic losses in the motor due to PWM voltage harmonics. Therefore, energy efficiency analyses of modern motor drive systems should include both the converter and the motor losses.

In this article, the losses of a commercially available 160 kW VSC are determined according to the new IEC61800-9-2 using both experimental methods; the input-output method and the calorimetric method, simultaneously. The measurement procedure and points in IEC 61800-9-2-standard are followed and the measurement results according to the standard are presented for the first time. A novel comparison between the electric power measurement uncertainty and the difference of the loss results obtained with both methods is presented.

In the experimental setup, the converter structure is the most used one in the industry, the input side of the converter is equipped with a diode rectifier bridge and a 2-level IGBT-bridge is used to modulate the output voltage using a continuous PWM method. The semiconductors are based on traditional silicon technology. The converter conversion efficiency is expected to be over 98%. The effect of the measurement uncertainty in the energy efficiency analysis of the converters and motors is discussed.

The paper is organized as follows: Section II gives a bibliographic review about topic and related standards. Section III introduces the experimental testing methods of the new IEC 61800-9-2 standard and presents the loss results obtained using the input-output method. In Section IV, the uncertainty analysis for the input-output method is performed using a frequency domain approach. Section V compares the results obtained with the input-output method and the calorimetric method. In addition, the input-output method is compared with the loss difference between the two methods. Finally, the paper discusses the importance of the results in the energy efficiency classification of VSCs in Section VI, followed by concluding remarks in Section VII.

II. Bibliographical Review

The energy efficiency of electric equipment is regulated by

different authorities and new energy efficiency standards have been launched recently. The scope of the regulated products is rapidly increasing. Minimum required efficiency levels for electric motors were already launched in the United States in the early 90s followed by a voluntary agreement of European Committee of Manufacturers of Electrical Machines and Power Systems (CEMEP) on efficiency classification in the late 90s. The motor efficiency classification has developed into the recently updated global standard IEC 60034-30-1 [2] for direct-on-line (DOL) machines and technical specification IEC/TS 60034-30-2 [3] for converter-fed machines. The determination methods of electrical machine losses for efficiency classification concerning DOL machines are given in IEC 60034-2-1 [4] and concerning converter-fed machines in IEC/TS 60034-2-3 [5].

The electric motors' efficiency levels [6], the methods to improve the motor efficiencies [7] and how the efficiencies of the electric machines are tested [8] as well as the uncertainty of the testing [9] have been of general interest of the scientific community during the latest years. The indirect method in the efficiency determination using loss segregation has been suggested in IEC and IEEE standards and a segregation of losses procedure has been also introduced to PMSMs [10] while the measurement uncertainty of direct and indirect uncertainty in the efficiency determination of PMSMs is analyzed in [11] .

Frequency converters have been used since the 1980's to control the speed and torque of electrical machines but they have neither had an efficiency classification nor standard methods to determine the losses of these devices even though it has been of interest for the scientific community and business for a long time [12].

The efficiency of the voltage or current source inverters and their topologies for medium voltage [13] and for high power applications are discussed e.g. in [14]. However, the low voltage drives and high voltage drives are not directly comparable since in high voltage drives, a relatively low switching frequency is used together with gate current profile optimization [15] to maximize the current handling capability and to minimize the system cost. In addition, several different modulation methods have been introduced to reduce the switching losses of the converters [16] and control methods to redistribute and regulate the losses between converter phases [17]. To overcome the problems associated with the efficiency determination of high efficiency semiconductor converters, a simple, open-loop, experimental dc-ac-dc back-to-back power conversion methodology is presented for the measurement of the combined losses of the power converter and passive filter in [18].

The first standard that introduced an efficiency classification for converters was the European standard EN 50598-2 launched in 2015. The frequency converters that are entitled as 'Complete Drive Modules' (CDMs) are labelled with energy efficiency classes in Europe [6]. The standard introduces IE0-IE2 classes for frequency converters and IES0–IES2 for power drive systems (PDSs) that include a converter and a motor. The EN 50598 standard designed by the European Committee for Electrotechnical Standardization

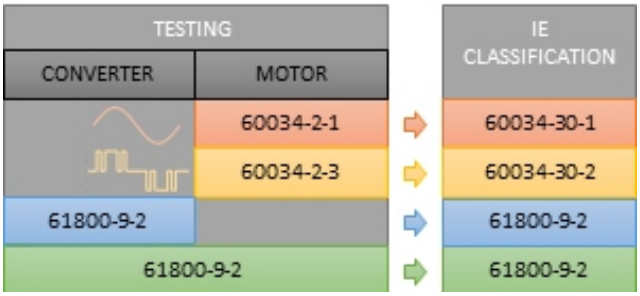

Fig. 1. Different IEC-standards for testing and energy efficiency classification of frequency converters, electric motors and converter-motor systems.

(CENELEC) was used as a base for the new international standard IEC 61800-9-2 with similar target [20]. An overview of standards related to electric motors and converter testing and their usage is given in Fig. 1.

The standard is applied to frequency converters that meet the following criteria; power rating range 0.12 kW–1000 kW, voltage range 100 V–1000 V and to low-voltage drive systems with asynchronous motors.

The contents of the European standard and its global counterpart are very similar and they both approve three methods to determine the losses of a voltage source converter (VSC). These methods input-output, calorimetric, and analytical methods. The methods are presented and characterized in [21], and their limitations are shown and compared.

A general overview of various loss measurement techniques is given in [22] and the electrical methods are briefly introduced. Sources of measurement errors are discussed. The article also gives the principles of the operation of various calorimetric types. The efficiency classification of the frequency converters is based on reference losses instead of efficiency boundaries that are used for electric motors. The loss limits as a function of the rated power of converter are shown in Fig. 2. The reference losses' relation to the rated power of the device is almost linear. If the losses of the device do not differ more than ±25% from the reference losses it will be labelled as IE1 while the devices with 25% more losses than the reference will be labelled as IE0 and converters with 25% less losses as IE2, respectively. The reference losses are Table values that are given in the standard. The loss boundaries for IE-classification are also converted here to efficiency boundaries, Fig. 3. In Fig. 3 it can be observed that the absolute values of the efficiency limits are relatively low and the limits remain constant for the rated powers above 160 kW where parallel power-semiconductor modules are commonly utilized and the device efficiency, therefore, remains constant. It should be noted that, in IES-classes for PDSs the loss boundary of 20% instead of 25% is used. The classes for CDMs and PDSs are defined up to IE2 only in the current standard and the IE and IES classes from 3 up to 9 are reserved to describe future technological improvements.

The calorimetric measurement was removed from the testing standard of general purpose electric motors after the IEC 34-2-1:1974 version [23] due to accuracy improvements in the torque transducers and power analyzers, but now it has been included as an approved method for the loss determination of power converters. Naturally, the converter

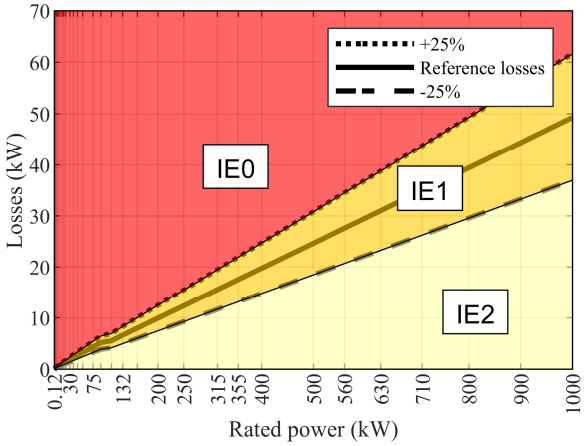

Fig. 2. Efficiency classification loss limits according to IEC 61800-9-2. The figure is created from the reference loss values given in the standard for different power ratings.

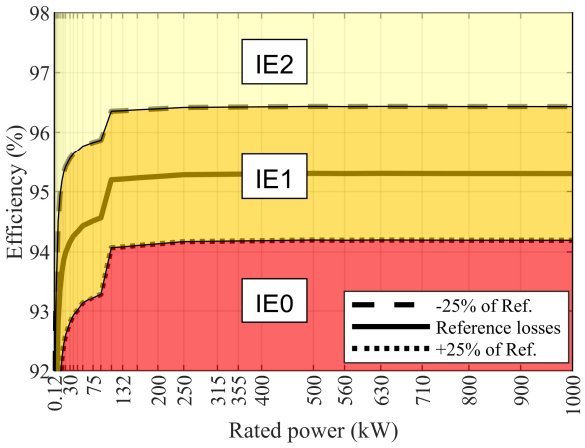

Fig. 3. IEC 61800-9-2 efficiency classification loss limits shown as efficiency limits as a function of device rated power.

loss determination with a calorimetric method is much easier to arrange with an adequate accuracy than the electrical machine measurement. The insulation of the motor stand and rotating shaft need special arrangements to avoid measurement reliability disturbing heat fluxes via them in the motor measurements while a metal frame with a ventilation fan can be easily used to mimic the converter. The development of insulation material properties is creating new possibilities for simple, low cost and highly accurate calorimetric systems. A measurement chamber with a low thermal conductivity wall and ceiling materials does not need an active control over the heat leakage through the walls. This will simplify the system, and it makes the systems more scalable to different sizes and economically more feasible.

Rigid polyurethane panels (PUR) sealed with polyurethane foam serve as an air tight and insulated test chamber which is easy to construct and is relatively cheap. Recently, the calorimetric measurement has been extensively adopted when measuring high-efficiency converter losses and efficiency.

In [24] a comparison between the calorimetric and the electrical method is made when measuring an active rectifier input LCL filter. In this ultimate case, the first power analyzer can catch only 44% from the actual expected loss and the state-of-the-art power analyzer can measure 91% of the losses with optimal settings.

The energy efficiency of an electric motor-drive system including a VSC and a synchronous reluctance motor is analyzed in [25] whereas in [26] a double chamber calorimeter with series chamber arrangement is introduced with a loss measurement accuracy below 1.5% of losses of the frequency converter in the loss range from 100 W to 400 W. The calorimeter efficiency uncertainty is analyzed to be very small, about 0.03%, and the power meter uncertainty with the input-output method 0.47% or 0.74% depending on the analysis method at the efficiency level of 97%. In [27], a new calorimetric loss measurement method is designed to implement a fast and accurate power loss measurement of WBG devices during the circuit operation. The measurement accuracy has been verified at 10 kW, 98.8% peak efficiency GaN-based three phase inverter. A highly accurate calorimetric system for power electronics loss determination is presented in [28] and is used especially for the loss determination of ultra-high efficiency silicon carbide power electronic circuits [29],[30].

An overview of the measurement methodology used in the power electronics loss determination is carried out in [31] and the measurement bandwidth requirement for the PWM power signal is examined in [32].

III. EXPERIMENTAL TESTS ACCORDING TO IEC 61800-9-2

Three alternative methods; input-output, calorimetric or analytic method, can be used to determine the losses of a VSC for the energy-efficiency classification according to IEC 61800-9-2. The analytical method is widely the most used one by the converter manufacturers but the parameters for the calculation method are not publicly available in general and these parameters subject to changes in the variable load conditions.

The analytical calculation procedure requires the knowledge of the converter's internal parameters such as semiconductor devices' threshold voltages, on-state resistances and switching losses. The analytical calculation procedure following the European standard EN50598 concluded in collaboration of converter manufacturer is presented in [33] for a 45 kVA VSC, but the results are not comprehensive and they are not given at the standardized test points.

A. Measurement points and conditions

The standard IEC 61800-9-2 contains 8 measurement points in the current-frequency plane shown in Fig. 4. The principle is to offer a good agreement of the loss results for common applications with a minimum number of measurement points. For example, points 1-4-7 can be used to estimate the losses in quadratic load profiles such as centrifugal blowers or pumps while the constant load points 1-2-3 are used for extruders, conveyer belts and hoisting machines. Points 3-4-5 can be roughly used to approximate winder or coiler applications.
The exact test load type for a converter is not specified in the standard and therefore an electronic load can be used instead

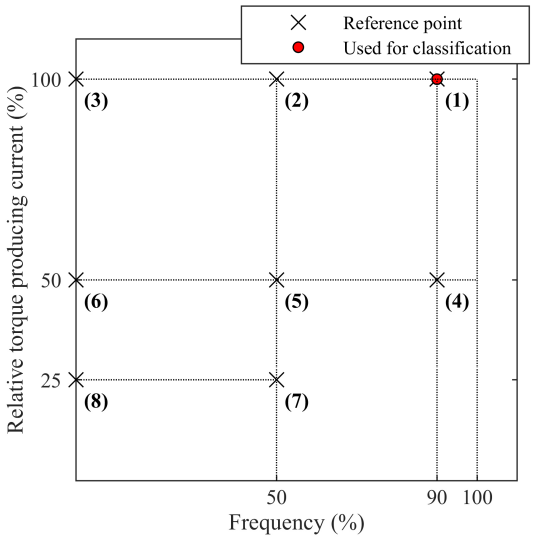

Fig. 4. Converter (CDM, Complete Drive Module) measurement points according to IEC 61800-9-2. The IE-classification is based on the losses in the point *f* = 90% (45 Hz) and *I* = 100%.

of a motor. Here, a standard 4-pole induction motor with 200 kW rated power was used as a test load, since it was already available in the laboratory. The measurement point current values given in the standard are minimum values and the actual test currents were slightly over the limits. The torque producing current values are given in Table I. The minimum relative test load currents given in Table I are related to the converter's rated current value. The usage of the different modulation index values has been limited in the standard by defining that the relative fundamental CDM output voltage (in per cent) shall not be lower than the relative CDM output frequency (in per cent).

Normally, the inverter bridge generates the majority of the losses that are the sum of the on-state losses and switching losses of both transistors and free-wheeling diodes. The on-state losses for the specified output power depend on the phase angle between the output voltage fundamental and current fundamental, and therefore the standard gives reference values for the displacement power factor for the load, Table II. For the converter testing a tolerance band of ±0.08 is allowed for the displacement power factors. It should be noted that the tests cannot be executed without a power analyzer that is capable of performing a harmonic analysis. The displacement power factor (DPF) is not the ratio of real power to apparent that is typically used for the power factor, but it is defined by the phase-shift angle between the fundamental output current and fundamental output voltage. In this case, the test load displacement power factor should be 0.86±0.08 at the test point with 100% torque producing current. The 200 kW induction motor as a load gives a power factor of 0.83 that is well between the limits. Similarly for the 50% torque producing current the obtained load displacement power factor 0.62 is inside the limits, but for the 25% current point the factor dropped to 0.1 that is far below the limit. In fact, it has been also noted in the standard that sometimes it is not possible to use the displacement power factor from the table in partial load operating points. If it is not possible, a displacement power factor as close as possible without

TABLE I
MINIMUM TEST LOAD CURRENTS AT DIFFERENT POINTS OF OPERATION

Torque producing current (%)	Test load current for the rated powers of				
	0.12 kW-0.75 kW	0.75 kW-5.5 kW	5.5 kW-45 kW	**45 kW-200 kW**	200 kW – 1000 kW
25	0.79	0.58	0.45	**0.42**	0.39
50	0.81	0.71	0.60	**0.58**	0.56
75	0.89	0.82	0.79	**0.78**	0.77
100	1.00	1.00	1.00	**1.00**	1.00

TABLE II
TEST LOAD DISPLACEMENT POWER FACTOR BETWEEN FUNDAMENTAL OUTPUT CURRENT AND FUNDAMENTAL OUTPUT VOLTAGE AT DIFFERENT POINTS

Torque producing current (%)	Test load displacement power factor for the power range of				
	0.12kW-0.75 kW	0.75 kW-5.5. kW	5.5 kW-45 kW	**45 kW-200 kW**	200 W-1000 W
25	0.34	0.38	0.49	**0.54**	0.57
50	0.51	0.60	0.71	**0.75**	0.78
75	0.64	0.72	0.80	**0.83**	0.85
100	0.73	0.79	0.85	**0.86**	0.87

changing the size of the motor shall be used and included in the documentation. The converters are commonly rated with a wide voltage level input range, and the input voltage level has a clear effect on the converter losses. However, all the testing conditions are recorded in the product documentation and it is expected that the manufacturer will test the converter with an appropriate input voltage. Therefore, the energy efficiency classification is fixed to a specific voltage level. The reference switching frequency is specified in the standard; 4 kHz for the devices with the rated power up to 90 kW and 2 kHz with the rated powers above 90 kW. Thus, 2 kHz is used here. To ensure exactly 2 kHz switching frequency at the rating point, the field weakening point is set to 50 Hz to avoid any field weakening at the 45 Hz point and the automatic thermal switching frequency decrease was disabled. The converter main ventilation fan was fed from an external three phase power supply and was set to full ventilation power as suggested in the standard. The losses were measured in the ten load points shown in the torque producing current – output frequency plane in Fig. 6. The first additional load point was at the no-load condition, where the output voltage reference is set to zero voltage and zero frequency (measurement point 10) to obtain the converter self-usage in the on-state, and another one was the rated current point (measurement point 0). The measurement points 0,1,2,5 and 7 were measured also with the calorimetric method simultaneously with the input-output measurements. In all the measurements, the converter was inside the calorimeter chamber to guarantee a stable ambient temperature for the converter. The data was collected when the converter was in its thermal equilibrium after it had been running at least 30 minutes with a constant load in the measurement points with 25 Hz, 45 Hz and 50 Hz frequencies. In the zero frequency point, the converter was first operated with 5 Hz output frequency and then the output frequency was decreased down to 0.5 Hz that was the minimum frequency where the system was running smoothly. The loss values are calculated using measured average input (P_{in}) and output power (P_{out}) values. The power analyzer observation window is set to 5 seconds and *N*=30 samples are used for zero

frequency points and one hundred N=100 samples for other points in the mean value of loss

$$P_{\mathrm{Loss,I-O}} = \frac{1}{N}\sum_{1}^{N} P_{\mathrm{in}N,5\ \mathrm{s}} - \frac{1}{N}\sum_{1}^{N} P_{\mathrm{out}N,5\ \mathrm{s}}. \quad (1)$$

It is expected that the random variation and the resulting type A uncertainty are reduced to a negligible [34] level because of the mean value calculation and it can be ignored in the uncertainty analysis presented in Chapter IV.

B. Experimental setup

The electric quantities were recorded using a Yokogawa WT1600 power analyzer equipped with a HITEC Zero-Flux current transducer system. As mentioned previously, also a calorimetric system was used simultaneously. The loss measurement system is an open and balance type calorimeter. The same calorimetric system is applied in [35], where the results of a European efficiency measurement for a 250-kW high-efficiency grid-connected solar inverter are presented and the loss results are verified with the calorimetric system. In high power solar inverter efficiency measurements the input is single phase distorted current drawn from the DC link of an active rectifier bridge and the output is a three-phase controlled voltage. The total heat generated by the device under test (DUT) in the thermal equilibrium inside the calorimeter can be expressed as

$$P_{\mathrm{Cal}} = \bar{c}_{\mathrm{p}} q_{\mathrm{m}} \Delta T_{\mathrm{air}} + U_{\mathrm{wall}} S_{\mathrm{wall}} \Delta T_{\mathrm{wall}}, \quad (2)$$

where $\bar{c}_{\mathrm{p}}$ is the specific heat capacity of moist air (J/(kgK)) calculated with the average temperatures of the inlet and outlet air, q_{m} the mass flow rate (kg/s), ΔT_{air} the temperature difference of the moist air between the inlet and outlet tubes (K), U_{wall} the overall heat transfer coefficient of the chamber (W/m^{2}K), S_{wall} the area of the chamber walls (m^2), and ΔT_{wall} the temperature gradient across the chamber walls (K). ΔT_{wall} is calculated based on the inside temperature T_{inside} and the outside temperature T_{outside}. The mass flow rate q_{m} is determined based on the known heater power P_{Cal} during the balance test. The balance test heating source mounted next to the converter is a steel-fixed resistor as shown in Fig. 5 with four 18 W DC-fans installed inside the resistor to extract the heat effectively to the chamber. These fans as well as the DUT ventilation fans are running continuously to keep the air circulation similar during both tests.

C. Input – output results

The losses at the measurement points and the interpolated losses in the torque-frequency plane are shown in Fig. 6. The ventilation losses are 270 W that is fed from the external supply and measured separately. The losses at this zero voltage modulation point were 339 W that is the self-consumption of the converter including the 270 W ventilation power. The control electronics power consumption is therefore only 69 W that is a remarkably low value for the converter of this size. The diode bridge losses and the losses in the intermediate circuit rise as a function of the output power, because the grid voltage and DC-link voltage remain relatively constant and the current drawn by the converter increases. The inverter bridge losses depend on the output current, voltage

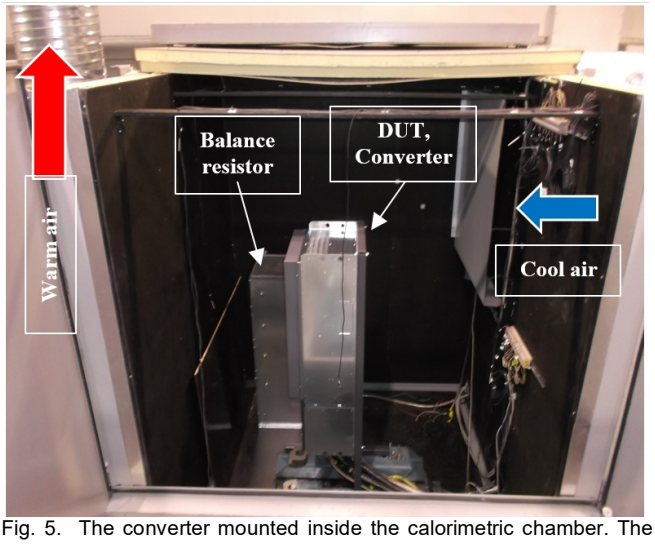

Fig. 5. The converter mounted inside the calorimetric chamber. The resistor is next to DUT to replicate the power losses during the balance test following directly the main test. The input air temperature is kept stably at 25°C while the output air temperature is 40°C that is controlled by the fluid flow by adjusting the exhaust blower rotational speed.

and power factor, since the converter is driven with a fixed switching frequency. The influence of the power factor is minimal on total losses since it mainly affects the power distribution between the power switch and the free-wheeling diode. When the motor is driven with a constant *U/f* ratio, the voltage increases linearly with the frequency. The rapid increase in the losses above 45 Hz is a result of overmodulation and increased harmonic content of the produced voltage. The conversion efficiency of the converter at the classification and rated point is 98.0% excluding the ventilation losses while the total efficiency at these points is 97.9%.

IV. Uncertainty Analysis of the Input-Output Method

One controversial topic has been the validity of the power values with distorted electrical waveforms when using the input-output method. Therefore, in the converter loss determination for IE-classification the measurement uncertainty is added to the converter loss value before it is used for energy efficiency classification. The power analyzer calculates the electric power (P_{active}) using N samples of the discrete instantaneous voltage $u(t)$ and current $i(t)$ values

$$P_{\mathrm{active}} = \frac{1}{N}\sum_{k=1}^{N} u_k(t) i_k(t), \quad (3)$$

and using DFT the active power can be presented using the frequency components from n to infinity,

$$P_{\mathrm{active}} = \sum_{n=1}^{n=\infty} U(n) I(n) \cos(\varphi(n)), \quad (4)$$

where $U(n)$ and $I(n)$ are the RMS values of the n^{th} components and $\varphi(n)$ the phase difference between the components. Each n^{th} harmonic can be a harmonic, an interharmonic or a subharmonic. Equation (4) shows that for

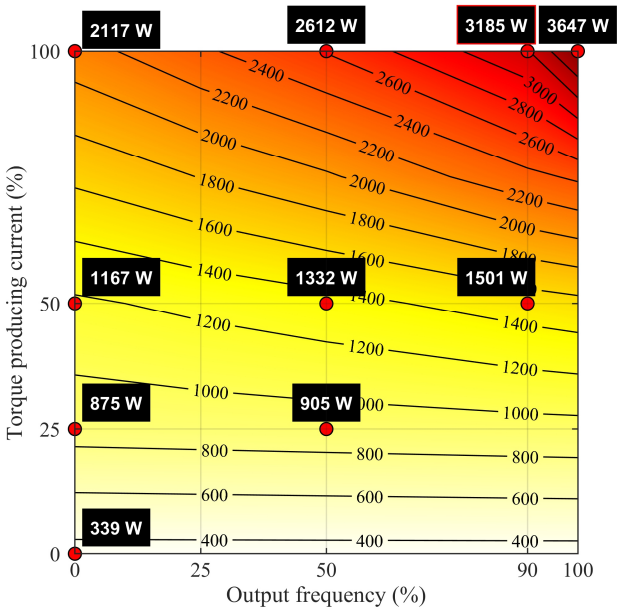

Fig. 6. Converter losses obtained using the input-output method as a function of the torque producing current and output frequency. The losses are obtained at 10 measurement points. The IE-classification is based on the losses at the point f = 90% (45 Hz) and I = 100%.

the power to exits at a specific frequency, all terms in the product must be non-zero. It also shows that there is always a frequency band limit in the active power that is either set by the voltage or the current measurement. When using a power analyser, the restrictive components are usually the external current sensors if the current values are above the permitted values of the power analyser internal channels that is typical in the motor and drives measurements. Here, the current measurement system's small signal bandwidth is 500 kHz. The total active power is split in the frequency bands using

TABLE III
LOSSES OBTAINED WITH CALORIMETRIC METHOD AND THE DIFFERENCE TO INPUT-OUTPUT LOSSES

Quantity	Measurement point				
	0	1	2	5	7
f	100%	90%	50%	50%	50%
I	100%	100%	100%	50%	25%
P_{Loss}	3647 W	3185 W	2612 W	1332 W	905 W
ΔP	8%	6%	10%	13%	9%

DFT. Both the input and output waveforms were analyzed in the measurement point '5' with 25 Hz output frequency and 50% torque producing current. The output power waveform behavior is considered to be average over the linear modulation region in this point and no significant differences between 5 Hz and 45 Hz operation points can be expected. The power distribution function in the frequency domain is presented in Fig. 7 together with the used power analyzer reading and range errors [36]. The power analyzer accuracy is optimal, 0.15% (1-year accuracy) of the power reading and 0.05% of the range, when the power lies in the frequency band between 45 Hz and 66 Hz, and it decreases strongly after 50 kHz. In the PWM output, the voltage and current fundamentals are transferring 97.8% of the total power and the total harmonic power is 2.2% of the total. The largest harmonic power exists at 4 kHz even though the average switching frequency over one second is 2 kHz. The power at the 4 kHz frequency is formed by the pulses with a length of 250 µs that is the most used one in the pulse pattern formed by this digital PWM. 99.7% of the PWM-power is in the frequency band below 10 kHz. For the rectifier bridge input, all the power is at frequencies below 1 kHz and the 5th and 7th harmonic waves are transferring the power in the reverse direction compared to the input fundamental waves. This explains the higher than 100 % value in the input power after 50 Hz.

For uncertainty analysis the power transferred by other than fundamental wave is insignificant, since the portion of the harmonic power does not have a significant effect on the total power uncertainty value. Therefore, the power measurement uncertainty analysis for the input and output can be performed using the fundamental wave values or using the total power values. The uncertainty analysis is performed similarly as in [34], but also the current measurement system accuracy is included in the analysis. In addition to reading and range errors (Fig. 7), also a lower power factor increases measurement uncertainty. The power analyzer's additional reading error caused by the power factor is shown in Fig. 8. The power factor error is a result of timestamp mismatch between the current and voltage values because of some differences between the channels. The additional power reading error rises non-linearly as a function of the power factor and in this case with the power factors lower than 0.7 it is already higher than the normal reading error of the best accuracy band.

The current measurement system accuracy is for AC-currents ±(0.01% reading + 0.002% range) and the phase difference is smaller than 0.01° [37]. The total power measurement uncertainty (u_c) can be calculated using an uncertainty budget [38]. The input estimate values x_i of the

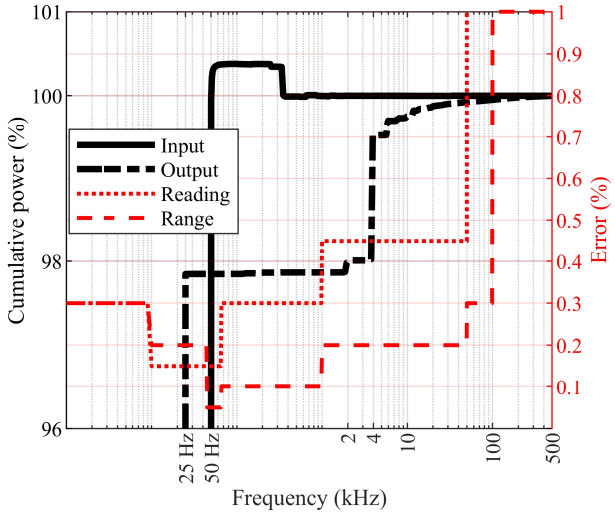

Fig. 7. The input and output active power and the power analyzer reading and range errors as a function of frequency. The electrical quantities have been recorded in the measurement point (5) with 50% torque producing current and 25 Hz output frequency from converter terminals. The fundamental waves are transferring 97.8% of the power in the output. At the input side, the 5th and 7th harmonic waves are transferring the power in the reverse direction (the power flows of these harmonics are from converter to grid) compared to the input fundamental waves.

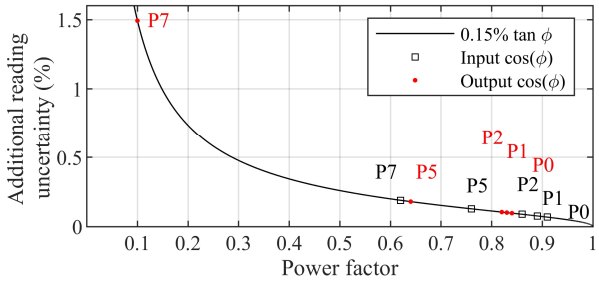

Fig. 8. The additional power reading error of the used power analyzer as a result of low power factor and the input and output power factors at points 0,1,2,5 and 7.

quantity X_i make up an output estimate according to the function $y = f(x_1, x_2, \ldots, x_N)$

$$u_c = \sqrt{\sum_i^N \left(\frac{\partial f}{\partial x_i}\right)^2 u^2(x_i)}. \quad (5)$$

In the analysis the amplitude and phase errors of the current measurement system are expected not to correlate as well as the total current measurement system and the power analyzer uncertainties. The relative proportions of the power range, power reading value, power factor influence (Add Rdg), current measurement system amplitude and phase error are (CT) shown in Fig. 9. In the uncertainty analysis the manufacturers' specifications are assumed to have a normal distribution with standard deviation $\sigma = 4$. The total expanded loss measurement uncertainty values (total height of the bars) with 95% confidence level are also given in Fig. 9.

The current measurement system influence on the power measurement uncertainty is relatively low for both the input and output powers because of the high accuracy of the system. The input and output uncertainties are almost equal in points 0, 1 and 2, while in 5 and 7 the power analyzer range error is the dominating factor in the output power uncertainty. The 25 Hz output frequency is outside the best accuracy band (0.05% of range) of the power analyzer and the range uncertainty is 4 times the uncertainty (0.2% of range) of the best accuracy band. The power analyzer relative power measurement uncertainty depends on how well the corresponding power value matches with the current power range that is controlled by the voltage and current ranges. The low power factor impairs the power measurement accuracy rapidly. The total loss measurement uncertainty is 385 W in the classification point (1) that is 12% of the determined losses or 0.26% of the output power.

V. COMPARISON OF THE RESULTS OBTAINED USING THE INPUT-OUTPUT AND CALORIMETRIC METHOD

As mentioned earlier the losses were obtained in five measurement points simultaneously using a calorimetric system described in [34]. The calorimeter accuracy is 0.4% of the losses in the loss range of 1 kW to 7 kW that has been validated using a series of resistor tests with known loss power. The accuracy includes the power analyzer measurement uncertainty that is used to control the resistor power. The data processing method described in [39] is used to improve the repeatability of the results if the air properties

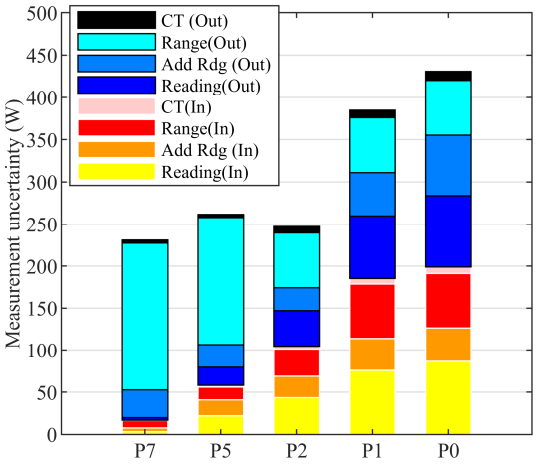

Fig. 9. Relative proportions of the different uncertainty contributors and the total electric measurement uncertainty values.

change during the measurement series. Yet, the air properties were extremely constant during the measurements and the maximum recorded difference in the barometric pressure was 600 Pa, in relative humidity 2.2% and in the inlet and outlet temperatures 0.1 K. These air properties' effects in the specific heat of the air are 0.6‰, 0.2‰ and 0.4‰ that are in direct relation to the loss result obtained with the calorimeter. All these maximum differences were recorded in separate measurement points but even if they would have existed simultaneously, the differences would not have had a significant effect on the determined losses. The losses and the difference to input-output losses are tabulated in Table III. When comparing the values obtained with the input-output method and with the calorimetric method, no significant differences in the scope of energy efficiency classification can be found. However, the magnitude of the difference might be very valuable in R&D work. In the classification point the loss difference is 6% between the input-output and calorimetric method that is 0.15% proportion of the output power. The total measurement uncertainty in losses and the loss difference between the input-output method and the calorimetric method in relation to output power are plotted in Fig. 10. It can be examined in Fig. 10 that the difference in the results obtained with the input-output and calorimetric methods behave similarly as the determined measurement uncertainty. The relative loss uncertainty is rapidly increasing when the output power is decreasing because the ratings of the measurement instruments are in good agreement near the rated values, but in the low power points they are overrated.

VI. DISCUSSION

In IEC 61800-9-2 the measurement uncertainty is added at the top of the determined value to remove possible problems in the accuracy of the loss determination. However, the analysis here shows that the measurement accuracy should not be a big problem in the energy-efficiency classification of converters when current efficiency classes are used with relatively low efficiency limit values. It should be noted that

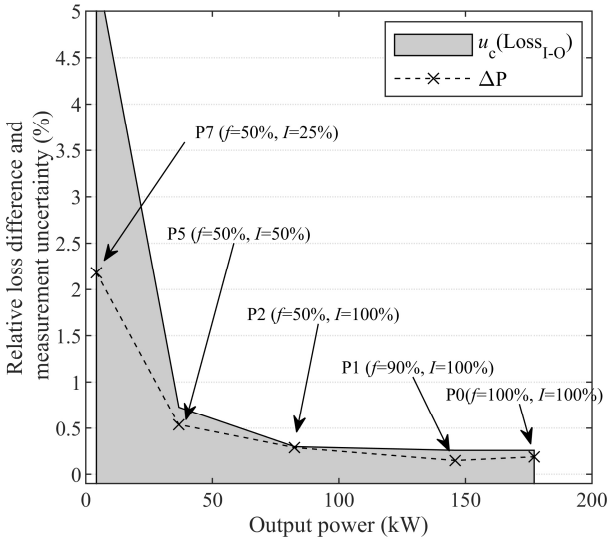

Fig. 10. Relative loss difference between the input-output and calorimetric method in relation to output power and the measurement uncertainty of the loss determination using the input-output method.

the power analyzer used here is not with the highest available accuracy. There are other models in the market that have higher accuracy specifications but the power analyzer used here represents well the instrumentation that is used in typical test setups of research institutes or manufacturers.

Fig. 11 shows the measured losses with both methods and the total measurement uncertainty in the losses and the IE-classification limits for 160 kW (200 kVA) converter. The sum of the determined losses and loss measurement uncertainty is used for the classification. The measurement results show that even a typical commercial product based on silicon technology has only half of the losses needed to obtain the highest available energy efficiency classification. Based on the authors' calculations, a similarly rated converter with silicon carbide inverter currently on the market should have about 30% less total losses than the product measured here. There is an urgent need either to modify the reference losses in the oncoming standard or to introduce more efficiency classes for converters. The first one could more feasible in this phase, when the classes are not yet widely adopted.

VII. Conclusion

The losses of the most used converter topology in industrial motor drives – voltage source converter with passive rectifier- and 2-level inverter bridge – with a rated power of 160 kW was examined according to IEC61800-9-2 using the input-output and the calorimetric method. The obtained losses indicate that the tested converter can be rated with the highest 'IE2' –class. The comparison of losses obtained with the two methods shows that even though there are differences in the results, they are not critical from the energy efficiency classification point of view. However, the final optimization of the converter energy-efficiency in R&D activities might need much higher loss measurement accuracy than the input-output method can provide.

The input and output power measurement uncertainty was analyzed in the frequency domain. The uncertainty analysis of

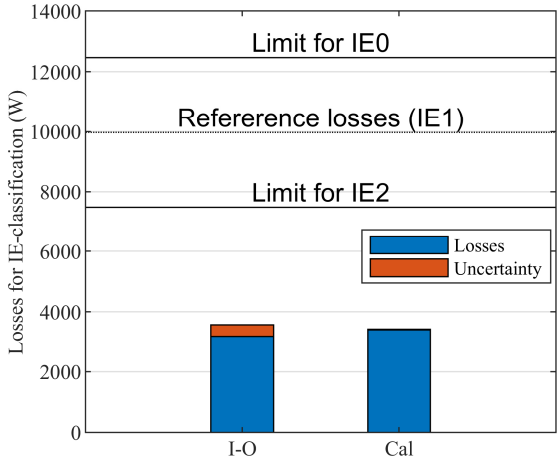

Fig. 11. VSC losses obtained with the input-output method and the related uncertainty added at the top of the determined losses. Also, the reference losses (IE1) for 200 kVA (160 kW) converter and the limits for IE0 and IE2 efficiency classes are given.

the frequency converter output waveforms in the frequency domain can be extended to converter-fed motors. The power measurement uncertainty analysis can be performed for converter-fed machines similarly as for direct-on-line machines. The input or output power measurement accuracy should not be a problem in the energy efficiency classification of electric machines or power converters. However, the problem with the loss uncertainty approaching infinity when the device efficiency is approaching unity should be noted in the testing of today's high efficiency devices. The IEC 61800-9-2 limits for the low-voltage VSCs intended to be used to supply motors are not pushing the manufacturers to use the latest technology, since even the Si-based converter measured here has only half of the losses allowed for the highest energy-efficiency class currently in use. Based on the results presented in this paper the IEC-loss limits should be reconsidered in the next revision of the standard in future.

References

[1] P. Waide, C. U. Brunner, "Energy-Efficiency Policy Opportunities for Electric Motor-Driven Systems –Working paper", International energy agency, Paris, France, 2011.

[2] Rotating electrical machines – Part 30-1: Efficiency classes of line operated AC motors (IE code), Ed. 1, IEC 60034-30-1, March 2014.

[3] Rotating electrical machines – Part 30-2: Efficiency classes of variable speed AC motors (IE-code) Ed. 1, IEC TS 60034-30-2, Dec. 2016.

[4] Rotating electrical machines – Part 2-1: Standard methods for determining losses and efficiency from tests (excluding machines for traction vehicles), Ed. 2, IEC 60034-2-1, June 2014.

[5] Rotating electrical machines – Part 2-3: Specific test methods for determining losses and efficiency of converter-fed AC induction motors, IEC TS 60034-2-3, Nov. 2013.

[6] A. T. de Almeida, F. J. T. E. Ferreira and G. Baoming, "Beyond Induction Motors—Technology Trends to Move Up Efficiency," in *IEEE Transactions on Industry Applications*, vol. 50, no. 3, pp. 2103-2114, May-June 2014.

[7] A. T. De Almeida, F. J. T. E. Ferreira and A. Q. Duarte, "Technical and Economical Considerations on Super High-Efficiency Three-Phase Motors," in *IEEE Transactions on Industry Applications*, vol. 50, no. 2, pp. 1274-1285, March-April 2014.

[8] W. Cao, "Comparison of IEEE 112 and New IEC Standard 60034-2-1," in *IEEE Transactions on Energy Conversion*, vol. 24, no. 3, pp. 802-808, Sept. 2009.

[9] G. Bucci, F. Ciancetta, E. Fiorucci and A. Ometto, “Uncertainty Issues in Direct and Indirect Efficiency Determination for Three-Phase Induction Motors: Remarks About the IEC 60034-2-1 Standard,” in IEEE Transactions on Instrumentation and Measurement, vol. 65, no. 12, pp. 2701-2716, Dec. 2016.
[10] B. Deusinger, M. Lehr and A. Binder, “Determination of efficiency of permanent magnet synchronous machines from summation of losses,” *2014 International Symposium on Power Electronics, Electrical Drives, Automation and Motion*, Ischia, 2014, pp. 619-624.
[11] N. Yogal, C. Lehrmann and M. Henke, “Determination of the Measurement Uncertainty of Direct and Indirect Efficiency Measurement Methods in Permanent Magnet Synchronous Machines,” 2018 XIII International Conference on Electrical Machines (ICEM), Alexandroupoli, 2018, pp. 1149-1156.
[12] T. Noguchi, H. Tomiki, S. Kondo and I. Takahashi, "Direct power control of PWM converter without power-source voltage sensors," in *IEEE Transactions on Industry Applications*, vol. 34, no. 3, pp. 473-479, May/Jun 1998.
[13] Y. Suh, J. K. Steinke and P. K. Steimer, "Efficiency Comparison of Voltage-Source and Current-Source Drive Systems for Medium-Voltage Applications," in *IEEE Transactions on Industrial Electronics*, vol. 54, no. 5, pp. 2521-2531, Oct. 2007.
[14] E. P. Wiechmann, P. Aqueveque, R. Burgos and J. Rodriguez, “On the Efficiency of Voltage Source and Current Source Inverters for High-Power Drives,” in *IEEE Transactions on Industrial Electronics*, vol. 55, no. 4, pp. 1771-1782, April 2008.
[15] G. Schmitt, R. Kennel and J. Holtz, "Voltage gradient limitation of IGBTS by optimised gate-current profiles," *2008 IEEE Power Electronics Specialists Conference*, Rhodes, 2008, pp. 3592-3596. doi: 10.1109/PESC.2008.4592512.
[16] A.M. Hava, R.J. Kerkman, and T.A. Lipo, “A high-performance generalized discontinuous PWM algorithm,” IEEE Trans. on Industry Applications, vol. 34, no. 5, pp. 1059-1071, Sep.-Oct. 1998.
[17] A. Anuchin, D. Aliamkin, M. Lashkevich, D. Shpak, A. Zharkov and F. Briz, “Minimization and redistribution of switching losses using predictive PWM strategy in a voltage source inverter,” *2018 25th International Workshop on Electric Drives: Optimization in Control of Electric Drives (IWED)*, Moscow, 2018, pp. 1-6.
[18] A. Kadavelugu, H. Suryanarayana, L. Liu, Z. Pan, C. Belcastro and E. Paatero, "A simple and accurate efficiency measurement method for power converters," *2017 IEEE Applied Power Electronics Conference and Exposition (APEC)*, Tampa, FL, 2017, pp. 3265-3270.
[19] I.P. Tsoumas, H. Tischmacher, and P. Kollensperger, “The European Standard EN 50598-2: Efficiency classes of converters and drive systems,” in Proc. 21th Int. Conf. on Electrical Machines, Berlin, Germany, Sep. 2014, pp. 929–935.
[20] Adjustable speed electrical power drive systems – Part 9-2: Ecodesign for power drive systems, motor starters, power electronics their driven applications – Energy efficiency indicators for power drive systems and motor starters. Ed. 1. IEC 61800-9-2, March 2017.
[21] F.W. Fuchs, J. Schroder, and B. Wittig, “State of the technology of power loss determination in power converters,” in Proc. 15th European Conf. on Power Electronics and Applications, Lille, France, Sep. 2013, pp. 1–10.
[22] C. Xiao, G. Chen, and W.G. Odendaal, “Overview of power loss measurement techniques in power electronics systems,” in Conf. Rec. of the 2002 IEEE Industry Applications Conference, vol. 2, Pittsburgh, PA, USA, Oct. 2002, pp. 1352–1359.
[23] Rotating electrical machines - Part 2: Methods for determining losses and efficiency of rotating electrical machinery form tests (excluding machines for traction vehicles) - Measurement of losses by the calorimetric method, IEC 34-2A, Genève, Switzerland, 1974.
[24] V. Mattsson, “Comparison of calorimetric and electrical loss measurement methods in a frequency converter research and development application,” *2011 IEEE Energy Conversion Congress and Exposition*, Phoenix, AZ, 2011, pp. 1026-1030.
[25] L. Aarniovuori *et al*., “Application of Calorimetric Method for Loss Measurement of a SynRM Drive System,” in *IEEE Transactions on Industrial Electronics*, vol. 63, no. 4, pp. 2005-2015, April 2016.
[26] Xiaofeng Gong *et al*., “Measurement of a variable frequency drive loss and efficiency using both calorimeter and powermeter,” *2012 IEEE International Symposium on Industrial Electronics*, Hangzhou, 2012, pp. 700-707.
[27] H. Li, X. Li, Z. Zhang, J. Wang, L. Liu and S. Bala, "A simple calorimetric technique for high-efficiency GaN inverter transistor loss measurement," *2017 IEEE 5th Workshop on Wide Bandgap Power Devices and Applications (WiPDA)*, Albuquerque, NM, 2017, pp. 251-256.
[28] D. Christen, U. Badstuebner, J. Biela, and J. W. Kolar, “Calorimetric power lossmeasurement for highly efficient converters,” in *Proc. 2010 Int. Power Electron. Conf. (ECCE Asia)*, Sapporo, Japan, Jun. 2010, pp. 1438–1445.
[29] A. Stupar, T. Friedli, J. Minibock and J. W. Kolar, "Towards a 99% Efficient Three-Phase Buck-Type PFC Rectifier for 400-V DC Distribution Systems," in *IEEE Transactions on Power Electronics*, vol. 27, no. 4, pp. 1732-1744, April 2012.
[30] L. Schrittwieser, M. Leibl, M. Haider, F. Thöny, J. W. Kolar and T. B. Soeiro, "99.3% Efficient Three-Phase Buck-Type All-SiC SWISS Rectifier for DC Distribution Systems," in *IEEE Transactions on Power Electronics*, vol. 34, no. 1, pp. 126-140, Jan. 2019.
[31] Xiao, C., Chen, G., Odendaal, W.G.H.: ‘Overview of power loss measurement techniques in power electronics systems’, IEEE Trans. Ind. Appl., 2007, 43, (3), pp. 657–664.
[32] D. Lindenthaler and G. Brasseur, "Signal-Bandwidth Evaluation for Power Measurements in Electric Automotive Drives," in *IEEE Transactions on Instrumentation and Measurement*, vol. 64, no. 6, pp. 1336-1343, June 2015.
[33] L. Aarniovuori, T. Musikka, A. Kosonen, M. Niemelä and J. Pyrhönen, “Three alternative methods to determine voltage source converter losses,” *2015 17th European Conference on Power Electronics and Applications (EPE'15 ECCE-Europe)*, Geneva, 2015, pp. 1-10.
[34] H. Kärkkäinen, L. Aarniovuori, M. Niemelä and J. Pyrhönen, “Advanced Uncertainty Calculation Method for Frequency Converter Loss Determination,” *2018 20th European Conference on Power Electronics and Applications (EPE'18 ECCE Europe)*, Riga, 2018, pp. P.1-P.10.
[35] L., Aarniovuori, A. Kosonen, P. Sillanpää, M. Niemelä, “High-Power Solar Inverter Efficiency Measurements by Calorimetric and Electric Methods,” in *IEEE Trans. Power Electron*., vol.28, no.6, pp.2798-2805, June 2013.
[36] *WT1600 Digital Power Meter User’s Manual (4th Edition)*, Yokogawa Electric Corporation, Tokyo, Japan, 2004,
[37] Zero-flux™ Current Sensors & Precision Power Meters: Hitec & Yokogawa – A perfect ACCURACY match, Yokogawa Europe, Amersfoot, The Netherlands, 2009.
[38] Evaluation of measurement data – Guide to the expression of uncertainty in measurement, Ed. 1, JCGM 100:2008, September 2008, pp. 1–134.
[39] A. Kosonen, L. Aarniovuori, J. Ahola, J. Backman, J. Pyrhönen and M. Niemelä, “Loss Definition of Electric Drives by a Calorimetric System With Data Processing,” in *IEEE Transactions on Industrial Electronics*, vol. 61, no. 8, pp. 4432-4442, Aug. 2014.

Lassi Aarniovuori (M’14,) received D.Sc. degree in Electric drives technology from Lappeenranta University of Technology (LUT), Lappeenranta, Finland, 2010.

He is currently an Adjunct Professor of Electrical Machines and Drives at LUT-University, Finland. After receiving a doctorate degree, Dr. Aarniovuori has worked seven years as a full time researcher in various university-industry collaboration projects in the field of electric motor drives at LUT. From 2017 to 2019, he worked as a Marie Curie Fellow with the School of Engineering and Applied Science, Aston University, Birmingham, U.K.

Dr. Aarniovuori’s current research interests include the field of electric motor drives, especially wide band-gap power switches, modulation methods, simulation of electric drives, efficiency measurements, and calorimetric measurement systems.

Hannu Kärkkäinen (STM’17) was born in Imatra, Finland, in 1980. He received the M.Sc. degree in electrical engineering from Lappeenranta University of Technology (LUT), Lappeenranta, Finland, in 2015.

He is currently a Junior Researcher with the Department of Electrical Engineering, LUT. His research interests include electric drive systems, particularly loss and efficiency measurements of motors and drives.

Alecksey Anuchin (M'13–SM'19) received his B.Sc., M.Sc., Ph.D., and Dr. Eng. Sc. degrees from Moscow Power Engineering Institute in 1999, 2001, 2004, and 2018, respectively.

He has more than 20 years of experience covering control systems of electric drives, hybrid powertrains, and real-time communications. He is the author of three textbooks on the design of real-time software for the microcontroller of the C28 family and Cortex-M4F, and control system of electric drives (in Russian).

He has published more than 100 conference and journal papers. He delivers lectures on "Control Systems of Electric Drives", "Real-time Software Design", "Electric Drives," and "Science Research Writing" in Moscow Power Engineering Institute. He is in a head position at the Electric Drives Department for the last 8 years.

Juha J. Pyrhönen (M'06–SM'17) born in 1957 in Kuusankoski, Finland, received the Doctor of Science (D.Sc.) degree from Lappeenranta University of Technology (LUT), Finland in 1991.

He became Professor of Electrical Machines and Drives in 1997 at LUT. He is engaged in research and development of electric motors and power-electronic-controlled drives.

Prof. Pyrhönen has wide experience in the research and development of special electric drives for distributed power production, traction and high-speed applications. Permanent magnet materials and applying them in machines have an important role in his research. Currently he is also studying possibilities of using carbon-based materials in electrical machines.

Pia Lindh (M'04–SM'17) born in Helsinki in 1969, received her M.Sc. degree in energy technology in 1998 and her D.Sc. degree in electrical engineering (Technology) in 2004 from Lappeenranta University of Technology (LUT), Lappeenranta, Finland.

She is currently serving as an associate professor at the Department of Electrical Engineering in LUT Energy, Lappeenranta, where she is engaged in teaching and research of electric motors and electric drives.

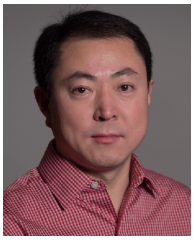

Wenping Cao (M'05–M'11) received the B.Eng in electrical engineering from Beijing Jiaotong University, Beijing, China, in 1991, and the Ph.D. degree in electrical machines and drives from the University of Nottingham, Nottingham, U.K., in 2004. He is currently Chair Professor of Electrical Power Engineering at Aston University, Birmingham, U.K., and also a Visiting Professor at School of Electrical Engineering and Automation, Anhui University, P. R. China.

Prof. Cao is presently the Chairman for the Industrial Electronics Society, IEEE UK and Ireland Section, and also a "*Royal Society Wolfson* Research *Merit Award" holder, U.K.* He was a semi-finalist at the "Annual MIT-CHIEF Business Plan Contest", U.S.A., in 2015; the "Dragon's Den Competition Award" winner from Queen's University Belfast, U.K., in 2014, the "Innovator of the Year Award" winner from Newcastle University, U.K., in 2013. His research interests include fault analysis and condition monitoring of electrical machines and power electronics.

ACTA UNIVERSITATIS LAPPEENRANTAENSIS

920. HONKANEN, JARI. Control design issues in grid-connected single-phase converters, with the focus on power factor correction. 2020. Diss.

921. KEMPPINEN, JUHA. The development and implementation of the clinical decision support system for integrated mental and addiction care. 2020. Diss.

922. KORHONEN, SATU. The journeys of becoming ang being an international entrepreneur: A narrative inquiry of the "I" in international entrepreneurship. 2020. Diss.

923. SIRKIÄ, JUKKA. Leveraging digitalization opportunities to improve the business model. 2020. Diss.

924. SHEMYAKIN, VLADIMIR. Parameter estimation of large-scale chaotic systems. 2020. Diss.

925. AALTONEN, PÄIVI. Exploring novelty in the internationalization process - understanding disruptive events. 2020. Diss.

926. VADANA, IUSTIN. Internationalization of born-digital companies. 2020. Diss.

927. FARFAN OROZCO, FRANCISCO JAVIER. In-depth analysis of the global power infrastructure - Opportunities for sustainable evolution of the power sector. 2020. Diss.

928. KRAINOV, IGOR. Properties of exchange interactions in magnetic semiconductors. 2020. Diss.

929. KARPPANEN, JANNE. Assessing the applicability of low voltage direct current in electricity distribution - Key factors and design aspects. 2020. Diss.

930. NIEMINEN, HARRI. Power-to-methanol via membrane contactor-based CO2 capture and low-temperature chemical synthesis. 2020. Diss.

931. CALDERA, UPEKSHA. The role of renewable energy based seawater reverse osmosis (SWRO) in meeting the global water challenges in the decades to come. 2020. Diss.

932. KIVISTÖ, TIMO. Processes and tools to promote community benefits in public procurement. 2020. Diss.

933. NAQVI, BILAL. Towards aligning security and usability during the system development lifecycle. 2020. Diss.

934. XIN, YAN. Knowledge sharing and reuse in product-service systems with a product lifecycle perspective. 2020. Diss.

935. PALACIN SILVA, VICTORIA. Participation in digital citizen science. 2020. Diss.

936. PUOLAKKA, TIINA. Managing operations in professional organisations – interplay between professionals and managers in court workflow control. 2020. Diss.

937. AHOLA, ANTTI. Stress components and local effects in the fatigue strength assessment of fillet weld joints made of ultra-high-strength steels. 2020. Diss.

938. METSOLA, JAAKKO. Good for wealth or bad for health? Socioemotional wealth in the internationalisation process of family SMEs from a network perspective. 2020. Diss.

939. VELT, HANNES. Entrepreneurial ecosystems and born global start-ups. 2020. Diss.

940. JI, HAIBIAO. Study of key techniques in the vacuum vessel assembly for the future fusion reactor. 2020. Diss.

941. KAZARNIKOV, ALEXEY. Statistical parameter identification of reaction-diffusion systems by Turing patterns. 2020. Diss.

942. SORMUNEN, PETRI. Ecodesign of construction and demolition waste-derived thermoplastic composites. 2020. Diss.

943. MANKONEN, ALEKSI. Fluidized bed combustion and humidified gas turbines as thermal energy conversion processes of the future. 2020. Diss.

944. KIANI OSHTORJANI, MEHRAN. Real-time efficient computational approaches for hydraulic components and particulate energy systems. 2020. Diss.

945. PEKKANEN, TIIA-LOTTA. What constrains the sustainability of our day-to-day consumption? A multi-epistemological inquiry into culture and institutions. 2021. Diss.

946. NASIRI, MINA. Performance management in digital transformation: a sustainability performance approach. 2021. Diss.

947. BRESOLIN, BIANCA MARIA. Synthesis and performance of metal halide perovskites as new visible light photocatalysts. 2021. Diss.

948. PÖYHÖNEN, SANTERI. Variable-speed-drive-based monitoring and diagnostic methods for pump, compressor, and fan systems. 2021. Diss.

949. ZENG, HUABIN. Continuous electrochemical activation of peroxydisulfate mediated by single-electron shuttle. 2021. Diss.

950. SPRINGER, SEBASTIAN. Bayesian inference by informative Gaussian features of the data. 2021. Diss.

951. SOBOLEVA, EKATERINA. Microscopy investigation of the surface of some modern magnetic materials. 2021. Diss.

952. MOHAMMADI ASL, REZA. Improved state observers and robust controllers for non-linear systems with special emphasis on robotic manipulators and electro-hydraulic servo systems. 2021. Diss.

953. VIANNA NETO, MÁRCIO RIBEIRO. Synthesis and optimization of Kraft process evaporator plants. 2021. Diss.

954. MUJKIC, ZLATAN. Sustainable development and optimization of supply chains. 2021. Diss.

955. LYYTIKÄINEN, JOHANNA. Interaction and barrier properties of nanocellulose and hydrophobically modified ethyl(hydroxyethyl)cellulose films and coatings. 2021. Diss.

956. NGUYEN, HOANG SI HUY. Model based design of reactor-separator processes for the production of oligosaccharides with a controlled degree of polymerization. 2021. Diss.

957. IMMONEN, HEIKKI. Application of object-process methodology in the study of entrepreneurship programs in higher education. 2021. Diss.

ISBN 978-952-335-647-4
ISBN 978-952-335-648-1 (PDF)
ISSN-L 1456-4491
ISSN 1456-4491
Lappeenranta 2021